



NOAA Technical Memorandum NMFS-AFSC-360

doi:10.7289/V5/TM-AFSC-360

Model-based Essential Fish Habitat Definitions for Aleutian Island Groundfish Species

K. Turner, C. N. Rooper, E. Laman, S. Rooney,
D. Cooper, and M. Zimmermann

U.S. DEPARTMENT OF COMMERCE
National Oceanic and Atmospheric Administration
National Marine Fisheries Service
Alaska Fisheries Science Center

August 2017

NOAA Technical Memorandum NMFS

The National Marine Fisheries Service's Alaska Fisheries Science Center uses the NOAA Technical Memorandum series to issue informal scientific and technical publications when complete formal review and editorial processing are not appropriate or feasible. Documents within this series reflect sound professional work and may be referenced in the formal scientific and technical literature.

The NMFS-AFSC Technical Memorandum series of the Alaska Fisheries Science Center continues the NMFS-F/NWC series established in 1970 by the Northwest Fisheries Center. The NMFS-NWFSC series is currently used by the Northwest Fisheries Science Center.

This document should be cited as follows:

Turner, K., C. N. Rooper, E. A. Laman, S. C. Rooney, D. W. Cooper, and M. Zimmermann. 2017. Model-based essential fish habitat definitions for Aleutian Island groundfish species. U.S. Dep. Commer., NOAA Tech. Memo. NMFS-AFSC-360, 239 p.

Document available: <https://www.afsc.noaa.gov/Publications/AFSC-TM/NOAA-TM-AFSC-360.pdf>

Reference in this document to trade names does not imply endorsement by the National Marine Fisheries Service, NOAA.



NOAA Technical Memorandum NMFS-AFSC-360

doi:10.7289/V5/TM-AFSC-360

Model-based Essential Fish Habitat Definitions for Aleutian Island Groundfish Species

by
K. Turner, C. N. Rooper, E. Laman, S. Rooney,
D. Cooper, and M. Zimmermann

Resource Assessment and Conservation Engineering Division
Alaska Fisheries Science Center
7600 Sand Point Way NE
Seattle WA 98115

www.afsc.noaa.gov

U.S. DEPARTMENT OF COMMERCE

Wilbur L. Ross Jr., Secretary

National Oceanic and Atmospheric Administration

Benjamin Friedman, Acting Under Secretary and Administrator

National Marine Fisheries Service

Chris Oliver, Assistant Administrator for Fisheries

August 2017

This document is available to the public through:

National Technical Information Service
U.S. Department of Commerce
5285 Port Royal Road
Springfield, VA 22161

www.ntis.gov

ABSTRACT

Defining essential habitats for fishes is important for managing groundfish in Alaska. Species distribution models have been widely used in conservation biology and terrestrial systems to define the potential habitat for organisms of interest. The models themselves can take a number of forms, from relatively simple frameworks such as generalized linear or additive models to complex modeling frameworks such as boosted regression trees, maximum entropy models, two-stage models or other formulations. We used a variety of modeling methods and data sets from scientific surveys and commercial fisheries to define the habitats for over 30 fish species in the Aleutian Islands, Alaska. Adult, juvenile, larval and egg stages were modeled in four seasons where data were available. Depth was the most important variable determining the distribution of most adult and juvenile life history stages whereas sea surface temperature was the most important variable for egg and larval stages. Using the models, maps were developed that identified local hot spots for each species and life stage. These maps will be used for marine spatial planning and assessing impacts of anthropogenic activities in Alaska's marine environment.

CONTENTS

| | |
|---|-----|
| ABSTRACT..... | iii |
| INTRODUCTION | 1 |
| METHODS | 3 |
| Study Area and Species..... | 3 |
| Species Distribution Data – Recruitment Processes Data..... | 6 |
| Species Distribution Data – Groundfish Bottom Trawl Surveys | 9 |
| Species Distribution Data – Commercial Catch (observer) Data..... | 13 |
| Habitat Variables..... | 14 |
| Modeling Methods – Recruitment Processes Data | 24 |
| Modeling Methods – Bottom Trawl Survey Data..... | 24 |
| Modeling Methods – Commercial Catch (observer) Data | 26 |
| Model Validation..... | 26 |
| Essential Fish Habitat Maps..... | 27 |
| RESULTS | 28 |
| Flatfishes | 28 |
| Arrowtooth Flounder (<i>Atheresthes stomais</i>)..... | 28 |
| Kamchatka Flounder (<i>Atheresthes evermanni</i>) | 38 |
| Northern Rock Sole (<i>Lepidopsetta polyxystra</i>) | 47 |
| Southern Rock Sole (<i>Lepidopsetta bilineata</i>)..... | 57 |
| Greenland Turbot (<i>Reinhardtius hippoglossoides</i>)..... | 61 |
| Flathead Sole (<i>Hippoglossoides elassodon</i>) | 69 |
| Rex Sole (<i>Glyptocephalus zachirus</i>) | 79 |
| Dover Sole (<i>Microstomus pacificus</i>) | 89 |
| Roundfishes..... | 95 |
| Atka Mackerel (<i>Pleurogrammus monopterygius</i>) | 95 |
| Pacific Cod (<i>Gadus macrocephalus</i>)..... | 105 |
| Walleye Pollock (<i>Gadus chalcogrammus</i>)..... | 114 |
| Sablefish (<i>Anoplopoma fimbria</i>) | 125 |
| Great Sculpin (<i>Myoxocephalus polyacanthocephalus</i>) | 132 |
| Yellow Irish Lord (<i>Hemilepidotus jordani</i>)..... | 139 |

| | |
|---|-----|
| Bigmouth Sculpin (<i>Hemitripterus bolini</i>)..... | 147 |
| Rockfishes | 154 |
| Pacific Ocean Perch (<i>Sebastes alutus</i>)..... | 154 |
| Northern Rockfish (<i>Sebastes polyspinis</i>)..... | 164 |
| Shortraker Rockfish (<i>Sebastes borealis</i>) | 172 |
| Rougheye Rockfish (<i>Sebastes aleutianus</i>) | 180 |
| Blackspotted Rockfish (<i>Sebastes melanostictus</i>) | 183 |
| Dusky Rockfish (<i>Sebastes variabilis</i>)..... | 188 |
| Harlequin Rockfish (<i>Sebastes variegatus</i>) | 195 |
| Shortspine Thornyhead (<i>Sebastolobus alascanus</i>) | 202 |
| Skates | 210 |
| Alaska Skate (<i>Bathyraja parmifera</i>) and Leopard Skate (<i>Bathyraja panthera</i>) | 210 |
| Aleutian Skate (<i>Bathyraja aleutica</i>) | 218 |
| Invertebrates | 226 |
| Golden King Crab (<i>Lithodes aequispinus</i>) | 226 |
| Pacific Giant Octopus (<i>Enteroctopus dofleini</i>)..... | 232 |
| ACKNOWLEDGMENTS | 235 |
| CITATIONS | 237 |

INTRODUCTION

The 1996 reauthorization of the Magnuson-Stevens Fishery Conservation and Management Act (MSFCMA) mandates NMFS to identify habitats essential for managed fish and invertebrate species and conserve habitats from adverse effects of fishing and other anthropogenic activities. Essential Fish Habitat (EFH) is defined under the act as ‘those waters and substrates necessary to fish for spawning, breeding, feeding or growth to maturity’. As part of this mandate, EFH descriptions for all species listed under a Fisheries Management Plan in Alaska waters are needed. In addition, these descriptions are routinely revisited under a 5-year cycle that reviews and updates EFH information (including species descriptions) with new data and research.

Essential fish habitat descriptions consist of maps of EFH and text descriptions. Although useful, they could be easily refined both in terms of spatial extent and life history stage using species distribution models and available data from a variety of sources. Distribution models have been widely used in conservation biology and terrestrial systems to define the potential habitat for organisms of interest (e.g., Delong and Collie 2004, Lozier et al. 2009, Elith et al. 2011, Sagarese et al. 2014). Recently species distribution models have been developed for coral and sponge species in the eastern Bering Sea, Gulf of Alaska, and Aleutian Islands (Rooper et al. 2014, Sigler et al. 2015, Rooper et al. 2016).

Species distribution models themselves can take a number of forms, from relatively simple frameworks such as generalized linear or additive models to more complex methods including computer learning methods (e.g., boosted regression trees, maximum entropy models, random forest models) or multi-stage models. The models can be used to predict potential

habitat, probability of presence or even abundance, but they all have some features in common: 1) the underlying data consists of some type of independent variables (predictors) and a dependent response variable (presence, presence/absence or abundance), 2) raster maps of independent variables are used to predict a response map, 3) confidence bounds on the predictions and partitioning of the data can produce test statistics useful for evaluating the model. The outputs of species distribution models are designed to be raster maps that can show the predicted abundance of a species at each of the raster cells. This type of product is useful for EFH descriptions, as it lends itself to producing maps of areas of high abundance or hotspots of distribution and the models themselves can be used to refine the required text descriptions.

The goal of this study was to produce species distribution models of EFH for all major species of groundfish and invertebrates in the Aleutian Islands. The species distribution models predicted either abundance (for bottom trawl survey data) or probability of suitable habitat based on presence observations (for early life history data, commercial catch data, and some bottom trawl survey data for rarer species). The species distribution models used were generalized additive models (GAM or hurdle-GAM) for abundance data and maximum entropy models (MaxEnt) for presence-only data. Accompanying Data Reports were generated for Gulf of Alaska (Rooney et al. in prep.) and eastern Bering Sea (Laman et al. 2017) fishes and invertebrates. We used several sources of both measured and model derived data to parameterize both the early life history and adult fish distribution models. After model parametrization, we extend our analysis to predict condition in those areas not sampled throughout the Aleutian Islands. We generated models of EFH for each species in the Aleutian Islands where data exists for egg, larval, juvenile, and adult life history stages in four seasons. In addition, we produced distribution maps that showed the location of EFH for all major groundfish species. It is

anticipated that this research establishes a foundation for future updates and integration of new data and studies.

METHODS

Study Area and Species

The Aleutian Islands is a chain of volcanic islands stretching from southwest Alaska across the North Pacific, separating the western Gulf of Alaska from the Bering Sea (Fig. 1). The continental shelf and upper continental slope represent a diverse mosaic of benthic habitats from Unimak Pass (165°W) in the eastern Aleutian Islands to Stalemate Bank in the western Aleutian Islands (170.5°E). The Alaska Coastal Stream flows westward on the Pacific side of the Aleutian Islands, while on the Bering Sea side, the Aleutian North Slope Current flows eastward (Stabeno et al. 1999, Stabeno et al. 2002, Ladd et al. 2005). There is extensive transport to the north through passes in the island chain from the Pacific side to the Bering Sea. In the Aleutian Islands, there is a very narrow and deep continental shelf. The continental shelf ranges in width from 20 km to greater than 200 km and the continental slope is steep and features periodic passes cutting through the continental shelf (Fig. 1). The seafloor of the Aleutian Islands is diverse, with extensive rocky substrate resulting from volcanic activity. Much of the continental shelf is dominated by rocky substrate.

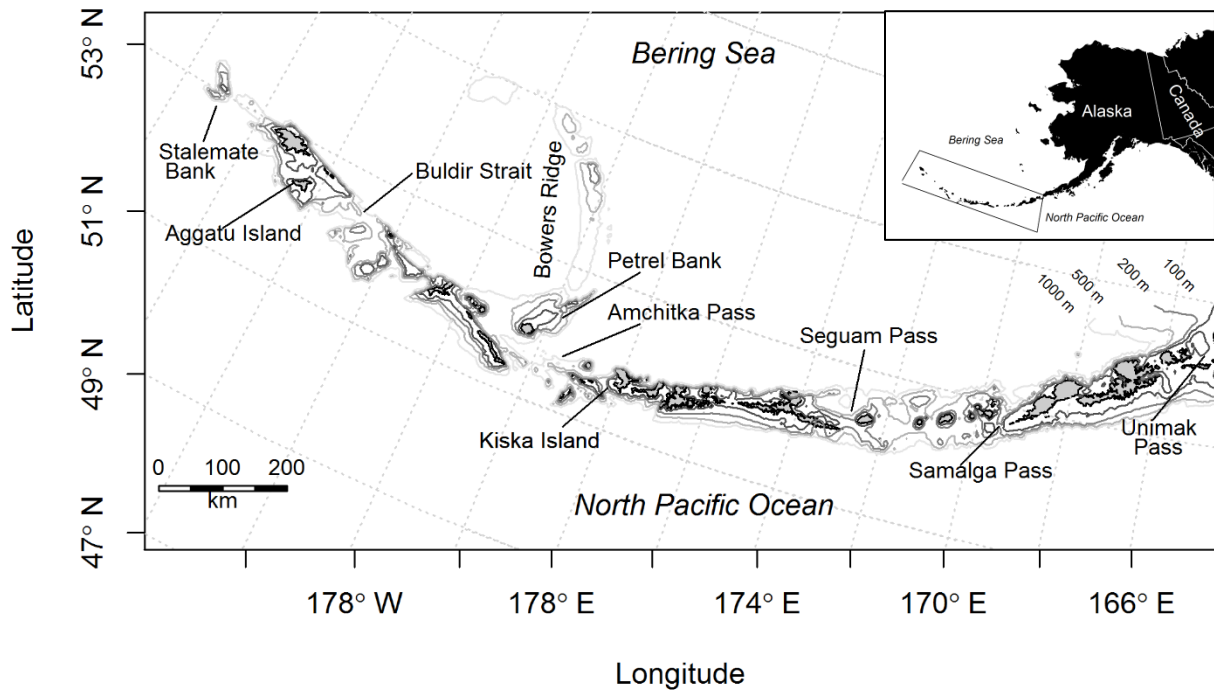


Figure 1. -- Aleutian Islands from Unimak Pass to Stalemate Bank where this modeling study was carried out.

The species and life stages of fishes and invertebrates examined for this study focused on managed species in the Aleutian Islands and where there was sufficient data for modeling (Table 1). Some species included in this study, such as the sculpins, are managed as a complex, but were considered here as individual species since adequate data were available for modeling. The data available for early life history stages (egg, larval, and early juvenile) was primarily from the Ecosystems & Fisheries-Oceanography Coordinated Investigations (EcoFOCI) ECODAAT database. The summer distributions of juvenile and adult life history stages were modeled using the Resource Assessment and Conservation Division (RACE) Aleutian Islands bottom trawl survey database (RACEBASE). The non-summer adult distributions were modeled using commercial catch data from the observer catch-in-areas database (CIA Database). All the

data were divided into four seasons for analyses: fall (October-November), winter (December-February), spring (March-May), and summer (June-September).

Table 1. -- Species of fishes and invertebrates that were modeled for essential fish habitat in the Aleutian Islands based on available distribution data from bottom trawl surveys, ichthyoplankton surveys, and/or commercial fisheries data.

| Species |
|--|
| Arrowtooth flounder (<i>Atheresthes stomias</i>) |
| Kamchatka flounder (<i>Atheresthes evermanni</i>) |
| Northern rock sole (<i>Lepidopsetta polyxystra</i>) |
| Southern rock sole (<i>Lepidopsetta bilineata</i>) |
| Rex sole (<i>Glyptocephalus zachirus</i>) |
| Dover sole (<i>Microstomus pacificus</i>) |
| Flathead sole (<i>Hippoglossoides elassodon</i>) |
| Greenland turbot (<i>Reinhardtius hippoglossoides</i>) |
| Walleye pollock (<i>Gadus chalcogrammus</i>) |
| Pacific cod (<i>Gadus macrocephalus</i>) |
| Sablefish (<i>Anoplopoma fimbria</i>) |
| Atka mackerel (<i>Pleurogrammus monopterygius</i>) |
| Great sculpin (<i>Myoxocephalus polyacanthocephalus</i>) |
| Yellow Irish lord (<i>Hemilepidotus jordani</i>) |
| Bigmouth sculpin (<i>Hemitripterus bolini</i>) |
| Pacific ocean perch (<i>Sebastes alutus</i>) |
| Northern rockfish (<i>Sebastes polyspinis</i>) |
| Shortraker rockfish (<i>Sebastes borealis</i>) |
| Rougheye rockfish (<i>Sebastes aleutianus</i>) |
| Blackspotted rockfish (<i>Sebastes melanostictus</i>) |
| Harlequin rockfish (<i>Sebastes variegatus</i>) |
| Dusky rockfish (<i>Sebastes variabilis</i>) |
| Shortspine thornyhead (<i>Sebastolobus alascanus</i>) |
| Alaska skate (<i>Bathyraja parmifera</i>) |
| Aleutian skate (<i>Bathyraja aleutica</i>) |
| Pacific giant octopus (<i>Enteroctopus dofleini</i>) |
| Golden king crab (<i>Lithodes aequispinus</i>) |

Species Distribution Data – Recruitment Processes Data

FOCI's ECODAAT database contains historical catches from limited geographical locations in the Aleutian Islands (Fig. 2). The data considered includes catches from 1991 to 2013 and was primarily from the eastern Aleutian Islands. These samples were collected during different types of surveys with different survey objectives and target species. Gear types varied in mesh size and included the bongo and Methot nets and samples were collected from varying depths in the water column. Samples collected varied across all months and years; not all month-year combinations occurred in the database. For this reason, the data were combined across years for analysis.

Each species in the ECODAAT database was classified as either egg, larval or pelagic juvenile (we considered all juveniles to be “pelagic” juveniles, as they were found in the water column rather than the benthos). We used these data for presence-only models where the number of presence observations in a species-life stage combination exceeded 50. The numbers of catches for each species, season and life stage are shown in Table 2.

An important caveat to the species distribution models developed using the ECODAAT database is that these data were not collected over the entire area of the Aleutian Islands, only from about 165°W longitude to 178°W longitude. **The distribution of sampling effort should be considered when drawing conclusions from maps produced from these data.**

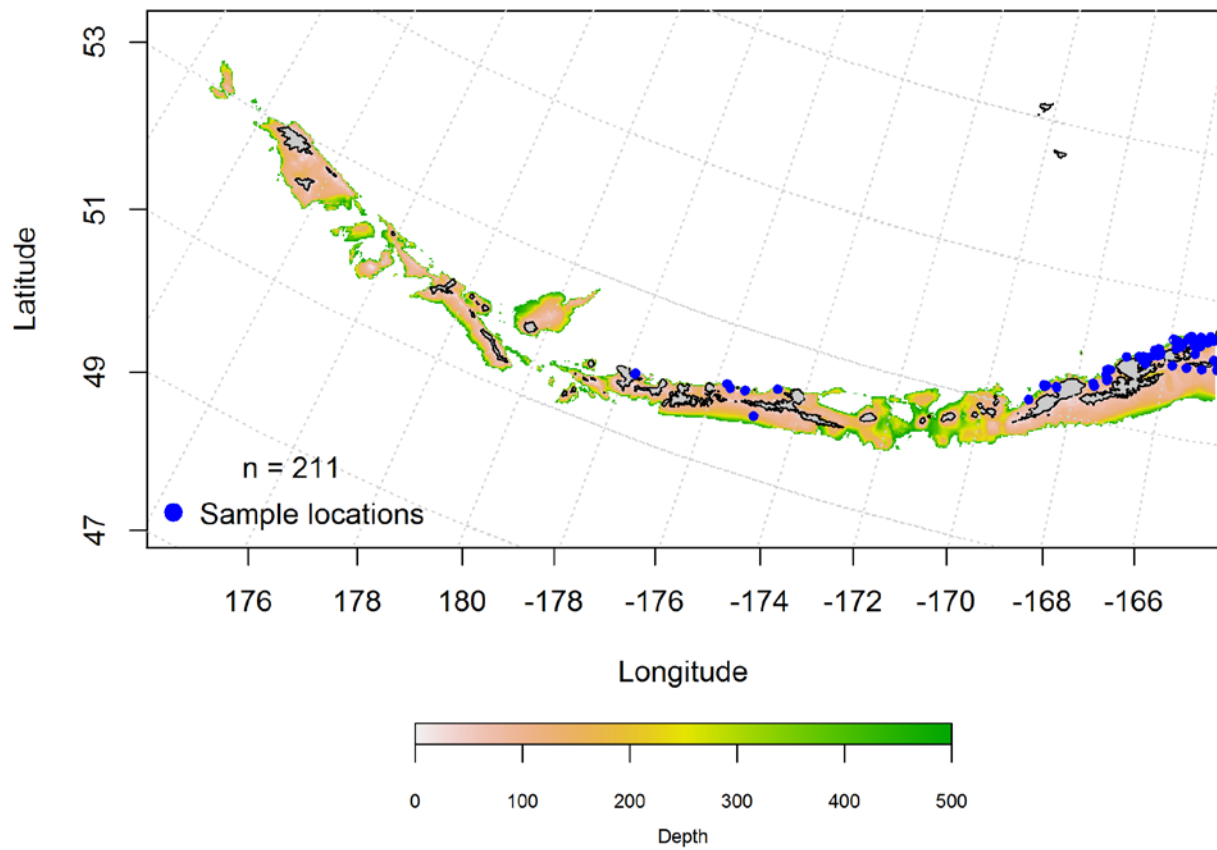


Figure 2. -- Locations of ichthyoplankton data collections in the Aleutian Islands from 1991 to 2013. These data were used in the modeling of early life history stages of fish and invertebrate essential fish habitat.

Table 2. -- Temporal periodicity (months) and prevalence (indicated in parentheses by the number of presence records from the ECODAAT database) of early life history stages of taxa collected during EcoFOCI ichthyoplankton surveys of the Aleutian Islands (1991 to 2013).

| Species | Eggs | Larvae | Pelagic juveniles |
|--|-----------------|-----------------|-------------------|
| <i>Atheresthes</i> spp. | Feb (5) | Feb - July (80) | -- |
| Atka mackerel (<i>Pleurogrammus monopterygius</i>) | * | May (11) | -- |
| Bigmouth sculpin (<i>Hemitripterus bolini</i>) | -- | May (1) | -- |
| Dover sole (<i>Microstomus pacificus</i>) | May - July (10) | July (1) | -- |
| Greenland turbot (<i>Reinhardtius hippoglossoides</i>) | Feb - Mar (4) | Apr - May (11) | -- |
| Flathead sole (<i>Hippoglossoides elassodon</i>) | Apr - Jun (118) | Apr - Sep (47) | -- |
| Northern rock sole (<i>Lepidopsetta polyxystra</i>) | -- | Apr - Jul (106) | -- |
| Pacific cod (<i>Gadus macrocephalus</i>) | Apr - May (3) | Apr - Jul (101) | Jul (3) |
| Rex sole (<i>Glyptocephalus zachirus</i>) | Apr - Jun (65) | Jun (2) | -- |
| Rockfish (<i>Sebastes</i> spp.) | -- | Apr - Sep (130) | -- |
| Sablefish (<i>Anoplopoma fimbria</i>) | -- | May - Jul (9) | -- |
| Southern rock sole (<i>Lepidopsetta bilineata</i>) | -- | May - Jul (21) | -- |
| Walleye pollock (<i>Gadus chalcogrammus</i>) | Feb - Sep (177) | Mar - Jul (143) | Jul - Aug (7) |
| Yellow Irish lord (<i>Hemilepidotus jordani</i>) | -- | May (6) | Apr - May (4) |

* locations for Atka mackerel eggs taken from Lauth et al. 2007 (n = 106)

Species Distribution Data – Groundfish Bottom Trawl Surveys

The species distribution data for groundfish and invertebrates were collected with during The National Marine Fisheries Service (NMFS), Alaska Fisheries Science Center (AFSC) bottom-trawl surveys of the Aleutian Islands ecosystem (Fig. 3). These data were the most comprehensive of the three types of data analyzed, as they are all from the summer season (May – August) and are conducted with a rigorous statistical design. A stratified-random sampling design was used for the survey of is primarily conducted in trawlable areas shallower than 500 m across the Aleutian archipelago (Fig. 1). The survey area extends on the north side of the Aleutian Islands from Unimak Pass in the east (165°W) to Stalemate Bank in the west (170°E); on the south side of the Aleutian archipelago, the survey extends from Samalga Pass (170°E) to Stalemate Bank in the west. The survey is divided into depth strata and are based on four intervals: 1–100 m, 101–200 m, 201– 300 m, and 301–500 m) and are also divided into relatively contiguous features based on bottom topography and separation by passes.

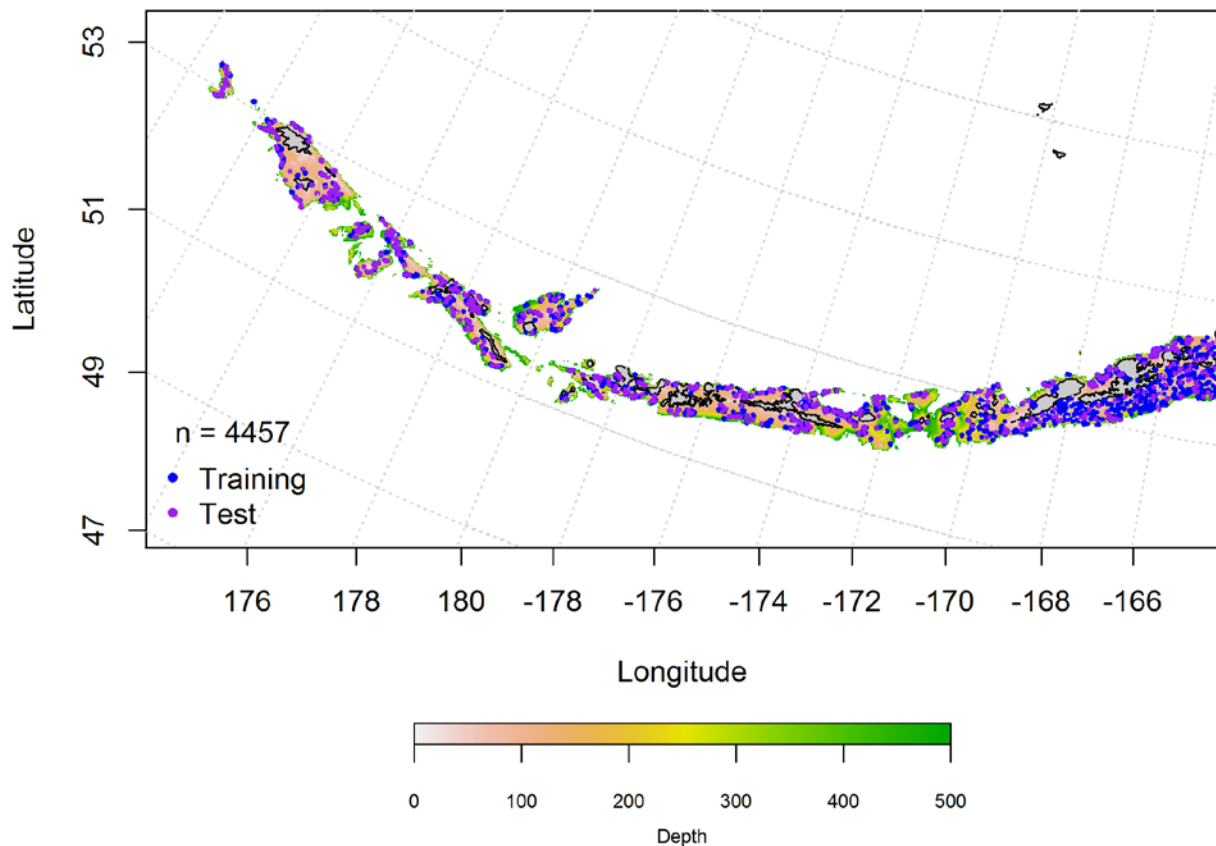


Figure 3. -- NMFS bottom trawl survey locations in the Aleutian Islands from 1991-2014 used in modeling essential fish habitat for fishes and invertebrates. Training data were used to parameterize the models, while testing data were used to test model performance (see Model Validation section for details).

A modified Neyman optimum allocation sampling strategy (Cochran 1977) was used to provide representative samples of fishes and invertebrates occurring at each sampling location within each stratum.

The gear used in the Aleutian Islands bottom trawl survey is a poly Nor'Eastern high-opening bottom trawl with 24.2 m roller gear constructed with 36 cm rubber bobbins separated by 10 cm rubber disks (Stauffer 2004). Trawl tows were conducted at a target speed of 5.6 km h^{-1} (3 knots) for 15 (since 1996) or 30 min (prior to 1996). Bottom contact and net dimensions were recorded throughout each trawl using net mensuration equipment. For these

analyses, records were only used if trawl performance was satisfactory and if the distance fished, geographic position, average depth, and water temperature were recorded. Tows were deemed satisfactory if the net opening was within a predetermined normal range, the roller gear maintained contact with the seafloor, and the net suffered little or no damage during the tow. Data from a total of 3,617 bottom-trawl tows were used for this analysis.

All fishes and invertebrates captured during a survey tow were sorted either by species or into higher level taxonomic groups and the total weight of each taxon in the catch was determined. Catch per unit effort (CPUE, no.*ha⁻¹) for each taxonomic group was calculated using the area swept which was computed from the net width for each tow multiplied by the distance towed recorded with the vessel's GPS. For some species both juvenile and adult sizes were captured during the bottom trawl survey. In these cases an approximate length at first maturity was used to partition the catches into juvenile and adult stages (Table 3). For some species only a subset of years was used in the modeling due to taxonomic changes that have occurred throughout the time series. For example, dusky and dark rockfishes were considered one species prior to the 1996 survey, so only data from surveys beginning in this year were used to model these two species.

Table 3. -- Species modeled using bottom trawl survey data. Years included in each of the modeling efforts, the percentage of positive catches (frequency of occurrence) in the bottom trawl hauls for juvenile and adult life history stages, and the maximum size considered to be the juvenile stage is shown.

| Species | Years modeled | Percent positive catches - Juveniles | Percent positive catches - adults | Maximum juvenile length (cm) |
|--|---------------|--------------------------------------|-----------------------------------|------------------------------|
| Alaska skate (<i>Bathyraja parmifera</i>) | Post 1990 | 5% | 9% | 92 |
| Aleutian skate (<i>Bathyraja aleutica</i>) | Post 1990 | 9% | 5% | 132 |
| Arrowtooth flounder (<i>Atheresthes stomias</i>) | Post 1993 | 55% | 70% | 35 |
| Atka mackerel (<i>Pleurogrammus monopterygius</i>) | All | 14% | 39% | 27 |
| Bigmouth sculpin (<i>Hemitripterus bolini</i>) | All | | 2% | 51 |
| Blackspotted rockfish (<i>Sebastes melanostictus</i>) | Post 2007 | 18% | 13% | 43 |
| Dover sole (<i>Microstomus pacificus</i>) | All | 6% | 6% | 38 |
| Dusky rockfish (<i>Sebastes variabilis</i>) | Post 1996 | | 8% | 29 |
| Flathead sole (<i>Hippoglossoides elassodon</i>) | All | 16% | 28% | 29 |
| Golden king crab (<i>Lithodes aequispinus</i>) | All | | 21% | |
| Great sculpin (<i>Myoxocephalus polyacanthocephalus</i>) | All | 4% | 4% | 51 |
| Greenland turbot (<i>Reinhardtius hippoglossoides</i>) | All | 3% | 8% | 65 |
| Harlequin rockfish (<i>Sebastes variegatus</i>) | All | | 2% | 23 |
| Kamchatka flounder (<i>Atheresthes evermanni</i>) | Post 1993 | 40% | 20% | 52 |
| Northern rock sole (<i>Lepidopsetta polyxystra</i>) | Post 2001 | 41% | 64% | 30 |
| Northern rockfish (<i>Sebastes polyspinis</i>) | All | 9% | 36% | 25 |
| Pacific giant octopus sp. (<i>Enteroctopus dofleini</i>) | All | | 12% | |
| Pacific cod (<i>Gadus macrocephalus</i>) | All | 30% | 63% | 46 |
| Pacific ocean perch (<i>Sebastes alutus</i>) | All | 23% | 52% | 25 |
| Walleye pollock (<i>Gadus chalcogrammus</i>) | All | 6% | 36% | 29 |
| Rex sole (<i>Glyptocephalus zachirus</i>) | All | 2% | 3% | 24 |
| Rougeye rockfish (<i>Sebastes aleutianus</i>) | Post 2007 | | 10% | 43 |
| Sablefish (<i>Anoplopoma fimbria</i>) | All | 7% | 11% | 40 |
| Shortraker rockfish (<i>Sebastes borealis</i>) | All | 7% | 18% | 44 |
| Shortspine thornyhead (<i>Sebastolobus alascanus</i>) | All | 11% | 18% | 21 |
| Southern rock sole (<i>Lepidopsetta bilineata</i>) | Post 2001 | 19% | 53% | 30 |
| Yellow Irish lord (<i>Hemilepidotus jordani</i>) | All | 4% | 22% | 22 |

| |
|-----------------------|
| Standard GAM model |
| Hurdle GAM model |
| Maximum entropy model |

Species Distribution Data – Commercial Catch (observer) Data

Data from the catch-in-areas (CIA) observer database was used to model adult life history stages of fishes caught in commercial catches during the non-summer seasons (Table 4). The CIA data was provided by Steve Lewis and John V. Olson and of the NMFS Alaska Regional Office (AKRO). The data from observed hauls and all gear types were combined across years for analysis. We used the observations of catch by species in the data for presence-only models where the number of presence observations for a given species exceeded 50. The numbers of catches for each species and season are shown in Table 4. None of these fish and invertebrates could be split by life history stages. Only the fall, winter and spring seasons were considered, as the summer distributions were modeled using bottom trawl survey data.

Commercial fishing activity occurred throughout the Aleutians, however, an important caveat to the species distribution models developed using the CIA database is that for most species, the **distribution of catches represent the distribution of fishing activity**. So, instead of being a standardized survey conducted over a defined grid, these observations were typically clustered in areas of high densities for a target species. As such, they should be viewed with some caution compared to the bottom trawl survey distribution maps.

Table 4. -- Numbers of presence records by species available from the CIA database in the Aleutian Islands. Maximum entropy modeling was conducted for species and season where the number of presence observations exceeded 50.

| Species | Fall | Winter | Spring |
|--|-------|--------|--------|
| Alaska skate (<i>Bathyraja parmifera</i>) | 517 | 756 | 1,037 |
| Aleutian skate (<i>Bathyraja aleutica</i>) | 264 | 249 | 467 |
| Arrowtooth flounder (<i>Atheresthes stomias</i>) | 891 | 1,394 | 2,637 |
| Atka mackerel (<i>Pleurogrammus monopterygius</i>) | 1,699 | 1,767 | 1,304 |
| Bigmouth sculpin (<i>Hemitripterus bolini</i>) | 129 | 231 | 268 |
| Dusky rockfish (<i>Sebastes variabilis</i>) | 605 | 611 | 707 |
| Flathead sole (<i>Hippoglossoides elassodon</i>) | 263 | 952 | 1,335 |
| Golden king crab (<i>Lithodes aequispinus</i>) | 57 | | 156 |
| Great sculpin (<i>Myoxocephalus polyacanthocephalus</i>) | | 69 | 160 |
| Greenland turbot (<i>Reinhardtius hippoglossoides</i>) | 174 | 111 | 614 |
| Harlequin rockfish (<i>Sebastes variegatus</i>) | 183 | 158 | 72 |
| Kamchatka flounder (<i>Atheresthes evermanni</i>) | 282 | 417 | 852 |
| Rock sole (<i>Lepidopsetta</i> spp.) | 814 | 1,947 | 3,466 |
| Northern rockfish (<i>Sebastes polyspinis</i>) | 1,470 | 1,877 | 1,817 |
| Pacific cod (<i>Gadus macrocephalus</i>) | 1,410 | 2,750 | 4,432 |
| Pacific ocean perch (<i>Sebastes alutus</i>) | 1,252 | 1,372 | 1,077 |
| Rex sole (<i>Glyptocephalus zachirus</i>) | 244 | 443 | 805 |
| Sablefish (<i>Anoplopoma fimbria</i>) | 262 | 110 | 894 |
| Shortraker rockfish (<i>Sebastes borealis</i>) | 130 | 89 | 580 |
| Shortspine thornyhead (<i>Sebastolobus alascanus</i>) | 131 | 55 | 738 |
| Walleye pollock (<i>Gadus chalcogrammus</i>) | 1,300 | 1,442 | 1,518 |
| Yellow Irish lord (<i>Hemilepidotus jordani</i>) | 206 | 231 | 548 |

Habitat Variables

Independent variables for modeling included the standard suite of habitat variables typically collected on the bottom trawl survey as well as a few derived and modeled variables (Table 5, Fig. 4). These variables were chosen for their availability and for their potential influence on the distribution of fishes based on previous studies. Separate sets of habitat variables were used to model early life history stages (EcoFOCI data), adult and juvenile stages (trawl data) and seasonal data (CIA data). The variables used to model each data set are highlighted in Table 5.

The early life history stages of each taxon were generally sampled in pelagic waters. Therefore, surface water temperature, surface current speed and surface current direction were chosen as potential variables to explain early life history distributions. Surface current direction variability was used as an indication of potential eddy vorticity or other current variability processes that might be present. These variables were derived from a regional ocean modeling system (ROMS) model runs from 1969 to 2005 provided by A. Hermann (Danielson et al. 2011). The data used to parameterize the model were average monthly values for oceanographic variables on a 10 km × 10 km grid. The model derived variables used in this study were interpolated via inverse distance weighting to a 1 km² grid and summarized by season. The ROMS derived variables were only used to model early life history stages and not adult fish distributions from the bottom trawl survey.

Additional variables used for modeling the early life history stages of fish species included the depth, slope, ocean color (as a proxy for chlorophyll a/primary production estimates), and tidal current. To model depth and slope, we used a 100 m × 100 m gridded bathymetry raster for the Aleutian Islands region that was derived from bathymetric point data (n > 2.1 million soundings) on National Ocean Service (NOS) smooth sheets (Zimmermann and Benson 2013, Zimmermann et al. 2013). Slope for each 100 m × 100 m raster grid cell was computed as the maximum difference between the depth at a cell and its surrounding cells using the raster package in R software (R Core Development Team 2013). For the analysis of early life history data, these two layers were averaged to a 1 km × 1 km grid.

To estimate average ocean productivity (g C m⁻² day⁻¹) at each of the bottom trawl survey sites, we used moderate resolution imaging spectroradiometer (MODIS) ocean color data for five spring-summer months (May-September over 8 years (2003 to 2011) for the Aleutian Islands

region (Behrenfeld and Falkowski 2007). These ocean color data are available on a spatial grid. These values were averaged by spatial location by month (for May-September) and then averaged by year (to account for differences in the number of samples at each spatial location). These grid averages were then interpolated to a 1 km² raster grid using inverse distance weighting.

Tidal speeds were estimated for 369 consecutive days (1 January 2009 to 3 January 2010) using a tidal inversion program parameterized for the Aleutian Islands on a 1 km² grid (Egbert and Erofeeva 2002). This tidal speed prediction model was used to produce a series of one lunar year of tidal currents for spring and neap cycles at each bottom trawl survey location. The maximum tidal speed value from the series of predicted tidal current was then extracted for the position of each bottom trawl survey haul. This maximum value was used as a habitat variable in the modeling. Maximum tidal current speed at each bottom trawl survey site were also interpolated to the entire Aleutian Islands using ordinary kriging and an exponential semi-variogram using R software. When evaluated using leave-one-out cross-validation, the kriging model fit the observations very well ($n = 3,051$, mean squared error = 407, $R^2 = 0.93$). The kriging model was then used to interpolate a raster of maximum current speed values on a 1 km² grid that was used for modeling early life history stages.

For bottom trawl survey data a different suite of habitat variables was used for modeling (Table 5). Haul position and depth were collected during each NMFS bottom trawl haul. A start and end position for the vessel during the on-bottom portion of each haul were collected using the vessel-mounted GPS receiver. Vessel position was corrected for the position of the bottom trawl itself by triangulating how far the net was behind the vessel (based on the seafloor depth and the wire out) and subtracting this distance from the vessel position in the direction of the

bottom trawl haul. We assumed that the bottom trawl was directly behind the vessel during the haul and that all bottom trawl hauls were conducted in a straight line from the beginning point to the end point. The mid-point of the start and end positions of the net was used as the location variable in the modeling. The longitude and latitude data for each haul (and all other geographical data including the raster layers described below) were projected into Alaska Albers Equal Area Conic projection (center latitude = 50° N and center longitude = -154° W) and degrees of latitude and longitude were transformed into $100\text{ m} \times 100\text{ m}$ square grids of eastings and northings for modeling. The location variable was used to capture any significant spatial trends across the Aleutian Islands region in bottom trawl survey catches.

The depth for each haul was estimated from a SeaBird SBE-39 microbathymograph attached to the headrope of the net and the measured net height. Mean depth during the haul was calculated for inclusion as an explanatory variable in the modeling. Mean slope for each bottom trawl haul was estimated from the $100\text{ m} \times 100\text{ m}$ bathymetry raster described above. The bathymetry raster of the entire Aleutian Islands region (Zimmermann et al. 2013) was used for prediction, but not for parameterizing the models.

The average summer temperature was estimated from data collected during Aleutian Islands bottom trawl surveys from 1993 to 2014. Bottom temperatures were collected during each bottom trawl haul using the SBE-39 attached to the headrope of the net. Mean bottom temperatures for each haul were interpolated to the $100\text{ m} \times 100\text{ m}$ grid for the entire Aleutian Islands region. These data were interpolated using ordinary kriging (Venables and Ripley 2002) with an exponential semi-variogram model using R software. This resulted in a single temperature raster layer that reflects the mean temperature conditions in surveys from 1993 to 2014. When evaluated using leave-one-out cross-validation, the kriging model was a statistically

significant fit to the observations ($n = 2,814$, mean squared error = 0.19, $R^2 = 0.38$), capturing the spatial trend in the temperature data. The temperature data used in our models were primarily designed to reflect long-term averages that could be compared spatially to the distribution of fishes and invertebrates. Bottom temperature averaged over the length of each bottom trawl haul was used as a habitat variable in the modeling. The $100 \text{ m} \times 100 \text{ m}$ raster layers of mean temperature were used for prediction.

Two measures of water movement and its potential interaction with the seafloor were used as habitat variables in modeling and prediction. The first variable for model parameterization was the maximum tidal speed at the site of each bottom trawl haul as described above for the analyses of EcoFOCI data. The second water movement variable was the bottom water layer current speed estimated from ROM's model runs for 1969-2005 (Danielson et al. 2011). These long-term current speed and direction estimates were available as points on a $10 \text{ km} \times 10 \text{ km}$ grid. The ROM's model was based on a three-dimensional grid with 60 depth tiers for each grid cell. For example, a point at 60 m water depth would have 60 depth bins at 1 m intervals, while a point at 120 m depth would have 60 depth bins at 2 m depth intervals. The model estimates of current speed and direction for the deepest depth bin at each point (closest to the seafloor) was used in this analysis. To obtain estimated current speed and direction for each bottom trawl survey haul, the values from this raster at each of the haul location were extracted and the mean value computed for the path of each bottom trawl survey haul; this raster was also used for prediction. To reflect average ocean productivity ($\text{g C m}^{-2} \text{ day}^{-1}$) at each of the bottom trawl survey sites, we used the MODIS ocean color data described above interpolated to a $100 \text{ m} \times 100 \text{ m}$ raster.

The final variables included in the modeling of bottom trawl survey data were the catches of structure forming invertebrates (corals, sponges and pennatulaceans). The presence of each of these categories of invertebrates was a binomial (presence or absence) term in the model. Distribution models for each of these species were used for prediction on a 100 m ×100 m raster (Rooper et al. 2014, Rooper et al. unpublished model).

The same process and variables used to model and predict fish and invertebrate distributions with the NMFS bottom trawl survey data were used for the commercial catch data (CIA data), with the exception of the structure forming invertebrate layers; Table 5).

There was some collinearity in the habitat variables included in the models of bottom trawl survey data (Table 6). The largest correlations were between latitude and longitude ($r = 0.60$) and slope and depth ($r = 0.53$). The remaining pairwise correlations among variables were < 0.5 . Variance inflation factors (VIF) were calculated using the method of Zuur et al. (2009) for each of the variables to be included in the modeling, resulting in values ranging from 1.2 to 1.6. These values were all acceptable (below 5.0) allowing inclusion of all variables in the models. For the models of CIA data, the VIFs were also less than 5.0. However, tidal current, surface current speed and surface current variability (variables used in EcoFOCI models were highly correlated ($r \sim 0.8$) resulting in a VIF of > 7.0 for current variability. Since these were used in presence-only models, which have less stringent collinearity assumptions, all variables were included in the EcoFOCI modeling.

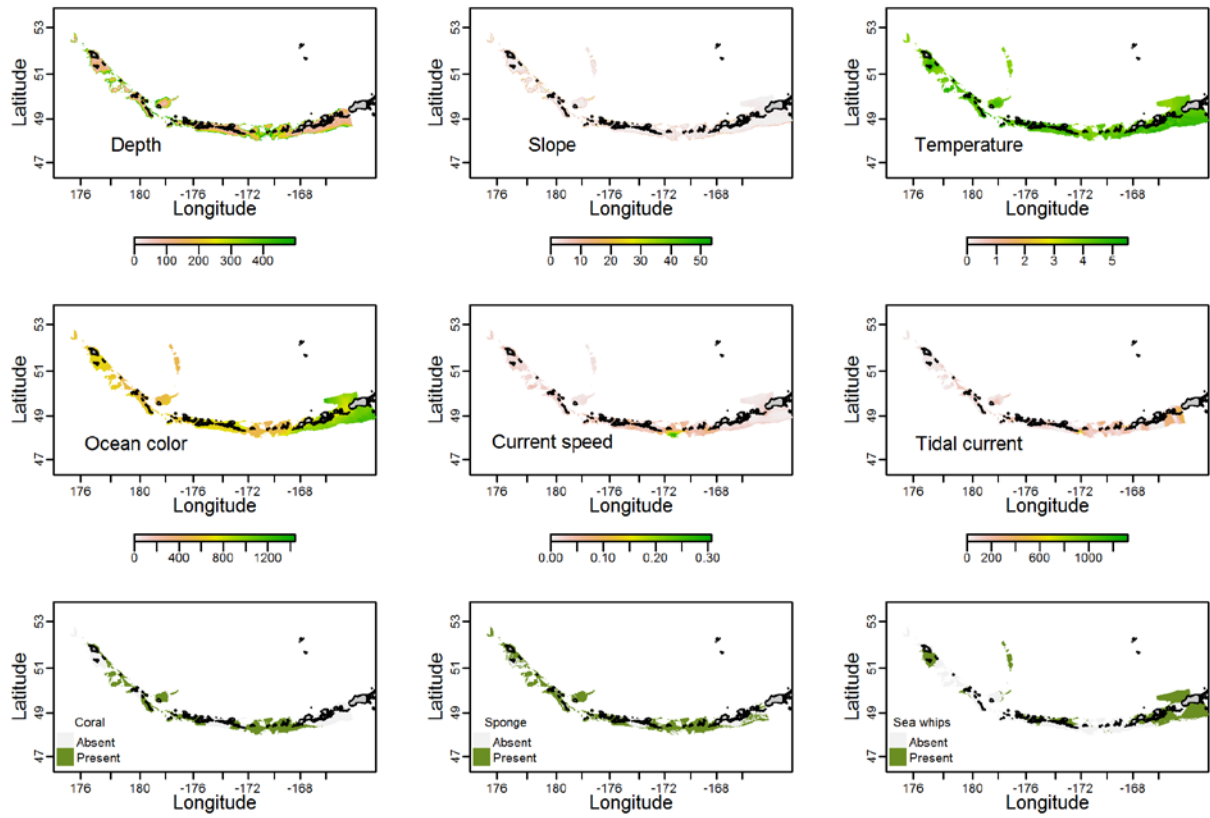


Figure 4. -- Environmental variables used to model the distribution of life history stages of fishes and invertebrates.

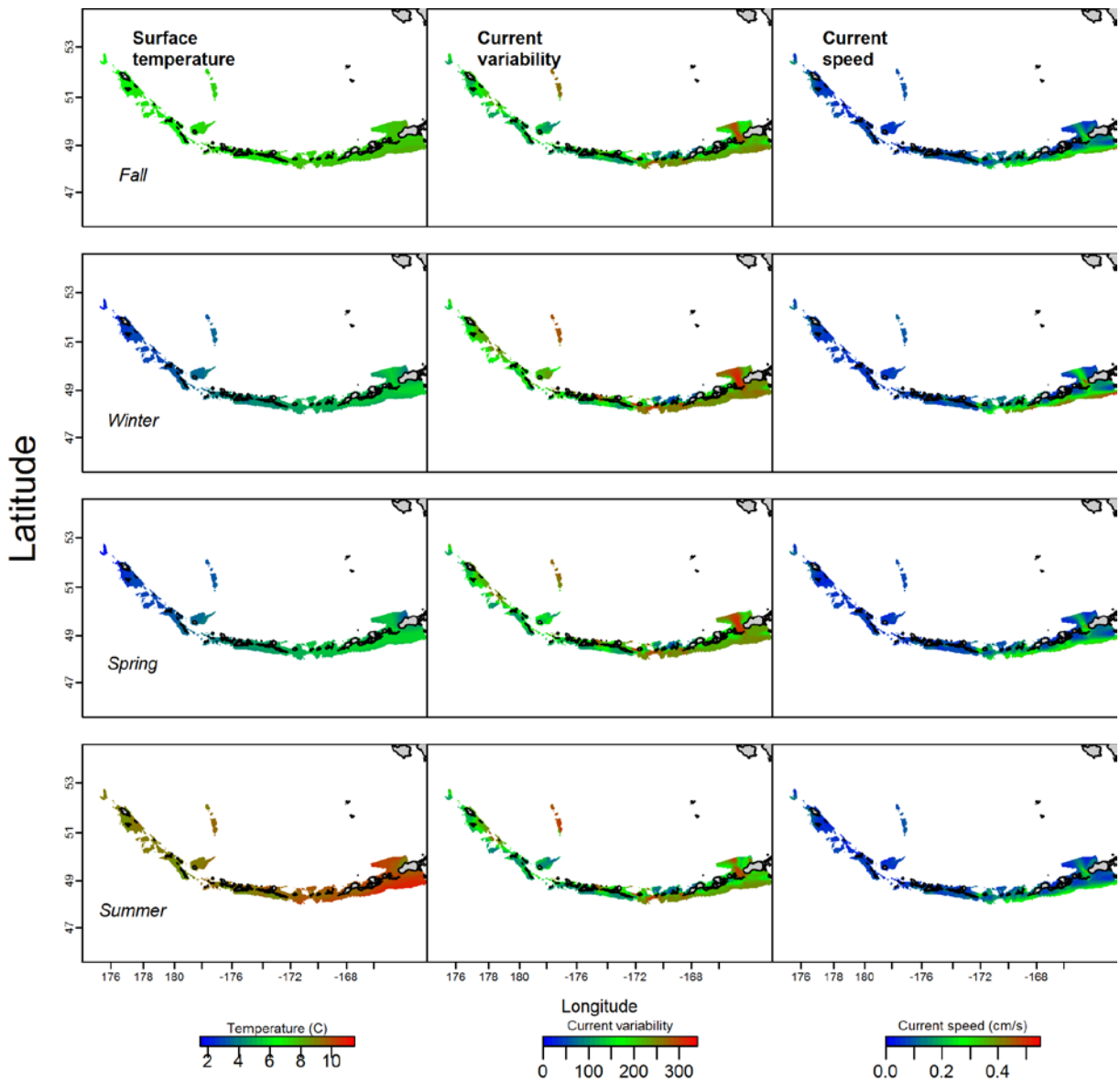


Figure 5. -- Oceanographic variables used for modeling early life history stages of fishes and invertebrates. Averages for each variable is shown for summer (June-September), fall (October-November), winter (December-February) and spring (March-May).

Table 5. -- Variables used in modeling the distributions of fishes and invertebrates in the Aleutian Islands.

| Variable | Unit | Used to model | Definition | Interpolation method | Source |
|---|---|--|---|----------------------------|---|
| Position | eastings, northings | Trawl data | Latitude and longitude of bottom trawl hauls in Alaska Albers projection corrected for the position of the trawl net relative to the vessel | -- | DGPS collected at bottom trawl hauls |
| Depth | m | EcoFOCI data, Trawl data, CIA data | Bathymetry of the seafloor based on digitized and position corrected NOS charts | Linear interpolation | Mean depth of bottom trawl hauls (modeling), Zimmermann et al. 2013 |
| Slope | percent | EcoFOCI data, Trawl data, CIA data | Maximum difference between a depth measurement and its adjoining cells | -- | Zimmermann et al. 2013 |
| Bottom temperature | °C | Trawl data, CIA data | Mean summer bottom temperature for the region measured during bottom trawl surveys from 1996-2010 | Ordinary kriging | Temperature data collected at bottom trawl hauls |
| Surface temperature | °C | EcoFOCI data | Ocean current speed predicted from the ROMS model during the years 1970-2004 and averaged on a 10 km by 10 km grid | Inverse distance weighting | Danielson et al. 2011 |
| Ocean color | Carbon*m ⁻² *day ⁻¹ | EcoFOCI data, Trawl data, CIA data | Net primary production in surface waters in May to September averaged by 1080 by 2160 grid cells then averaged across years (2002-2011) | Inverse distance weighting | Behrenfeld and Falkowski 1997 |
| Mean bottom ocean current | m*sec ⁻¹ | Trawl data, CIA data | Seafloor ocean current speed predicted from the ROMS model during the years 1970-2004 and averaged on a 10 km by 10 km grid | Inverse distance weighting | Danielson et al. 2011 |
| Maximum tidal current | cm*sec ⁻¹ | EcoFOCI data, Trawl data, CIA data | Maximum of the predicted tidal current at each bottom trawl location over a 1-year cycle | Ordinary kriging | Egbert and Erofeeva 2000 |
| Mean surface ocean current speed | m*sec ⁻¹ | EcoFOCI data | Surface ocean current speed predicted from the ROMS model during the years 1970-2004 and averaged on a 10 km by 10 km grid | Inverse distance weighting | Danielson et al. 2011 |
| Mean surface ocean current direction | angle | EcoFOCI data | Surface ocean current direction predicted from the ROMS model during the years 1970-2004 and averaged on a 10 km by 10 km grid | Inverse distance weighting | Danielson et al. 2011 |
| Surface ocean current direction variability | -- | EcoFOCI data | Variability in surface ocean current direction predicted from the ROMS model during the | Inverse distance weighting | Danielson et al. 2011 |

years 1970-2004 and averaged on a 10 km by 10 km grid

| | | | | | |
|-----------------------------------|----|------------|--|----|--|
| Coral presence or absence | -- | Trawl data | Coral presence or absence in bottom trawl catch and raster of predicted presence or absence of coral | -- | Catch data from bottom trawl hauls (modeling), Rooper et al. (2014) (prediction) |
| Sponge presence or absence | -- | Trawl data | Sponge presence or absence in bottom trawl catch and raster of predicted presence or absence of Sponge | -- | Catch data from bottom trawl hauls (modeling), Rooper et al. (2014) (prediction) |
| Pennatulacean presence or absence | -- | Trawl data | Pennatulacean presence or absence in bottom trawl catch and raster of predicted presence or absence of Pennatulacean | -- | Catch data from bottom trawl hauls (modeling), Rooper et al. (unpublished data) (prediction) |

Table 6. -- Variance inflation factors for Aleutian Islands data used in the modeling.

| Variable | Variance inflation factor (Trawl survey data) | Variance inflation factor (CIA data) | Variance inflation factor (FOCI data) |
|-----------------------------|---|--------------------------------------|---------------------------------------|
| Depth | 1.60 | 1.51 | 1.87 |
| Slope | 1.31 | 1.40 | 2.36 |
| Temperature | 1.30 | 1.16 | |
| Ocean color | 1.54 | 1.17 | 1.22 |
| Current speed | 1.23 | 1.20 | |
| Tidal current | 1.16 | 1.06 | 4.40 |
| Coral | 1.17 | | |
| Sponge | 1.41 | | |
| Sea whips | 1.33 | | |
| Surface temperature | | | 1.70 |
| Surface current speed | | | 7.85 |
| Surface current variability | | | 4.85 |

Modeling Methods – Recruitment Processes Data

The maximum entropy (MaxEnt) modeling method was used for estimating species distribution for early life history stages in the EcoFOCI ECODAAT database (Phillips et al. 2006, Elith et al. 2011). It was implemented in R software using the *dismo* package. MaxEnt models use only presence observations and are based on raster grids of explanatory variables (habitat variables) and point observations of presence. The model predicts the probability of suitable habitat based on habitat related variables (i.e., given the depth, temperature, slope and current speed at each grid cell – what is the probability that this is suitable for a canary rockfish?), not probability of presence. For all species, separate training (80%) and testing (20%) data were randomly selected from the total available observations of presence for assessing the model performance.

Modeling Methods – Bottom Trawl Survey Data

Three types of distribution modeling were used for the bottom trawl survey data based on the frequency of occurrence for each species in the catch. For species that occurred in > 30% of bottom trawl hauls, such as arrowtooth flounder (Table 3), a standard Generalized Additive Modeling (GAM) method was used to produce maps of predicted density. Generalized additive models (Hastie and Tibshirini 1990) using the *mgcv* package in R (Wood 2006) were used to predict the dependent variables using the suite of untransformed habitat variables. In each case, the basis degrees of freedom used in the smoothing function was limited to ≤ 4 for univariate variables and ≤ 30 for the bivariate term (location). Insignificant terms were sequentially

removed. In this case model terms were removed until there was no reduction in the Akaike Information Criterion (AIC) values (Wood 2006). For each species, the model with the lowest AIC score was deemed the best fitting model and used for further prediction and model validation. For the standard GAMs, the CPUE was fourth-root transformed prior to analyses and the number of inflection points were limited and insignificant terms were sequentially removed to determine the best-fitting model.

For species where frequency of occurrence was between 10% and 30% a hurdle model (Cragg 1971, Potts and Elith 2006; hurdle-GAM) predicting spatial distribution of fishes was used (Table 3). Hurdle models predict the spatial distribution of abundance in three stages: 1) probability of presence is predicted from presence-absence data using a GAM model and binomial distribution for each species; 2) a threshold presence probability is determined that defines presence or absence of the species; 3) a separate GAM model is constructed that predicts abundance by modeling the forth-root transformed CPUE data from the bottom trawl survey where the species was present in the catch.

For species with $< 10\%$ frequency of occurrence, but > 50 presence observations, the MaxEnt methodology was used to develop suitable habitat models (Phillips et al. 2006, Elith et al. 2011). MaxEnt models use only presence observations and are based on raster grids of explanatory variables (habitat variables) and point observations of presence.

For all models, separate training (80%) and testing (20%) data were randomly selected from the total available bottom trawl hauls for assessing the performance of each type of modeling. The training and testing data sets were the same across all species for the analysis of bottom trawl survey data.

Modeling Methods – Commercial Catch (observer) Data

The MaxEnt modeling method was used for estimating species distribution for commercial catch data in the CIA database (Phillips et al. 2006, Elith et al. 2011). It was implemented in R software using the dismo package. MaxEnt models use only presence observations and are based on raster grids of explanatory variables (habitat variables) and point observations of presence. As with the other models, separate training (80%) and testing (20%) data were randomly selected for MaxEnt model developed in order to assess model performance.

Model Validation

To test the performance of the best-fitting models, the predictions were compared to the observations. For presence and presence-absence models the area under the curve (AUC) was computed to judge model performance. The AUC calculates the probability that a randomly chosen presence observation would have a higher probability of presence than a randomly chosen absence observation using rank data. We used the scale of Hosmer and Lemeshow (2005), where AUC value > 0.5 is estimated to be better than chance, a value > 0.7 is estimated to be acceptable, and values > 0.8 and 0.9 are excellent and outstanding, respectively.

Confidence intervals for the AUC (95%) were calculated according to the methodology of DeLong et al (1988). For abundance models the performance was directly tested by correlating the predictions with the observations. Model testing was also performed on the 20% of the data withheld at random, using the same metrics. Because of space limitations, figures showing the model validation results are not shown, except where deviations from model assumptions or

models with very poor predictive ability relative to the testing data are highlighted. Where these occur, the results of the modeling may not be robust.

Essential Fish Habitat Maps

Maps of essential habitat based on model predictions were developed for each life history stage and season modeled. These maps were produced as population quantiles from predictions of the distribution of suitable habitat (in cases where MaxEnt was used) or predictions of the distribution of abundance (for species where CPUE was modeled using either a GAM or hurdle-GAM). For each map of model predictions, 300,000 points were randomly sampled from the raster surface. These values were then ordered by cumulative distribution; zero abundance values and probabilities of suitable habitat < 0.05 were removed. Four population quantiles were selected from these cumulative distributions (5%, 25%, 50% and 75%). These quantiles were then used as break points to translate the model predictions (maps of suitable habitat or abundance) into maps of the distribution quantiles. For example, if the 5% quantile of species A was $0.024 \text{ individuals}\cdot\text{ha}^{-1}$, then this meant that 95% of the population occurred at values higher than 0.024. Similarly, a 75% quantile of species A at $2.1 \text{ individuals}\cdot\text{ha}^{-1}$ meant that values above 2.1 represented the top 25% of the population of predictions, or the predicted highest abundance areas. The four population quantiles for each species, life history stage, and season were mapped to show the distribution of the areas containing 95%, 75%, 50% and 25% of the population. It is important to note that these values were chosen somewhat arbitrarily, with the exception of the 95% level which is the current definition of EFH in Alaska, and other values could be equally appropriate.

RESULTS

Flatfishes

Arrowtooth Flounder (*Atheresthes stomais*)

Early life history stages of *Atheresthes* -- Arrowtooth flounder eggs and larvae cannot be distinguished from the other species in the genus, Kamchatka flounder (*Atheresthes evermanni*), so results from the genus *Atheresthes* are combined and presented here. There were only five instances of *Atheresthes* eggs observed in the EcoFOCI database, not enough to run the model. There were 80 catches of *Atheresthes* larvae in winter, spring and summer months (Fig. 6), with most instances occurring in the eastern Aleutian Islands (AI). The most important variables in the spring MaxEnt model of *Atheresthes* larvae were sea surface temperature, surface current speed, ocean color, current direction, and current variability (relative importance: 30.3%, 19.6%, 15.1%, 14.1, and 10.8%, respectively). The model resulted in an AUC of 0.97 for the training data and 0.91 for the testing data, indicating a good model fit. Predicted probability of suitable habitat for *Atheresthes* larvae was limited to the eastern Aleutian Islands, primarily in the north (Fig. 6).

Juvenile and adult arrowtooth flounder distribution in the bottom trawl survey -- A GAM predicting the abundance of juvenile arrowtooth flounder explained 40% of the variability in bottom trawl survey CPUE. Depth, geographic location and tidal current were the most important variables in the distribution model of juvenile arrowtooth flounder. The model fit the test data set well, explaining 37% of the variability. Highest abundance was predicted in the eastern and western Aleutian Islands at depths around 200 m and at low tidal currents (Fig. 7).

As with the juveniles, the best-fitting GAM model for adult arrowtooth flounder indicated that bottom depth and geographic location were the most important factors correlated to adult arrowtooth flounder distribution with peak biomass around 220 m in the eastern Aleutian Islands and near Attu Island in the west (Fig. 8). Interestingly, arrowtooth flounder decreased with the presence of deep-sea coral and sponge (Fig. 8). The model explained 32% of the training data variability in bottom trawl CPUE, and 34% of the variability in the test data set.

Arrowtooth flounder distribution in commercial fisheries -- Observed instances of adult arrowtooth flounder in the Aleutian Islands in commercial fisheries catches were generally consistent throughout all seasons. In the fall, bottom depth and ocean color were the most important variables determining suitable habitat of adult arrowtooth flounder (relative importance: 36.4% and 33.7%). The AUC of the fall MaxEnt model was 0.90 for the training data and 0.79 for the test data. The model predicted probable suitable habitat of arrowtooth flounder throughout the Aleutian Islands, though slightly more probable in the east near Unalaska Island and Seguam Pass (Fig. 9).

In the winter, the pattern was generally consistent with fall observations. Ocean color and bottom depth were the most important variables determining the probability of suitable habitat of arrowtooth flounder (relative importance: 46% and 32.1%). The AUC of the winter MaxEnt model was 0.94 for the training data and 0.80 for the test data. The model predicted probable suitable habitat of arrowtooth flounder throughout the Aleutian Islands, though slightly more probable in the east and near Atka and Agattu Islands (Fig. 10).

In the spring, there were more observed instances of adult arrowtooth flounder in the Aleutian Islands from commercial fisheries catches, than in the fall and winter. Again bottom depth and ocean color were the most important variables determining the probability of suitable

habitat of spring arrowtooth flounder (relative importance: 49% and 35.4%, respectively). The AUC of the spring MaxEnt model was 0.89 for the training data and 0.74 for the test data. As with the fall and winter, the model predicted probable suitable habitat of arrowtooth flounder throughout the Aleutian Islands and slightly higher at Agattu, Atka, and Unalaska islands (Fig. 11).

Arrowtooth flounder essential fish habitat maps and conclusions -- Essential fish habitat (EFH) of larval *Atheresthes* as predicted by the modeling is largely concentrated in the eastern Aleutian Islands on the northern side of the chain (Fig. 12). It should be noted that EcoFOCI sampling did not occur in the western Aleutians and was limited in the central AI.

In general, juvenile and adult arrowtooth flounder EFH is widely distributed through the Aleutian Islands chain and overlaps in most areas. Essential fish habitat predicted from fisheries catch data generally agrees with the bottom trawl survey data in all seasons (Fig. 12). These similarities can be observed in both areas of high) and low abundance (e.g., large passes). There does not appear to be much seasonal variability to the EFH distribution, although the fishery model in winter predicts a lower probability of EFH for arrowtooth flounder in the area around Unalaska Island. This may in part be due to lower fishing effort in the area during that season.

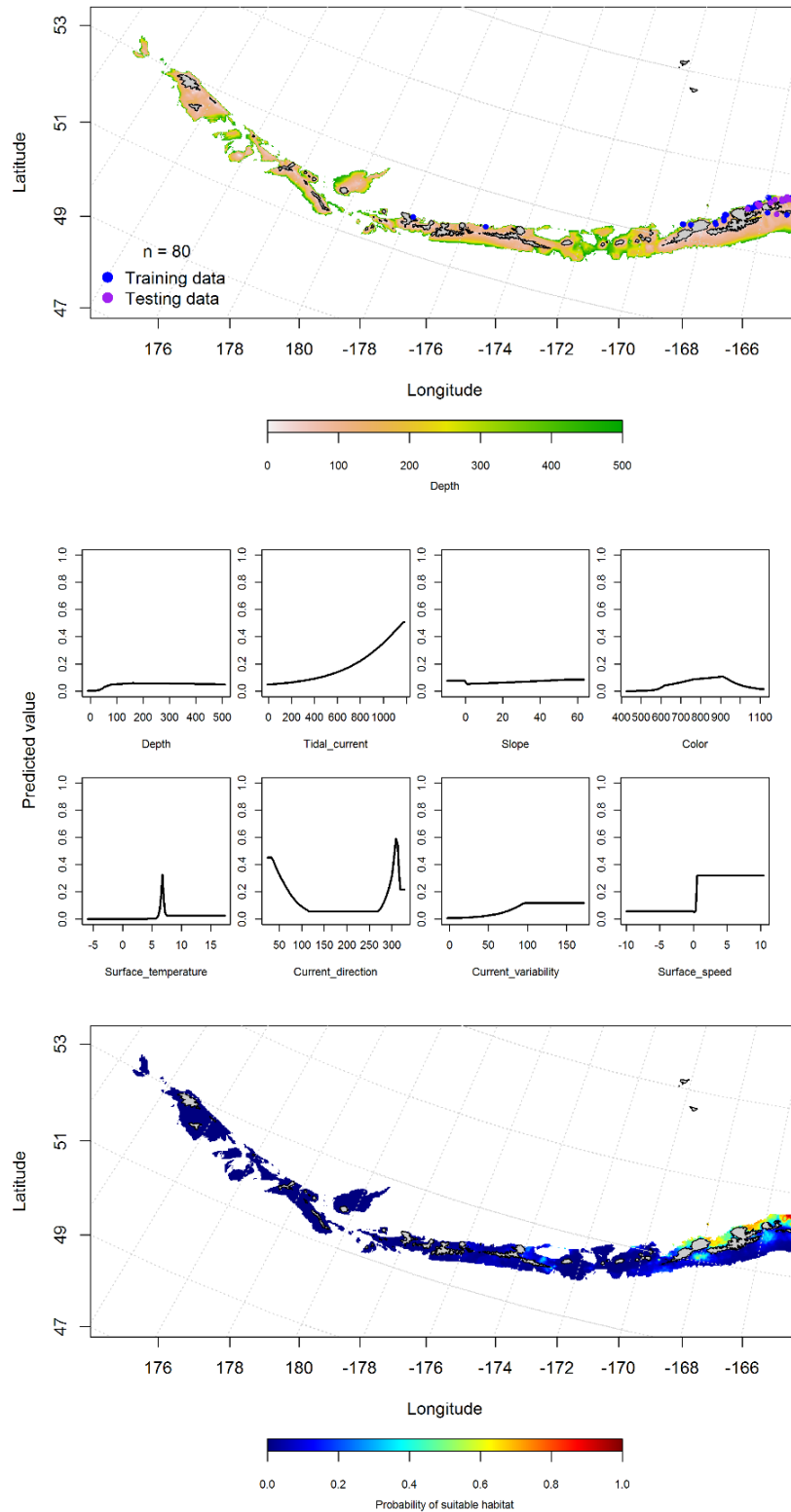


Figure 6. -- Observations of larval *Atheresthes* from the Aleutian Islands (top panel), relationships with environmental variables (middle panel) and predicted probability of suitable habitat based on EcoFOCI data and maximum entropy modeling.

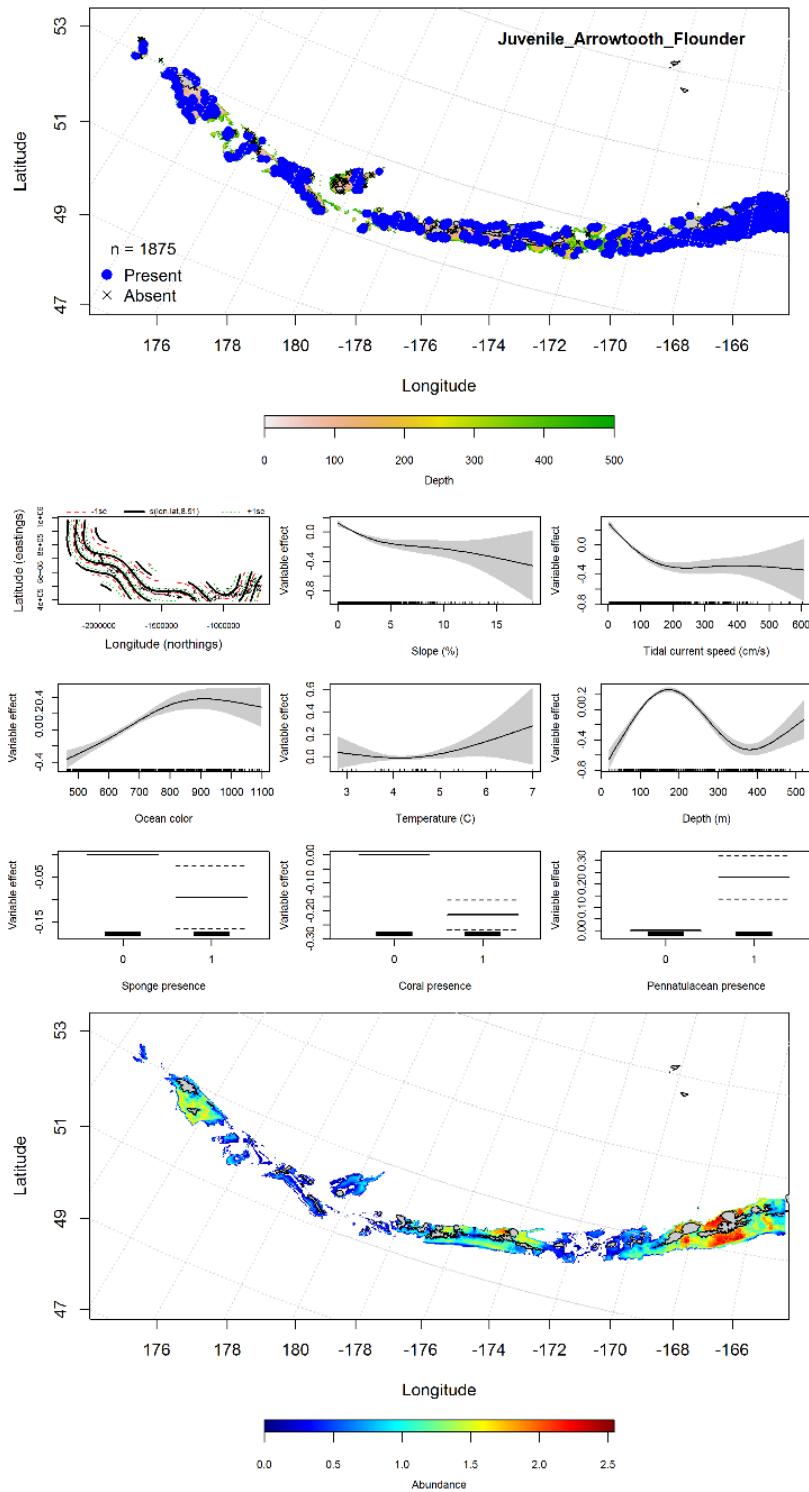


Figure 7. -- Distribution of catches of juvenile arrowtooth flounder in bottom trawl surveys (top panel), significant relationships between CPUE and environmental variables for the best-fitting generalized additive model of juvenile arrowtooth flounder (middle panels), and predicted abundance of juvenile arrowtooth flounder based on the model (bottom panel).

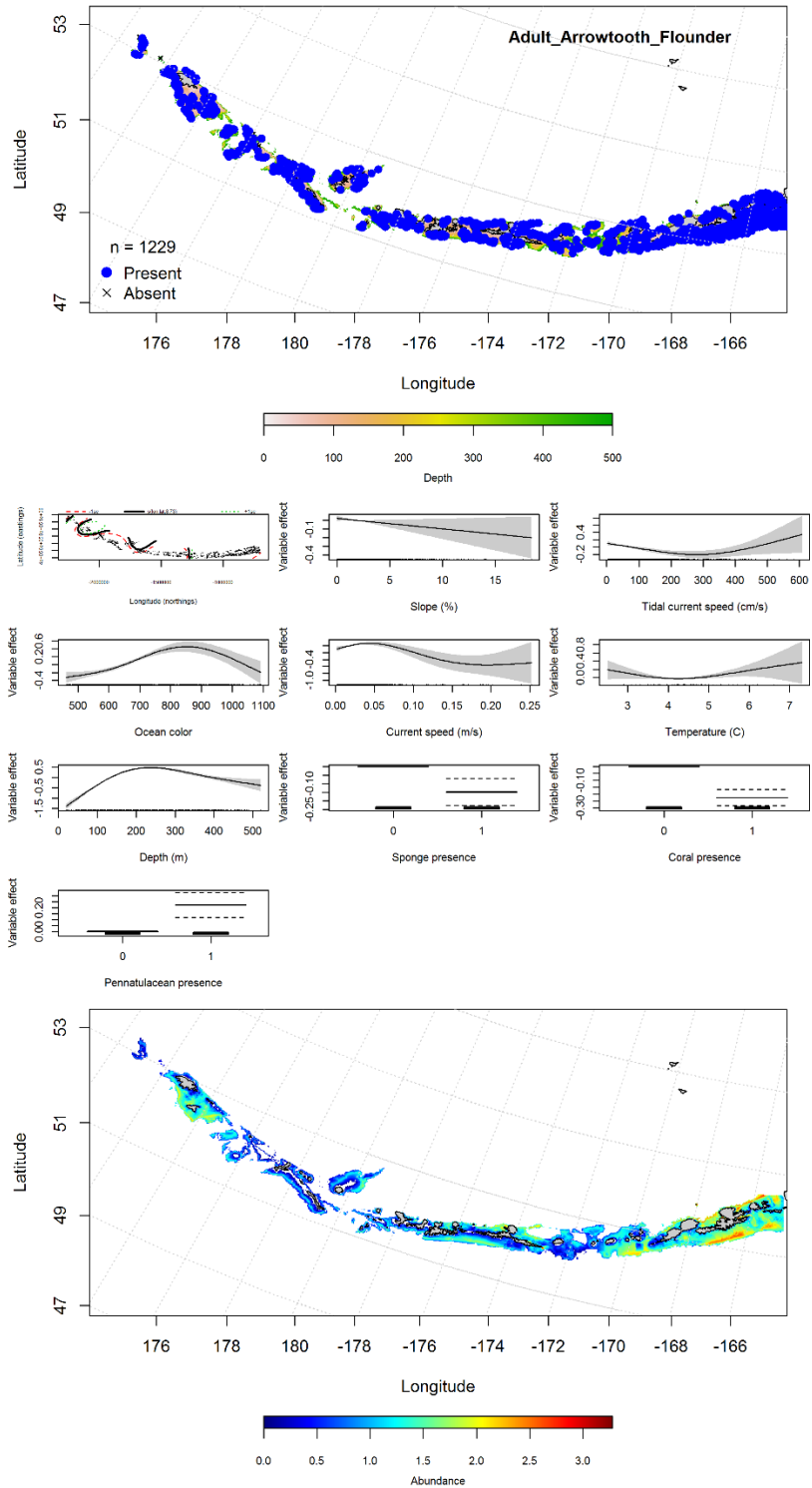


Figure 8. -- Distribution of catches of adult arrowtooth flounder in bottom trawl surveys (top panel), significant relationships between CPUE and environmental variables for the best-fitting generalized additive model of adult arrowtooth flounder (middle panels), and predicted abundance of adult arrowtooth flounder based on the model (bottom panel).

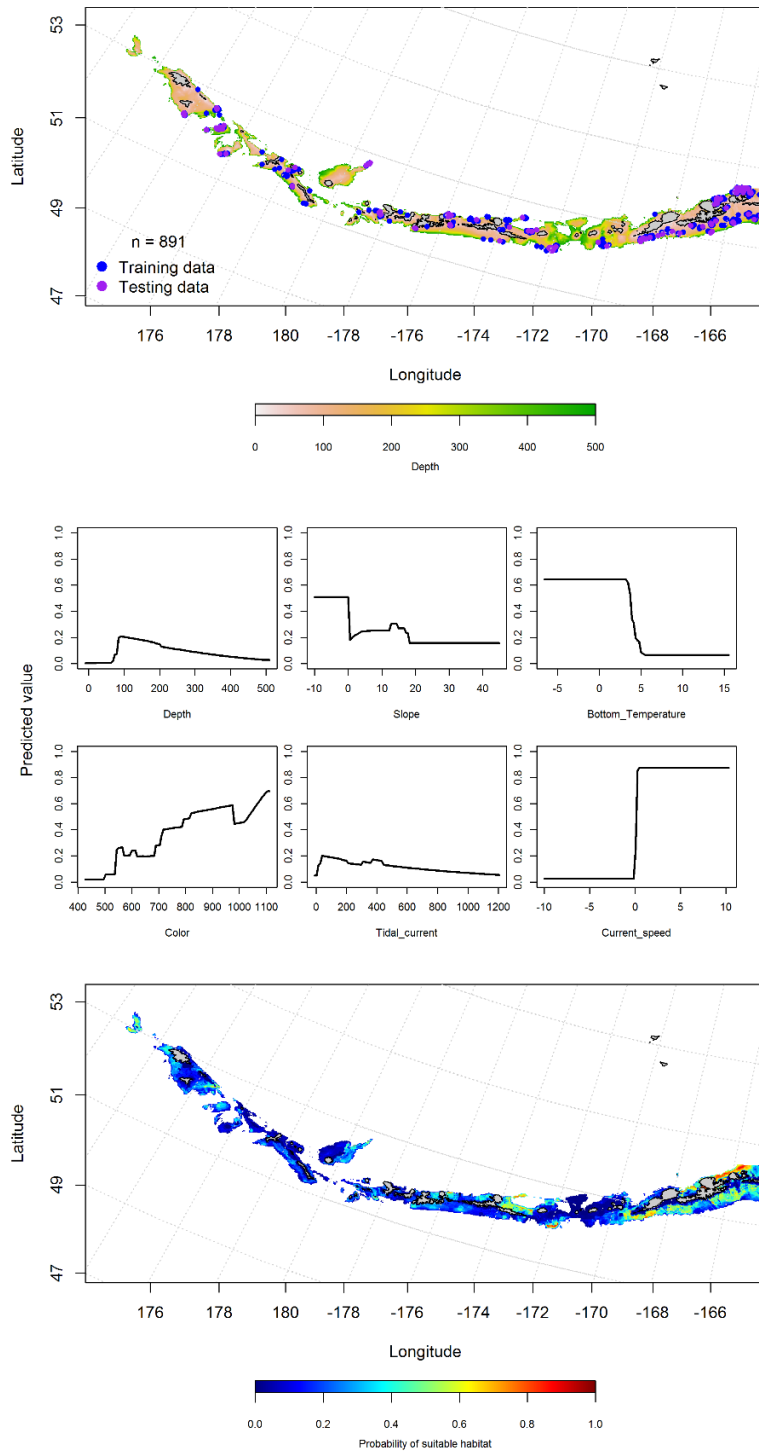


Figure 9. -- Locations of fall (September-November) commercial fisheries catches of arrowtooth flounder (top panel), relationships between probability of presence and environmental variables for the maximum entropy model (middle panels), and predicted probability of suitable habitat for arrowtooth flounder based on the model (bottom panel).

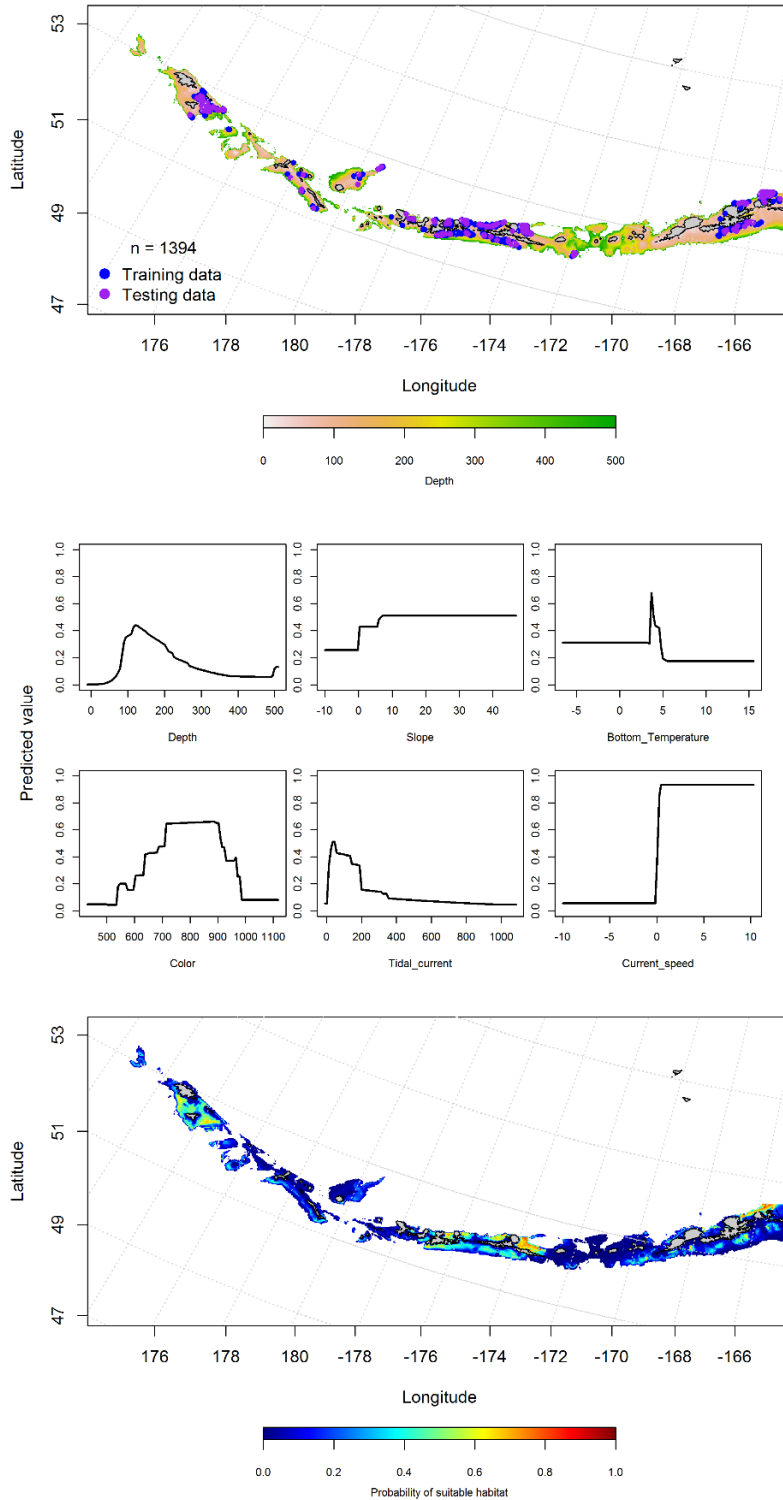


Figure 10. -- Locations of winter (December-February) commercial fisheries catches of arrowtooth flounder (top panel), relationships between probability of presence and environmental variables for the maximum entropy model (middle panels), and predicted probability of suitable habitat for arrowtooth flounder based on the model (bottom panel).

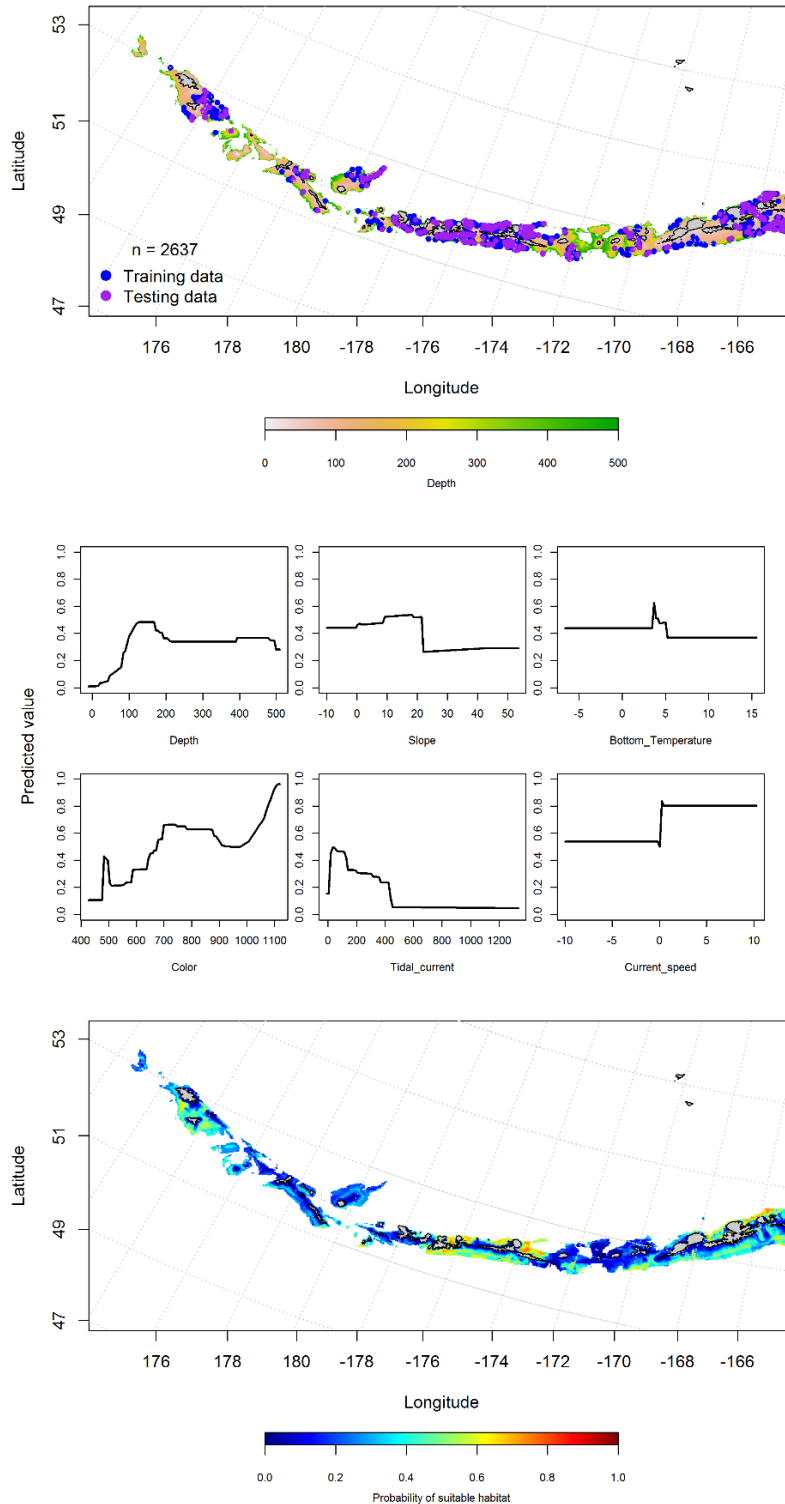


Figure 11. -- Locations of spring (March-May) commercial fisheries catches of arrowtooth flounder (top panel), relationships between probability of presence and environmental variables for the maximum entropy model (middle panels), and predicted probability of suitable habitat for arrowtooth flounder based on the model (bottom panel).

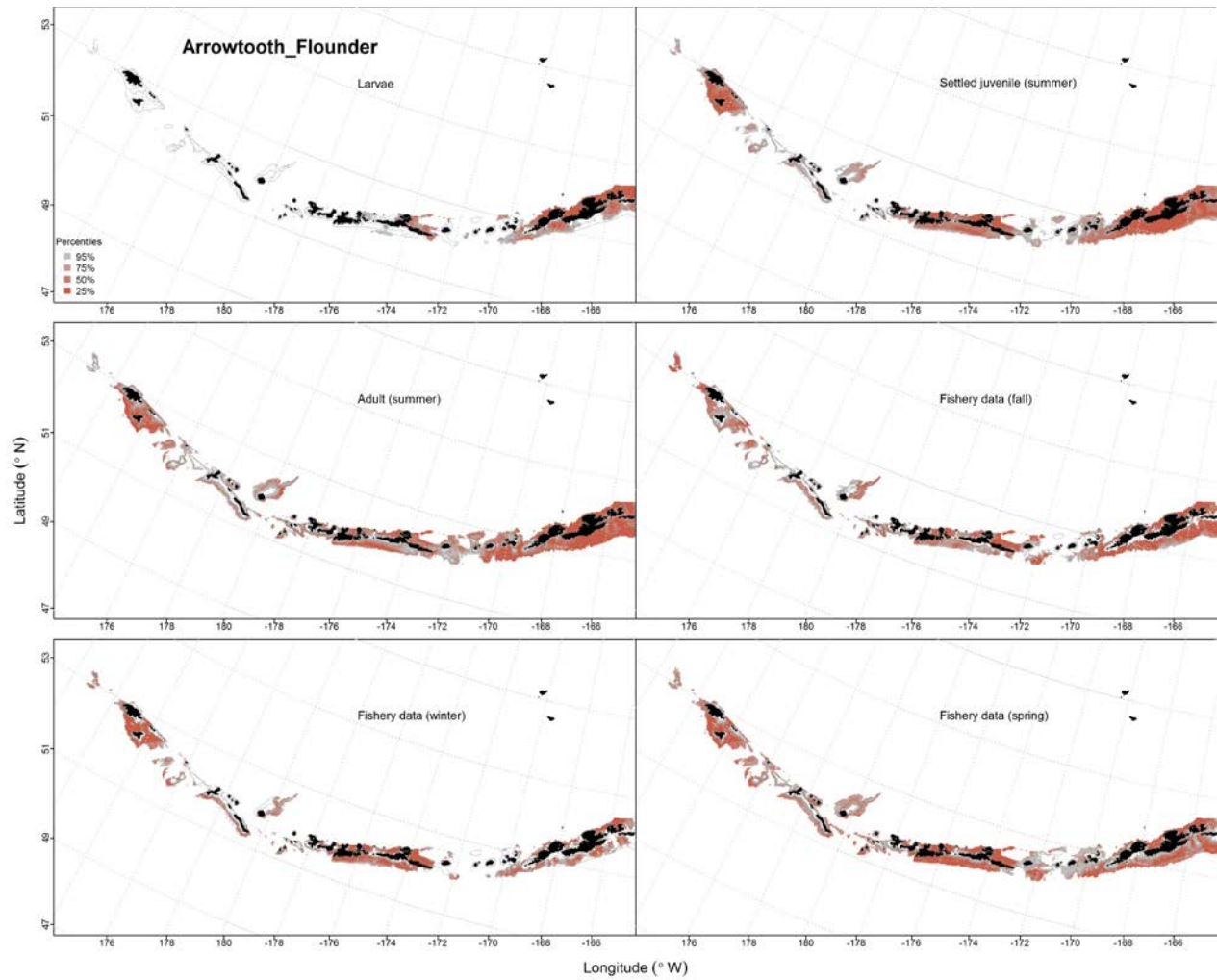


Figure 12. -- Predicted EFH quantiles for arrowtooth flounder life history stages based on species distribution modeling. Larval maps include both species of *Atheresthes* (*A. stomais* and *A. evermanni*). Settled juvenile and summer adult stages are based on bottom trawl survey data, while seasonal stages (winter, spring, fall) are from commercial fishery data.

Kamchatka Flounder (*Atheresthes evermanni*)

Early life history stages of Kamchatka flounder -- See section above (arrowtooth flounder) for the combined *Atheresthes* early life history stages.

Juvenile and adult Kamchatka flounder distribution in the bottom trawl survey -- The catch of Kamchatka flounder in summer bottom trawl surveys of the Aleutian Islands indicates this species is broadly distributed. Generalized additive models predicting the abundance of juvenile Kamchatka flounder explained 30% of the training data set variability in CPUE in the bottom trawl survey and 26% of the variability in the test data set. Geographic location and bottom depth were the most important variables explaining the distribution of juvenile Kamchatka flounder. The areas of predicted highest abundance were in the western Aleutian Islands and Atka Island (Fig. 13).

Adult Kamchatka flounder were modeled using a hurdle-GAM. The presence absence (PA) GAM predicted a higher probability of presence in the western Aleutian Islands, though was fairly similar across the islands. The best-fitting PA GAM indicated that bottom depth and geographic location were the most important factors controlling adult Kamchatka flounder distribution and the model explained 39% of the training data set variability. The AUC of the model was 0.90 for the training data and 0.89 for the test data set. The probability of suitable habitat for adult Kamchatka flounder was distributed across the AI, and was higher in areas with large passes (Fig. 14). The CPUE GAM model found that bottom depth and tidal current were the most important variables that explained the distribution of adult Kamchatka flounder. The model explained 31% of the training set variability in CPUE in the bottom trawl survey, 21% of the variability in the test data set. Adult Kamchatka flounder abundance was higher in deeper waters and near Seguam Pass (Fig. 14).

Kamchatka flounder distribution in commercial fisheries -- Observed instances of Kamchatka flounder in the Aleutian Islands in commercial fisheries catches was generally consistent throughout all seasons. In the fall, bottom depth and temperature were the most important variables determining suitable habitat of Kamchatka flounder (relative importance: 31.9% and 27.1%). The AUC of the fall MaxEnt model was 0.92 for the training data and 0.81 for the test data. The model predicted probable suitable habitat of Kamchatka flounder throughout the Aleutian Islands, though slightly more probable in the east near Unalaska Island and near Atka Island (Fig. 15).

In the winter the pattern was generally consistent with fall observations. Ocean color and bottom depth were the most important variables determining the probability of suitable habitat of Kamchatka flounder (relative importance: 32.5% and 32.3%, respectively). The AUC of the winter MaxEnt model was 0.97 for the training data and 0.89 for the test data. The model predicted probable suitable habitat of Kamchatka flounder throughout the Aleutian Islands, though slightly more probable in the east near Atka and Unalaska islands (Fig. 16).

In the spring, there were more observed instances of adult Kamchatka flounder in the Aleutian Islands from commercial fisheries catches, than in the fall and winter. Again bottom depth and ocean color were the most important variables determining the probability of suitable habitat of spring Kamchatka flounder (relative importance: 41.9% and 33.0%). The AUC of the spring MaxEnt model was 0.90 for the training data and 0.77 for the test data. As with the fall and winter, the model predicted probable suitable habitat of Kamchatka near Atka and Unalaska islands (Fig. 17).

Kamchatka flounder essential fish habitat maps and conclusions -- In general, juvenile Kamchatka flounder EFH was found to be widely distributed in the Aleutian Islands, with higher probability in the west near Agattu and Attu islands, in the central Aleutians and on Petrel Bank (Fig. 18). Adult EFH predicted from the bottom trawl survey tended to be deeper than the juvenile distribution and concentrated around Segoum Pass. Essential fish habitat predicted from fisheries catch data was more similar to the juvenile EFH from the bottom trawl survey (Fig. 18). These similarities may indicate that Kamchatka flounder, a non-target species, taken in the fisheries may be more likely to be juvenile stages.

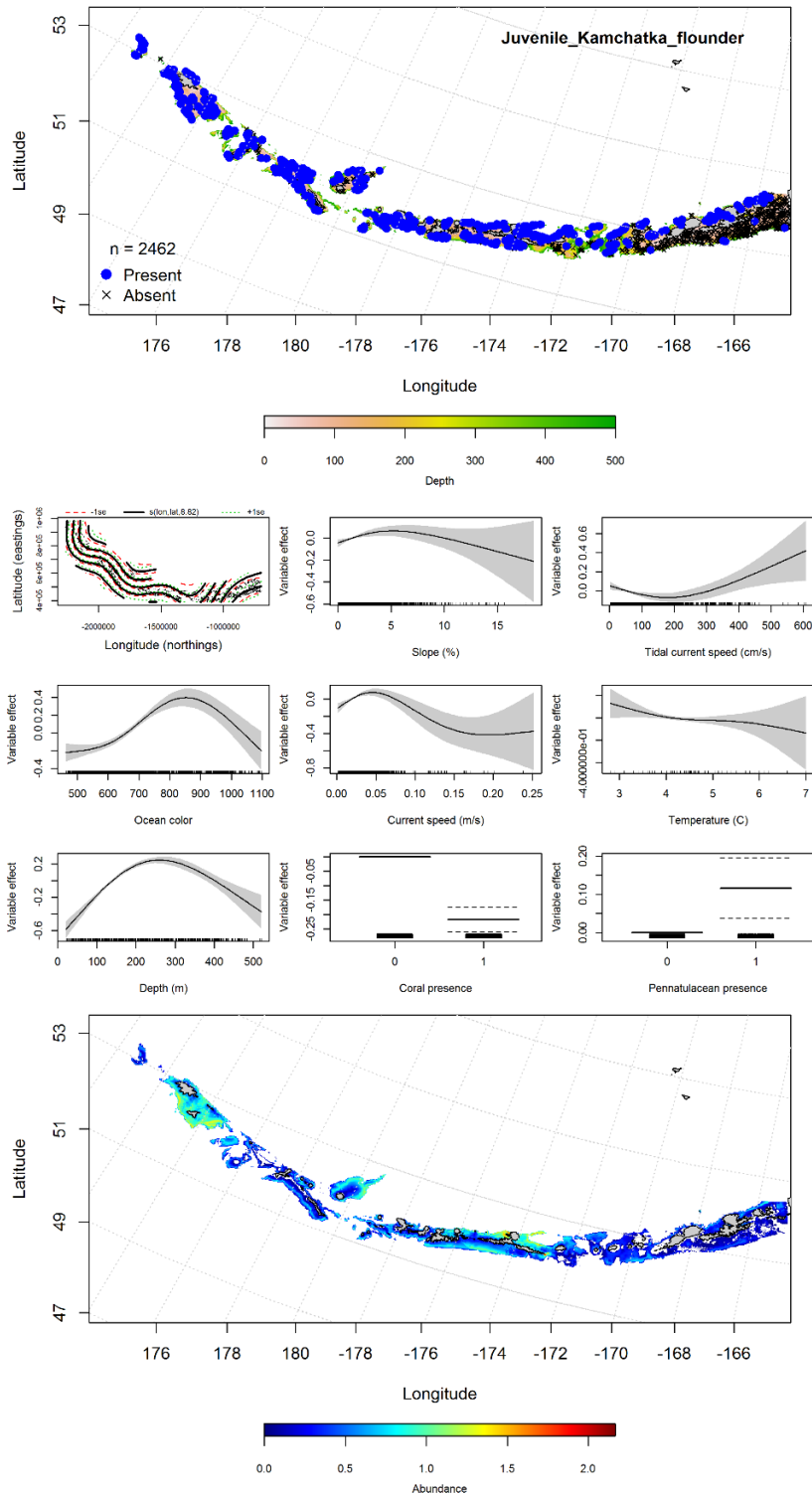


Figure 13. -- Distribution of catches of juvenile Kamchatka flounder in bottom trawl surveys (top panel), significant relationships between CPUE and environmental variables for the best-fitting generalized additive model of juvenile Kamchatka flounder (middle panels), and predicted abundance of juvenile Kamchatka flounder based on the model (bottom panel).

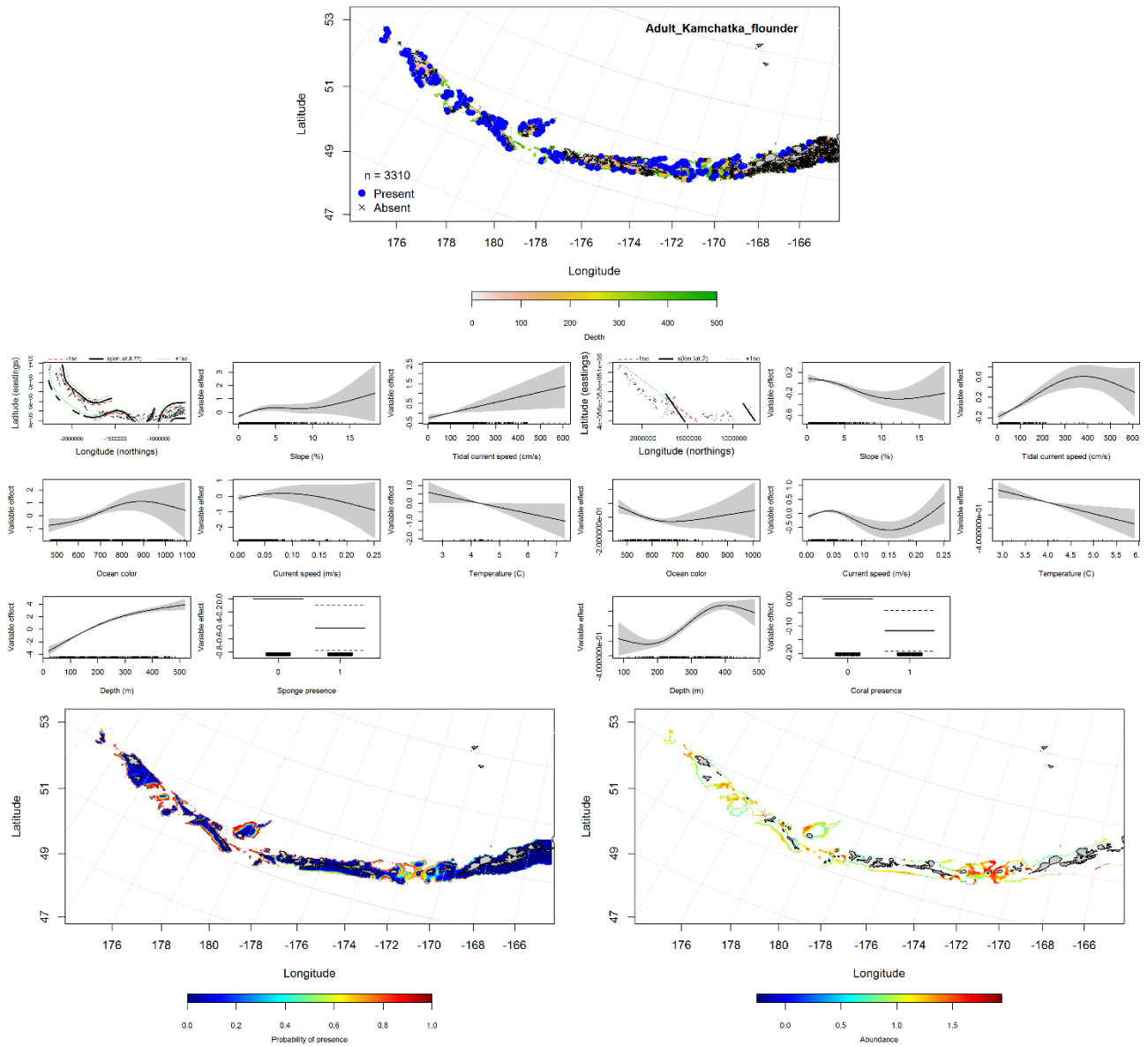


Figure 14. -- Distribution of catches of adult Kamchatka flounder in bottom trawl surveys (top middle panel), significant relationships between presence-absence and CPUE and environmental variables for the best-fitting generalized additive model of adult Kamchatka flounder (middle left and right panels), and predicted probability of presence and abundance of juvenile Kamchatka flounder based on the models (bottom left and right panels).

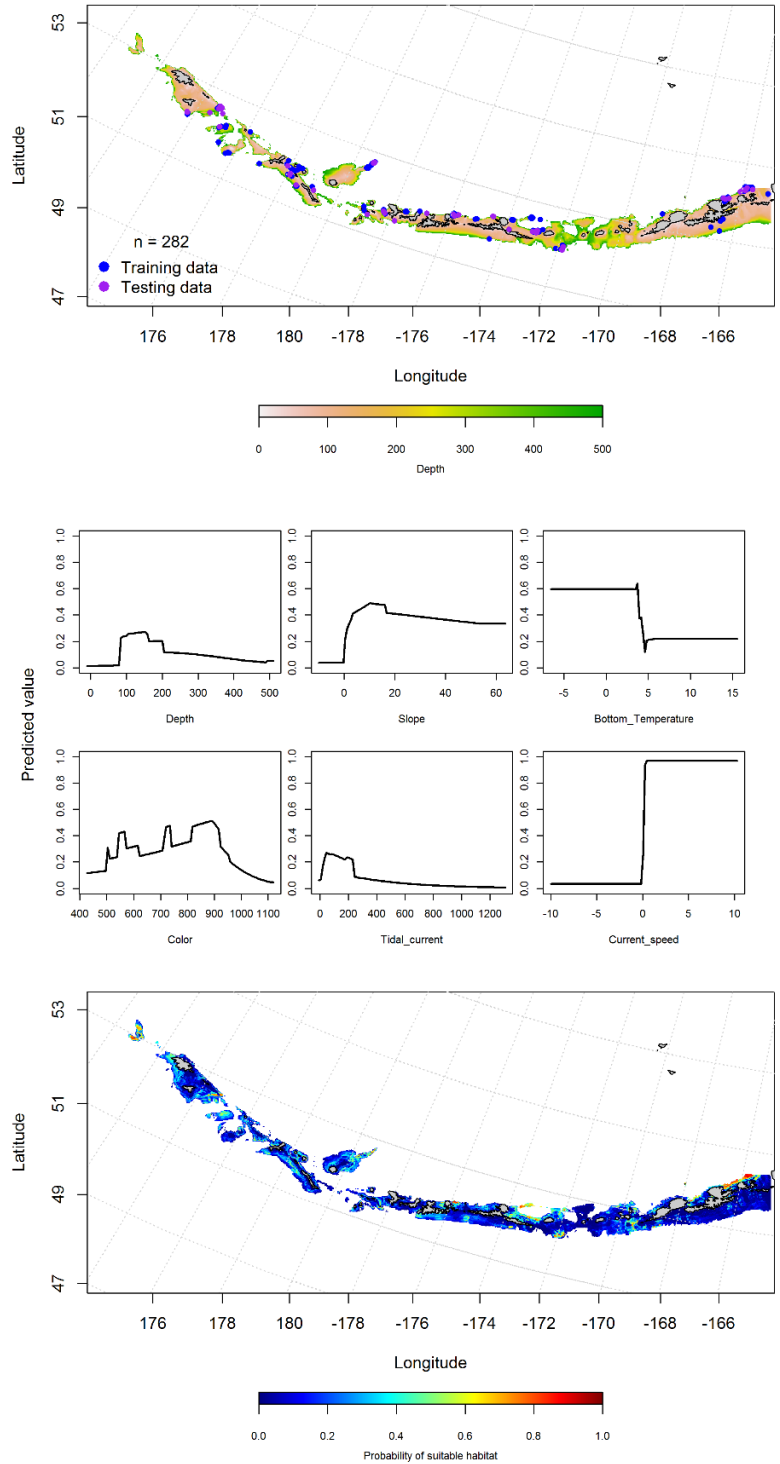


Figure 15. -- Locations of fall (September-November) commercial fisheries catches of Kamchatka flounder (top panel), relationships between probability of presence and environmental variables for the maximum entropy model (middle panels), and predicted probability of suitable habitat for Kamchatka flounder based on the model (bottom panel).

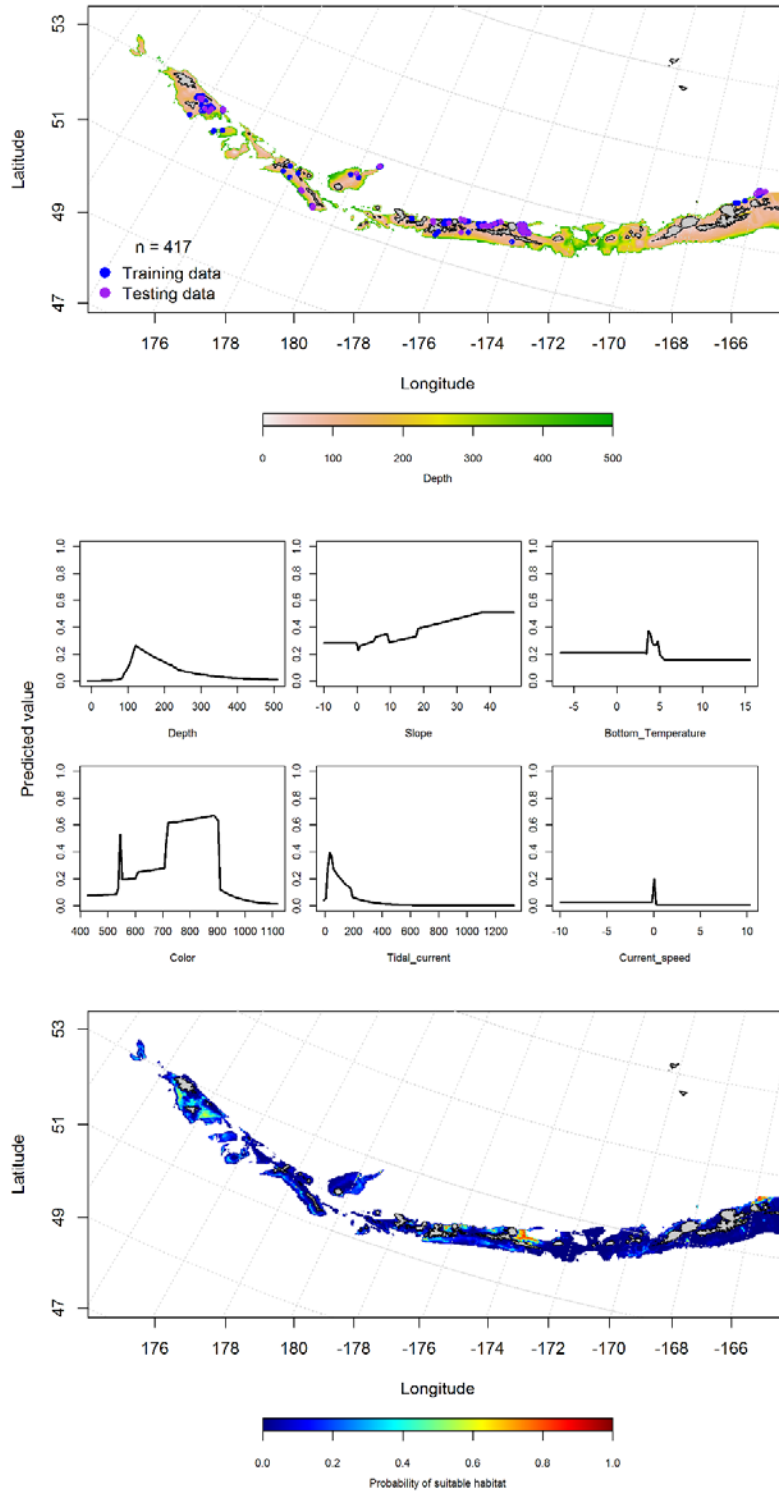


Figure 16. -- Locations of winter (December-February) commercial fisheries catches of Kamchatka flounder (top panel), relationships between probability of presence and environmental variables for the maximum entropy model (middle panels), and predicted probability of suitable habitat for Kamchatka flounder based on the model (bottom panel).

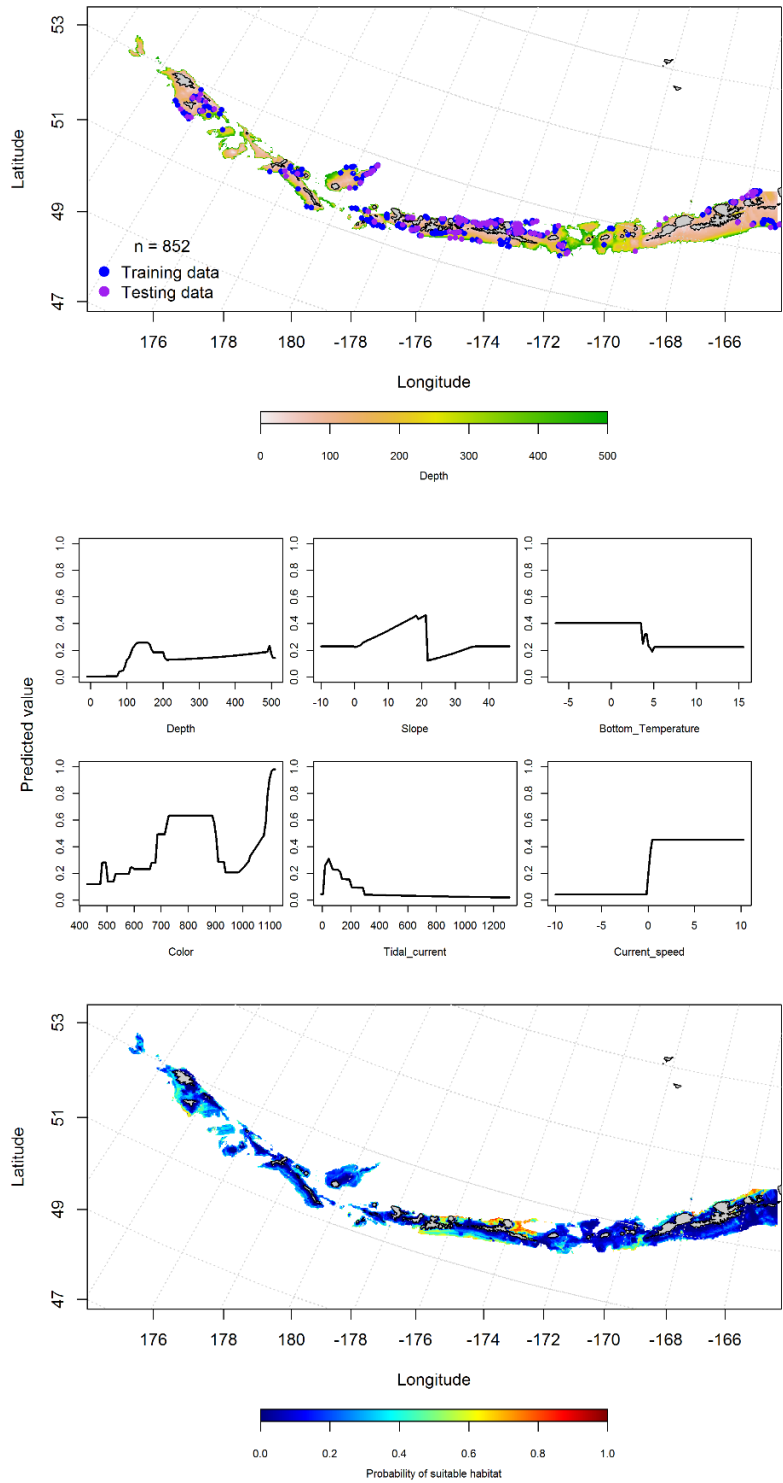


Figure 17. -- Locations of spring (December-February) commercial fisheries catches of Kamchatka flounder (top panel), relationships between probability of presence and environmental variables for the maximum entropy model (middle panels), and predicted probability of suitable habitat for Kamchatka flounder based on the model (bottom panel).

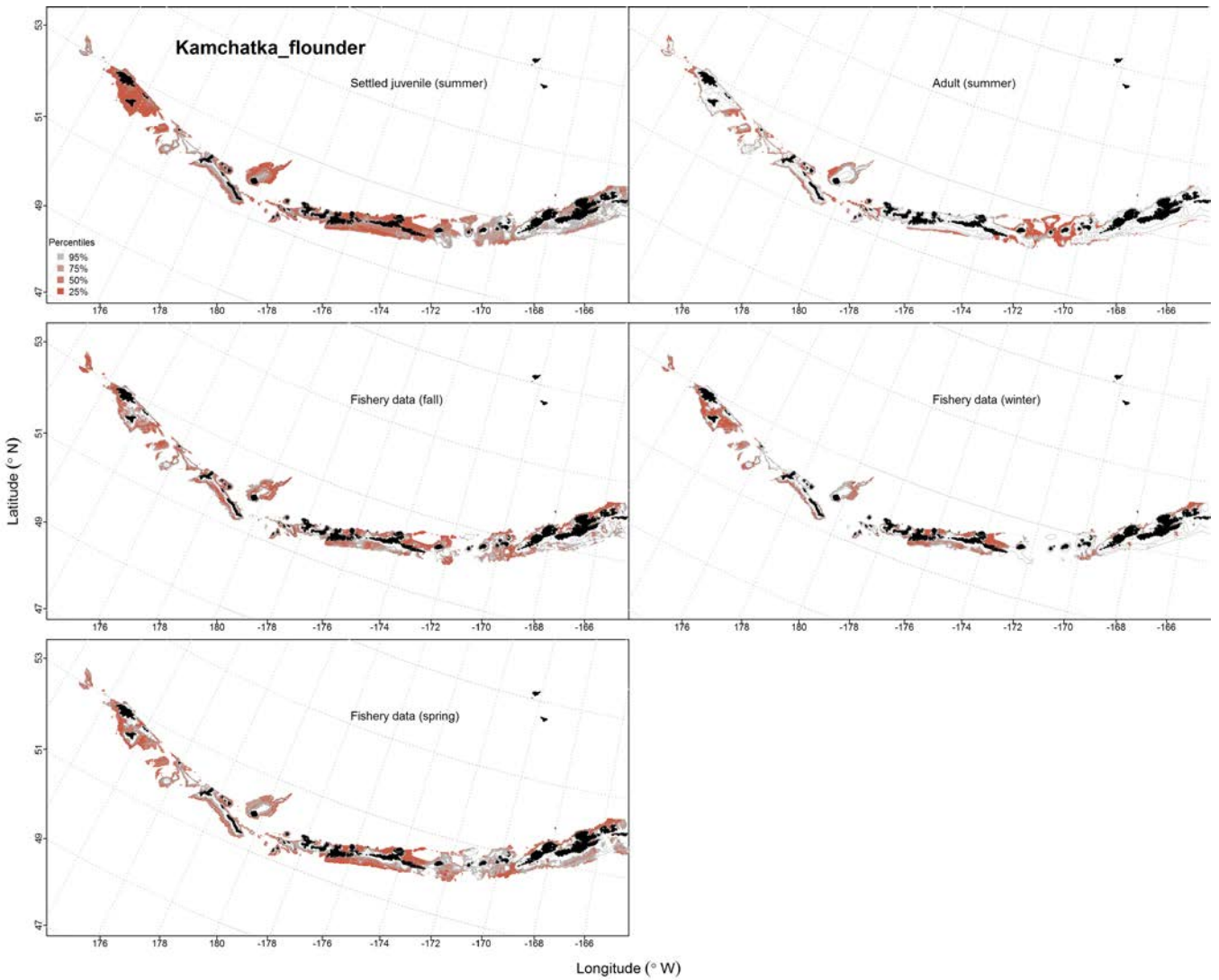


Figure 18. -- Predicted EFH quantiles for Kamchatka flounder life history stages based on species distribution modeling. Settled juvenile and summer adult stages are based on bottom trawl survey data, while seasonal stages (winter, spring, fall) are from commercial fishery data.

Northern Rock Sole (*Lepidopsetta polyxystra*)

Early life history stages of northern rock sole -- There were 106 instances of larval northern rock sole (NRS) observed in the EcoFOCI database limited to the eastern AI (Fig. 19). The most important variables in modeling probability of suitable habitat for larval NRS were surface current direction, ocean color and surface temperature (relative importance: 30%, 25.3%, and 21.2%, respectively). The AUC was 0.97 for the training data and 0.86 for the testing data, indicating a good model fit. The model correctly classified 91% of the training and 86% of the test data. The model predicted probable suitable habitat of larval NRS in the eastern Aleutian Islands (Fig. 19).

Juvenile and adult northern rock sole distribution in the bottom trawl survey -- The catch of northern rock sole in summer bottom trawl surveys of the Aleutian Islands indicates this species is broadly distributed (Fig. 20). Generalized additive models predicting the abundance of juvenile northern rock sole explained 50% of the variability in CPUE in the bottom trawl survey using training data, 50% of the variability in the test data. Bottom depth, ocean color and geographic location were the most important variables predicting probable habitat of juvenile northern rock sole. The model predicted suitable habitat of juvenile northern rock sole in shallow waters throughout the AI (Fig. 20).

The best-fitting GAM model for adult northern rock sole indicated that bottom depth and geographic location were the most important factors controlling the probability of suitable habitat. The model explained 47% of the variability of the training data and 46% of the variability of the test data. Adult northern rock sole were distributed similarly to the juveniles, across the AI in shallower waters (Fig. 21).

Rock sole distribution in commercial fisheries -- Northern and southern rock sole are not well distinguished in the commercial fisheries observer database (D. Stevenson, RACE Division, pers. comm.). Thus, these two species were considered as a group for seasonal modeling using MaxEnt methods. Distribution of adult rock sole in the Aleutian Islands in commercial fisheries catches was not consistent throughout all seasons. In the fall, depth and ocean color were the most important variables in the modeling (relative importance was 0.564 and 0.132, respectively). Most of the catches were south of Umnak Island (Fig. 22). The AUC of the fall MaxEnt model was 0.93 for the training data and 0.82 for the testing data. The model correctly classified 85% of the training observations and 82% of the testing observations. The model predicted suitable habitat near of Umnak and Unalaska islands, with some spots near Petrel Bank (Fig. 22).

In the winter, depth, ocean color, and tidal current were the most important variables in the modeling (relative importance was 0.539, 0.193 and 0.141 respectively). Most of the catches were in the central AI (Fig. 23). The AUC of the fall MaxEnt model was 0.93 for the training data and 0.86 for the testing data. The model correctly classified 86% of the training observations and 86% of the testing observations. The model predicted suitable habitat in the central AI, with some suitable habitat between Agattu and Attu islands (Fig. 23).

In the spring, depth, ocean color, and tidal current were the most important variables in the modeling (relative importance was 0.668, 0.147 and 0.133, respectively). Most of the catches were in the central AI (Fig. 24). The AUC of the fall MaxEnt model was 0.91 for the training data and 0.82 for the testing data. The model correctly classified 83% of the training and 82% testing observations. The model predicted suitable habitat in the eastern and central AI, with some suitable habitat between Agattu and Attu islands (Fig. 24).

Northern rock sole essential fish habitat maps and conclusions -- EFH for northern rock sole larvae was predicted in the eastern AI near Unalaska Island (Fig. 25). This likely reflects the distribution of EcoFOCI sampling rather than of northern rock sole larval distribution, since no sampling was conducted in the central or western AI. Juvenile and adult northern rock sole are widely distributed through the Aleutian Islands chain and co-occur in most places where they are found. Those collected in summertime bottom trawl surveys share similar predicted EFH distributions across the Aleutian Islands (Fig. 25). These similarities can also be observed in areas of low abundance (deeper waters and large passes). Seasonal distribution of adult EFH indicated that rock sole EFH was highest in all seasons in the central AI, similar to the results from bottom trawl survey models (Fig. 25).

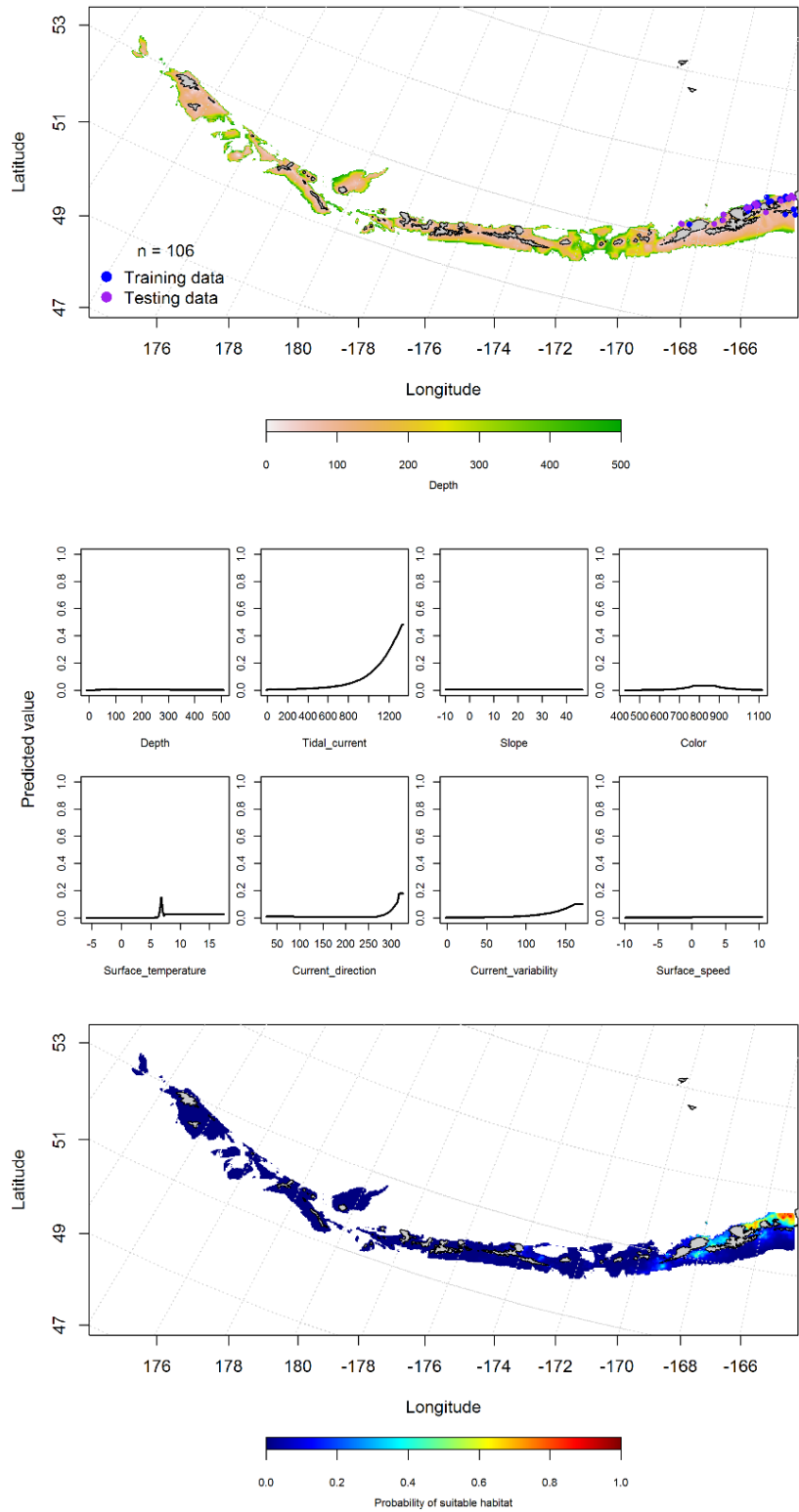


Figure 19. -- Observations of larval northern rock sole from the Aleutian Islands (top panel), relationships with environmental variables (middle panel) and predicted probability of suitable habitat based on EcoFOCI data and maximum entropy modeling.

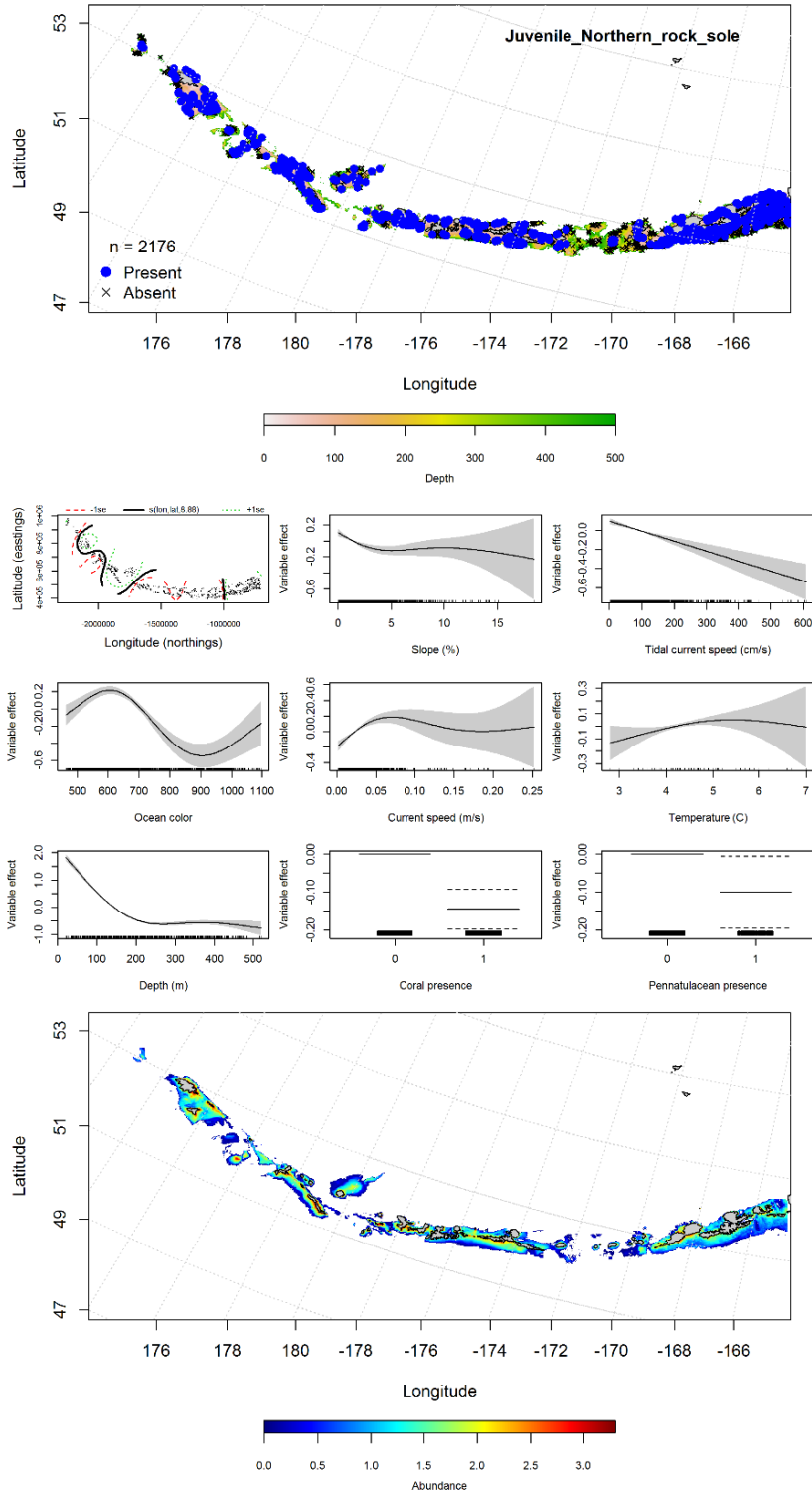


Figure 20. -- Distribution of catches of juvenile northern rock sole in bottom trawl surveys (top panel), significant relationships between CPUE and environmental variables for the best-fitting generalized additive model of juvenile northern rock sole (middle panels), and predicted abundance of juvenile northern rock sole based on the model (bottom panel).

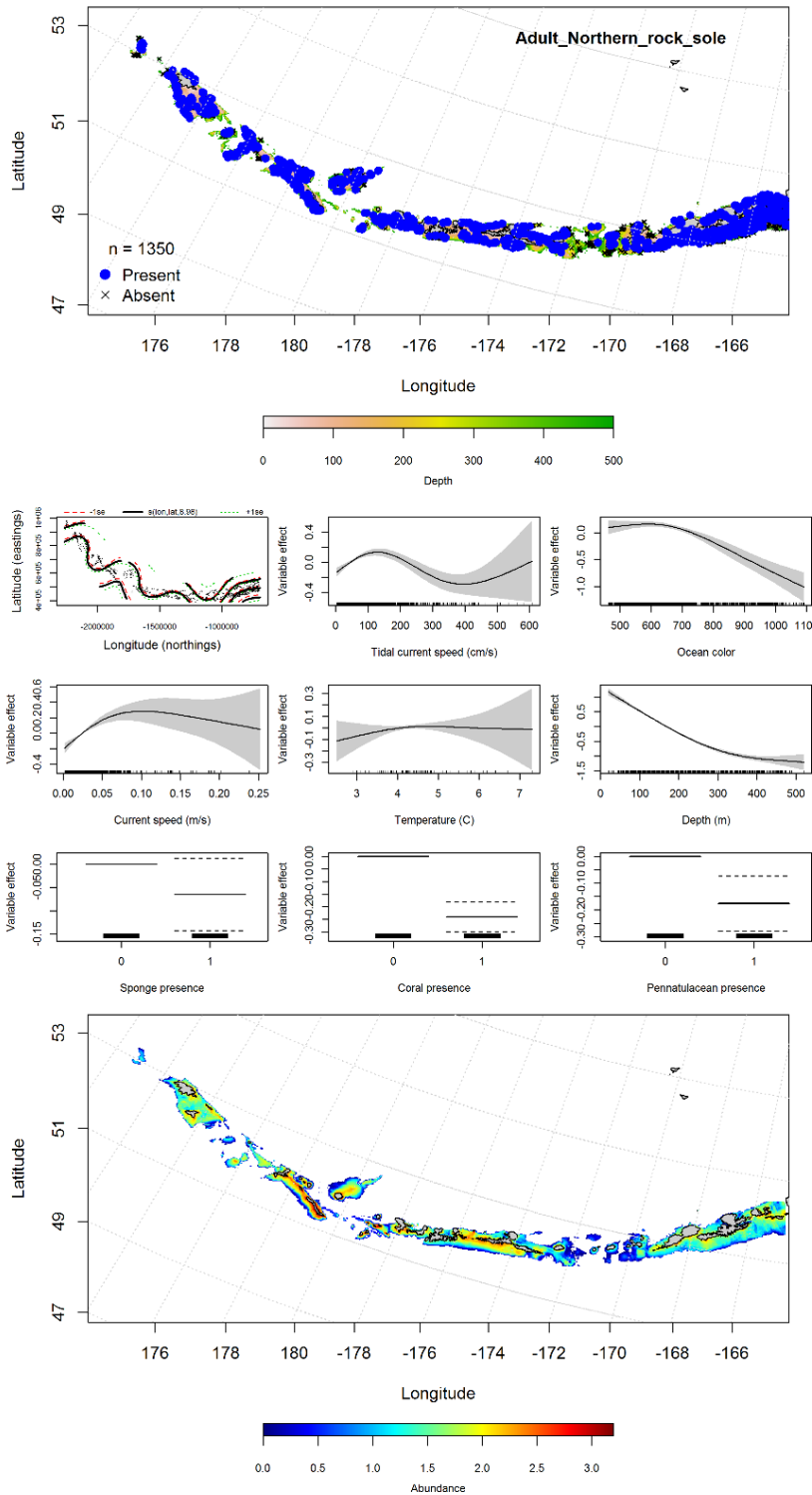


Figure 21. -- Distribution of catches of adult northern rock sole in bottom trawl surveys (top panel), significant relationships between CPUE and environmental variables for the best-fitting generalized additive model of adult northern rock sole (middle panels), and predicted abundance of adult northern rock sole based on the model (bottom panel).

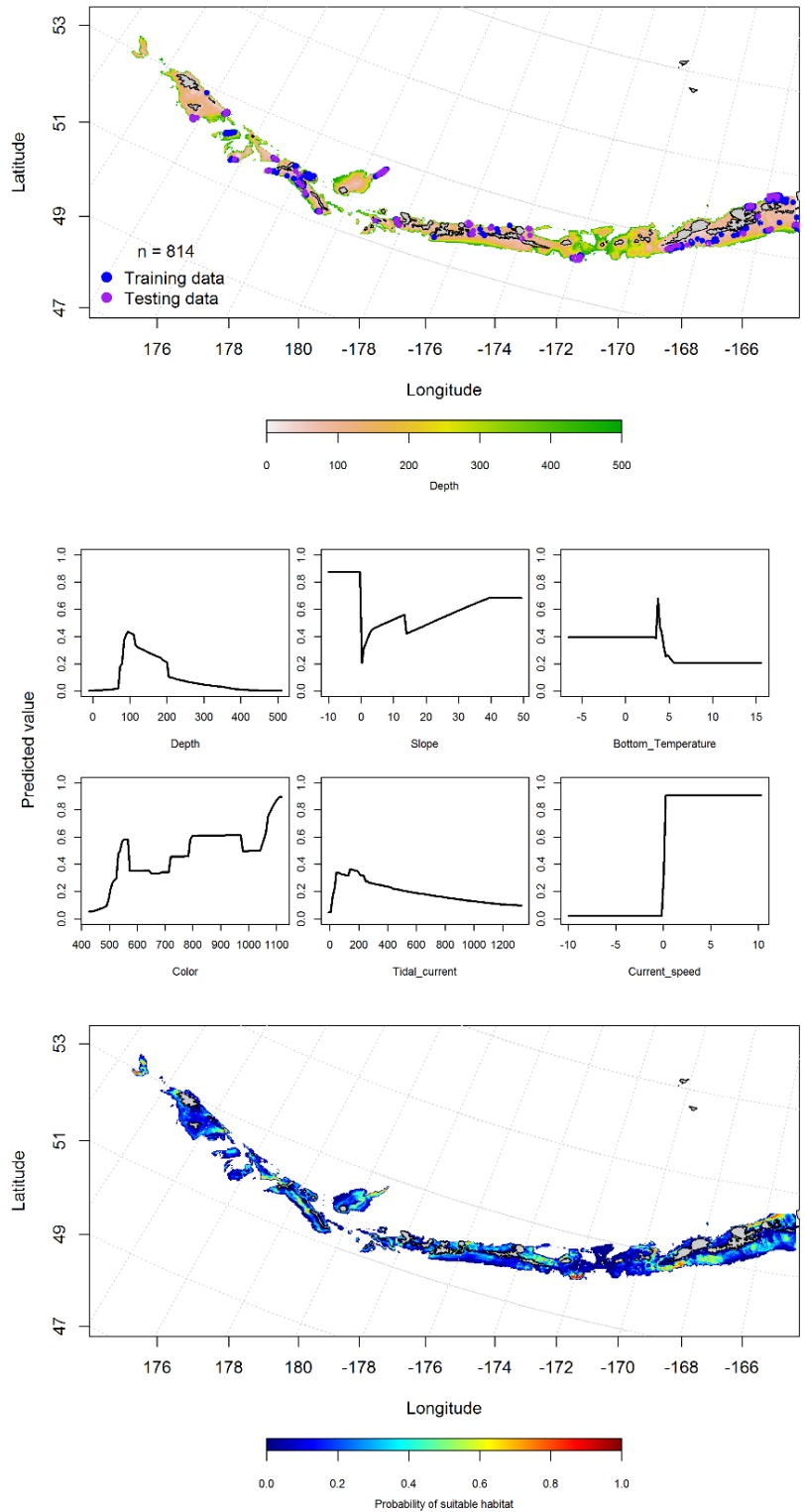


Figure 22. -- Locations of fall (September-November) commercial fisheries catches of rock sole (top panel), relationships between probability of presence and environmental variables for the maximum entropy model (middle panels), and predicted probability of suitable habitat for rock sole based on the model (bottom panel).

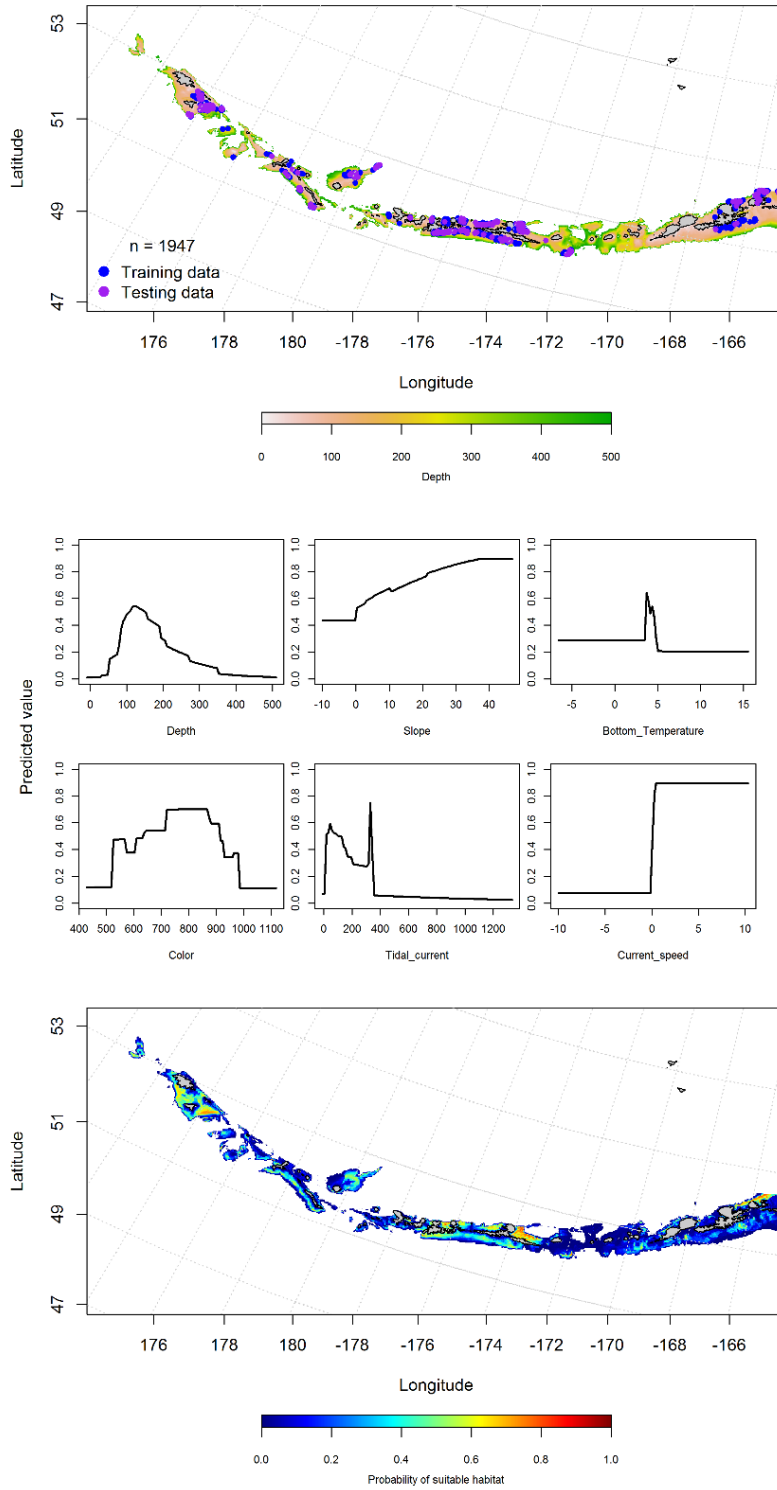


Figure 23. -- Locations of winter (December-February) commercial fisheries catches of rock sole (top panel), relationships between probability of presence and environmental variables for the maximum entropy model (middle panels), and predicted probability of suitable habitat for rock sole based on the model (bottom panel).

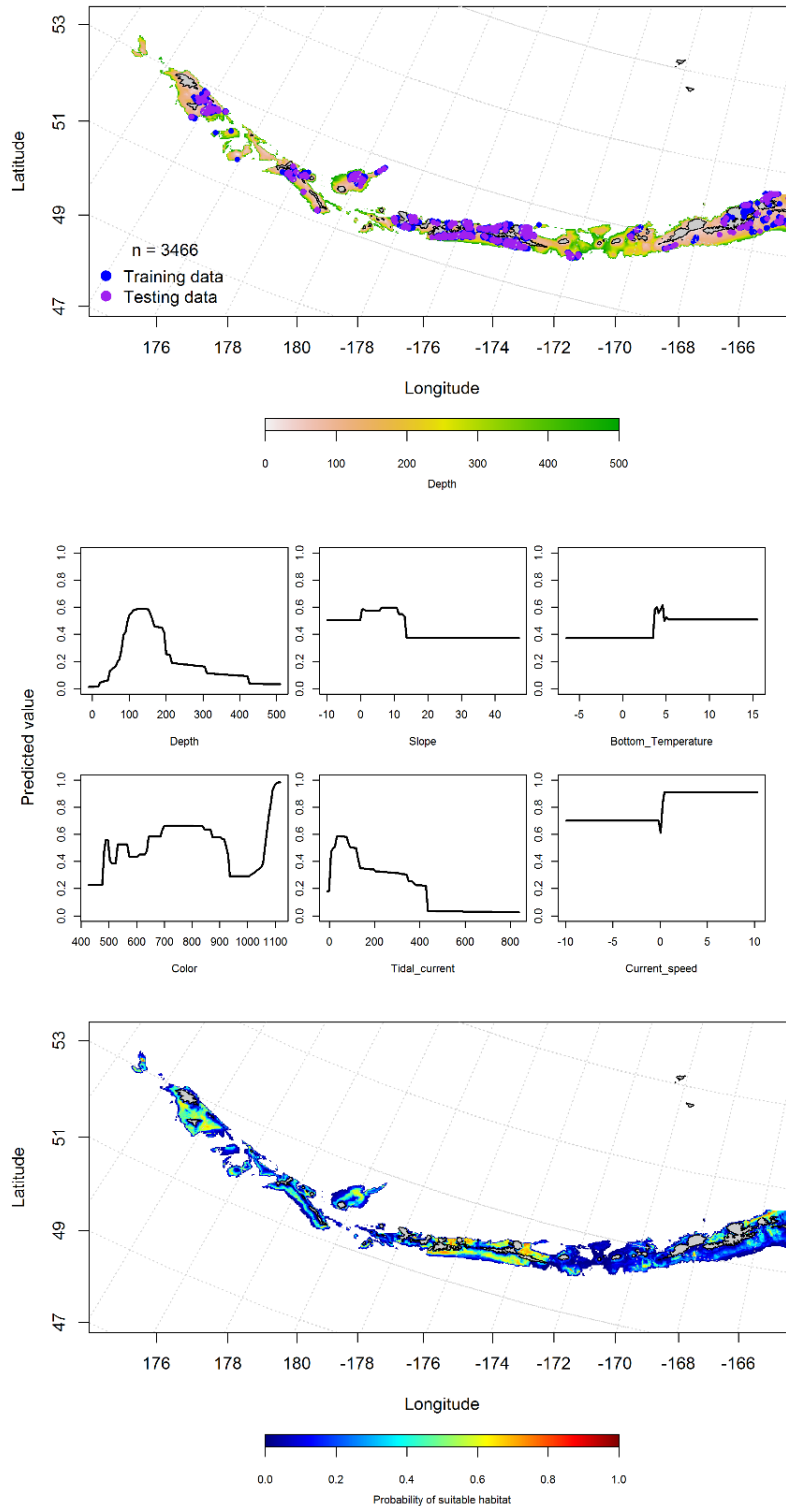


Figure 24. -- Locations of spring (March-May) commercial fisheries catches of rock sole (top panel), relationships between probability of presence and environmental variables for the maximum entropy model (middle panels), and predicted probability of suitable habitat for rock sole based on the model (bottom panel).

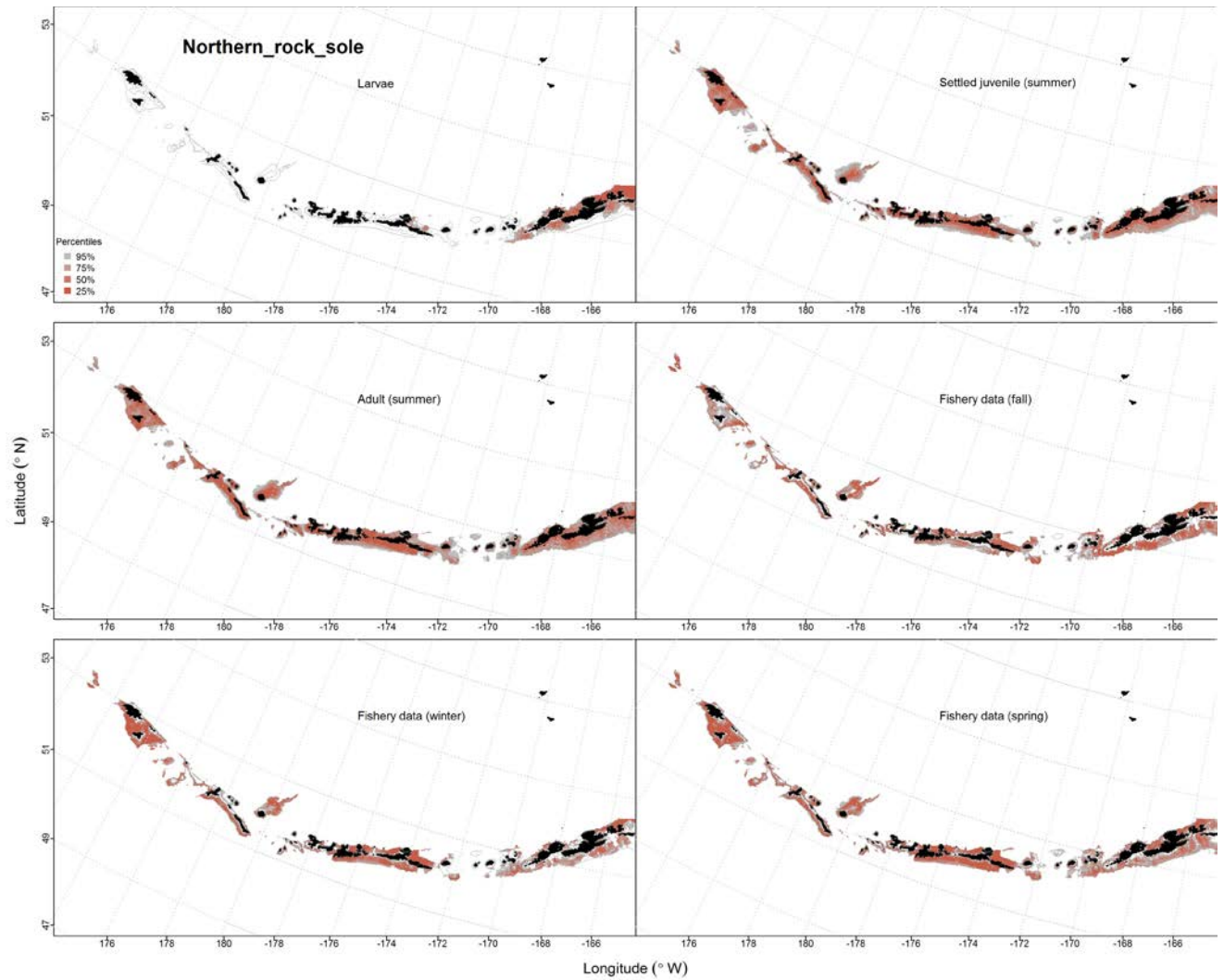


Figure 25. -- Predicted EFH quantiles for northern rock sole life history stages based on species distribution modeling. Larval stages are based on EcoFOCI data, settled juvenile and summer adult stages are based on bottom trawl survey data, while seasonal stages (winter, spring, fall) are from commercial fishery data. Seasonal stages combine both northern and southern rock sole.

Southern Rock Sole (*Lepidopsetta bilineata*)

Early life history stages of southern rock sole -- There were only eight instances of southern rock sole (SRS) larvae, all in the eastern AI, therefore they were not used in a model.

Juvenile and adult southern rock sole distribution in the bottom trawl survey -- A MaxEnt model was used to predict the EFH for juvenile southern rock sole. The AUC of the model was 0.92 for the training data and 0.75 for the test data. Ocean color and bottom depth were the most important variables explaining the probability of presence of juvenile southern rock sole suitable habitat. The model correctly classified 84% of the training data and 75% of the test data. The areas of predicted highest probability of presence for suitable habitat were in the eastern Aleutian Islands (Fig. 26).

A MaxEnt model was also used to predict the EFH for adult southern rock sole. The AUC of the model was 0.90 for the training data and 0.80 for the test data. Ocean color and bottom depth were the most important variables explaining the probability of presence of adult southern rock sole suitable habitat. The model correctly classified 82% of the training data and 80% of the test data. The areas of predicted highest probability of presence for suitable habitat were also in the eastern Aleutian Islands (Fig. 27).

Southern rock sole distribution in commercial fisheries -- Combined northern and southern rock sole are reported above with northern rock sole.

Southern rock sole essential fish habitat maps and conclusions -- EFH of southern rock sole was similar for juvenile and adult life stages (Fig. 28), concentrated in the east near Umnak and Unalaska islands, and uncommon in the central and western AI.

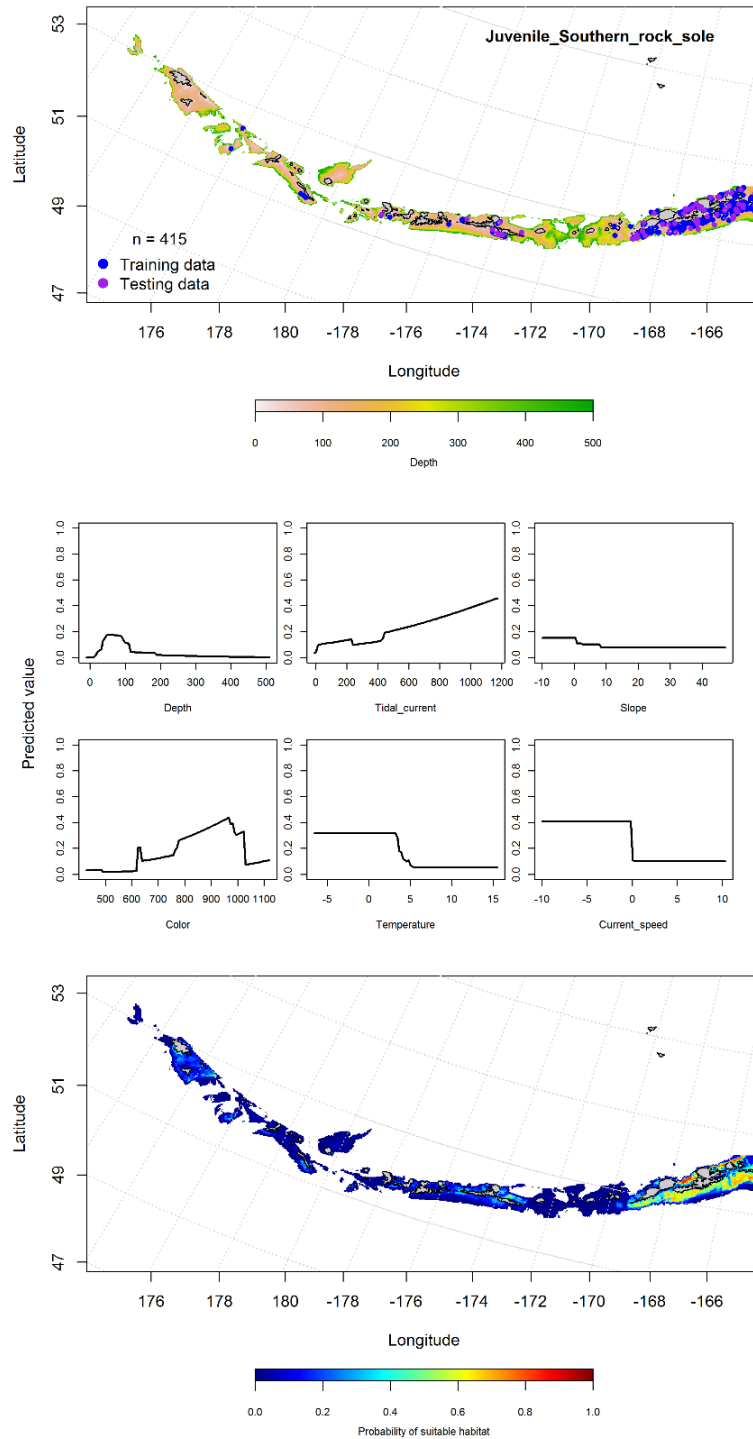


Figure 26. -- Distribution of catches of juvenile southern rock sole in bottom trawl surveys (top panel), relationships between presence and environmental variables for the maximum entropy model of juvenile southern rock sole (middle panels), and predicted probability of suitable habitat for juvenile southern rock sole based on the model (bottom panel).

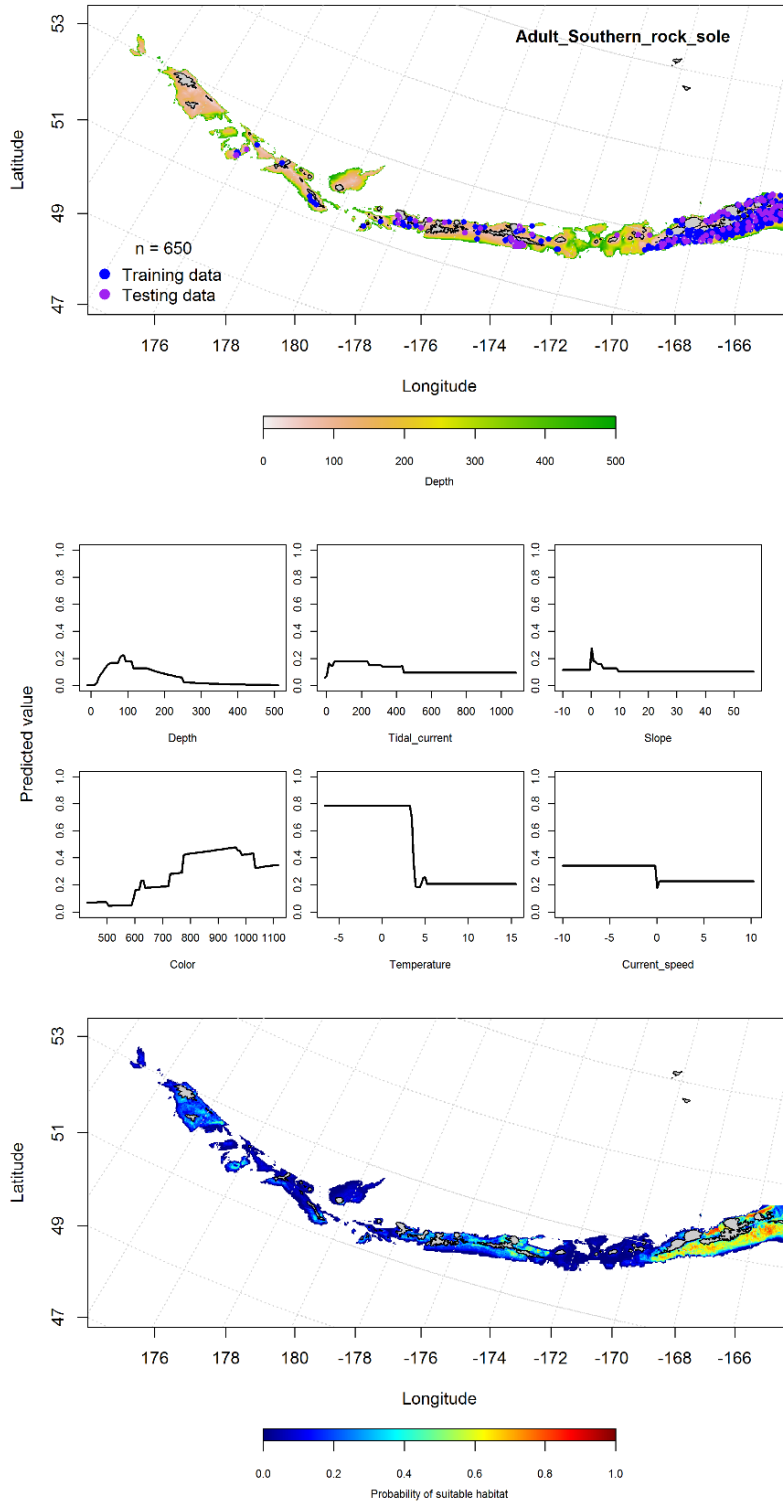


Figure 27. -- Distribution of catches of adult southern rock sole in bottom trawl surveys (top panel), relationships between presence and environmental variables for the maximum entropy model of adult southern rock sole (middle panels), and predicted probability of suitable habitat for adult southern rock sole based on the model (bottom panel).

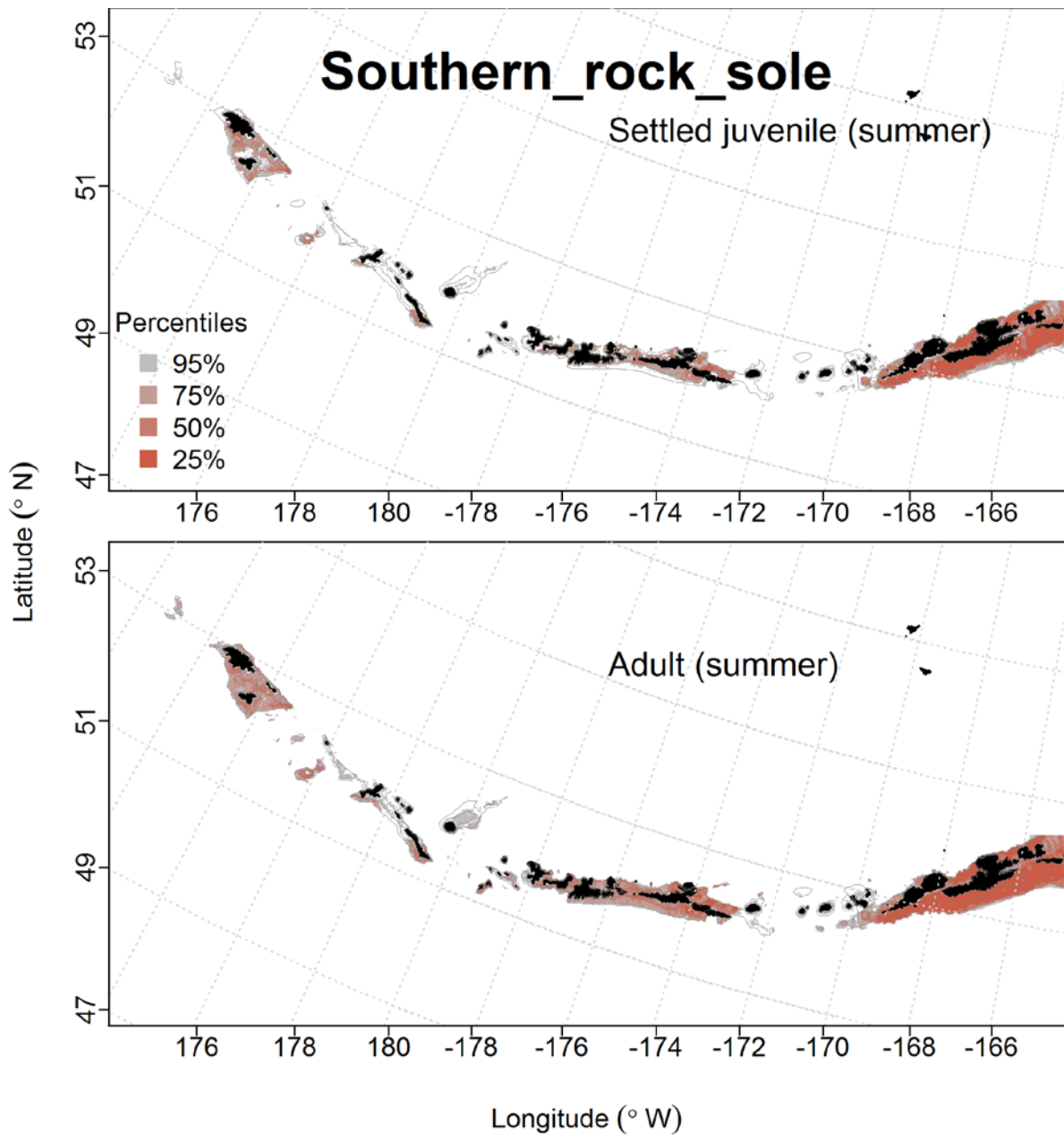


Figure 28. -- Predicted EFH quantiles for southern rock sole life history stages based on species distribution modeling. Settled juvenile and summer adult stages are based on bottom trawl survey data. Modeling for commercial fishery data was carried out with combined northern and southern rock sole and reported with northern rock sole.

Greenland Turbot (*Reinhardtius hippoglossoides*)

Early life history stages of Greenland turbot -- There were only three instances of Greenland turbot eggs and nine instances of larvae observed in the EcoFOCI database, all were limited to the eastern Aleutian Islands and thus were not modeled?

Juvenile and adult Greenland turbot distribution in the bottom trawl survey -- The MaxEnt model predicting the probable habitat of juvenile Greenland turbot fit the presence data well, with an AUC of 0.98 for training and 0.88 for testing data sets. Bottom depth and temperature were the most important variables explaining the distribution of juvenile Greenland turbot (relative importance: 0.611 and 0.329, respectively). The model fit the data set well, as 94% of the training data and 88% of the test data were correctly classified. The model predicted probable suitable habitat of juvenile Greenland turbot in the deeper passes of the AI (Fig. 29).

Adult Greenland turbot were distributed similarly to the juveniles. The MaxEnt model predicted presence of suitable adult Greenland turbot habitat in the deeper passes of the AI, although there were higher probabilities around Semisopchnoi Island, and in the far eastern AI (Fig. 30). In this model, the most important variables explaining the distribution were depth and temperature (relative importance = 0.483 and 0.437, respectively) and the AUC was 0.95 for training data and 0.86 for testing data. The model, correctly classified 87% of the training data and 86% of the test data.

Greenland turbot distribution in commercial fisheries -- Distribution of adult Greenland turbot in the Aleutian Islands in commercial fisheries catches was generally consistent throughout all seasons. In the fall, bottom depth, temperature, and ocean color were the most important variables determining probable suitable habitat of Greenland turbot (relative

importance: 27.1%, 26.9%, and 18.8%, respectively). The AUC of the fall MaxEnt model was 0.94 for the training data and 0.84 for the test data and 87% of the training data and 84% of the test data were predicted correctly. The model predicted probable suitable habitat of Greenland turbot was highest on Petrel Bank (Fig. 31).

In the winter, ocean color, bottom temperature, and bottom depth were the most important variables determining probable suitable habitat of Greenland turbot (relative importance: 0.389, 0.327, and 0.221, respectively). The AUC of the winter MaxEnt model was 0.96 for the training data and 0.84 for the test data and 88% of the cases in the training data and 84% of the test data sets were predicted correctly. In the fall, the model predicted the highest probable suitable habitat of Greenland turbot near Atka Island (Fig. 32).

In the spring, bottom depth, ocean color and slope were the most important variables determining probable suitable habitat of Greenland turbot (relative importance: 0.51, 0.21, and 0.14). The AUC of the spring MaxEnt model was 0.93 for the training data and 0.85 for the test data, and 87% of the training data and 85% of the test data was predicted correctly. As with the winter, the highest predicted probable suitable habitat of Greenland turbot was near Atka Island (Fig. 33).

Greenland turbot essential fish habitat maps and conclusions -- In general, juvenile and adult Greenland turbot were distributed through the Aleutian Islands in deeper water, although adult EFH was slightly more abundant in the eastern AI (Fig. 34). Similar to summertime bottom trawl survey data observations, the EFH predicted from commercial catches of Greenland turbot was distributed throughout the Aleutian Islands in deeper waters (Fig. 34). There does not appear to be much seasonal variability to the EFH distribution, as there were similar patterns across all life history stages and seasons.

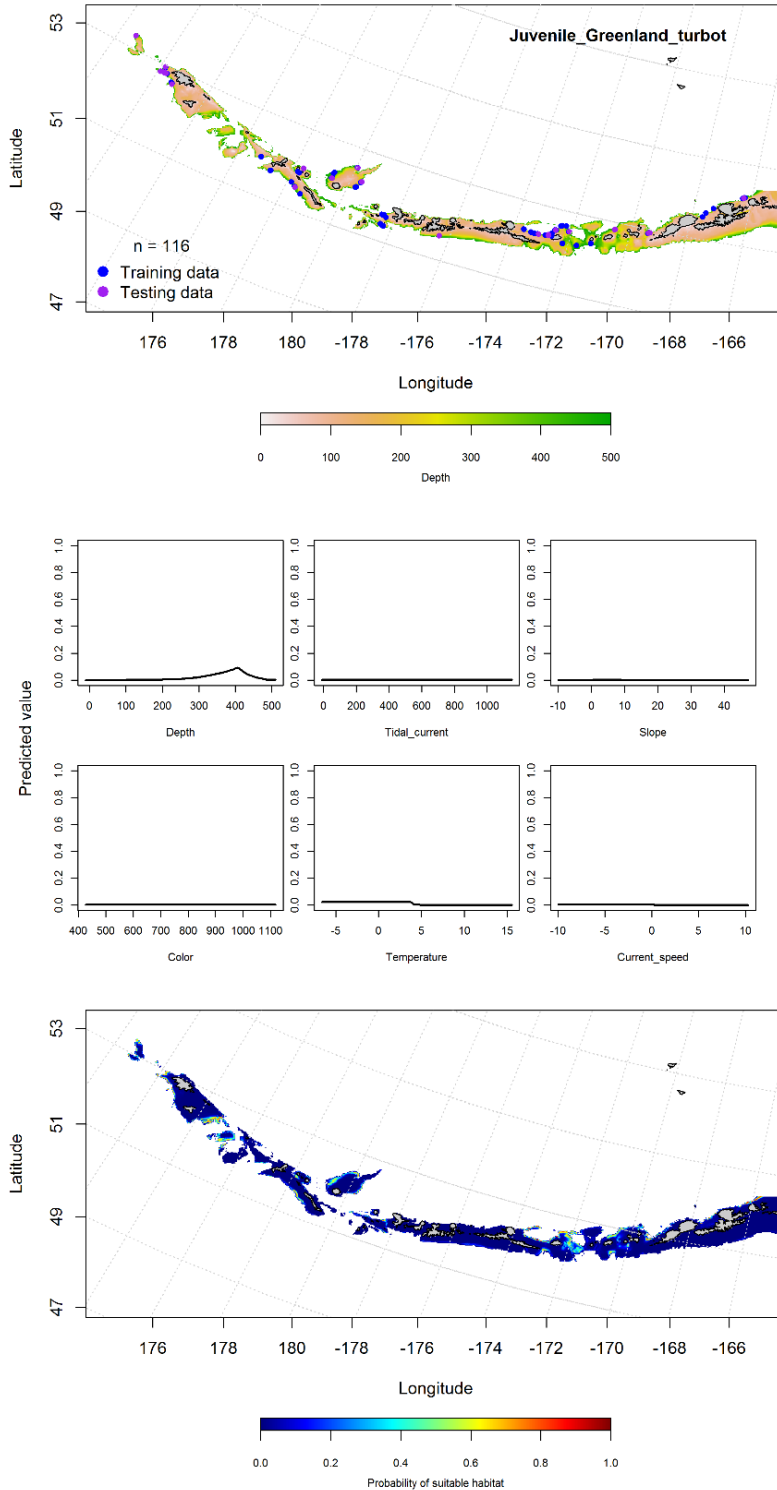


Figure 29. -- Distribution of catches of juvenile Greenland turbot in bottom trawl surveys (top panel), relationships between presence and environmental variables for the maximum entropy model of juvenile Greenland turbot (middle panels), and predicted probability of suitable habitat for juvenile Greenland turbot based on the model (bottom panel).

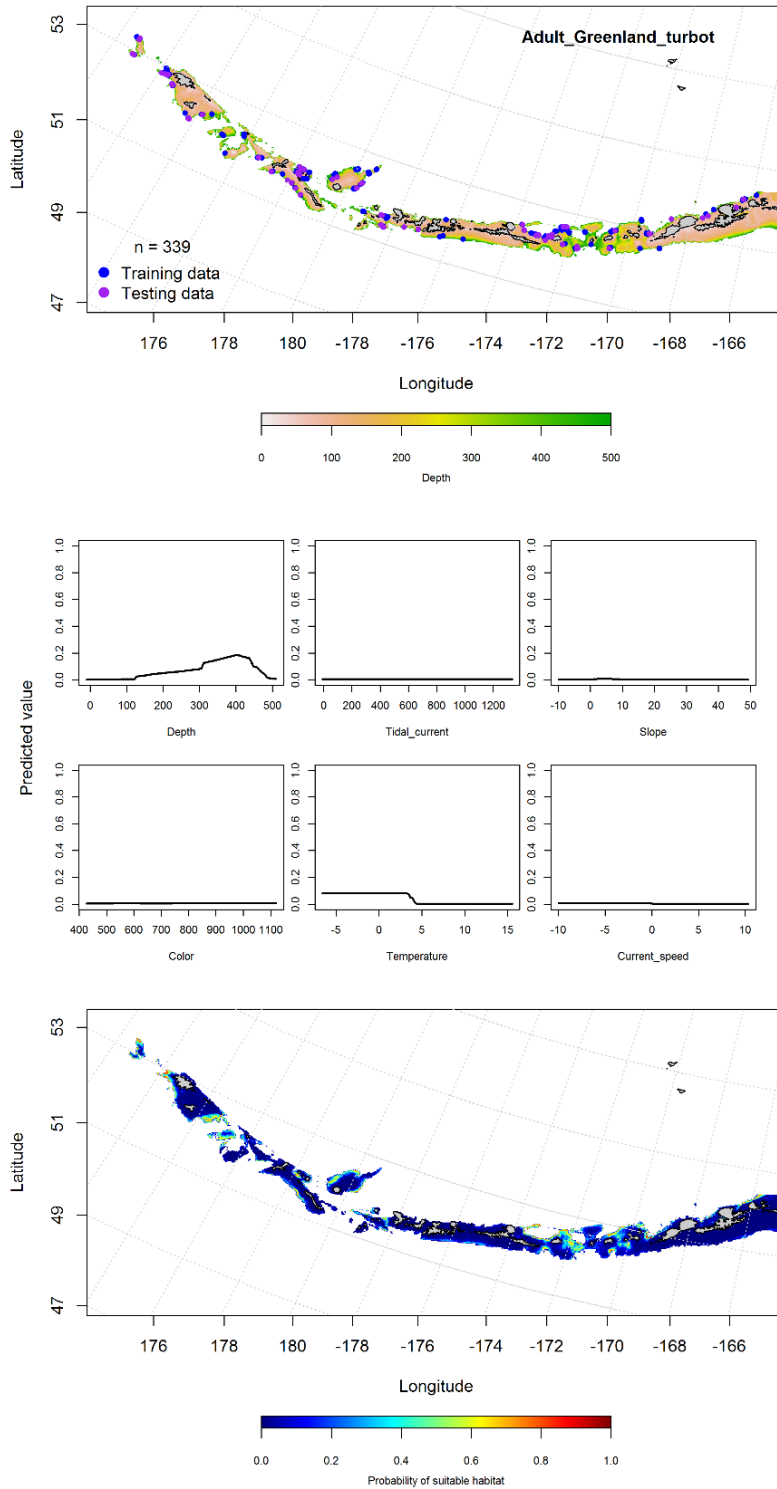


Figure 30. -- Distribution of catches of adult Greenland turbot in bottom trawl surveys (top panel), relationships between presence and environmental variables for the maximum entropy model of adult Greenland turbot (middle panels), and predicted probability of suitable habitat for adult Greenland turbot based on the model (bottom panel).

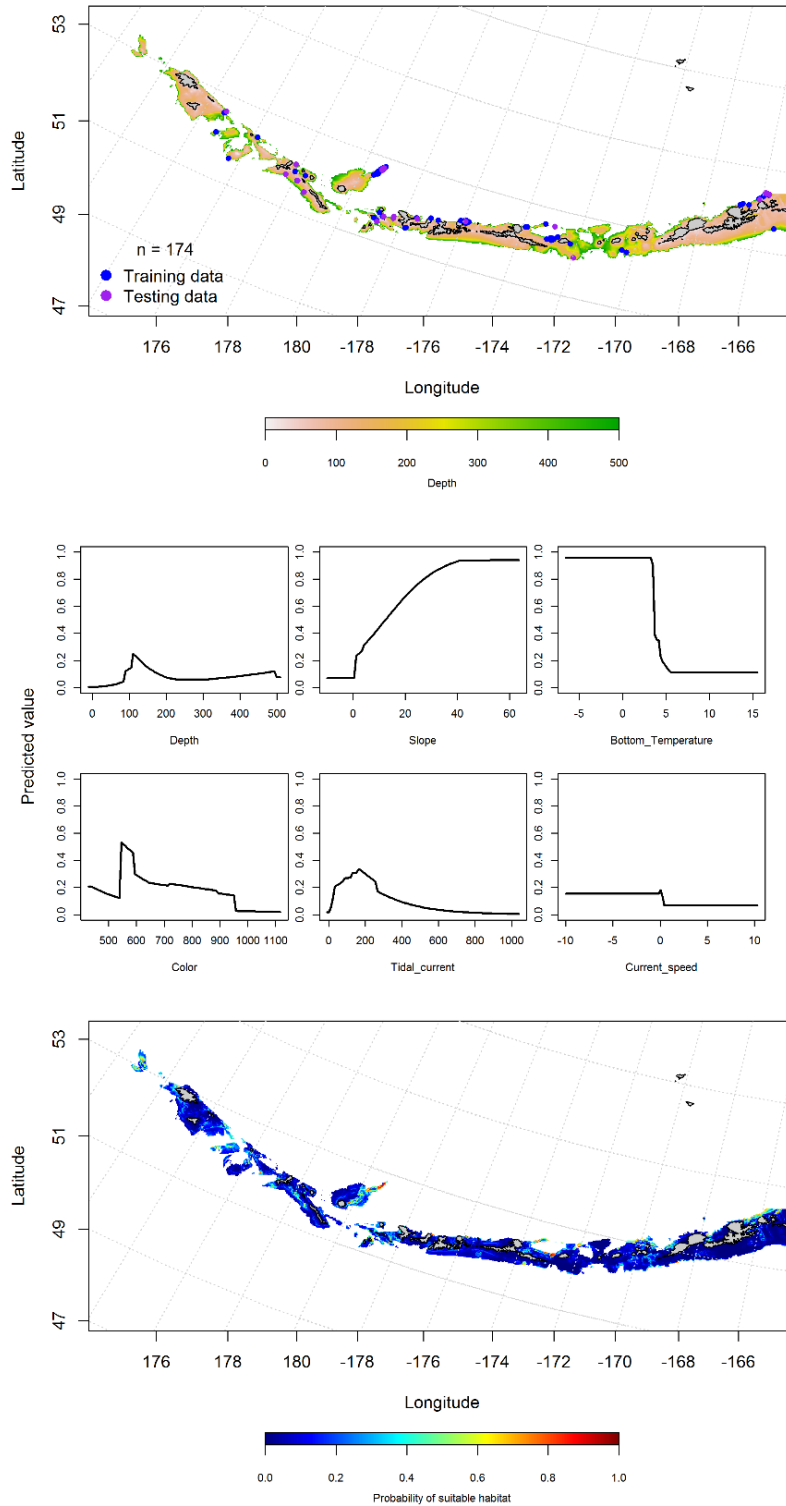


Figure 31. -- Locations of fall (September-November) commercial fisheries catches of Greenland turbot (top panel), relationships between probability of presence and environmental variables for the maximum entropy model (middle panels), and predicted probability of suitable habitat for Greenland turbot based on the model (bottom panel).

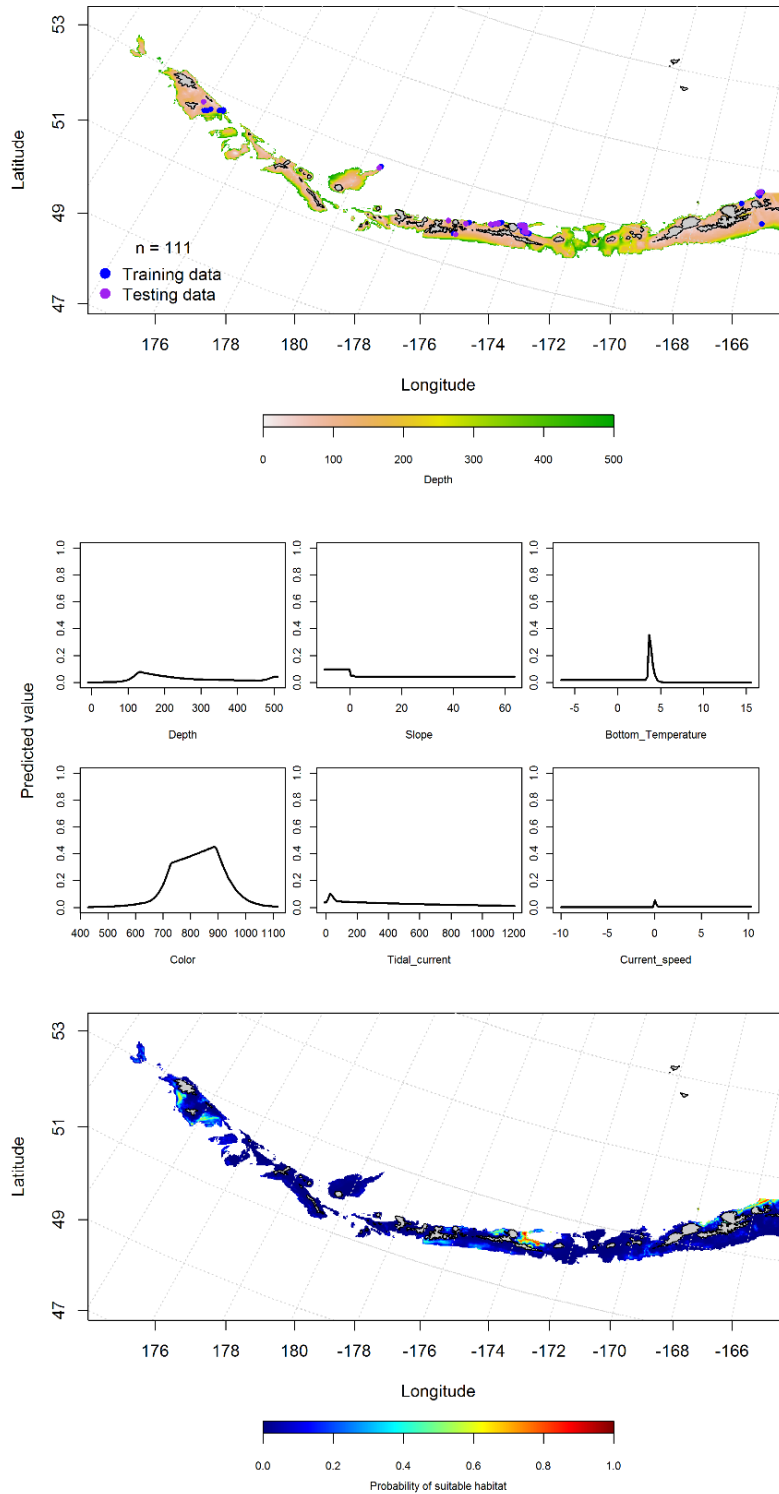


Figure 32. -- Locations of winter (December-February) commercial fisheries catches of Greenland turbot (top panel), relationships between probability of presence and environmental variables for the maximum entropy model (middle panels), and predicted probability of suitable habitat for Greenland turbot based on the model (bottom panel).

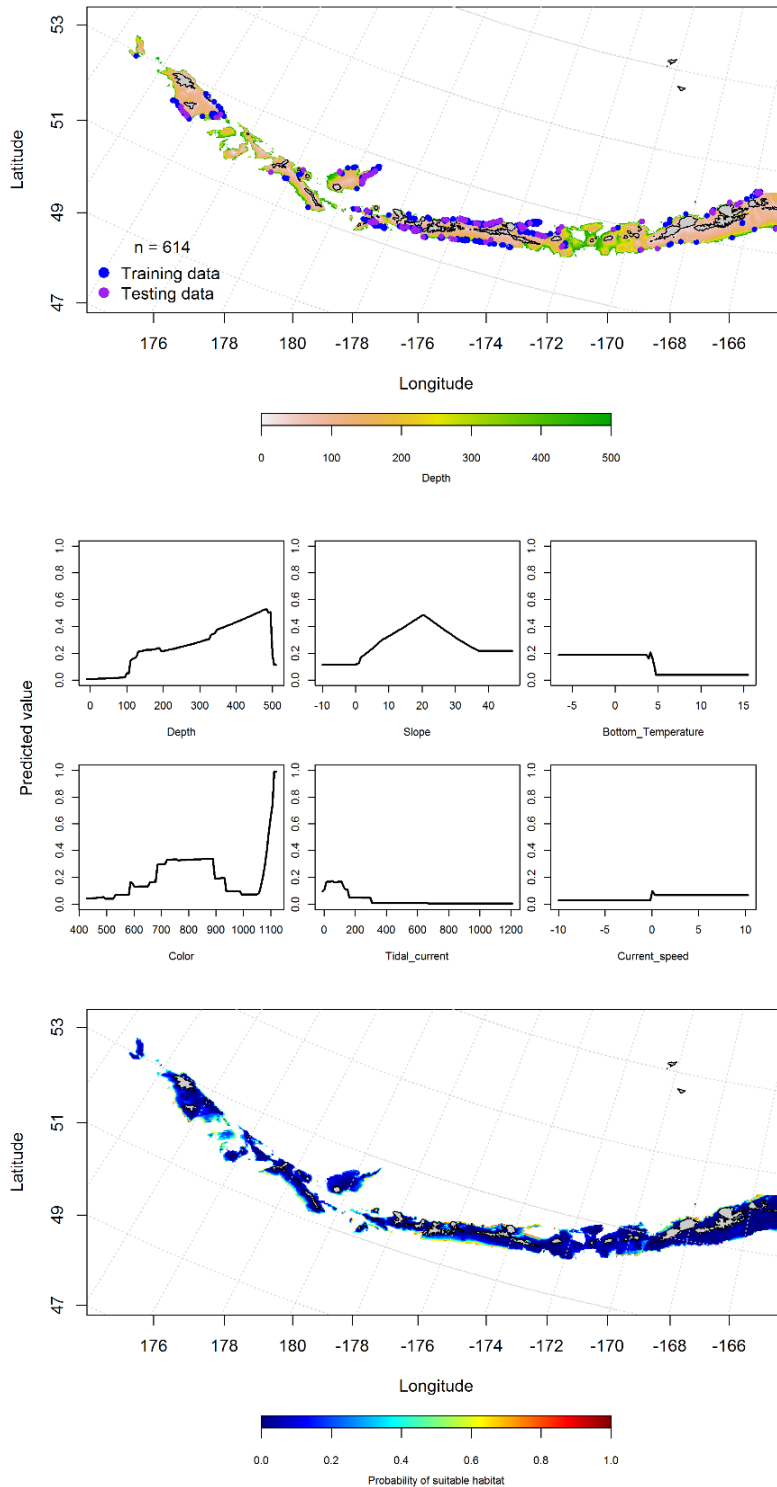


Figure 33. -- Locations of spring (March-May) commercial fisheries catches of Greenland turbot (top panel), relationships between probability of presence and environmental variables for the maximum entropy model (middle panels), and predicted probability of suitable habitat for Greenland turbot based on the model (bottom panel).

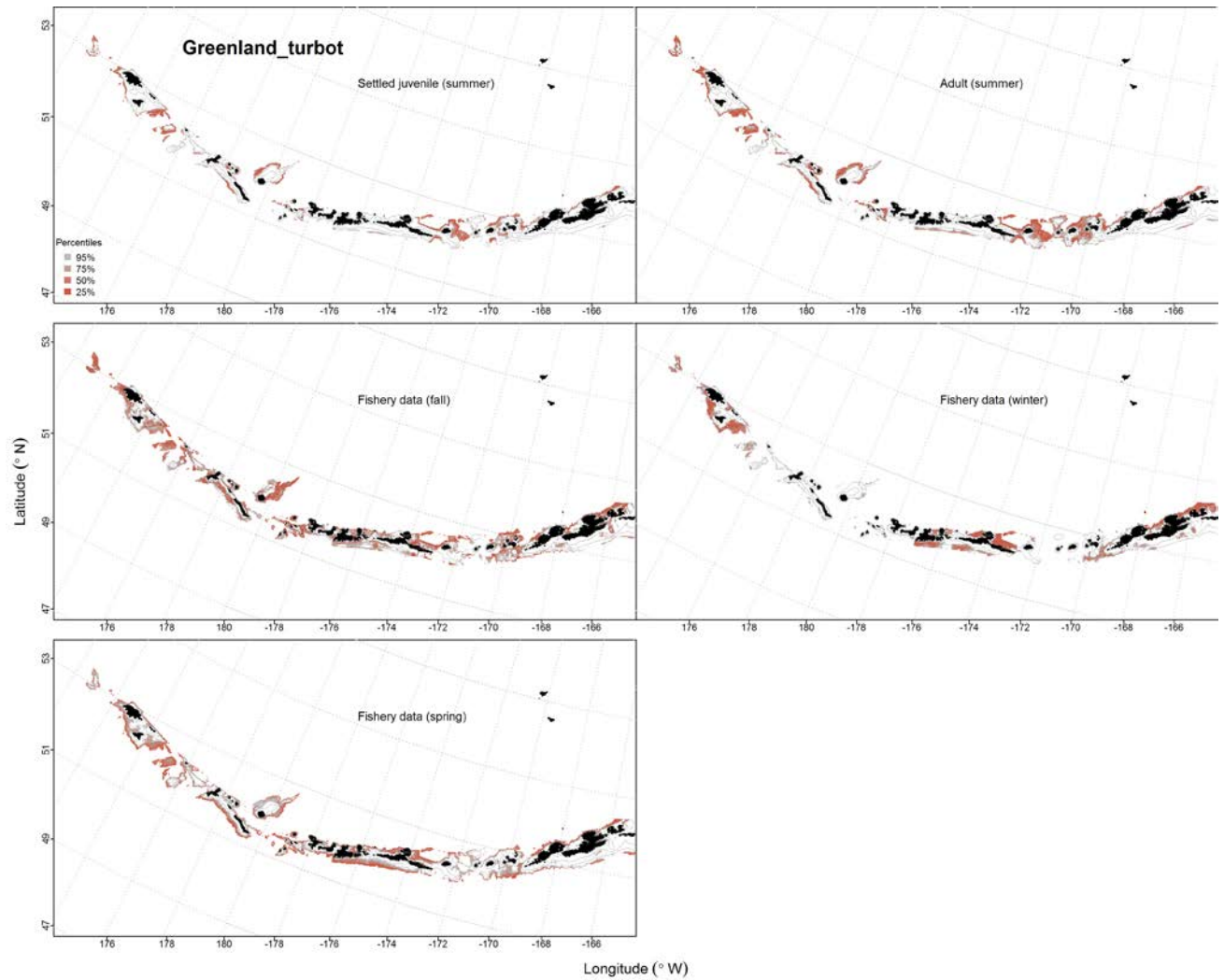


Figure 34. -- Predicted EFH quantiles for Greenland turbot life history stages based on species distribution modeling. Settled juvenile and summer adult stages are based on bottom trawl survey data, while seasonal stages (winter, spring, fall) are from commercial fishery data.

Flathead Sole (*Hippoglossoides elassodon*)

Early life history stages of flathead sole -- There were 118 instances of flathead sole eggs observed in the EcoFOCI database (Fig. 35). All observations were in the eastern AI, and the model predicted suitable habitat for flathead sole eggs in Unimak Pass and north of Unalaska Island. The most important variables in modeling egg distribution were ocean color, current speed, current direction, and surface temperature (relative importance: 0.26, 0.26, 0.20 and 0.15). For the spring model, the AUC was 1.0 for the training data and 0.98 for the test data, with 97% of the training data and 98% of the test data was correctly classified. There were only 47 observations of flathead sole larvae, all observations were found in the eastern AI. These were not modeled.

Juvenile and adult flathead sole distribution in the bottom trawl survey -- The catch of juvenile flathead sole in summer bottom trawl surveys of the Aleutian Islands indicates this species is broadly distributed (Fig. 36). A two-step hurdle-GAM predicting the presence absence (PA GAM) of juvenile flathead sole had an AUC of 0.90 for the training data and 0.92 for the test data. The most important variables included in the model were geographic location, depth and ocean color (Fig. 36). The areas of predicted highest probability of presence were concentrated around Agattu Island in the western AI, Atka Island in the central AI, and Unalaska Island in the east (Fig. 36). Geographic location and ocean color were the most important variables in the juvenile flathead sole CPUE GAM. Overall, the hurdle-GAM explained 29% of the variability of the training data and 32% of the test data. The areas of predicted highest abundance were around Agattu Island in the western AI, Atka Island in the central AI, and Unalaska Island in the eastern AI (Fig. 36).

The hurdle-GAM predicting the presence absence (PA GAM) of adult flathead sole had an AUC of 0.88 for the training data and 0.85 for the testing data. Geographic position, ocean color and depth were the most important variables explaining the distribution of adult flathead sole presence or absence (Fig. 37). The model correctly classified 81% of the training data and 79% of the test data. The areas of highest probability of presence were highest around Agattu, Adak and Unalaska islands (Fig. 37), similar to juvenile flathead sole. The adult flathead sole CPUE-GAM predicted the highest abundance near Agattu and Unalaska islands (Fig. 37), and the most important variables were geographic position and ocean color. Overall, the hurdle-GAM explained 30% of the variability of the training data set and 17% of the test data set.

Flathead sole distribution in commercial fisheries -- Flathead sole in the Aleutian Islands in commercial fisheries catch in fall was distributed in the east (Fig. 38). Ocean color, bottom temperature, and bottom depth were the most important variables determining probable suitable habitat of flathead sole (relative importance: 0.39, 0.26, 0.19). The AUC of the fall MaxEnt model was 0.96 for the training data and 0.91 for the test data. The model predicted suitable habitat of flathead was highest in the eastern AI (Fig. 38).

Like the fall, ocean color, bottom depth, and bottom temperature were the most important variables determining probability of suitable habitat of flathead sole (relative importance: 0.39, 0.22, and 0.14) in the winter model. The AUC of the winter MaxEnt model was 0.97 for the training data and 0.88 for the test data. 91% of the training data and 88% of the test data sets were correctly classified. The model predicted probable suitable habitat of flathead sole throughout the AI, but there was a clear clustering in the western, central and eastern AI around islands avoiding large passes (Fig. 39).

In the spring, ocean color and bottom depth were the most important variables determining probable suitable habitat of flathead sole (relative importance: 0.44 and 0.31). The AUC of the spring MaxEnt model was 0.94 for the training data and 0.86 for the test data. 86% of the training data and 86% of the test data were correctly classified. As with the winter, the model predicted probable suitable habitat of adult flathead sole throughout the AI, but there was a clear clustering in the western, central and eastern AI around islands avoiding large passes (Fig. 41).

Flathead sole essential fish habitat maps and conclusions -- Essential fish habitat for flathead sole eggs predicted by the modeling is concentrated in the eastern Aleutian Islands (Fig. 41). This likely reflects sampling biases.

In general, juvenile and adult flathead sole are predicted throughout the AI, but there are clear clusters in the western AI (Agattu Island), central (Atka Island) and the eastern AI (Unalaska Island) (Fig. 41). These similarities can be observed in both areas of high (areas of higher CPUE exist in the eastern, central, and western Aleutians) and low abundance (e.g., large passes).

The EFH predicted from commercial catches of flathead sole is distributed much the same as for the bottom trawl survey catches (Fig. 41). There does not appear to be much seasonal variability.

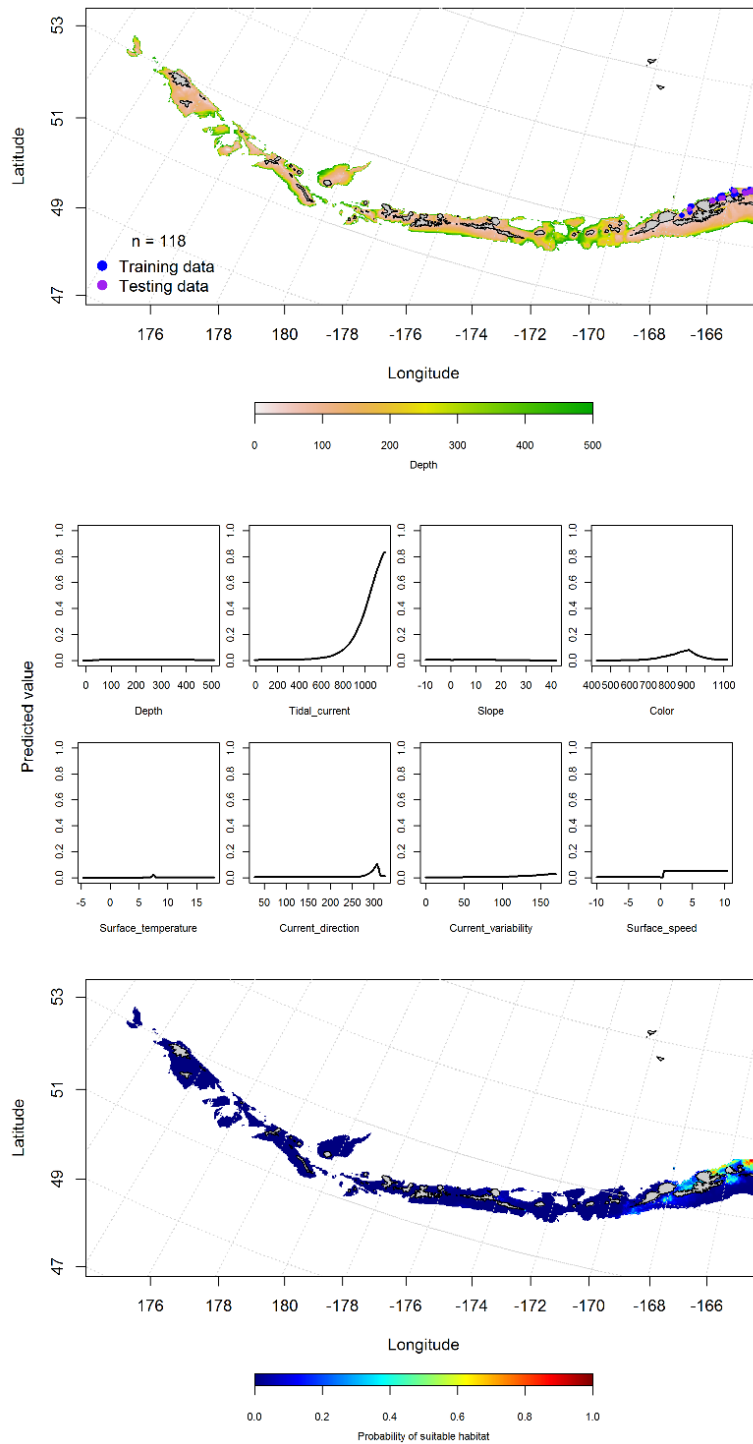


Figure 35. -- Observations of flathead sole eggs from the Aleutian Islands (top panel), relationships with environmental variables (middle panel) and predicted probability of suitable habitat based on EcoFOCI data and maximum entropy modeling.

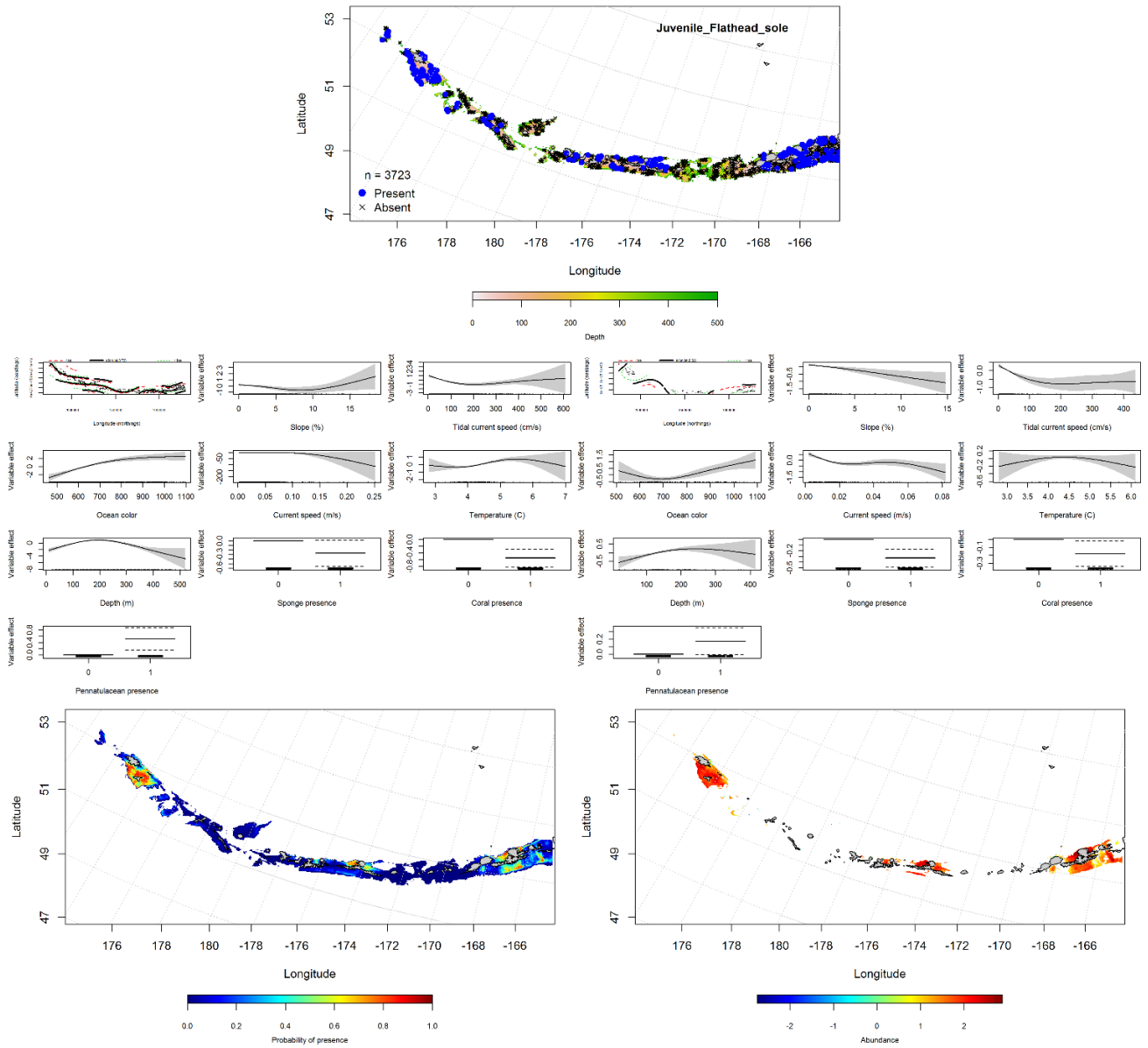


Figure 36. -- Distribution of catches of juvenile flathead sole in bottom trawl surveys (top middle panel), significant relationships between presence-absence and CPUE and environmental variables for the best-fitting generalized additive model of juvenile flathead sole (middle left and right panels), and predicted probability of presence and abundance of juvenile flathead sole based on the models (bottom left and right panels).

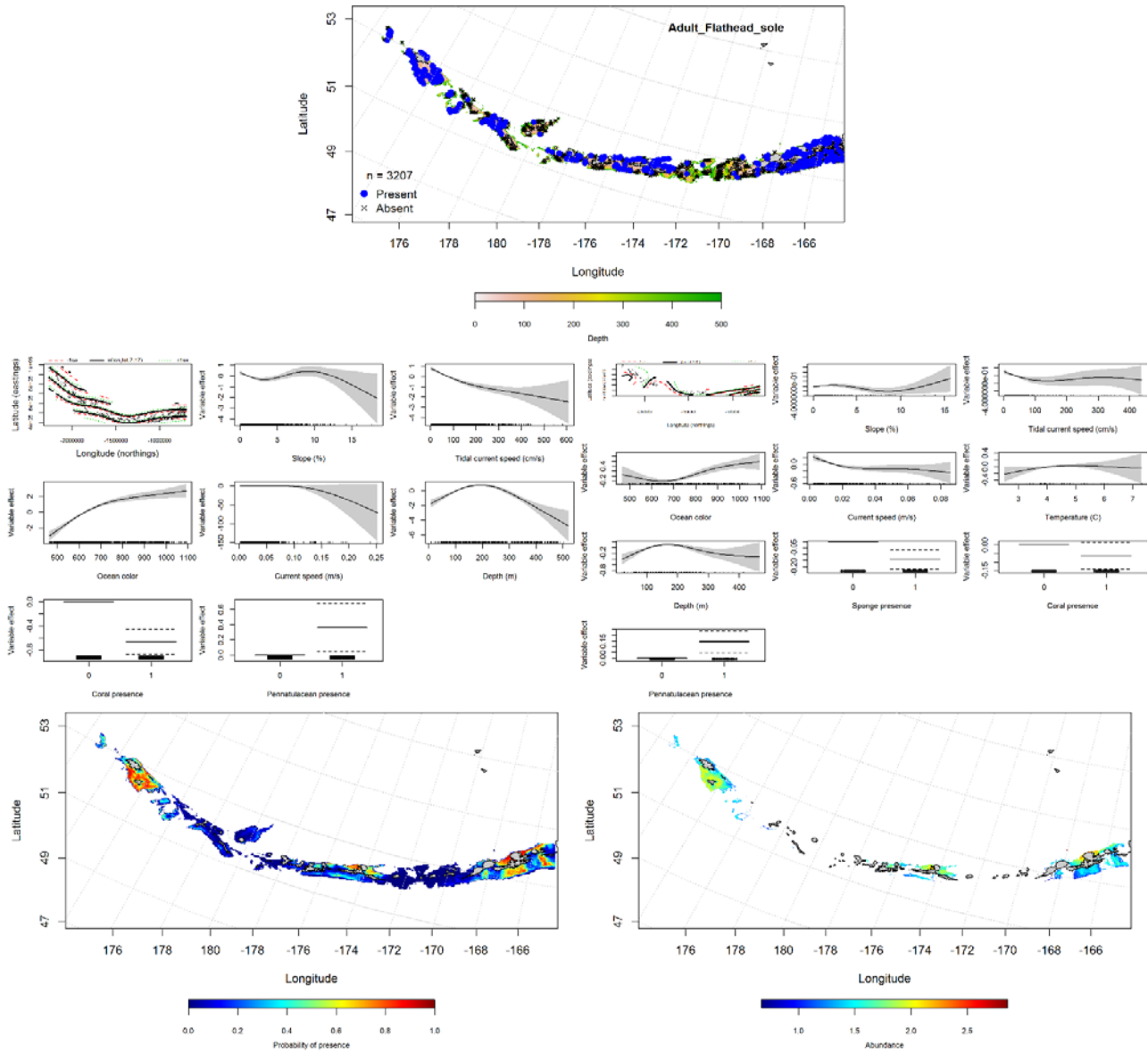


Figure 37. -- Distribution of catches of adult flathead sole in bottom trawl surveys (top middle panel), significant relationships between presence-absence and CPUE and environmental variables for the best-fitting generalized additive model of adult flathead sole (middle left and right panels), and predicted probability of presence and abundance of adult flathead sole based on the models (bottom left and right panels).

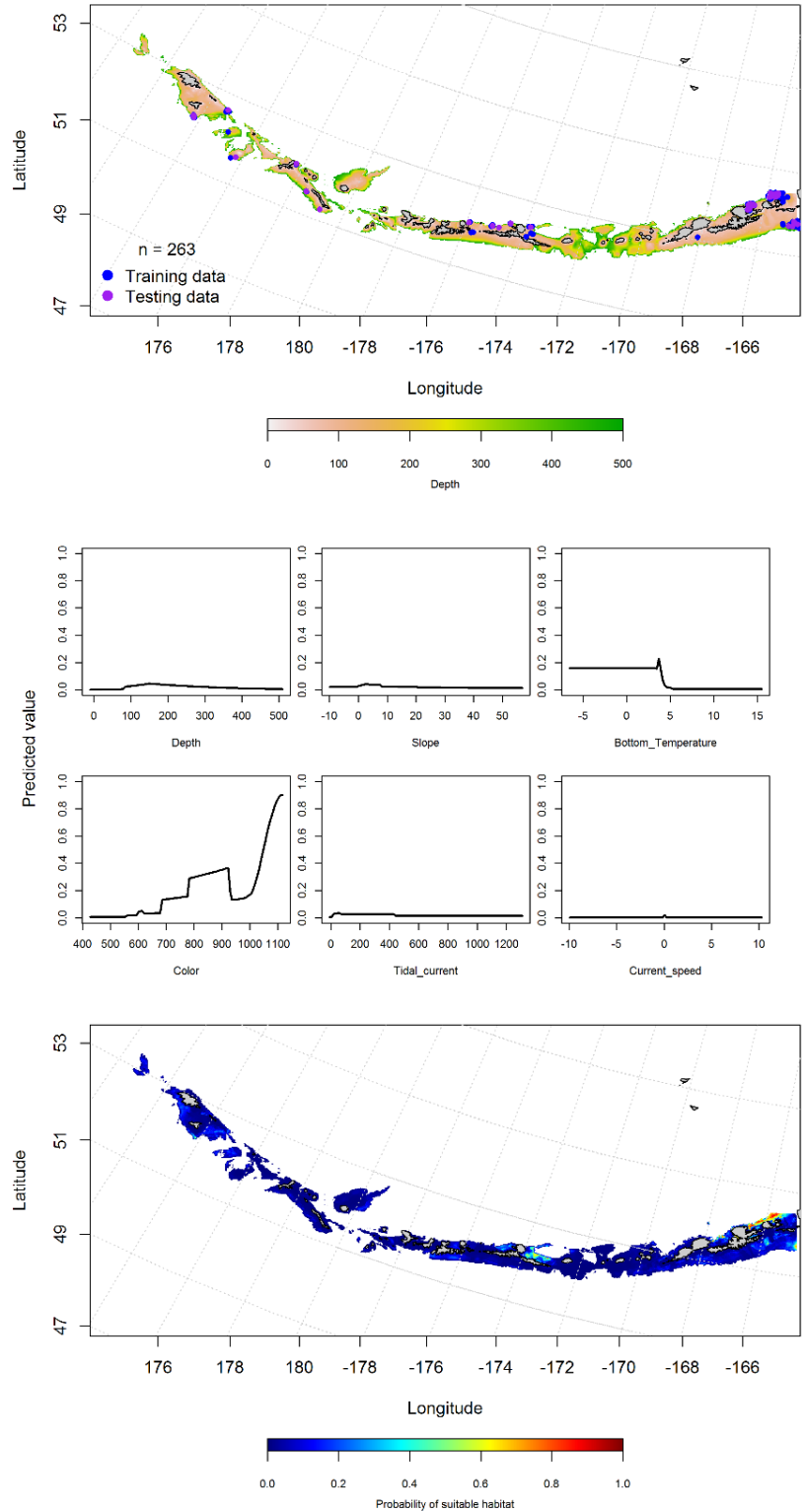


Figure 38. -- Locations of fall (September-November) commercial fisheries catches of flathead sole (top panel), relationships between probability of presence and environmental variables for the maximum entropy model (middle panels), and predicted probability of suitable habitat for flathead sole based on the model (bottom panel).

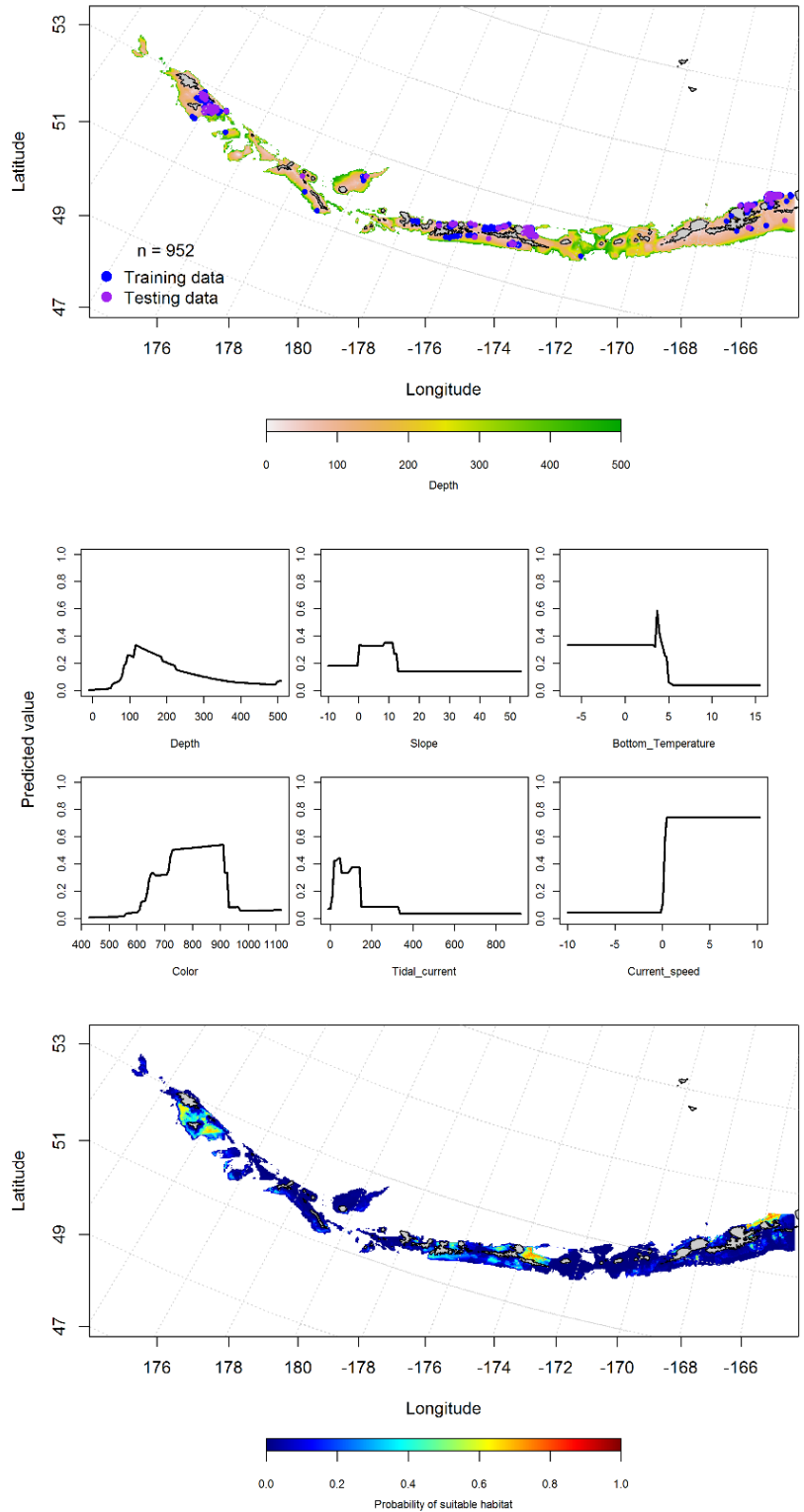


Figure 39. -- Locations of winter (December-February) commercial fisheries catches of flathead sole (top panel), relationships between probability of presence and environmental variables for the maximum entropy model (middle panels), and predicted probability of suitable habitat for flathead sole based on the model (bottom panel).

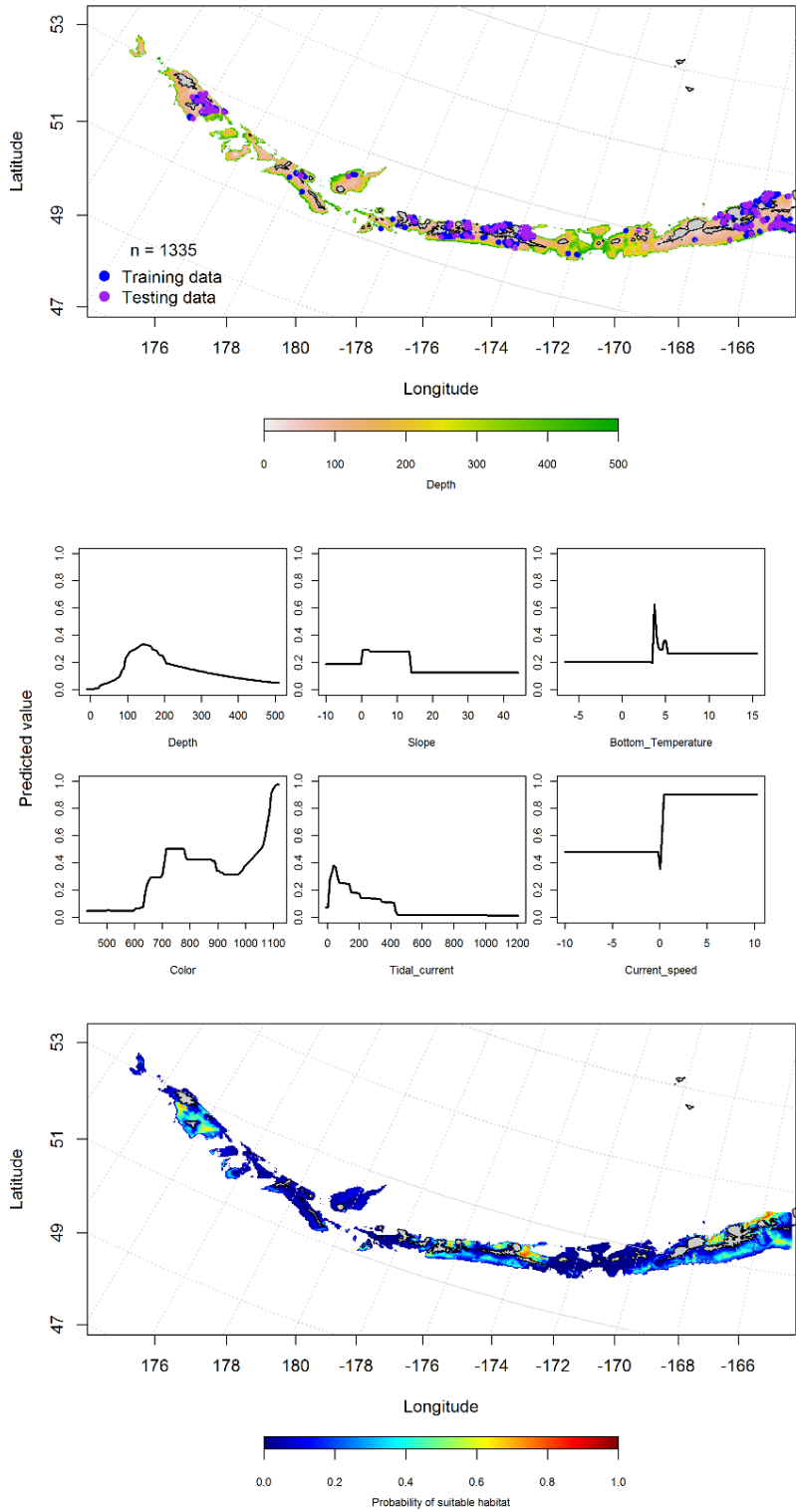


Figure 40. -- Locations of spring (March-May) commercial fisheries catches of flathead sole (top panel), relationships between probability of presence and environmental variables for the maximum entropy model (middle panels), and predicted probability of suitable habitat for flathead sole based on the model (bottom panel).

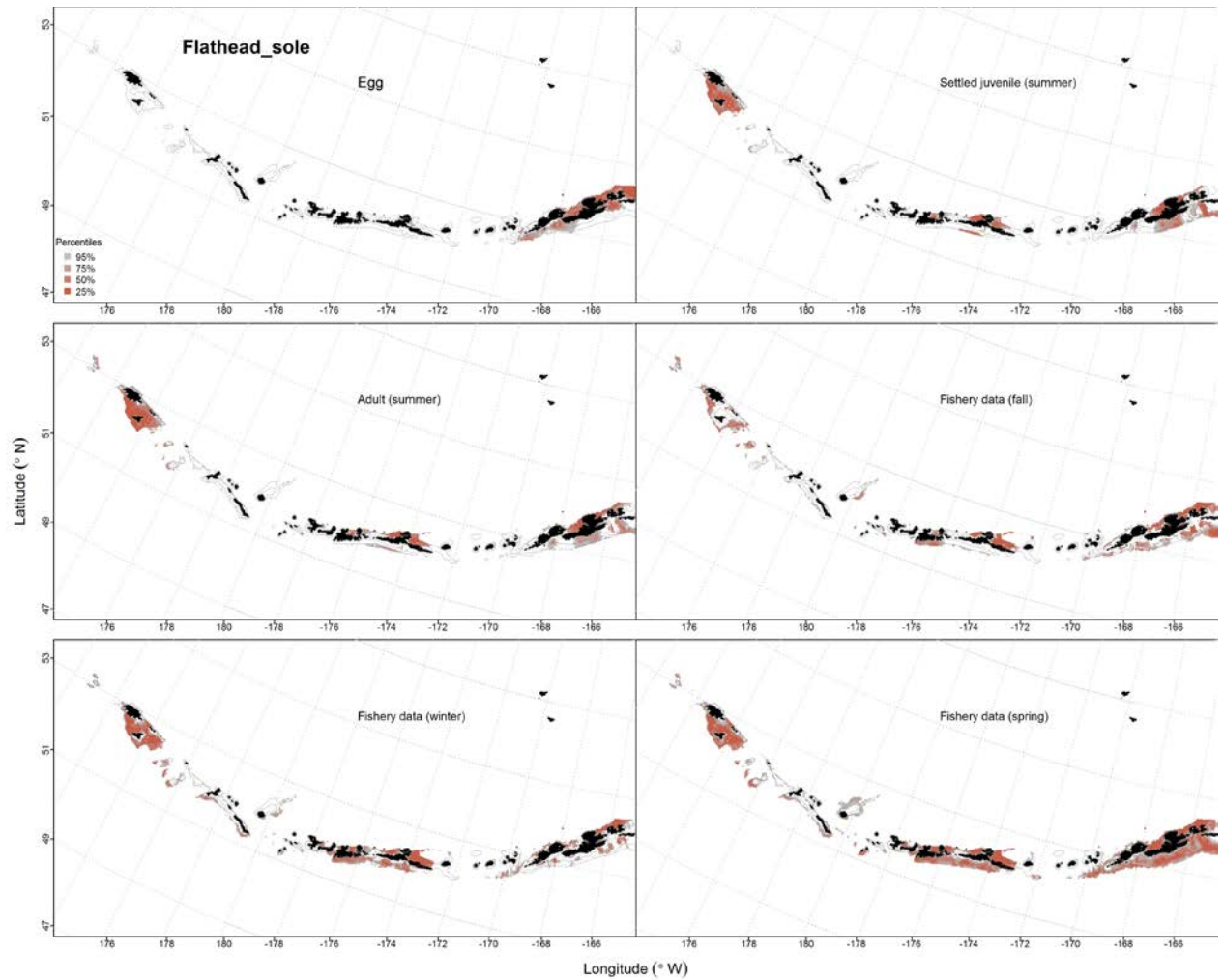


Figure 41. -- Predicted EFH quantiles for flathead sole life history stages based on species distribution modeling. Egg stage is based on EcoFOCI data. Settled juvenile and summer adult stages are based on bottom trawl survey data, while seasonal stages (winter, spring, fall) are from commercial fishery data.

Rex Sole (*Glyptocephalus zachirus*)

Early life history stages of rex sole -- There were only 65 instances of rex sole eggs observed in the FOCI database (Fig. 42), all in the eastern Aleutian Islands. The MaxEnt model of rex sole eggs indicated that current direction, surface temperature and ocean color were the most important variables determining egg distribution. The AUC for the model was 0.99 for the training data and 0.85 for the testing data. The model predicted rex sole eggs suitable habitat was more likely to occur in Unimak Pass and near Unalaska Island (Fig. 42). There were two observations of larval rex sole in the eastern AI.

Juvenile and adult rex sole distribution in the bottom trawl survey -- Juvenile rex sole were modeled using a hurdle-GAM. The PA GAM predicted a higher probability of presence in the eastern Aleutian Islands (Fig. 43). The PA GAM indicated that bottom depth, ocean color, and tidal current speed were the most important factors controlling juvenile rex sole distribution. The AUC was 0.82 for the training data and 0.81 for the test data. The important variables in the CPUE GAM were depth, slope and geographic location. Overall, the hurdle model explained 28% of the variability in training data and 25% in test data. The highest predicted juvenile rex sole abundance was near Unalaska Island (Fig. 43).

Adult rex sole were similarly distributed to juvenile rex sole in the AI (higher abundance in deeper areas of the eastern Aleutian Islands) (Fig. 44). The best-fitting GAM model indicated that bottom depth, surface ocean color, and geographic location were the most important factors controlling adult rex sole. The model explained 31% of the variability in the training data set and 31% of the variability in the test data set.

Rex sole distribution in commercial fisheries -- Distribution of adult rex sole in the Aleutian Islands in commercial fisheries catches was consistent throughout all seasons. In the fall, bottom temperature, ocean color, and depth were the most important variables determining probability of suitable habitat of rex sole. The AUC of the fall MaxEnt model was 0.98 for the training data and 0.95 for the test data. 91% of the training data and 95% of the cases in the test data were predicted correctly. The model predicted suitable habitat for rex sole in deeper waters across the Aleutian Islands (Fig. 45).

In the winter, ocean color, bottom depth, and bottom temperature were the most important variables determining probable suitable habitat of adult rex sole. The AUC of the winter MaxEnt model was 0.98 for the training data and 0.84 for the test data. 93% of the cases in the training data set, and 84% of the test data were predicted correctly. The model predicted suitable habitat was most abundant near Atka Islands and in northern Unimak Pass (Fig. 46).

Ocean color, bottom depth, and current speed were the most important variables determining probable suitable habitat of rex sole in the spring. The AUC of the spring MaxEnt model was 0.95 for the training data and 0.82 for the test data. 86% of the training data set and 82% of the test data set were correctly classified. The model predicted suitable habitat of rex sole in the spring was highest in the eastern AI (Fig. 47).

Rex sole essential fish habitat maps and conclusions -- Essential fish habitat for rex sole eggs was predicted to occur only in the eastern Aleutian Islands around Umnak and Unalaska islands (Fig. 48). Juvenile and adult rex sole essential fish habitat predicted by the modeling was distributed differently throughout the Aleutian Islands (Fig. 48). Juveniles were more sparsely distributed, with higher predicted abundance in the eastern AI. Adult rex sole were more widely distributed throughout the AI than the juveniles. Predicted fall, winter, and spring distributions

from commercial catches were similarly across seasons, but slightly more concentrated in the eastern AI in the spring. Areas with large passes were predicted to have low abundance in all seasons (Fig. 48).

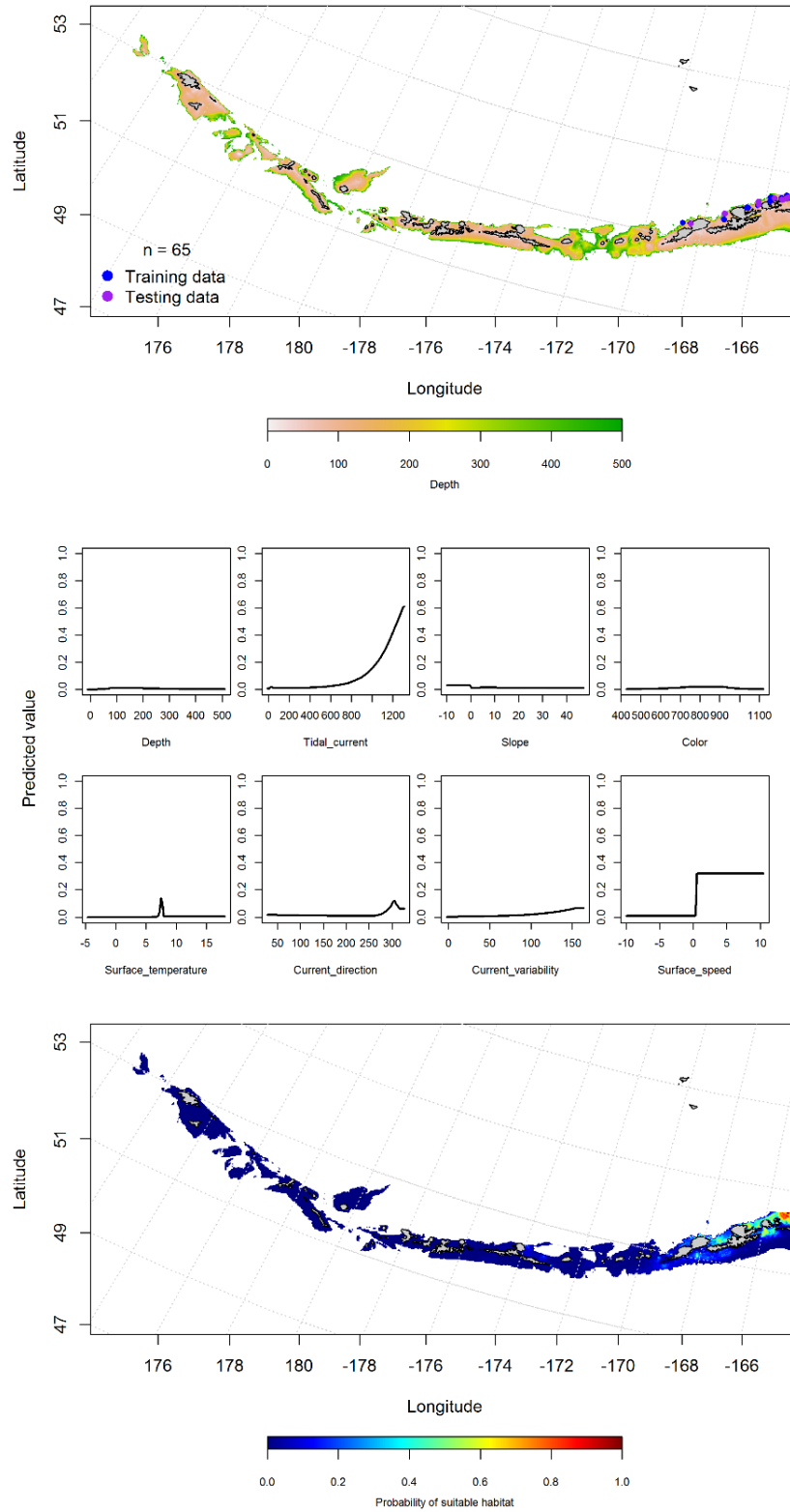


Figure 42. -- Observations of rex sole eggs from the Aleutian Islands (top panel), relationships with environmental variables (middle panel) and predicted probability of suitable habitat based on EcoFOCI data and maximum entropy modeling.

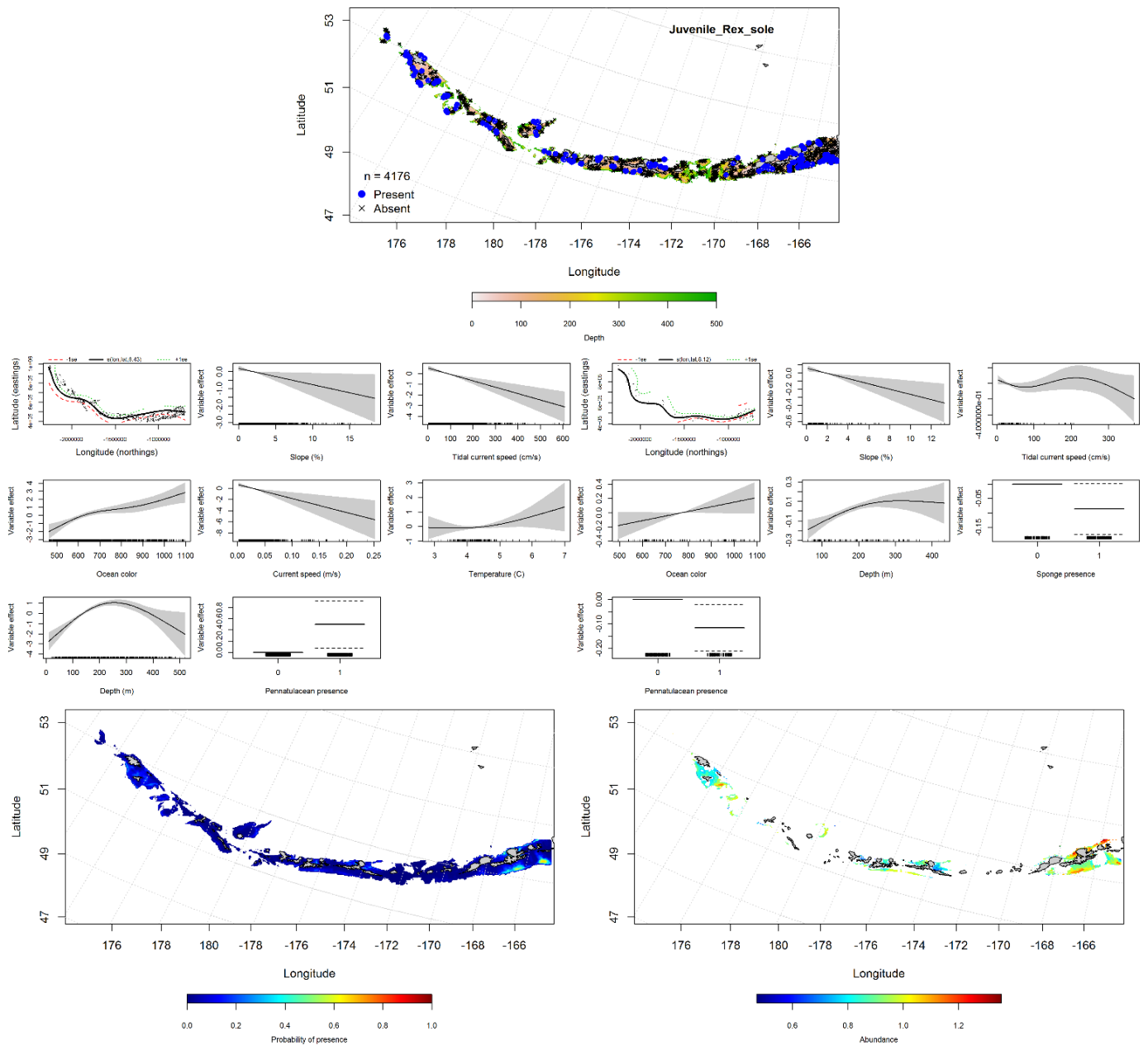


Figure 43. -- Distribution of catches of juvenile rex sole in bottom trawl surveys (top middle panel), significant relationships between presence-absence and CPUE and environmental variables for the best-fitting generalized additive model of juvenile rex sole (middle left and right panels), and predicted probability of presence and abundance of juvenile rex sole based on the models (bottom left and right panels).

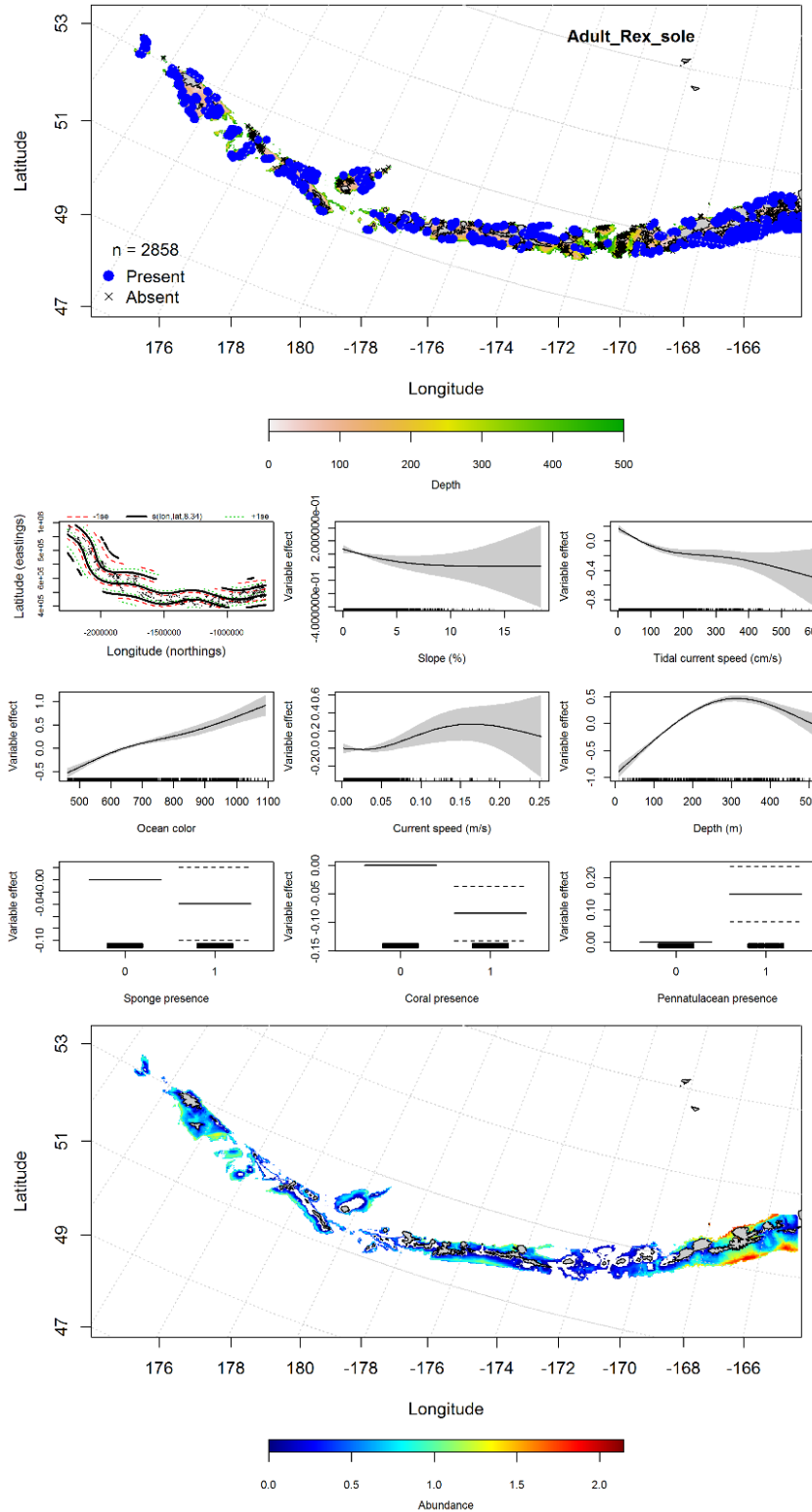


Figure 44. -- Distribution of catches of adult rex sole in bottom trawl surveys (top panel), relationships between presence and environmental variables for the maximum entropy model of adult rex sole (middle panels), and predicted probability of suitable habitat for adult rex sole based on the model (bottom panel).

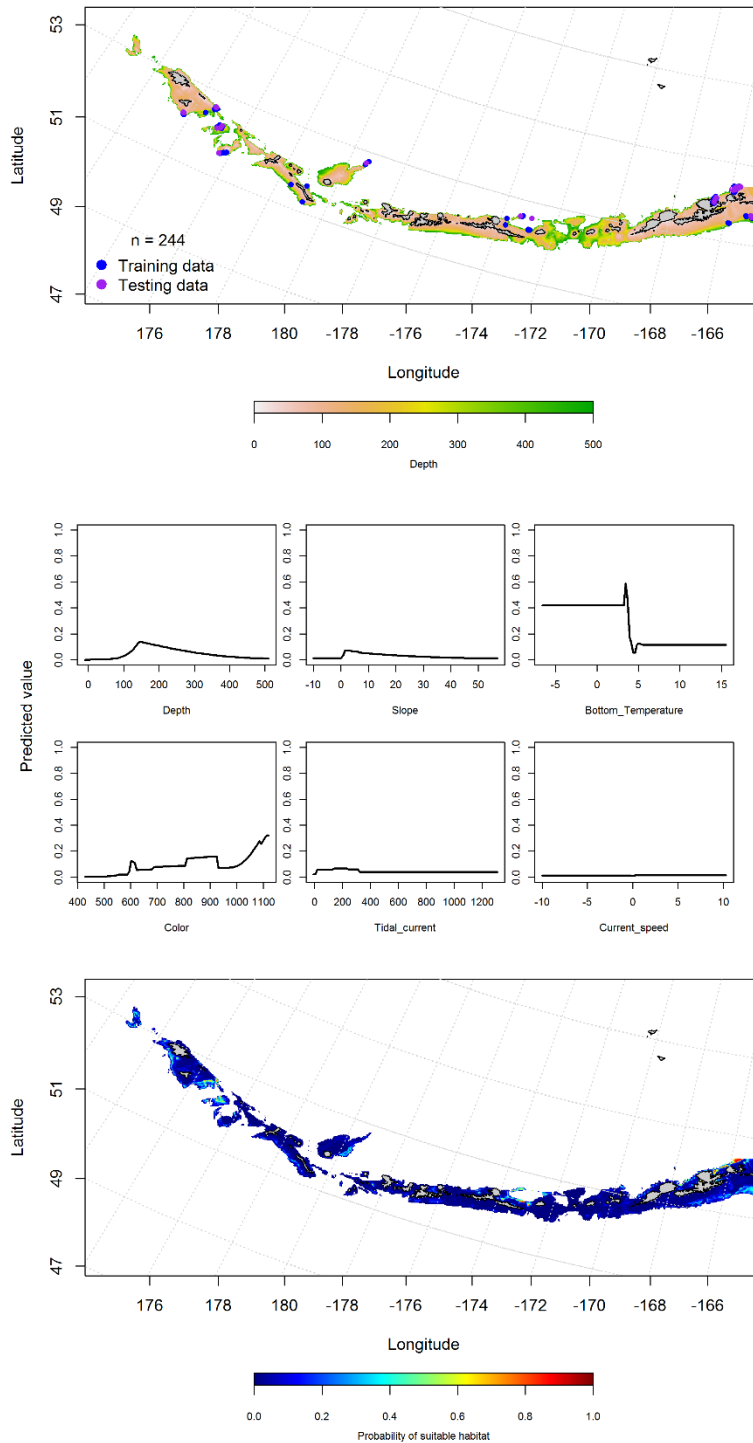


Figure 45. -- Locations of fall (September-November) commercial fisheries catches of rex sole (top panel), relationships between probability of presence and environmental variables for the maximum entropy model (middle panels), and predicted probability of suitable habitat for rex sole based on the model (bottom panel).

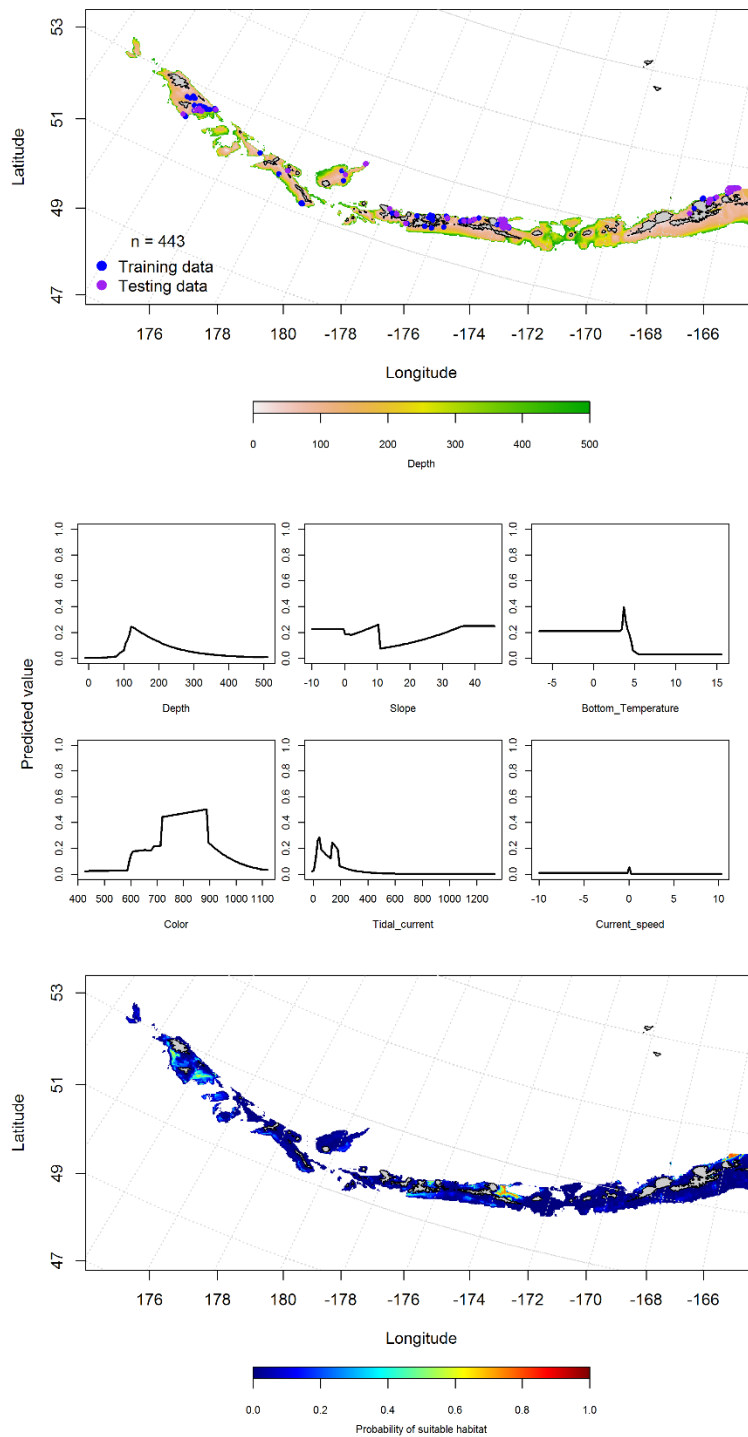


Figure 46. -- Locations of winter (December-February) commercial fisheries catches of rex sole (top panel), relationships between probability of presence and environmental variables for the maximum entropy model (middle panels), and predicted probability of suitable habitat for rex sole based on the model (bottom panel).

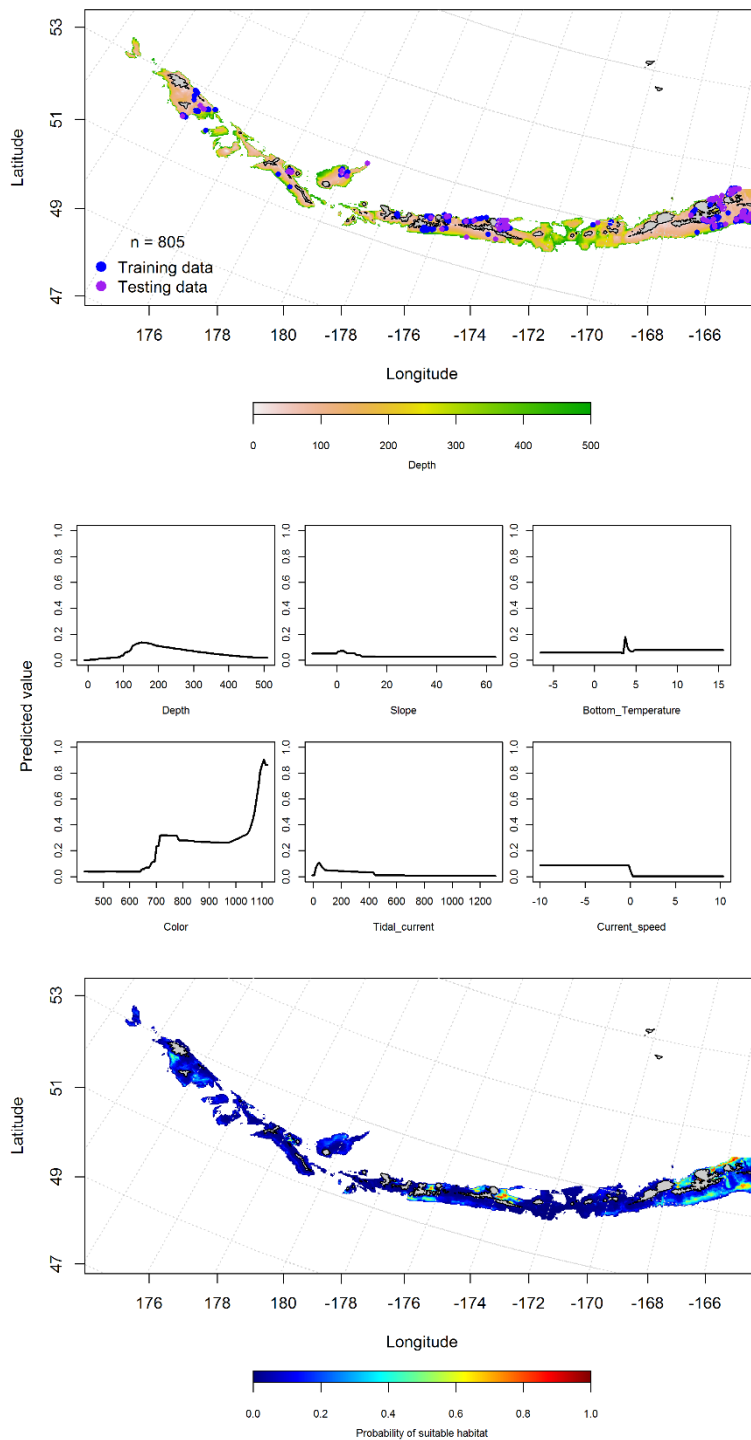


Figure 47. -- Locations of spring (March-May) commercial fisheries catches of rex sole (top panel), relationships between probability of presence and environmental variables for the maximum entropy model (middle panels), and predicted probability of suitable habitat for rex sole based on the model (bottom panel).

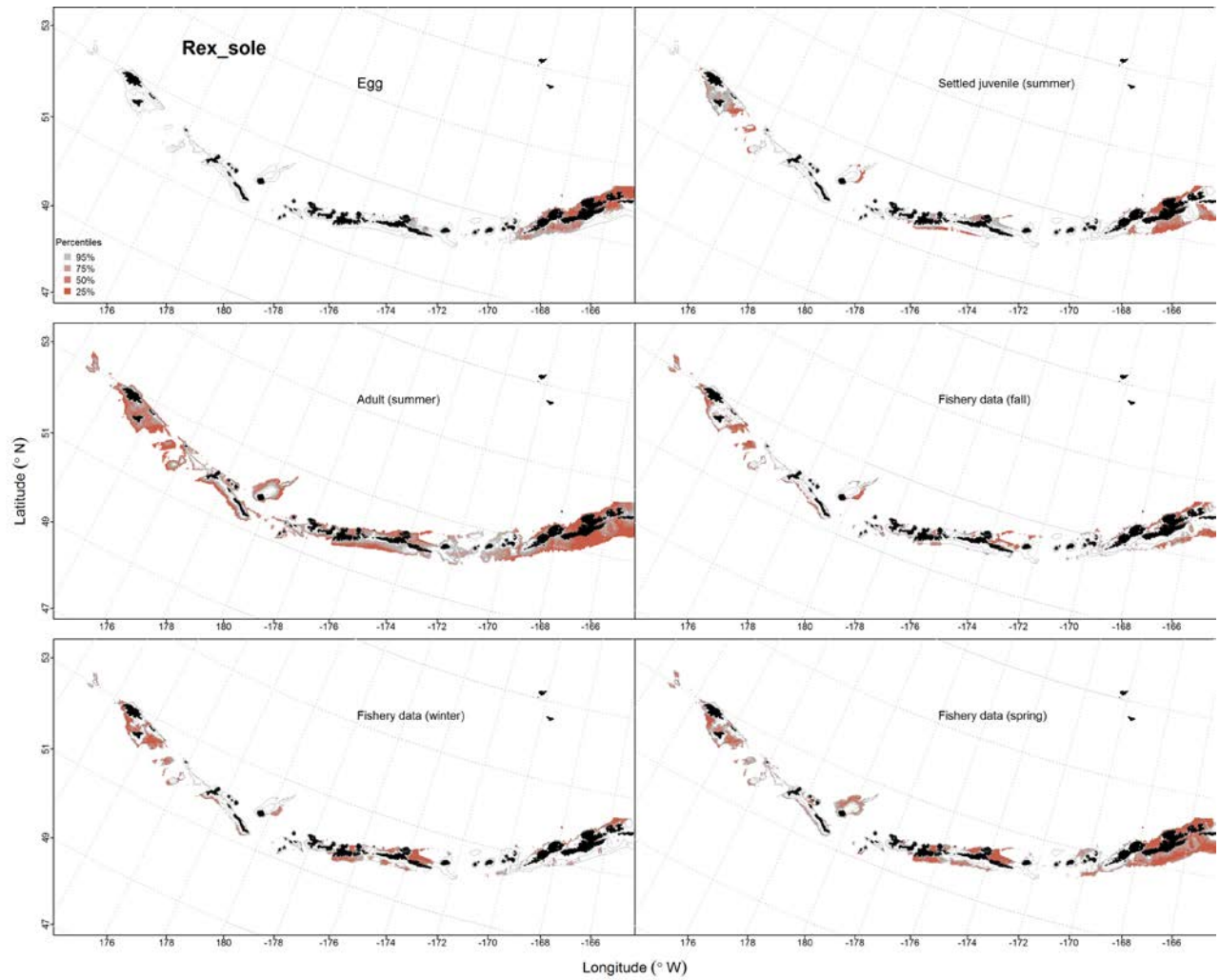


Figure 48. -- Predicted EFH quantiles for rex sole life history stages based on species distribution modeling. Egg stage is based on EcoFOCI data. Settled juvenile and summer adult stages are based on bottom trawl survey data, while seasonal stages (winter, spring, fall) are from commercial fishery data.

Dover Sole (*Microstomus pacificus*)

Early life history stages of Dover sole -- There were only 10 instances of Dover sole eggs and one instance of Dover sole larvae observed in the EcoFOCI database, therefore, there was no analysis.

Juvenile and adult Dover sole distribution in the bottom trawl survey -- Juvenile and adult Dover sole were modeled using a MaxEnt model. The model predicted probability of suitable habitat throughout the AI in deeper areas of the shelf and slope (Fig. 49). The model predicted suitable habitat at depths from 100-400 m and a low tidal currents. The AUC for the model was 0.88 for the training data (78% correctly classified) and 0.73 for the test data (73% correctly classified).

Depth, temperature, and current speed were the most important factors determining the probability of adult Dover sole suitable habitat (Fig. 50). The model AUC was 0.91 for the training data (83% correctly classified) and 0.84 for the test data (84% correctly classified). The probability of suitable habitat for adult Dover sole was highest in the deeper areas of the survey, especially in some of the deeper offshore banks (Stalemate Bank, Petrel Bank, Tahoma Reef)(Fig. 50).

The CPUE GAM model found that current speed was the most important variables that explained the distribution of adult Dover sole. The model explained 19% of the variability in training data set and 16% of the test data in CPUE in the bottom trawl survey data. The predicted abundance was similar to the presence/absence GAM (distributed throughout the AI) (Fig. 50).

Dover sole distribution in commercial fisheries -- There were only 28 and 15 instances of Dover sole observed in the commercial fisheries database in winter and spring. There were 56 fishery catches of Dover sole in the spring, so this was the only season modeled. In the spring, bottom depth, current speed, and ocean color were the most important variables determining probable suitable habitat of Dover sole. The AUC of the spring MaxEnt model was 0.93 for the training data and 0.82 for the test data. 82% of the training data and test data were predicted correctly. The model predicted suitable habitat for Dover sole at low levels throughout the deeper areas of the AI in the spring (Fig. 51).

Dover sole essential fish habitat maps and conclusions -- In general, juvenile and adult Dover sole share similar predicted EFH distributions across the Aleutian Islands (Fig. 52). Dover sole habitat tended to occur on offshore banks and in deeper areas of the shelf and slope. This was also consistent with the fishery data in the spring.

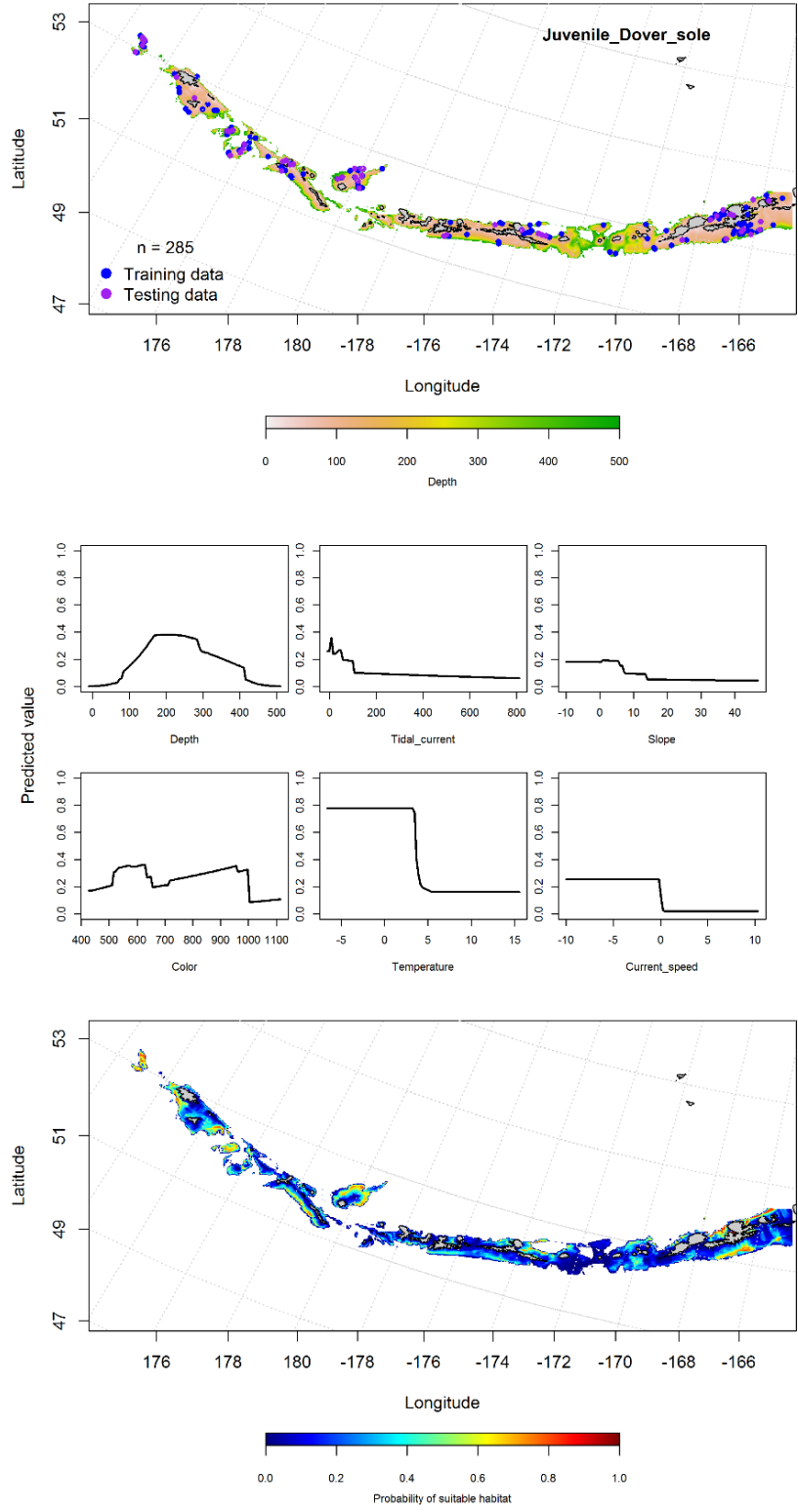


Figure 49. -- Distribution of catches of juvenile Dover sole in bottom trawl surveys (top panel), relationships between presence and environmental variables for the maximum entropy model of juvenile Dover sole (middle panels), and predicted probability of suitable habitat for juvenile Dover sole based on the model (bottom panel).

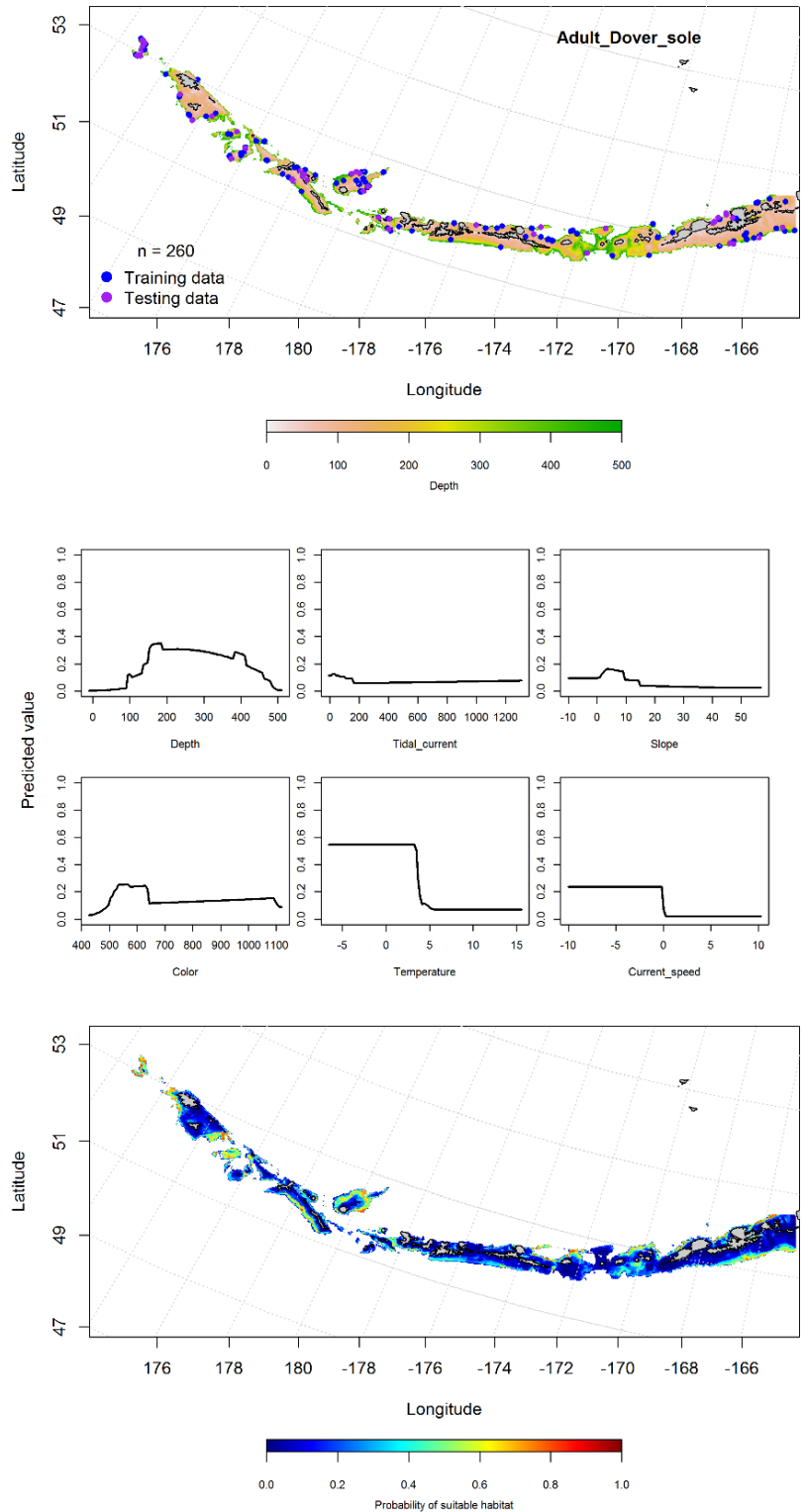


Figure 50. -- Distribution of catches of adult Dover sole in bottom trawl surveys (top panel), relationships between presence and environmental variables for the maximum entropy model of adult Dover sole (middle panels), and predicted probability of suitable habitat for adult Dover sole based on the model (bottom panel).

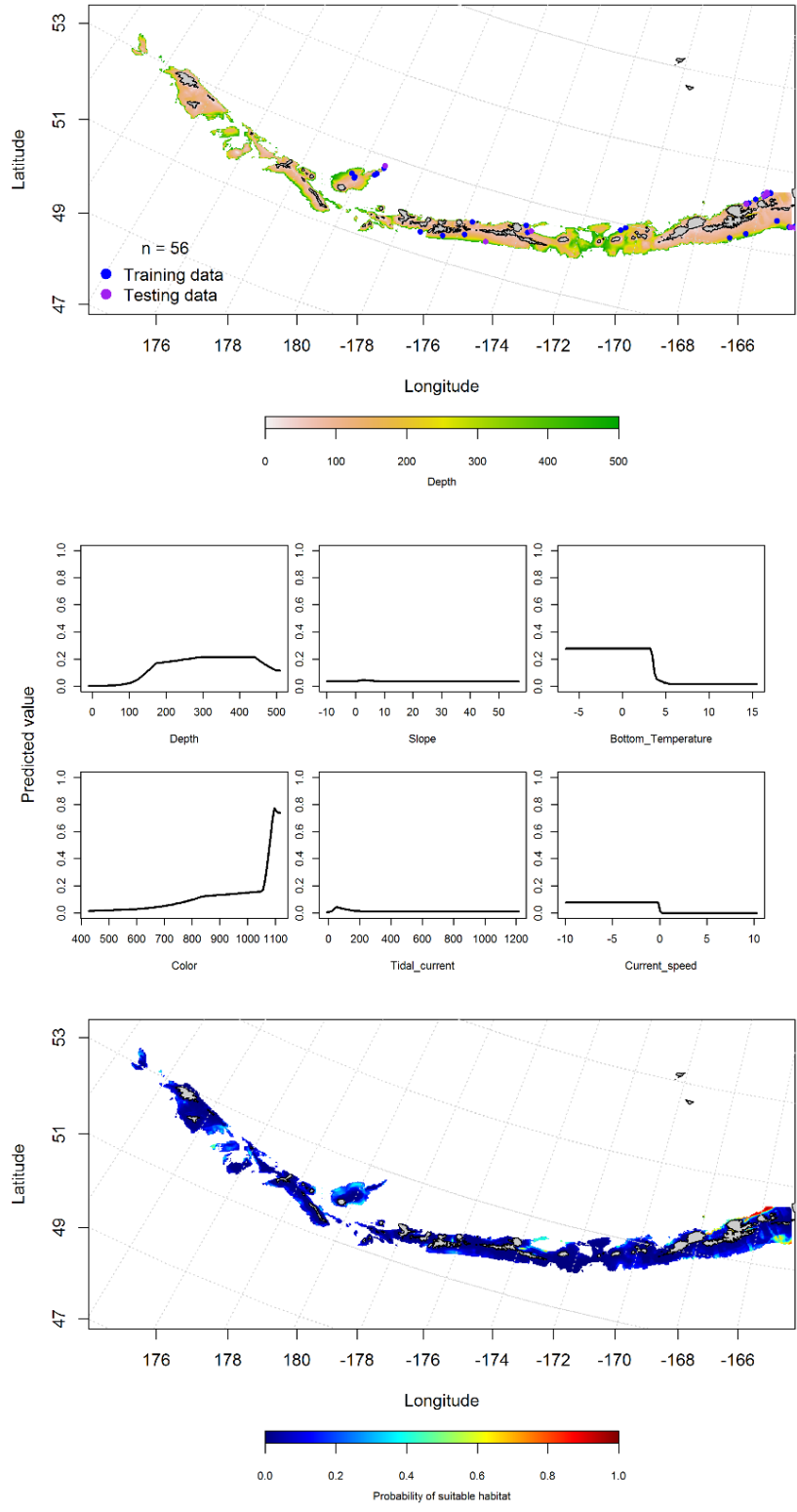


Figure 51. -- Locations of spring (March-May) commercial fisheries catches of Dover sole (top panel), relationships between probability of presence and environmental variables for the maximum entropy model (middle panels), and predicted probability of suitable habitat for Dover sole based on the model (bottom panel).

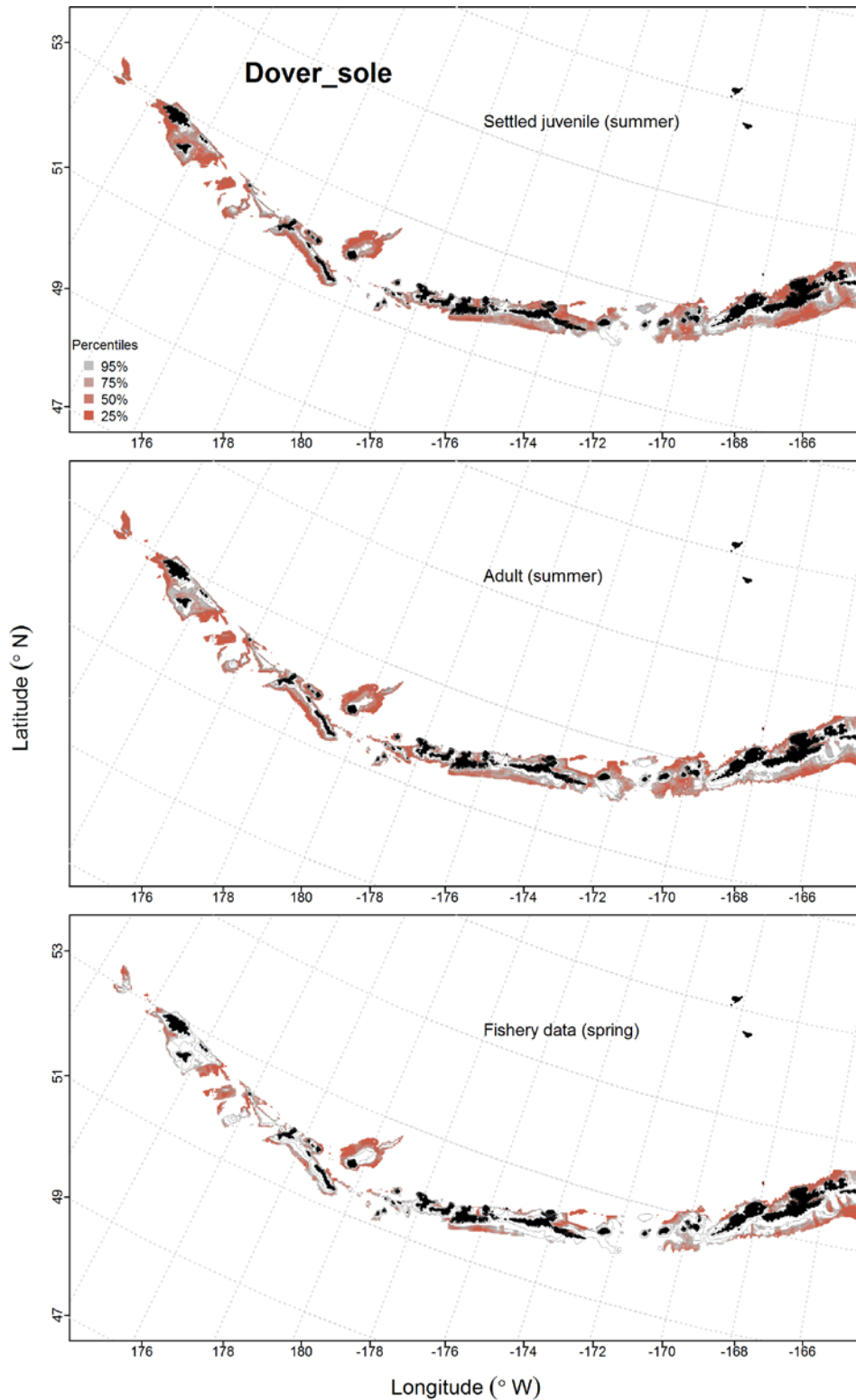


Figure 52. -- Predicted EFH quantiles for Dover sole life history stages based on species distribution modeling. Settled juvenile and summer adult stages are based on bottom trawl survey data, while seasonal stages (spring) are from commercial fishery data.

Roundfishes

Atka Mackerel (*Pleurogrammus monopterygius*)

Early life history stages of Atka mackerel -- Atka mackerel eggs were distributed throughout the AI (Fig. 53). All observations are taken from underwater camera work (Lauth et al. 2007), rather than the EcoFOCI database. Because Atka mackerel are demersal spawners/nesters, the same variables regularly used for the GAM models were used in this MaxEnt model. Bottom depth, ocean color and coral presence were the most important variables in modeling egg suitable habitat (Fig. 53). The AUC for the training data was 0.91, and 0.85 using the test data. 80% of the training data and 85% of the test data sets were correctly classified. The model predicted Atka mackerel egg probable suitable habitat throughout the AI in shallow waters, but especially near Samalga Pass and Seguam Pass (Fig. 53). There were only 11 instances of Atka mackerel larvae observed in the EcoFOCI database.

Juvenile and adult Atka mackerel distribution in the bottom trawl survey -- A hurdle-GAM predicting the presence absence (PA GAM) of juvenile Atka mackerel had an AUC of 0.89 for the training data and 0.87 for the testing data. The most important variables determining presence or absence were depth, geographic position and tidal current speed (Fig. 54). Juveniles were predicted to be distributed throughout the AI, though the highest predicted probability of presence was west of Kiska Island (Fig. 54). The CPUE-GAM indicated slope geographic location and tidal current speed were the most important variables explaining patterns in juvenile Atka mackerel abundance. Overall the hurdle-GAM explained 25% of the variability of the training data set and 15% of the test data set. The areas of predicted highest abundance were in the western AI (Fig. 54).

A GAM predicting the abundance of adult Atka mackerel explained 25% of the training and test data set variability in CPUE in the bottom trawl survey. Bottom depth, geographic location, slope and tidal current speed were the most important variables explaining the distribution of adult Atka mackerel. Adult Atka mackerel were distributed throughout the AI (Fig. 55).

Atka mackerel distribution in commercial fisheries -- Distribution of Atka mackerel in the Aleutian Islands in commercial fisheries catches was generally consistent throughout all seasons. In the fall, depth, temperature, and ocean color were the most important variables determining probability of suitable habitat of Atka mackerel. The AUC of the fall MaxEnt model was 0.93 for the training data and 0.84 for the test data. 85% of the cases in the training data set and 84% of the cases in the test data set were predicted correctly. The model predicted probable suitable habitat of Atka mackerel catches throughout the AI, though less abundant in areas with large passes (Fig. 56).

In the winter, depth, ocean color, and temperature were the most important variables determining the probability of suitable habitat of Atka mackerel (Fig. 57). The AUC of the winter MaxEnt model was 96% for the training data and 88% for the test data. 89% of the cases in both the training data sets and 88% in the test data were predicted correctly. As with the fall, the model predicted probable suitable habitat of Atka mackerel catches throughout the AI, though less abundant in areas with large passes (Fig. 57).

In the spring, depth and ocean color were the most important variables determining probable suitable habitat of Atka mackerel. The AUC of the spring MaxEnt model was 91% for the training data and 81% for the test data. The model correctly classified 83% of the training

data and 81% of the test data sets. As with the fall and winter, the model predicted probable suitable habitat of Atka mackerel catches throughout the AI (Fig. 58).

Atka mackerel essential fish habitat maps and conclusions -- Predicted EFH for Atka mackerel eggs was highest in the western and central AI (Fig. 59). Adult Atka mackerel are distributed throughout the AI whereas juveniles have a more limited predicted EFH in the western AI (Fig. 59). There were no seasonal differences in Atka mackerel EFH. Adults were distributed similarly through the Aleutian Islands (Fig. 59).

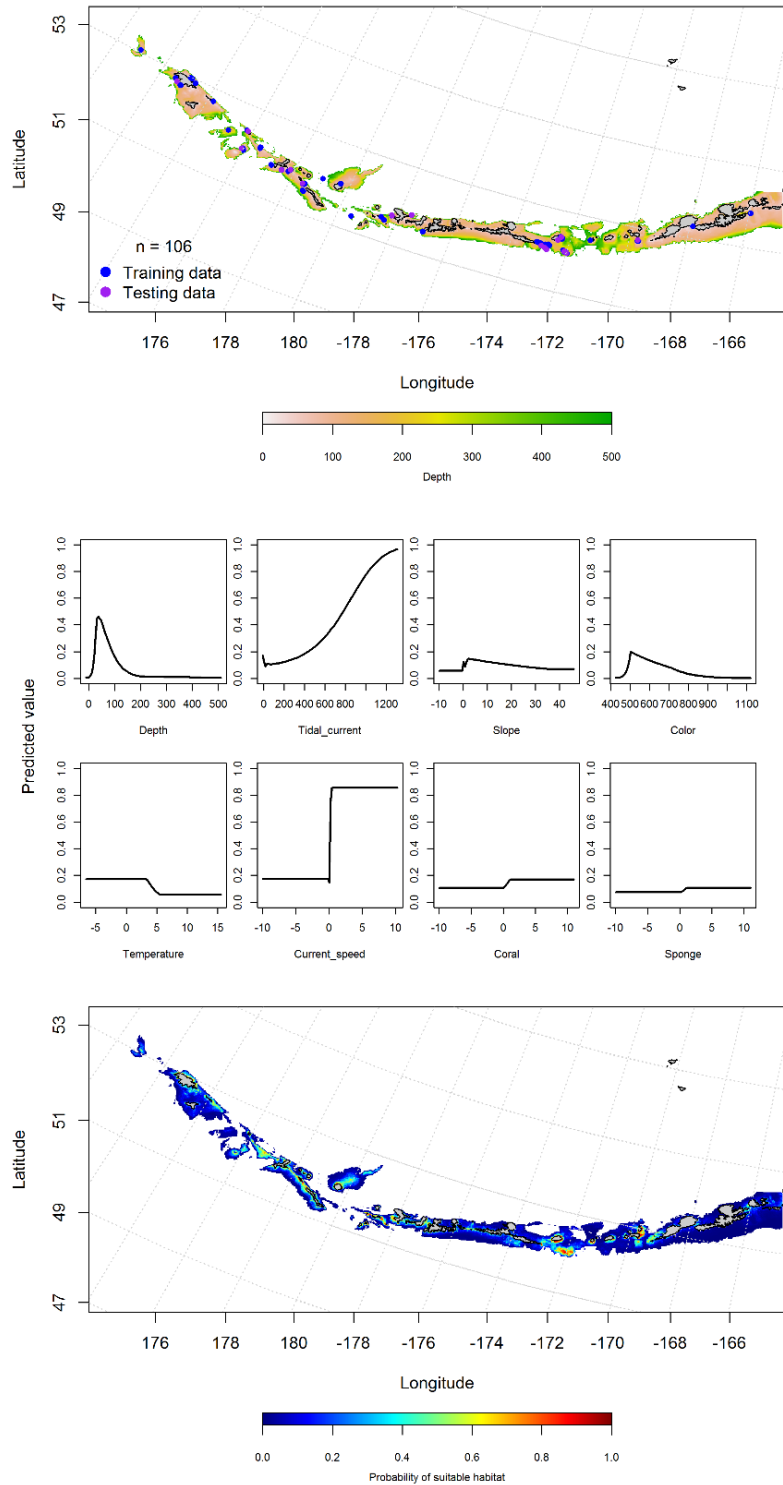


Figure 53. -- Observations of Atka mackerel eggs from the Aleutian Islands from underwater camera surveys (Lauth et al. 2007; top panel), relationships of suitable habitat and environmental variables (middle panels), and predicted probability of presence of suitable habitat for Atka mackerel eggs from MaxEnt modeling of the Aleutian Islands (bottom panel).

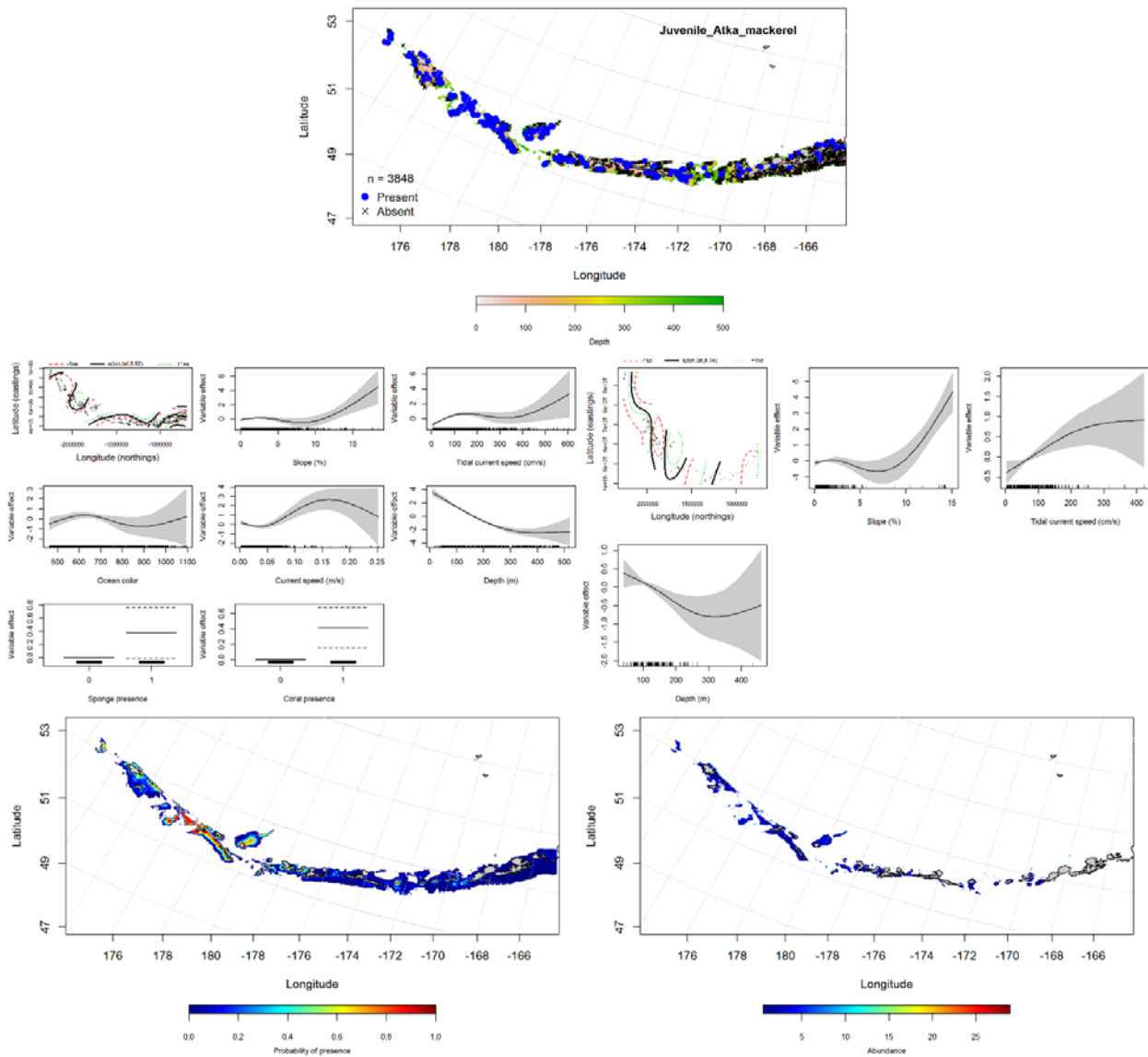


Figure 54. -- Distribution of catches of juvenile Atka mackerel in bottom trawl surveys (top middle panel), significant relationships between presence-absence and CPUE and environmental variables for the best-fitting generalized additive model of juvenile Atka mackerel (middle left and right panels), and predicted probability of presence and abundance of juvenile Atka mackerel based on the models (bottom left and right panels).

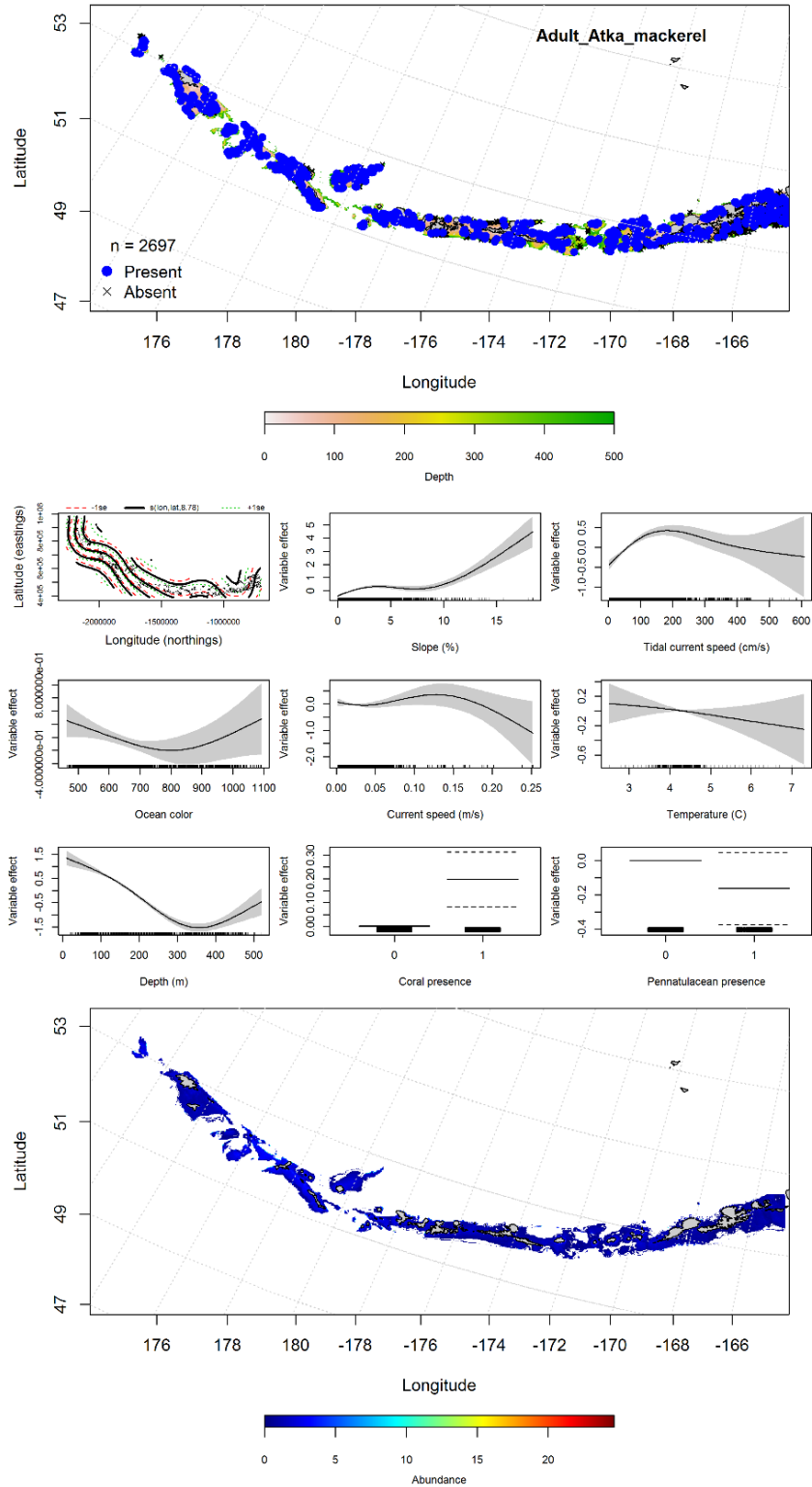


Figure 55. -- Distribution of catches of adult Atka mackerel in bottom trawl surveys (top panel), relationships between presence and environmental variables for the maximum entropy model of adult Atka mackerel (middle panels), and predicted probability of suitable habitat for adult Atka mackerel based on the model (bottom panel).

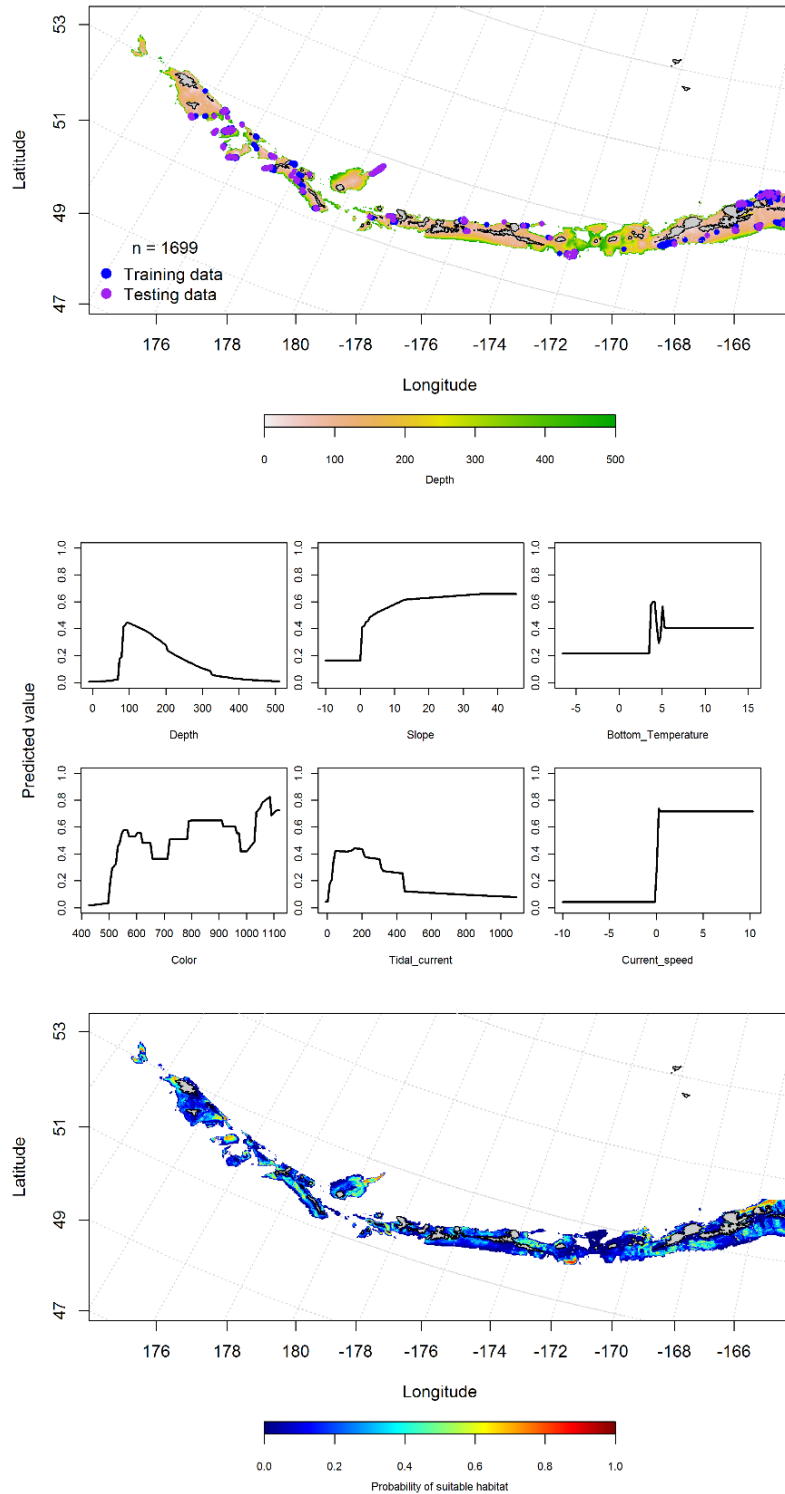


Figure 56. -- Locations of fall (September-November) commercial fisheries catches of adult Atka mackerel (top panel), relationships between probability of presence and environmental variables for the maximum entropy model (middle panels), and predicted probability of suitable habitat for Atka mackerel based on the model (bottom panel).

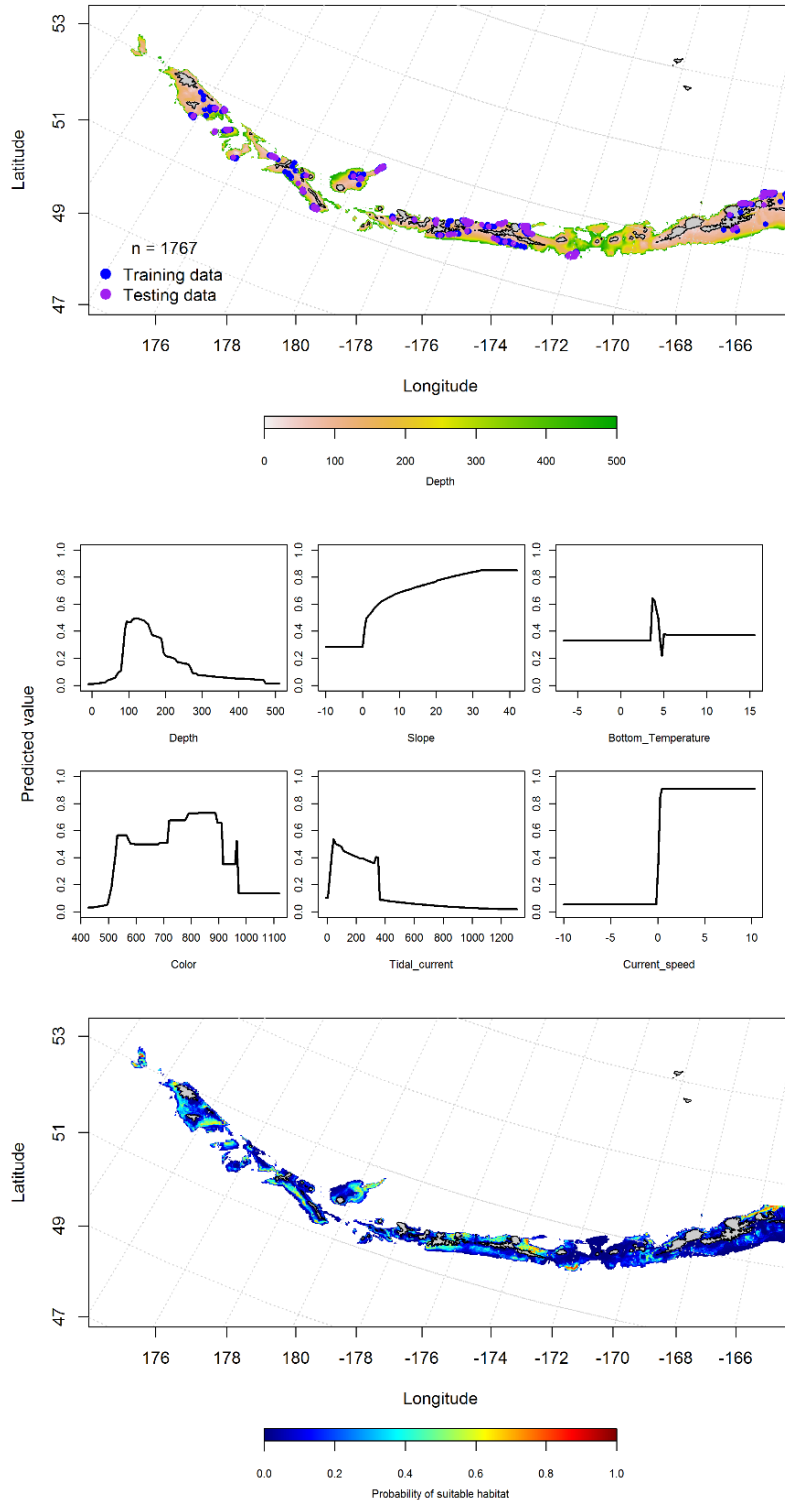


Figure 57. -- Locations of winter (December-February) commercial fisheries catches of adult Atka mackerel (top panel), relationships between probability of presence and environmental variables for the maximum entropy model (middle panels), and predicted probability of suitable habitat for Atka mackerel based on the model (bottom panel).

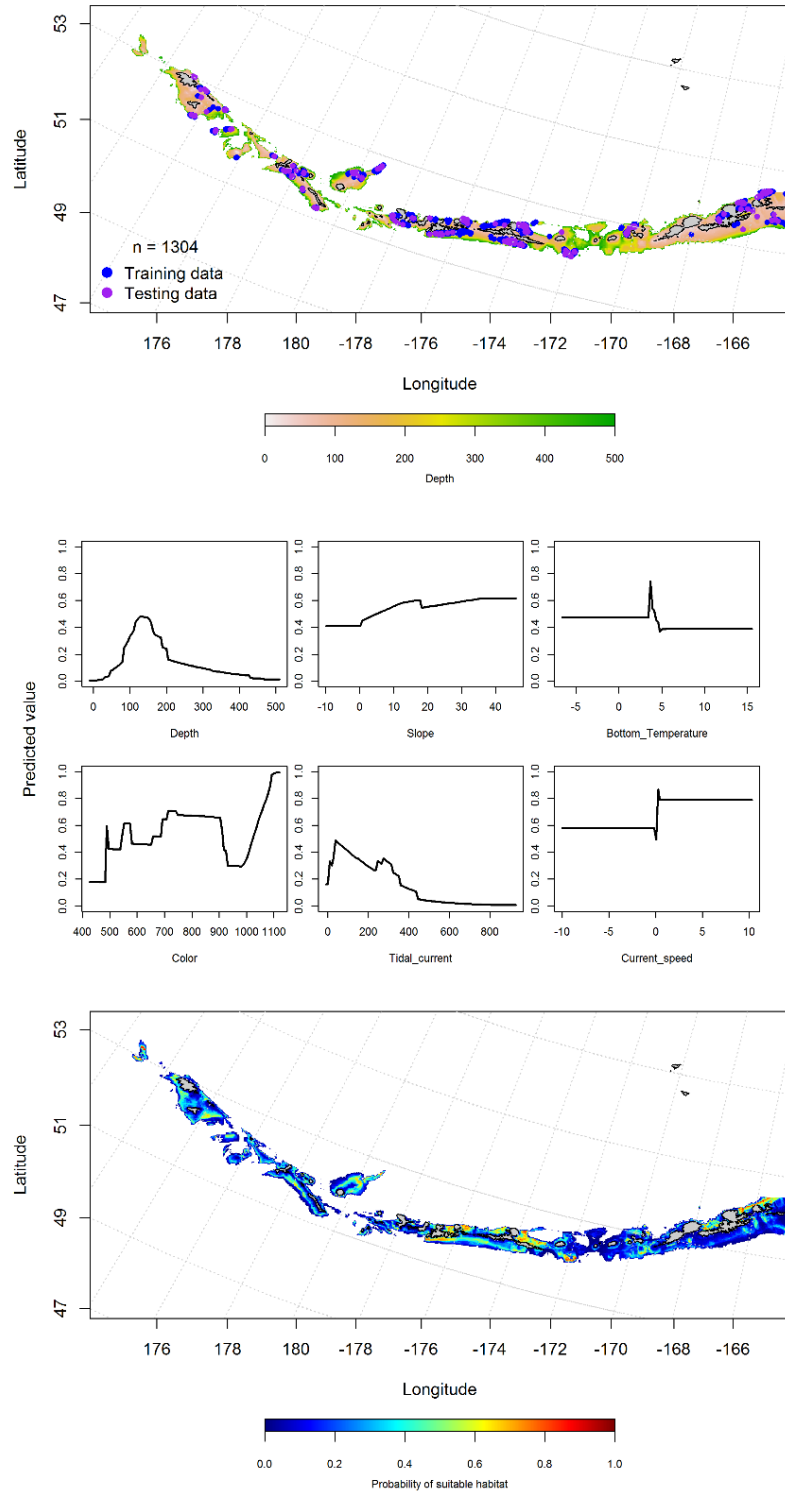


Figure 58. -- Locations of spring (March-May) commercial fisheries catches of adult Atka mackerel (top panel), relationships between probability of presence and environmental variables for the maximum entropy model (middle panels), and predicted probability of suitable habitat for Atka mackerel based on the model (bottom panel).

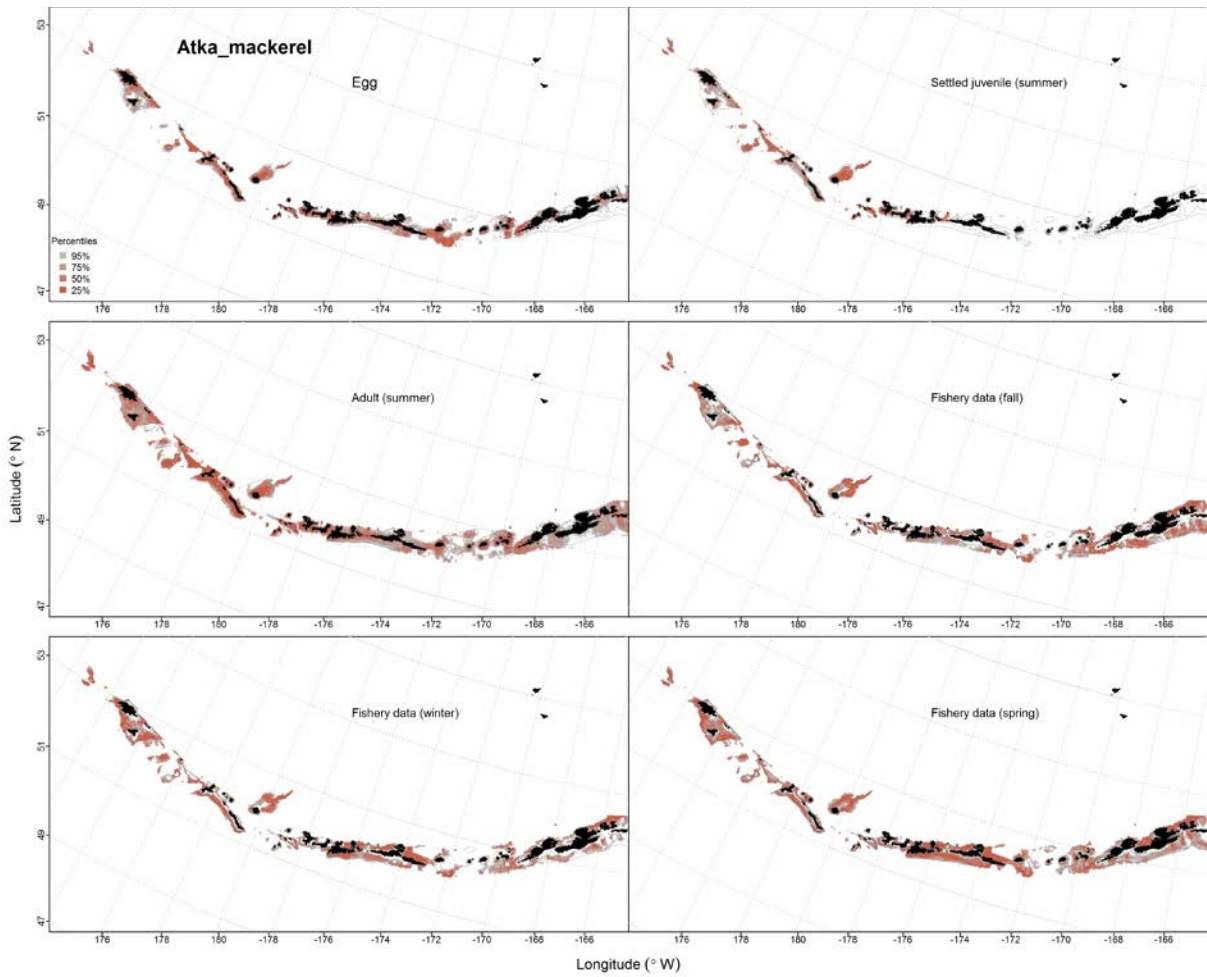


Figure 59. -- Predicted EFH quantiles for Atka mackerel life history stages based on species distribution modeling. Egg stage is based on Lauth et al. (2007) data. Settled juvenile and summer adult stages are based on bottom trawl survey data, while seasonal stages (winter, spring, fall) are from commercial fishery data.

Pacific Cod (*Gadus macrocephalus*)

Early life history stages of Pacific cod -- There were only three instances of Pacific cod eggs and three instances of Pacific cod pelagic juveniles observed in the EcoFOCI database, therefore, we did not do an analysis. There were 101 catches of Pacific cod larvae, with all occurring in the eastern Aleutian Islands (Fig. 60). The MaxEnt model indicated that current direction, current speed, ocean color and sea surface temperature were the most important factors explaining larval cod distribution. The model AUC's were 0.99 (training data) and 0.90 (test data). The model predicted suitable habitat for larval Pacific cod was limited to the eastern Aleutian Islands where most of the sampling was done (Fig. 60).

Juvenile and adult Pacific cod distribution in the bottom trawl survey -- The catch of juvenile Pacific cod in summer bottom trawl surveys of the Aleutian Islands indicates this species is broadly distributed (Fig. 61). A GAM predicting the abundance of juvenile Pacific cod explained 20% of the training data variability and 15% of the test data variability in CPUE from the bottom trawl survey. Bottom depth and geographic location were the most important variables explaining the distribution of juvenile Pacific cod. Juvenile Pacific cod are distributed throughout the AI, though areas of predicted highest abundance were in the eastern AI near Unimak Pass (Fig. 61).

A GAM predicting the abundance of adult Pacific cod explained 27% of the training data variability and 26% of the test data variability in CPUE from the bottom trawl survey. Bottom depth and geographic location were the most important variables explaining the distribution. Adults were distributed throughout the AI, but more heavily in the east (Fig. 62).

Pacific cod distribution in commercial fisheries -- Distribution of adult Pacific cod in the Aleutian Islands in commercial fisheries catches was generally consistent throughout all seasons. In the fall, bottom depth and ocean color were the most important variables determining probable suitable habitat of adult Pacific cod. The AUC of the fall MaxEnt model was 0.91 for the training data (83% correctly classified) and 0.78 for the test data (78% correctly classified). The model predicted suitable habitat of Pacific cod throughout the AI with areas of highest probability in the central and eastern AI (Fig. 63).

Bottom depth and ocean color were the most important variables determining suitable habitat of Pacific cod in the winter. The AUC of the winter MaxEnt model was 0.92 for the training data and 0.84 for the test data. As with the fall, the model predicted suitable habitat of Pacific cod across the AI with areas of highest abundance in the central and western AI (Fig. 64).

In the spring, bottom depth and ocean color were the most important variables determining suitable habitat of Pacific cod. The AUC of the spring MaxEnt model was 0.89 for the training data and 0.80 for the test data. The model correctly classified 81% of the training data and 80% of the test data. The model predicted probable suitable habitat of Pacific cod across the AI with areas of highest abundance in the central and western AI (Fig. 65).

Pacific cod essential fish habitat maps and conclusions -- Larval Pacific cod EFH was predicted to occur exclusively in the eastern AI, while juvenile and adult Pacific cod summer EFH was distributed broadly throughout the region (Fig. 66). The fall, winter, and spring distribution of Pacific cod EFH was essentially the same throughout the AI (Fig. 66).

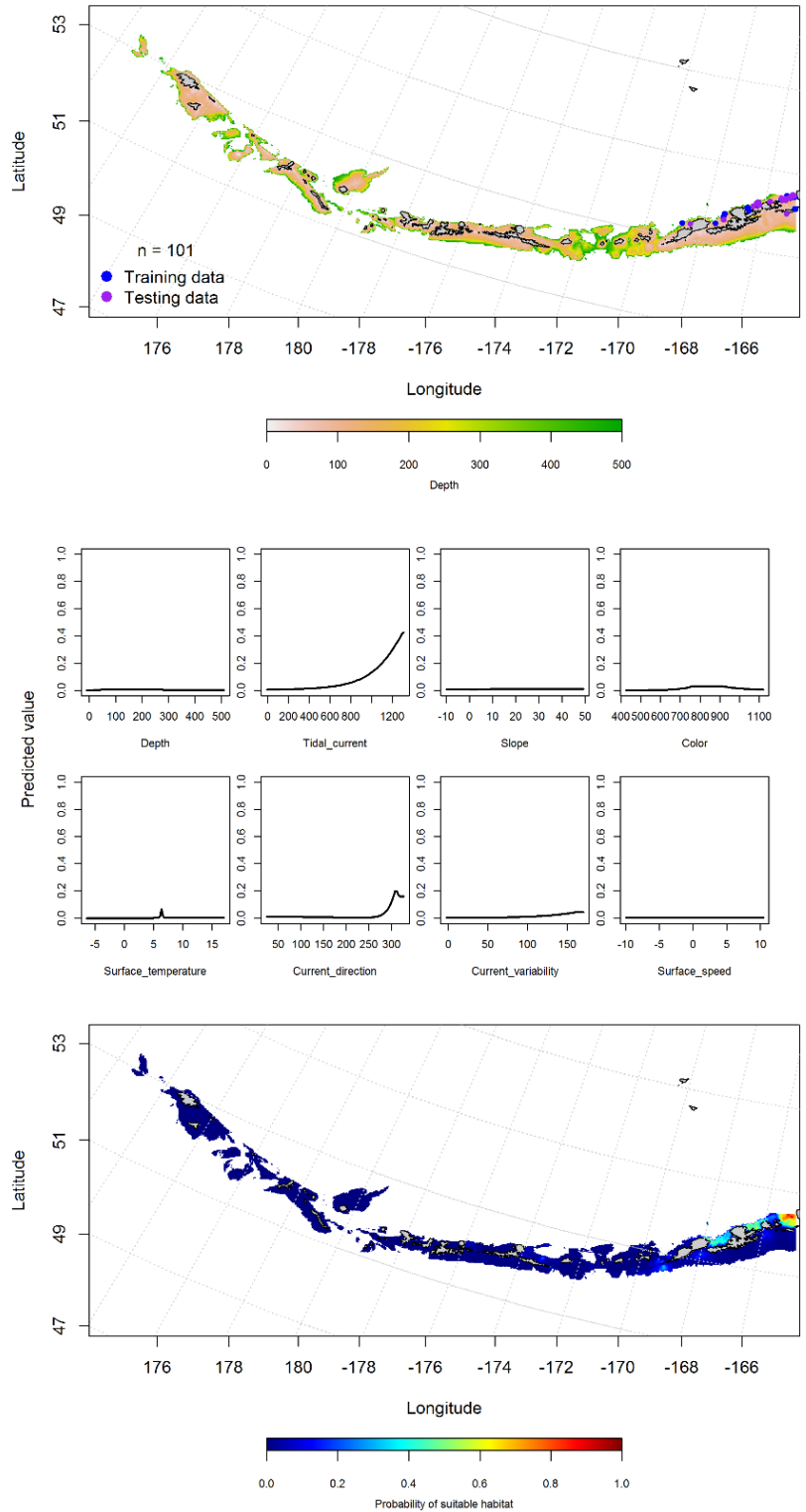


Figure 60. -- Observations of Pacific cod larvae from the Aleutian Islands the EcoFOCI data (top panel), relationships of suitable habitat and environmental variables (middle panels), and predicted probability of presence of suitable habitat for Pacific cod larvae from MaxEnt modeling of the Aleutian Islands (bottom panel).

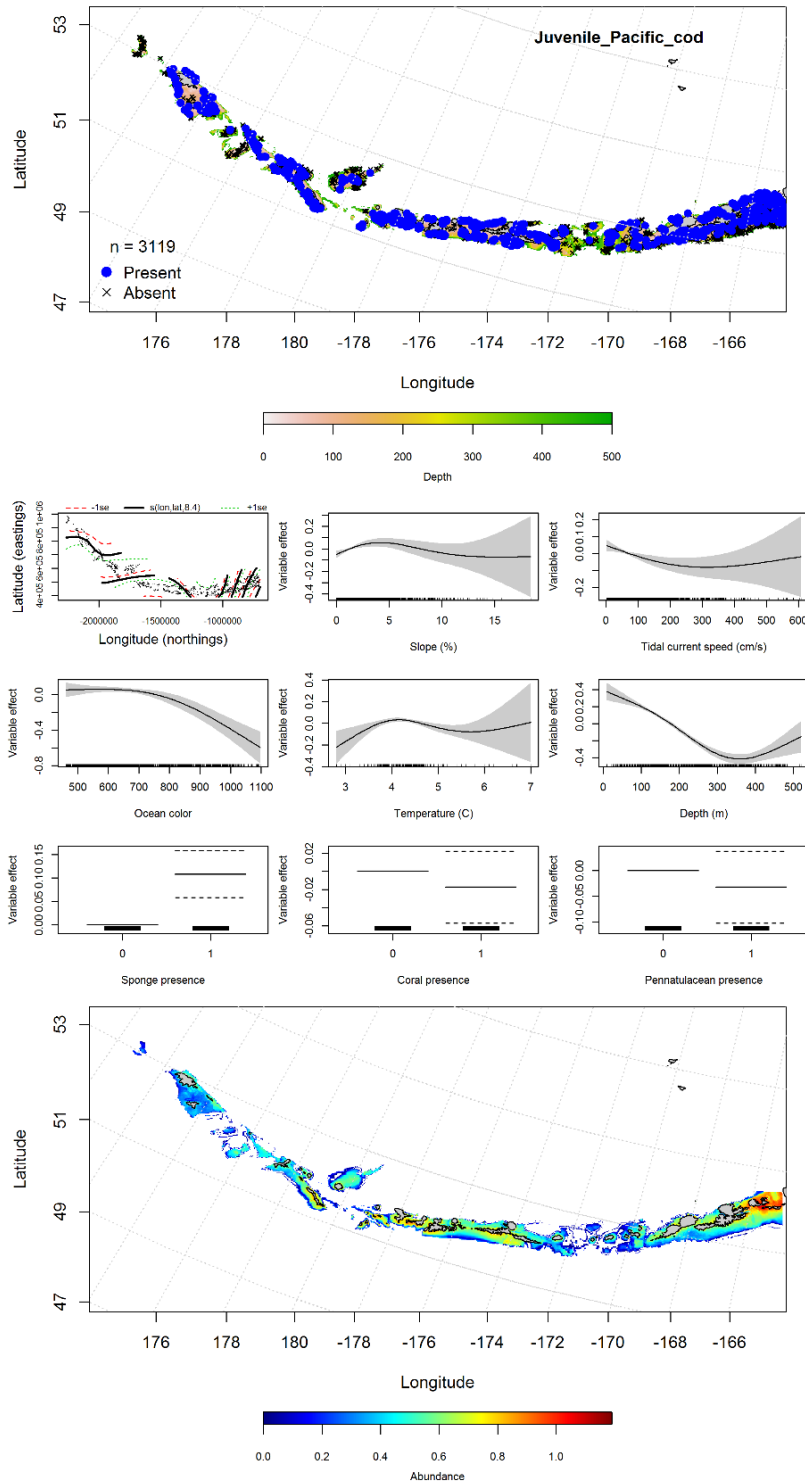


Figure 61. -- Distribution of catches of juvenile Pacific cod in bottom trawl surveys (top panel), relationships between presence and environmental variables for the maximum entropy model of juvenile Pacific cod (middle panels), and predicted probability of suitable habitat for juvenile Pacific cod based on the model (bottom panel).

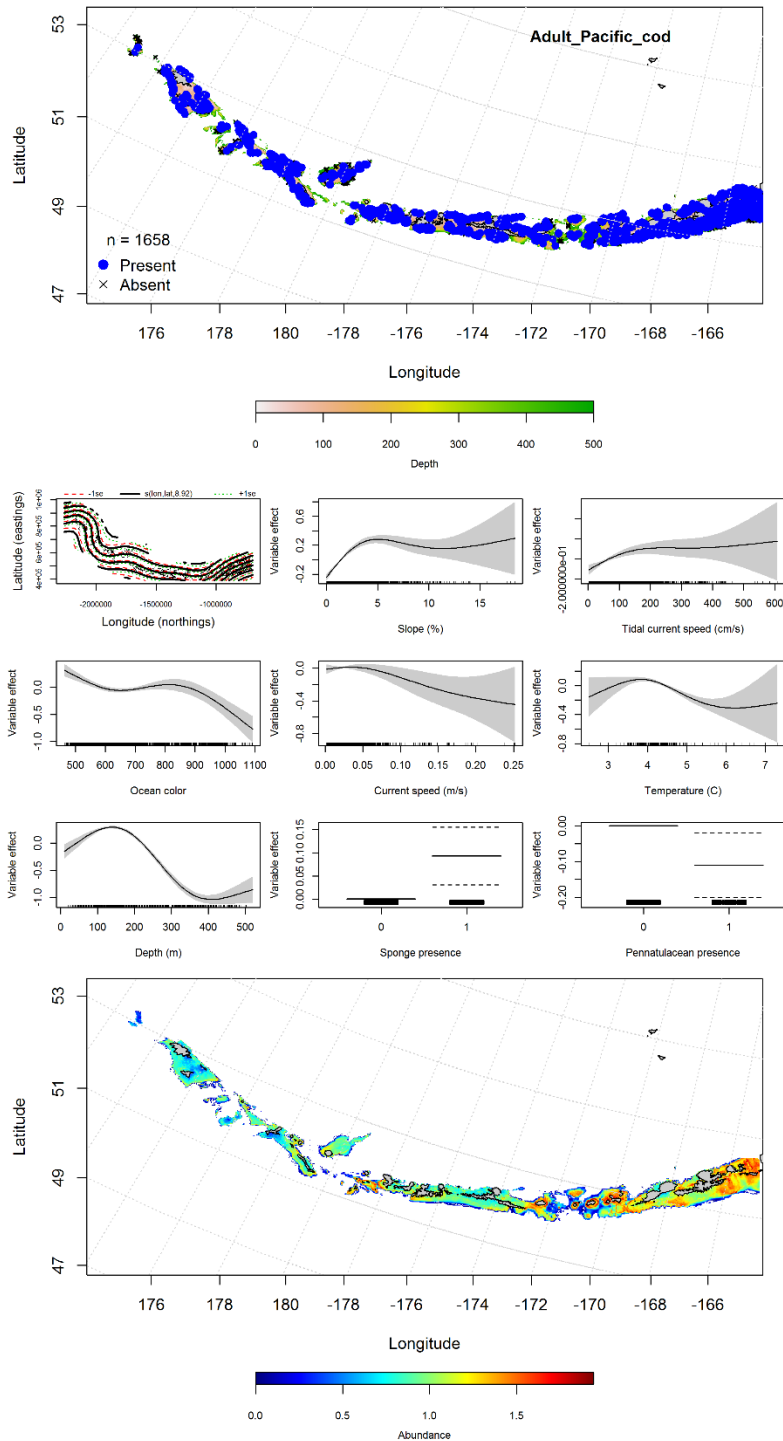


Figure 62. -- Distribution of catches of adult Pacific cod in bottom trawl surveys (top panel), relationships between presence and environmental variables for the maximum entropy model of adult Pacific cod (middle panels), and predicted probability of suitable habitat for adult Pacific cod based on the model (bottom panel).

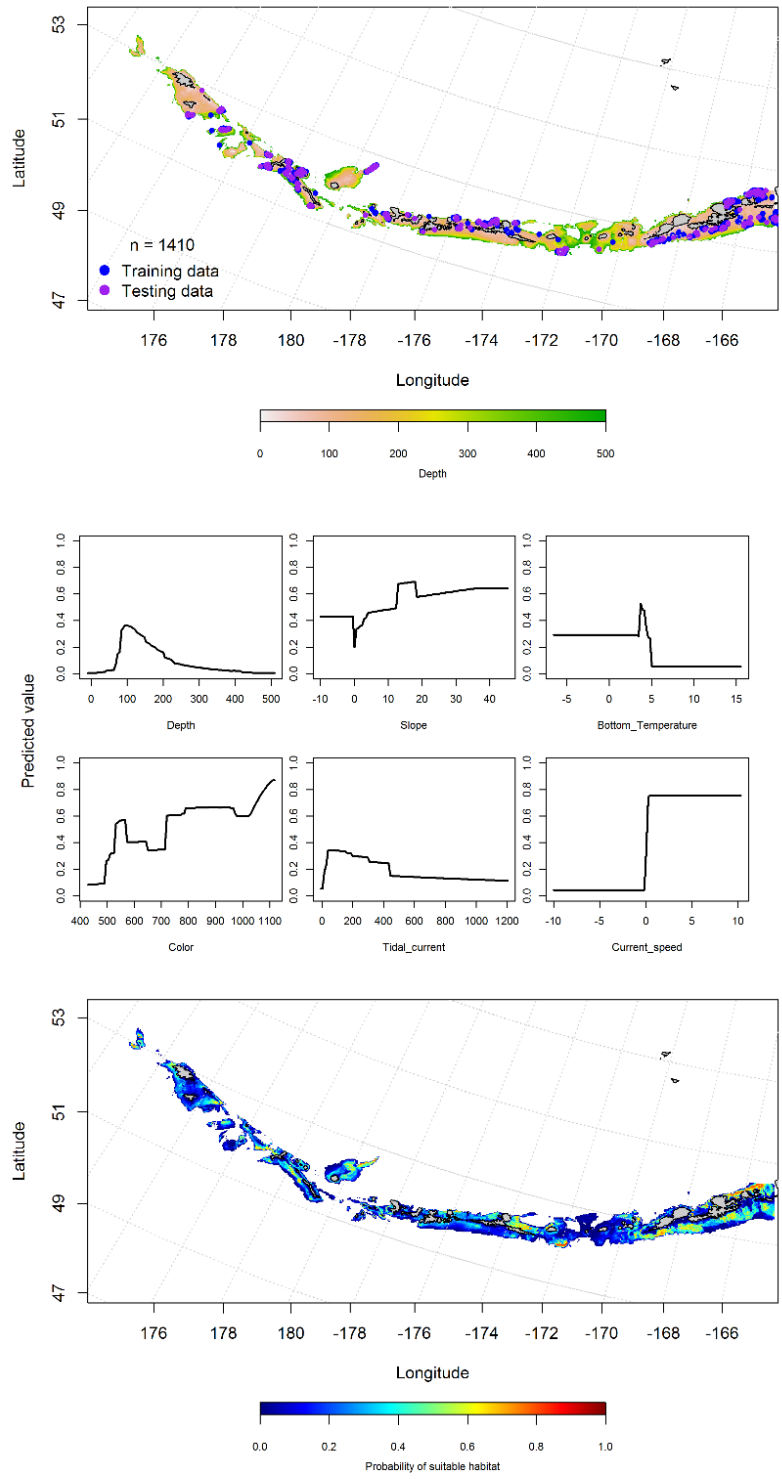


Figure 63. -- Locations of fall (September-November) commercial fisheries catches of Pacific cod (top panel), relationships between probability of presence and environmental variables for the maximum entropy model (middle panels), and predicted probability of suitable habitat for Pacific cod based on the model (bottom panel).

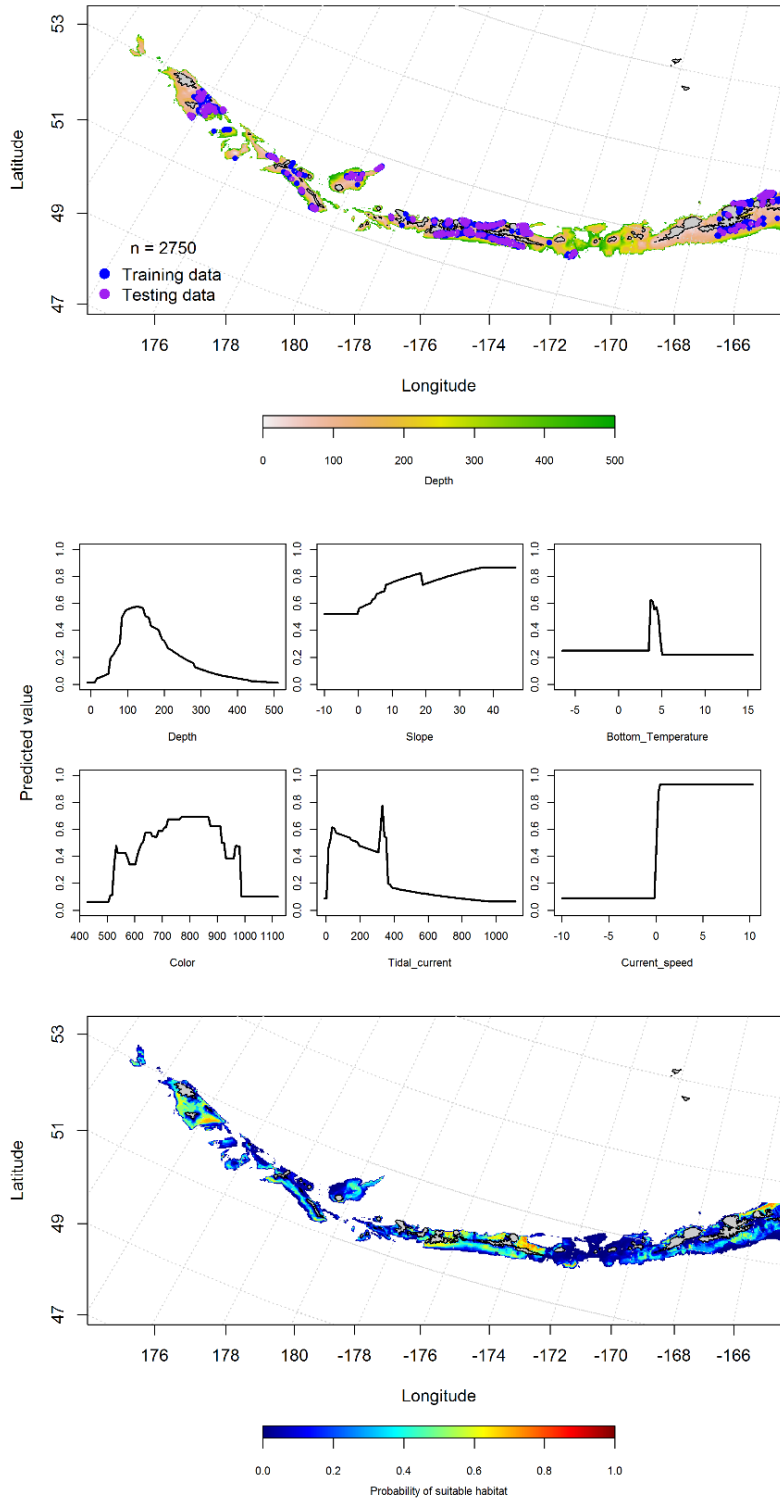


Figure 64. -- Locations of winter (December-February) commercial fisheries catches of adult Pacific cod (top panel), relationships between probability of presence and environmental variables for the maximum entropy model (middle panels), and predicted probability of suitable habitat for Pacific cod based on the model (bottom panel).

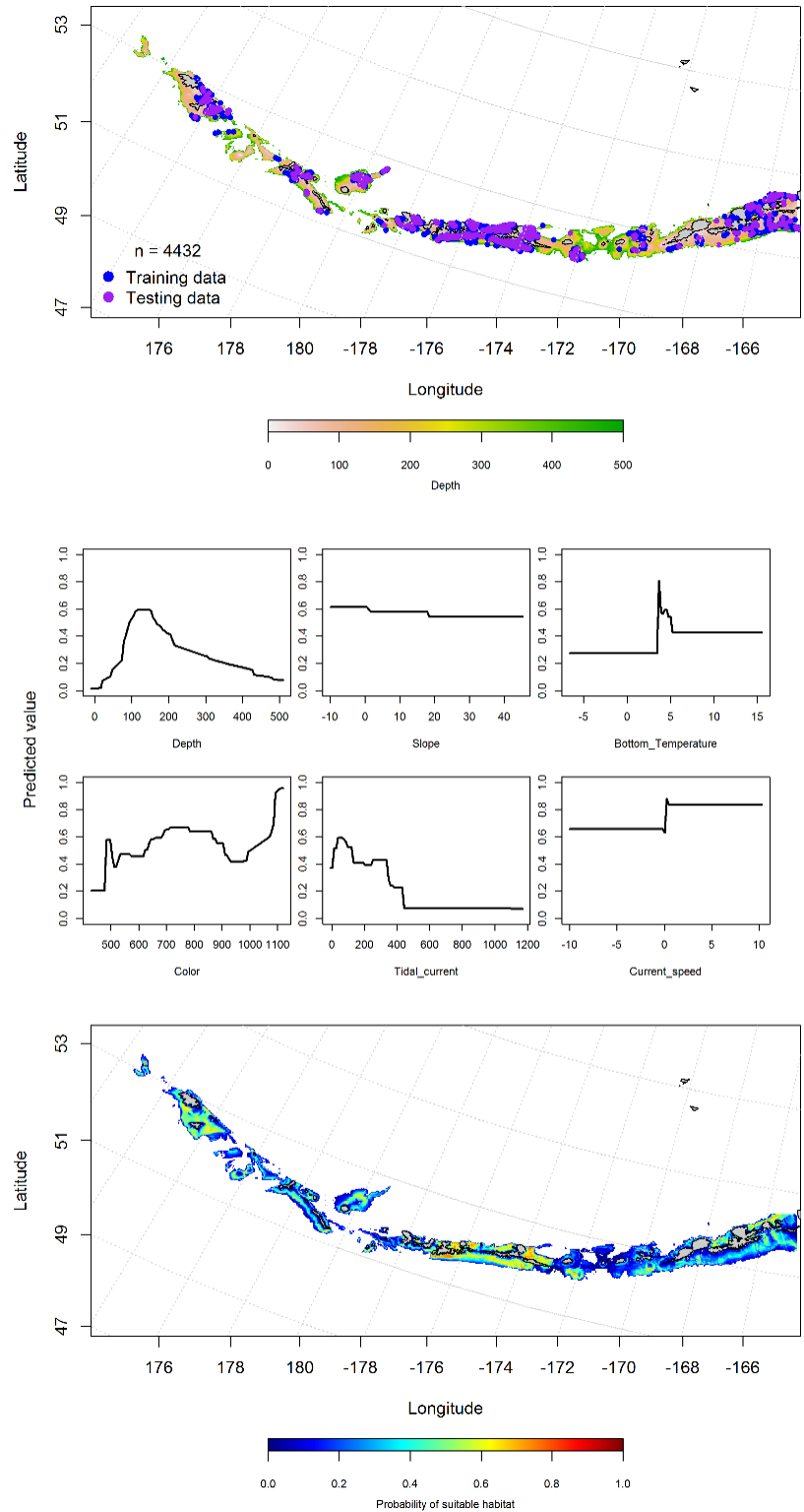


Figure 65. -- Locations of spring (March-May) commercial fisheries catches of Pacific cod (top panel), relationships between probability of presence and environmental variables for the maximum entropy model (middle panels), and predicted probability of suitable habitat for Pacific cod based on the model (bottom panel).

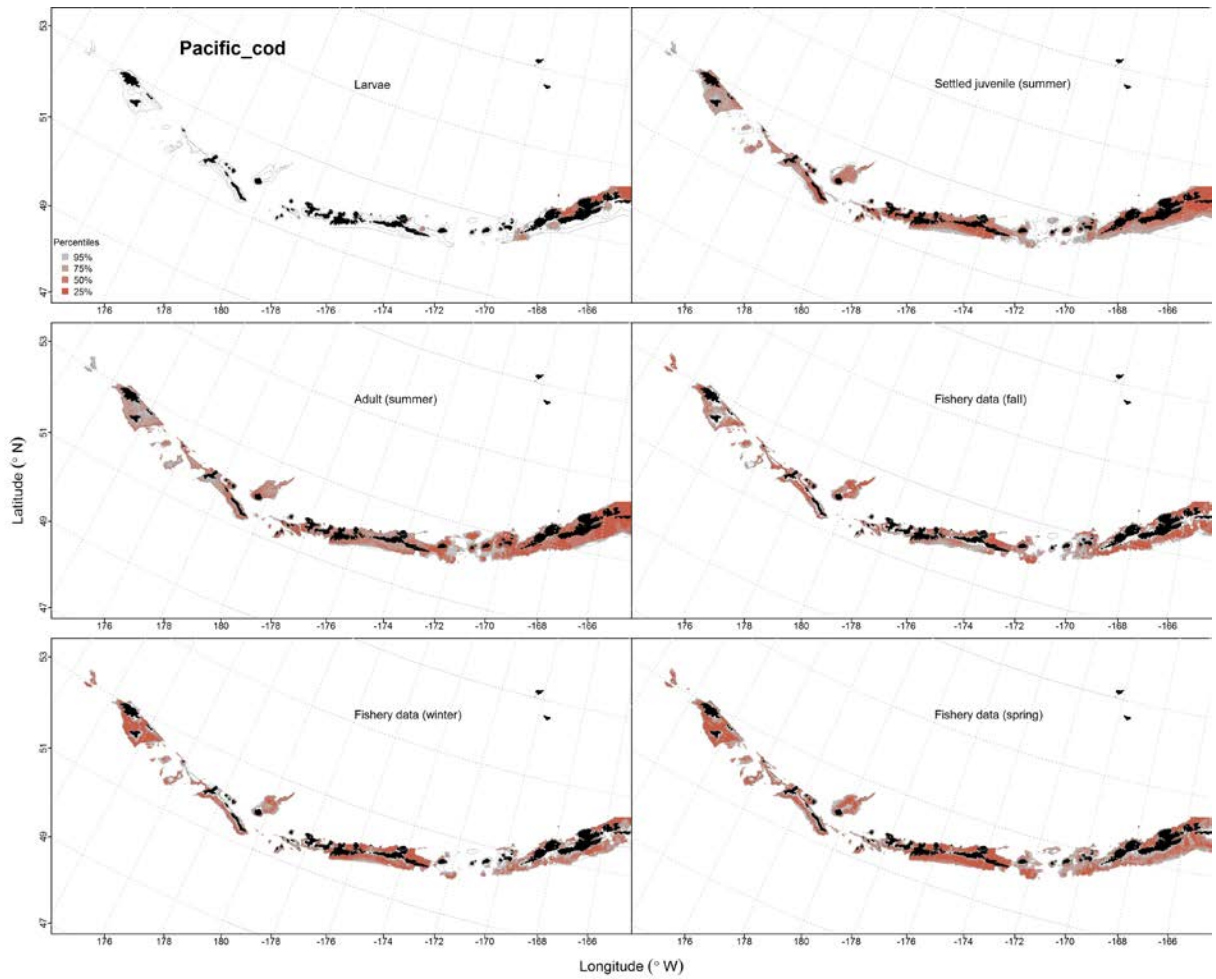


Figure 66. -- Predicted EFH quantiles for Pacific cod life history stages based on species distribution modeling. Larval stage is based on EcoFOCI data. Settled juvenile and summer adult stages are based on bottom trawl survey data, while seasonal stages (winter, spring, fall) are from commercial fishery data.

Walleye Pollock (*Gadus chalcogrammus*)

Early life history stages of walleye pollock -- There were 177 instances of walleye pollock eggs observed in the FOCI database all in the eastern AI (Fig. 67). Surface temperature, current speed, current direction and ocean color were the important variables for suitable habitat of pollock eggs. The training data AUC was 0.99, and 0.89 for the test data. The model correctly classified 96% of the training data and 89% of the test data. The predicted suitable habitat for pollock eggs was in the eastern AI (Fig. 67).

There were 143 observations of larval walleye pollock observed in the eastern AI (Fig. 68). The most important variables in the spring larval model were surface temperature, current direction, ocean color, current speed. The AUC was 0.99 for the training data and 0.95 for the testing data, indicating a good model fit. The model correctly classified 96% of training data and 95% of test data. The predicted suitable habitat for larvae was in the eastern AI (Fig. 68). There were only seven observations of juvenile pollock in the FOCI database.

Juvenile and adult walleye pollock distribution in the bottom trawl survey -- Juvenile walleye pollock were modeled using a hurdle-GAM. The PA GAM predicted areas of high and low abundance (e.g., areas with large passes) throughout the AI (Fig. 69). The best-fitting PA GAM indicated that bottom depth and ocean color were the most important factors controlling juvenile walleye pollock distribution with an AUC of 0.78 for both the training and test data sets. The model correctly classified 71% of the training data and test data. The CPUE GAM model found that depth and slope were the most important variables explaining the abundance of juvenile walleye pollock. The model explained only 7% of the variability in CPUE in the bottom trawl survey in the training data and explained 3% of the test data set. Juvenile pollock were

found in highest abundance in the eastern AI, with patches of high abundance in the central AI, on Petrel Bank and near Attu Island (Fig. 69).

A GAM predicting the abundance of adult pollock explained 25% of the training data set variability in CPUE, and 21% of the test data set variability. Bottom depth and geographic location were the most important variables explaining the distribution of adult walleye pollock. Adults were distributed throughout the AI along the shelf break, with highest predicted abundance in the eastern AI (Fig. 70).

Walleye pollock distribution in commercial fisheries --Distribution of adult walleye pollock in the Aleutian Islands in commercial fisheries catches was generally consistent throughout all seasons. In the fall, bottom depth, ocean color, current speed, and bottom temperature were the most important variables determining suitable habitat of walleye pollock. The AUC of the fall MaxEnt model was 0.94 for the training and 0.83 for the test data, and 87% of the training and 83% of the test data were correctly classified. The model predicted suitable habitat of pollock throughout the AI mostly along the shelf break (Fig. 71).

In the winter, ocean color, bottom depth, bottom temperature and current speed were the most important variables determining suitable habitat of pollock. The AUC of the winter MaxEnt model was 0.95 for the training data and 0.89 for the test data, with 88% of the training data and 89% of the cases in the test data predicted correctly. The model predicted suitable habitat of pollock across the AI, though more abundant near Agattu, Attu, and Atka islands (Fig. 72).

In the spring, depth, ocean color and tidal currents were the most important variables determining suitable habitat of pollock. The AUC of the spring MaxEnt model was 0.92 for the

training and 0.80 for the test data, with 84% of the training and 80% of the test data correctly classified. The model predicted suitable habitat of pollock throughout the AI (Fig. 73).

Walleye pollock essential fish habitat maps and conclusions -- Predicted EFH for pollock eggs and larvae was the most abundant in the eastern AI (Fig. 74). Juvenile walleye pollock had a more narrowly distributed EFH than the adults, though there were common areas of high abundance (Fig. 74). Predicted summertime EFH of juvenile walleye pollock was distributed throughout the AI, though less abundant in areas of large passes (such as Buldir Strait). Adult walleye pollock were distributed throughout the AI and most abundant in the eastern AI. The fall, winter and spring distribution of walleye pollock EFH from commercial catches was essentially the same throughout the seasons and spread throughout the AI (Fig. 74).

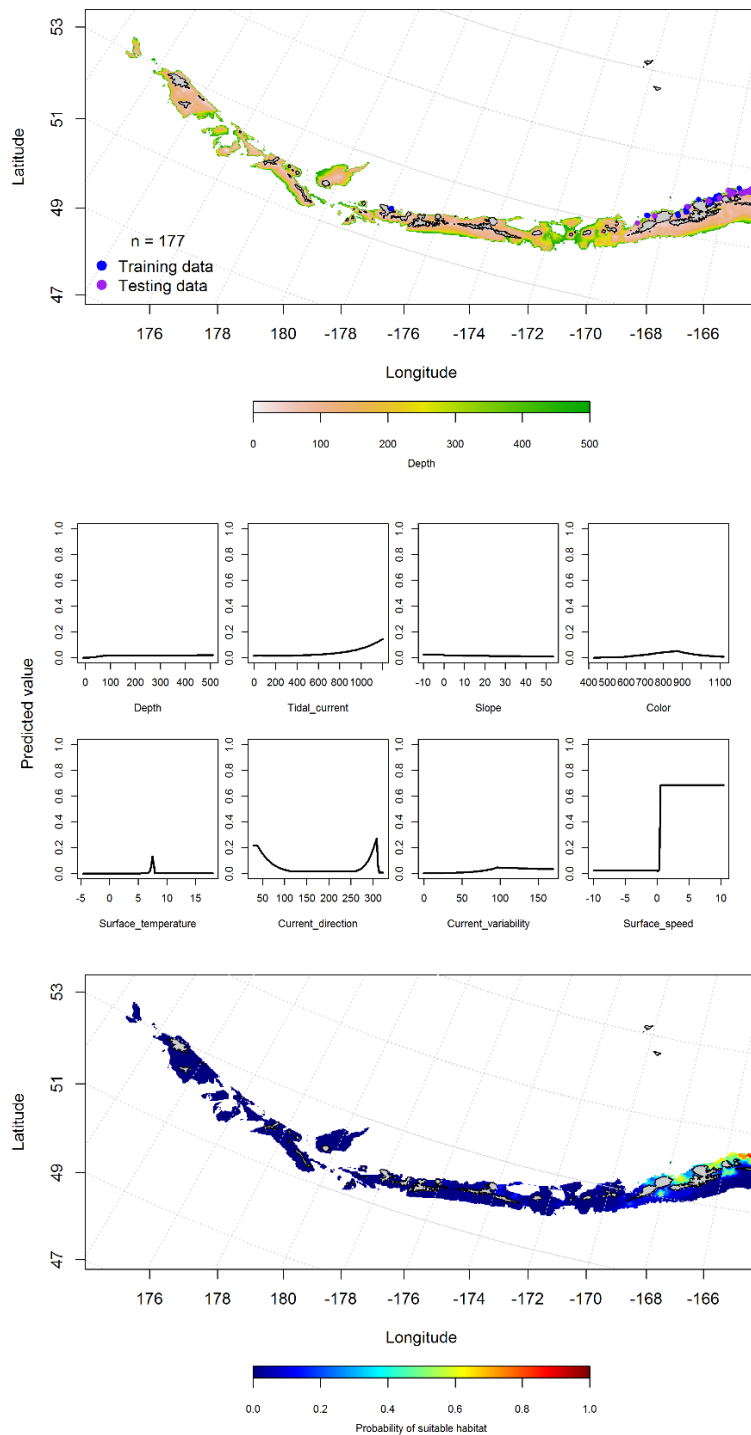


Figure 67. -- Observations of walleye pollock eggs from the Aleutian Islands the EcoFOCI data (top panel), relationships of suitable habitat and environmental variables (middle panels), and predicted probability of presence of suitable habitat for walleye pollock eggs from MaxEnt modeling of the Aleutian Islands (bottom panel).

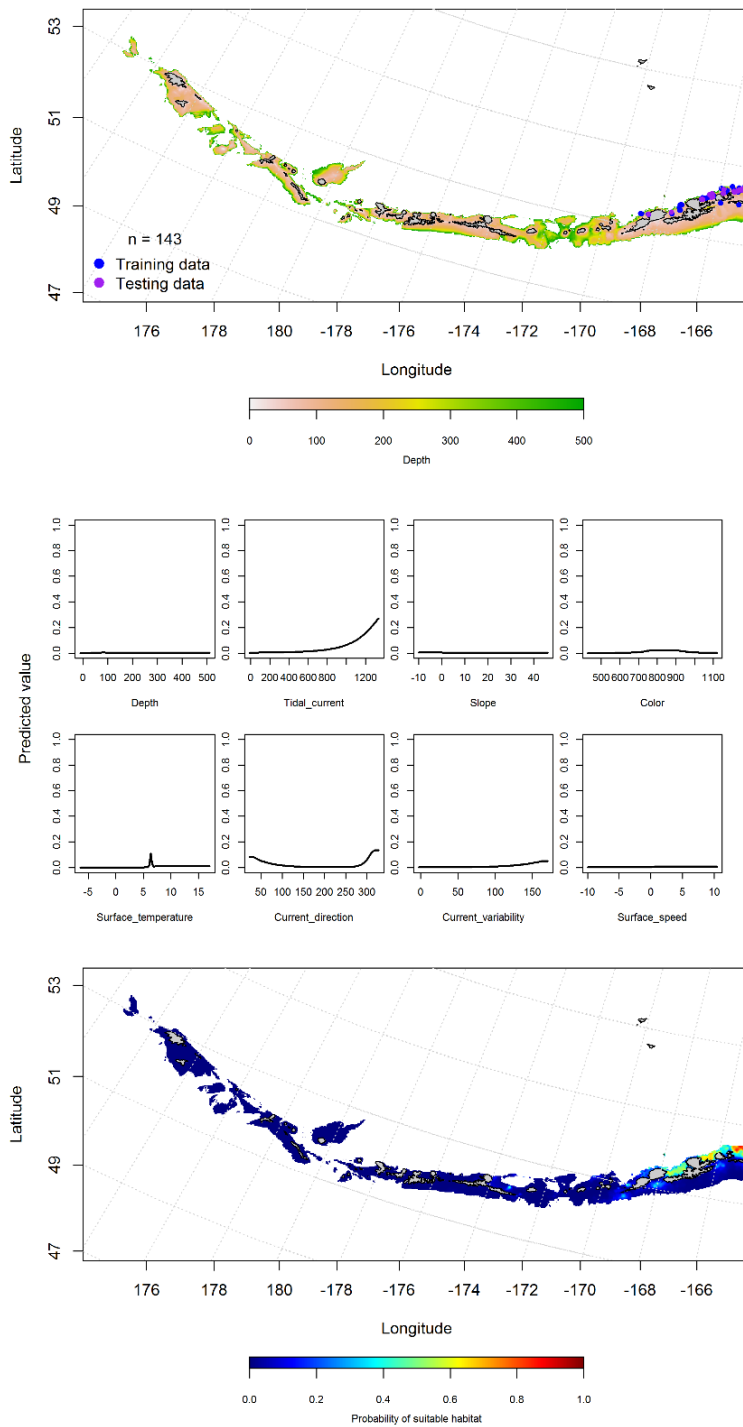


Figure 68. -- Observations of walleye pollock larvae from the Aleutian Islands the EcoFOCI data (top panel), relationships of suitable habitat and environmental variables (middle panels), and predicted probability of presence of suitable habitat for walleye pollock larvae from MaxEnt modeling of the Aleutian Islands (bottom panel).

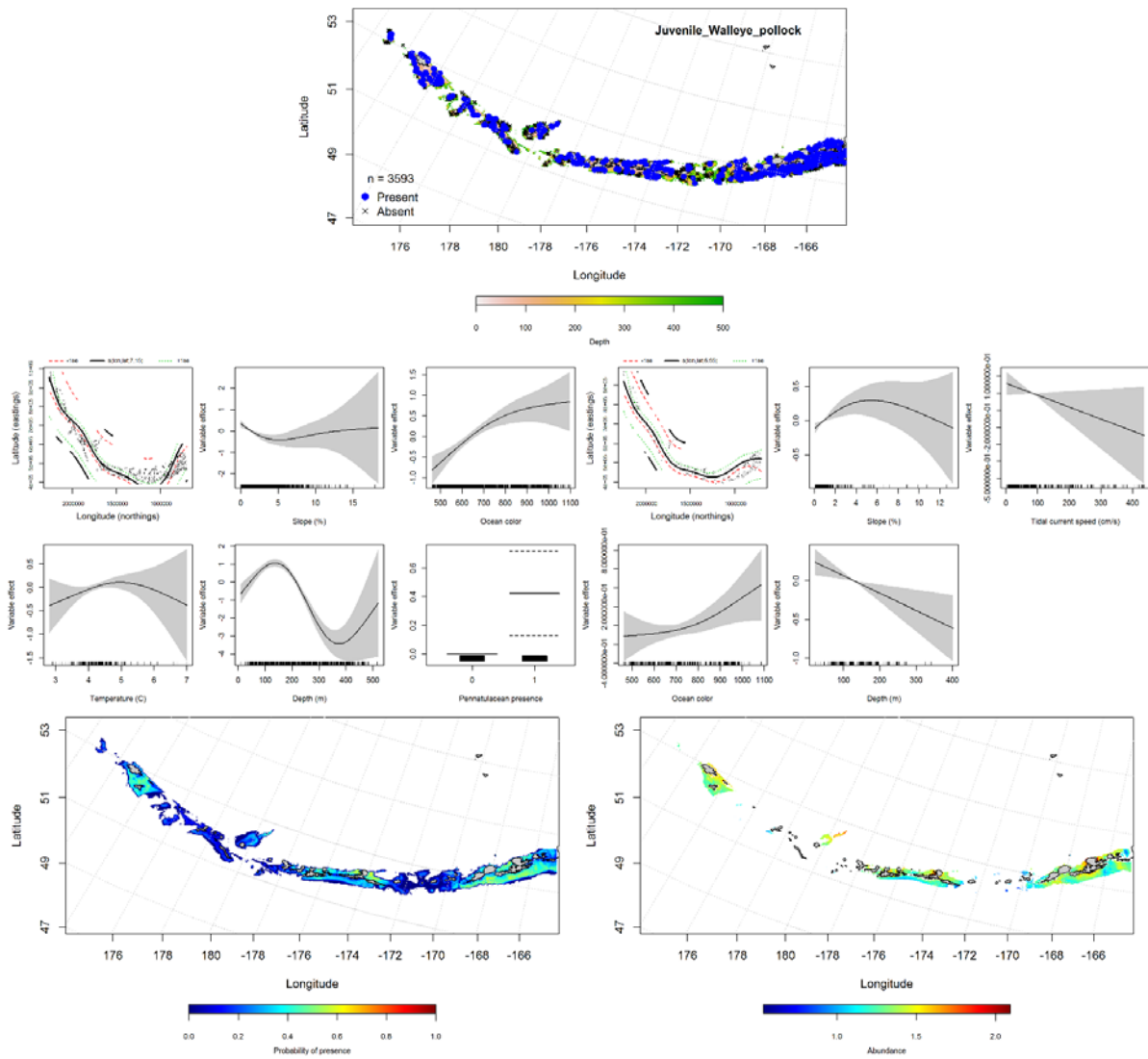


Figure 69. -- Distribution of catches of juvenile walleye pollock in bottom trawl surveys (top middle panel), significant relationships between presence-absence and CPUE and environmental variables for the best-fitting generalized additive model of juvenile walleye pollock (middle left and right panels), and predicted probability of presence and abundance of juvenile walleye pollock based on the models (bottom left and right panels).

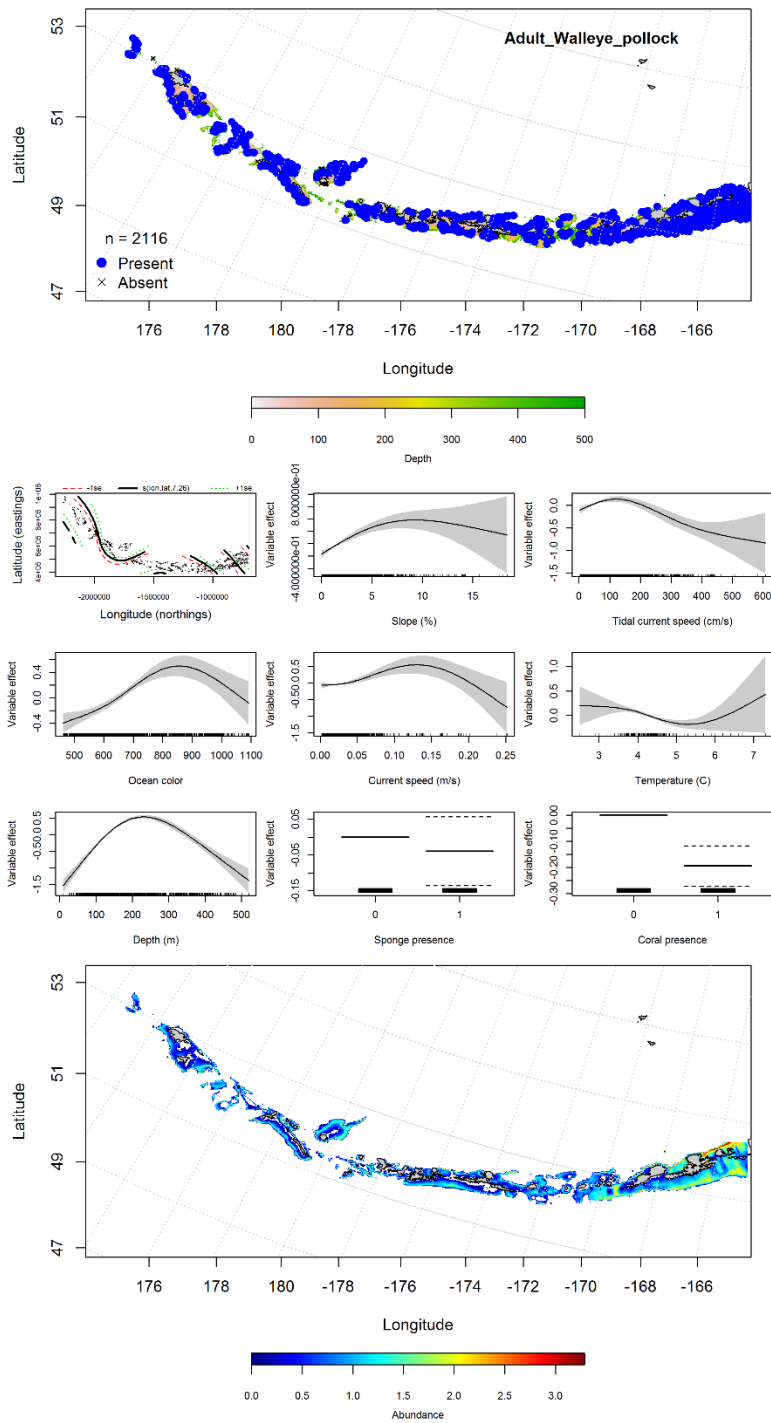


Figure 70. -- Distribution of catches of adult walleye pollock in bottom trawl surveys (top panel), relationships between presence and environmental variables for the GAM model of adult walleye pollock (middle panels), and predicted abundance of adult walleye pollock based on the model (bottom panel).

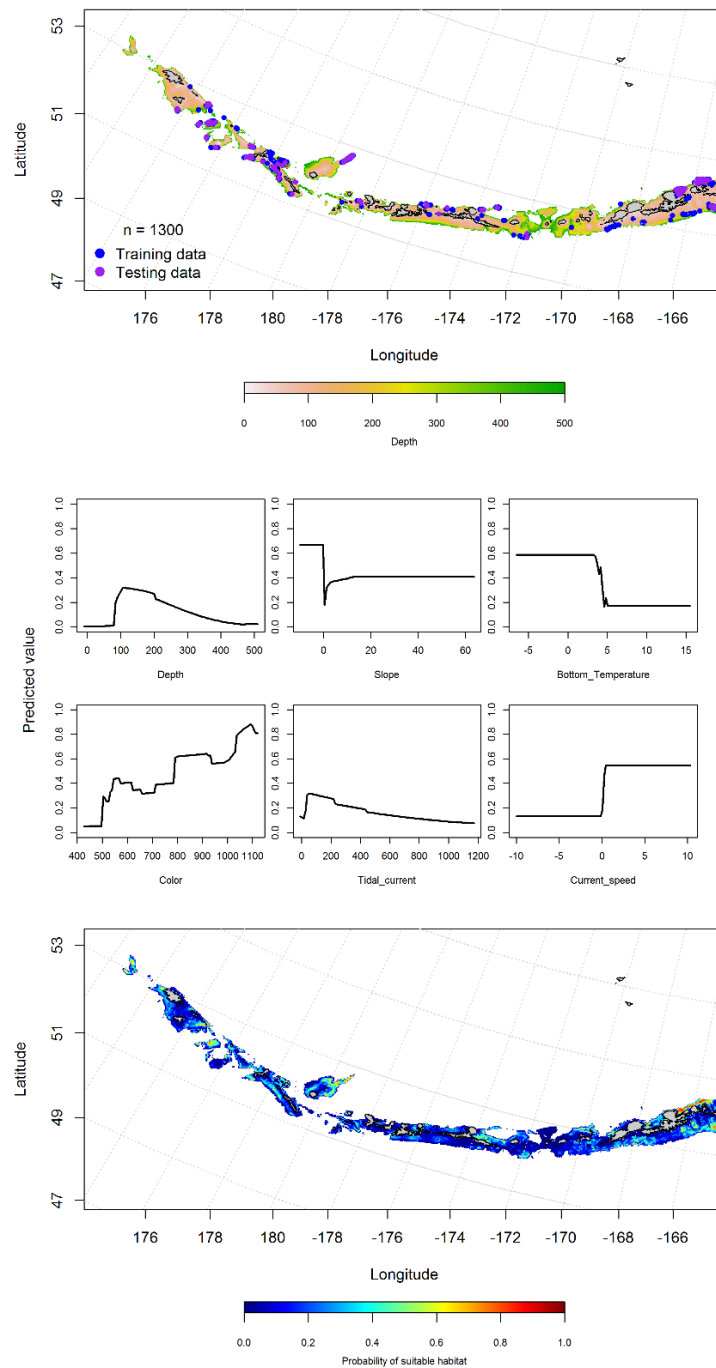


Figure 71. -- Locations of fall (September-November) commercial fisheries catches of adult walleye pollock (top panel), relationships between probability of presence and environmental variables for the maximum entropy model (middle panels), and predicted probability of suitable habitat for walleye pollock based on the model (bottom panel).

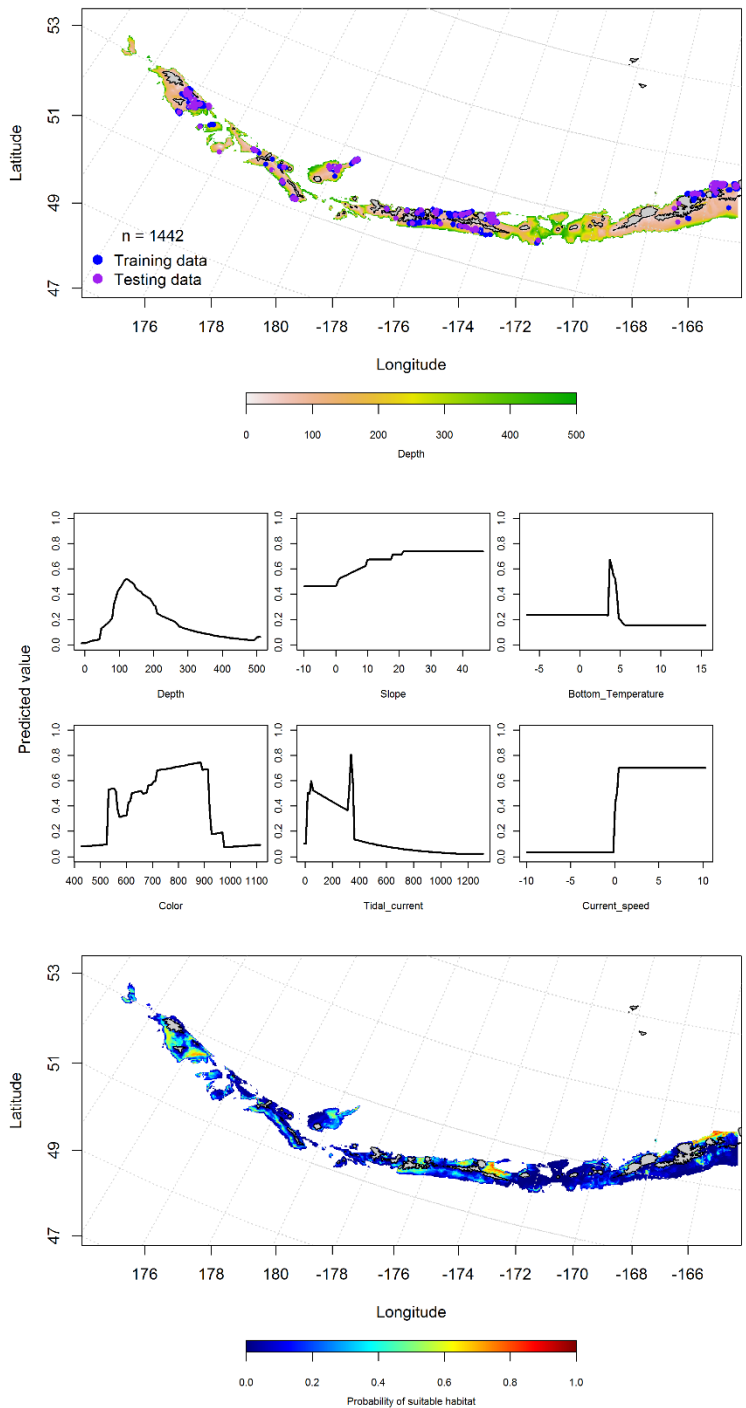


Figure 72. -- Locations of winter (December-February) commercial fisheries catches of adult walleye pollock (top panel), relationships between probability of presence and environmental variables for the maximum entropy model (middle panels), and predicted probability of suitable habitat for walleye pollock based on the model (bottom panel).

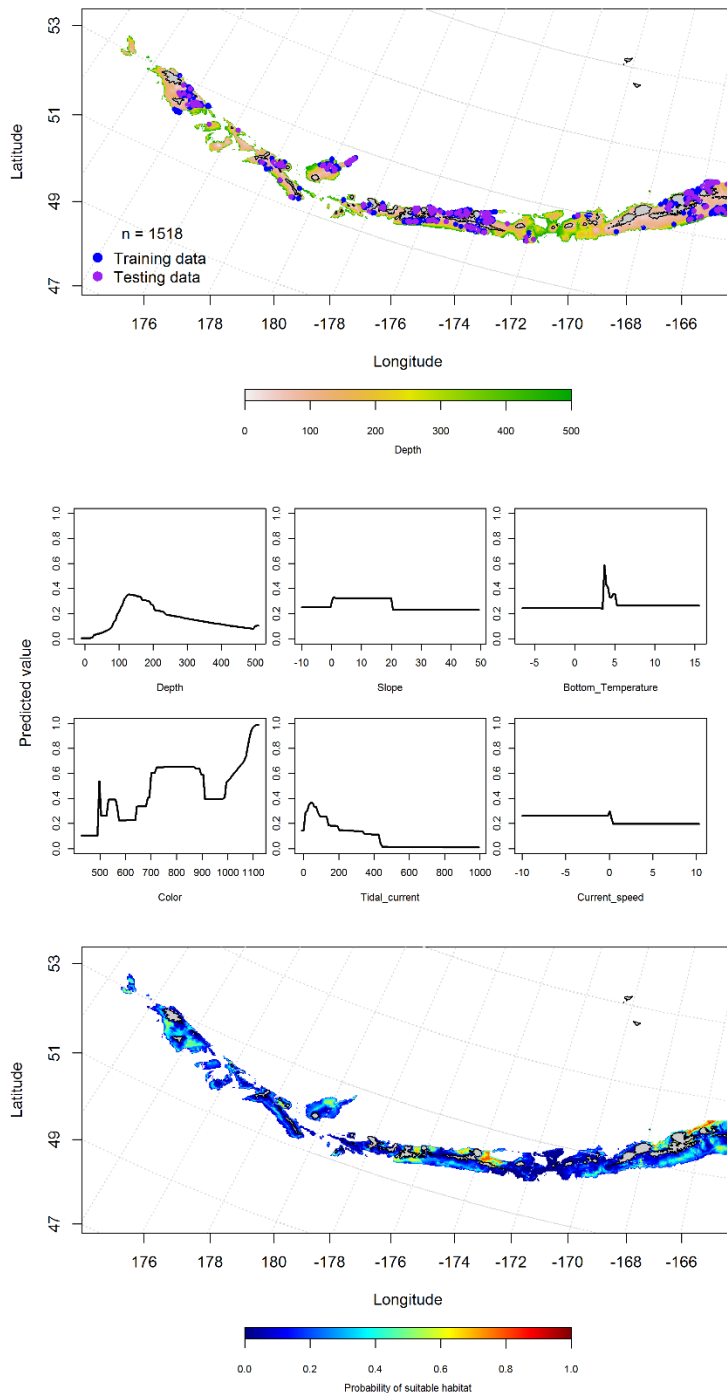


Figure 73. -- Locations of spring (March-May) commercial fisheries catches of adult walleye pollock (top panel), relationships between probability of presence and environmental variables for the maximum entropy model (middle panels), and predicted probability of suitable habitat for walleye pollock based on the model (bottom panel).

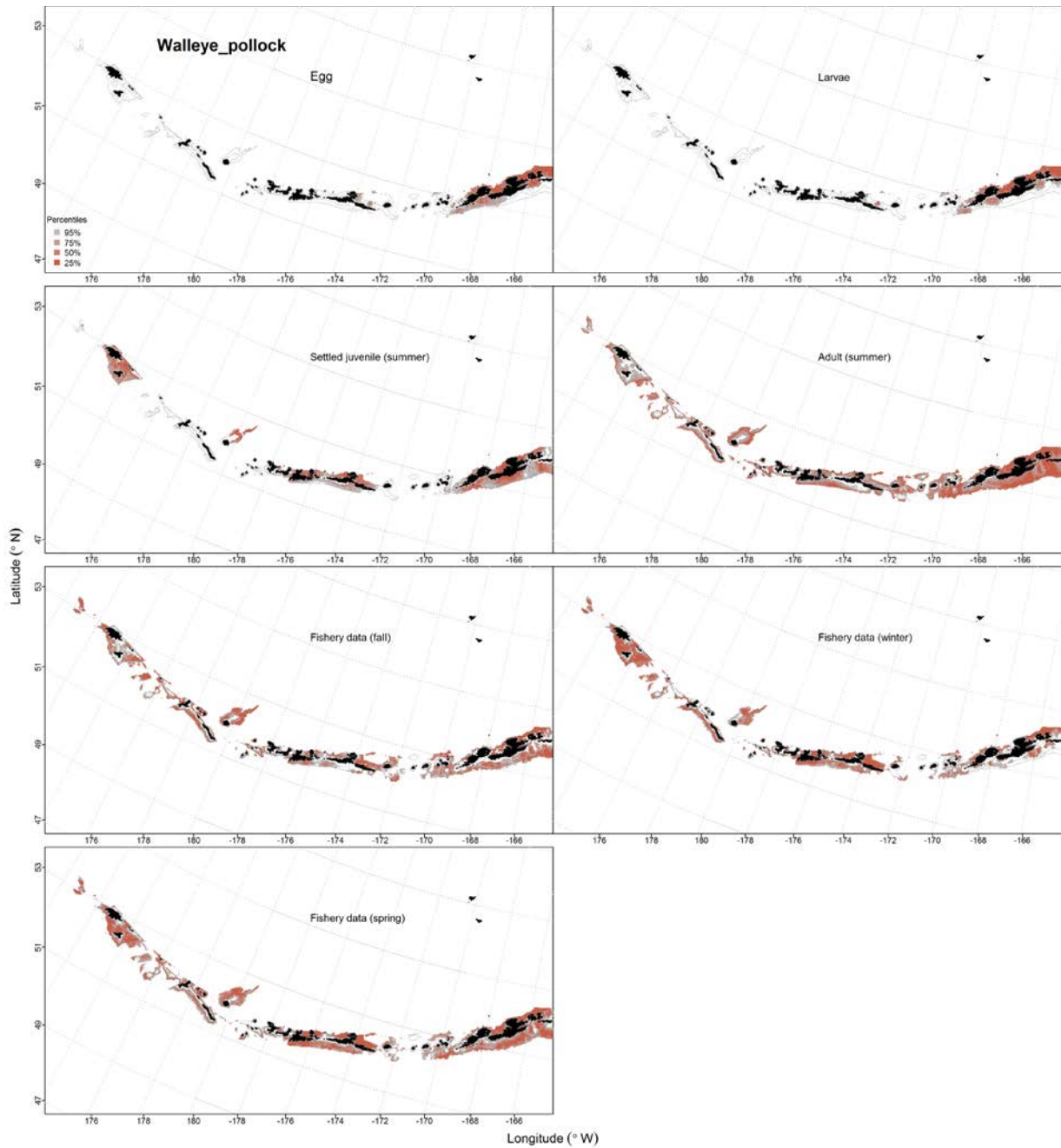


Figure 74. -- Predicted EFH quantiles for walleye pollock life history stages based on species distribution modeling. Egg and larval stage is based on EcoFOCI data. Settled juvenile and summer adult stages are based on bottom trawl survey data, while seasonal stages (winter, spring, fall) are from commercial fishery data.

Sablefish (*Anoplopoma fimbria*)

Early life history stages of sablefish -- There were only nine instances of larval sablefish observed in the EcoFOCI database, all observations occurred in eastern AI, therefore, we did not do an analysis.

Juvenile and adult sablefish distribution in the bottom trawl survey -- There were not enough instances (n = 14) of juvenile sablefish from the bottom trawl surveys for modeling. A MaxEnt model of adult sablefish catches in the bottom trawl survey indicated that depth and ocean color were the most important variables predicting sablefish habitat suitability. The AUC of the model was 0.92 for the training data and 0.81 for the testing data. The model predicted suitable habitat for adult sablefish in the Aleutian Islands was highest in the deeper regions of the survey area near Seguam Pass and south of Unalaska Island (Fig. 75).

Sablefish distribution in commercial fisheries -- Commercial fisheries catches of sablefish in the Aleutian Islands were generally consistent throughout the fall (Fig. 76) and winter (Fig. 77), though were more abundant in the western AI in the spring (Fig. 78) than in other seasons. In the fall, ocean color, bottom temperature, and bottom depth were the most important variables determining suitable habitat of adult sablefish. The AUC of the fall MaxEnt model was 0.91 for the training data and 0.76 for the test data, and 81% and 76%, respectively, of the cases in the test and training data sets were predicted correctly. The model predicted probable suitable habitat of adult sablefish across the AI though most probable in the eastern AI near Nikolski and Unalaska islands (Fig. 76).

In the winter, ocean color, bottom temperature, and tidal current were the most important variables determining suitable habitat of sablefish. The AUC of the winter MaxEnt model was

0.98 for the training data and 0.95 for the test data, with 95% of the training and test data cases predicted correctly. As with the fall, the winter model predicted probable suitable habitat of sablefish across the AI with a higher probability near Atka Island (Fig. 77).

In the spring, depth and ocean color were the most important variables determining probability of suitable habitat for sablefish. The AUC of the spring MaxEnt model was 0.93 for the training data and 0.83 for the test data. The model correctly classified 85% of the training data and 83% of the test data. The model predicted suitable habitat of sablefish across the AI (Fig. 78).

Sablefish essential fish habitat maps and conclusions -- Summertime EFH of sablefish was located in deeper waters along the shelf break and around Seguam Pass (Fig. 79). The fall and spring predicted EFH of sablefish were similar whereas there was lower probability in the winter (Fig. 79).

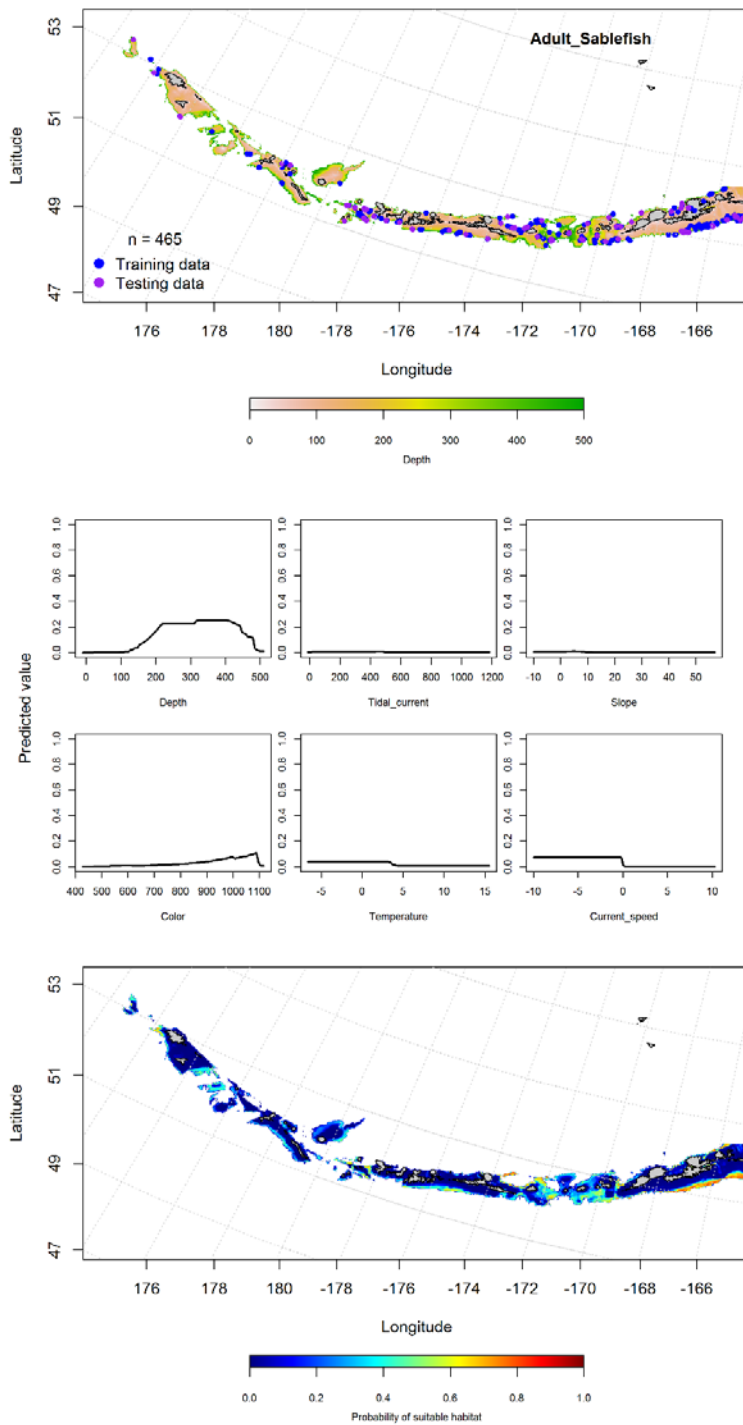


Figure 75. -- Distribution of catches of adult sablefish in bottom trawl surveys (top panel), relationships between presence and environmental variables for the maximum entropy model of adult sablefish (middle panels), and predicted probability of suitable habitat for adult sablefish based on the model (bottom panel).

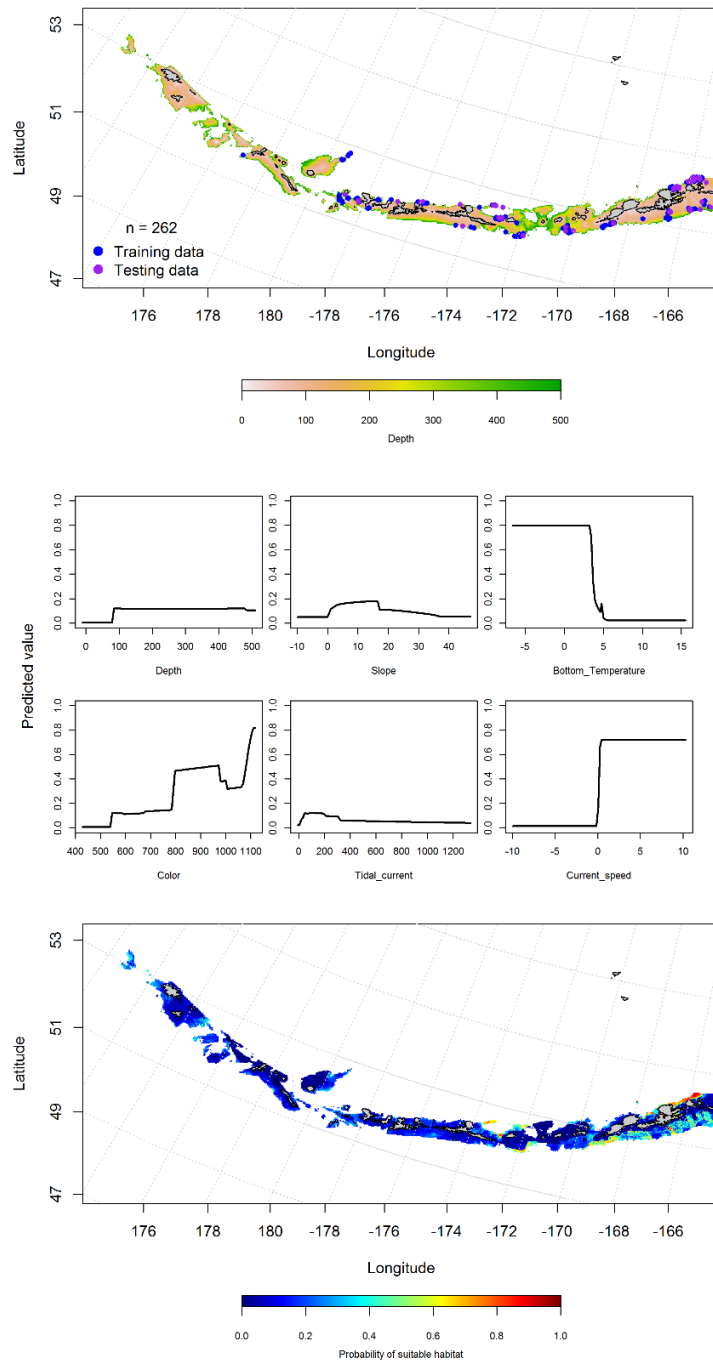


Figure 76. -- Locations of fall (September-November) commercial fisheries catches of adult sablefish (top panel), relationships between probability of presence and environmental variables for the maximum entropy model (middle panels), and predicted probability of suitable habitat for sablefish based on the model (bottom panel).

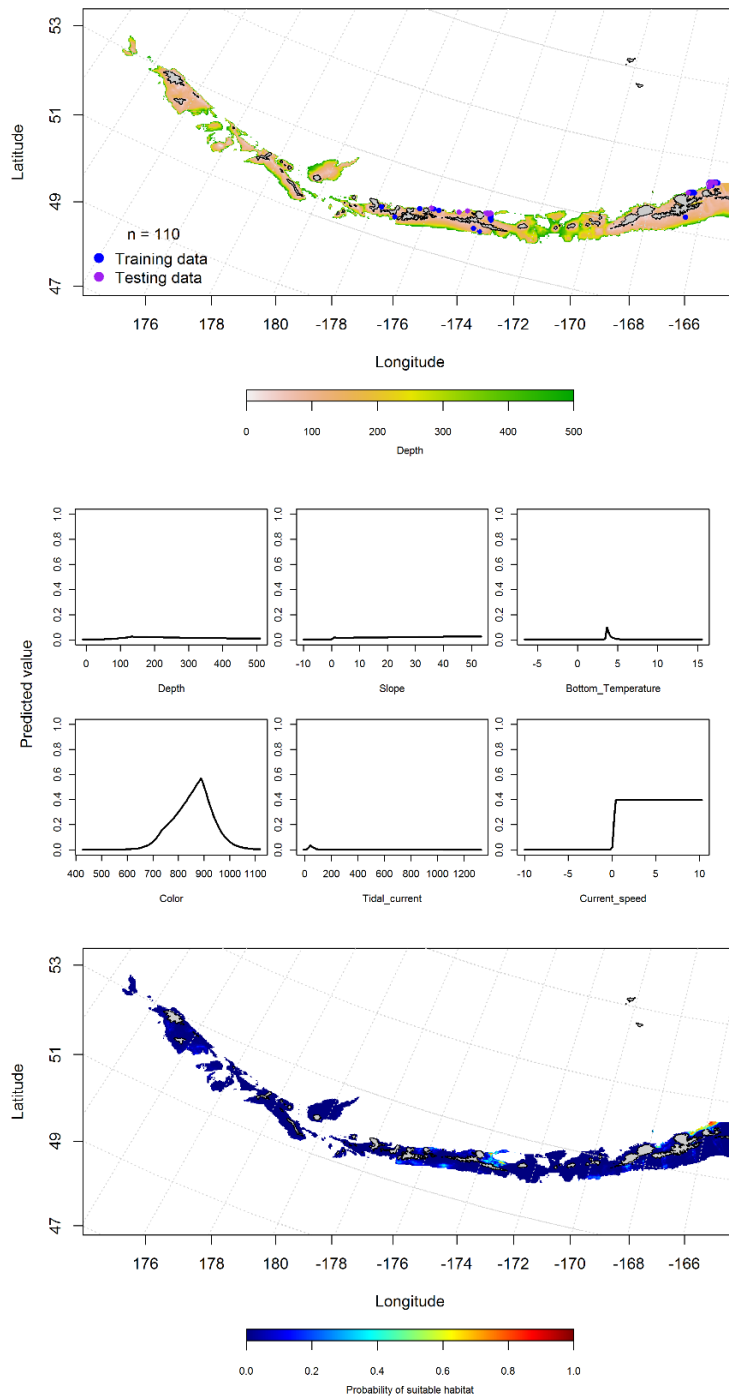


Figure 77. -- Locations of winter (December-February) commercial fisheries catches of adult sablefish (top panel), relationships between probability of presence and environmental variables for the maximum entropy model (middle panels), and predicted probability of suitable habitat for sablefish based on the model (bottom panel).

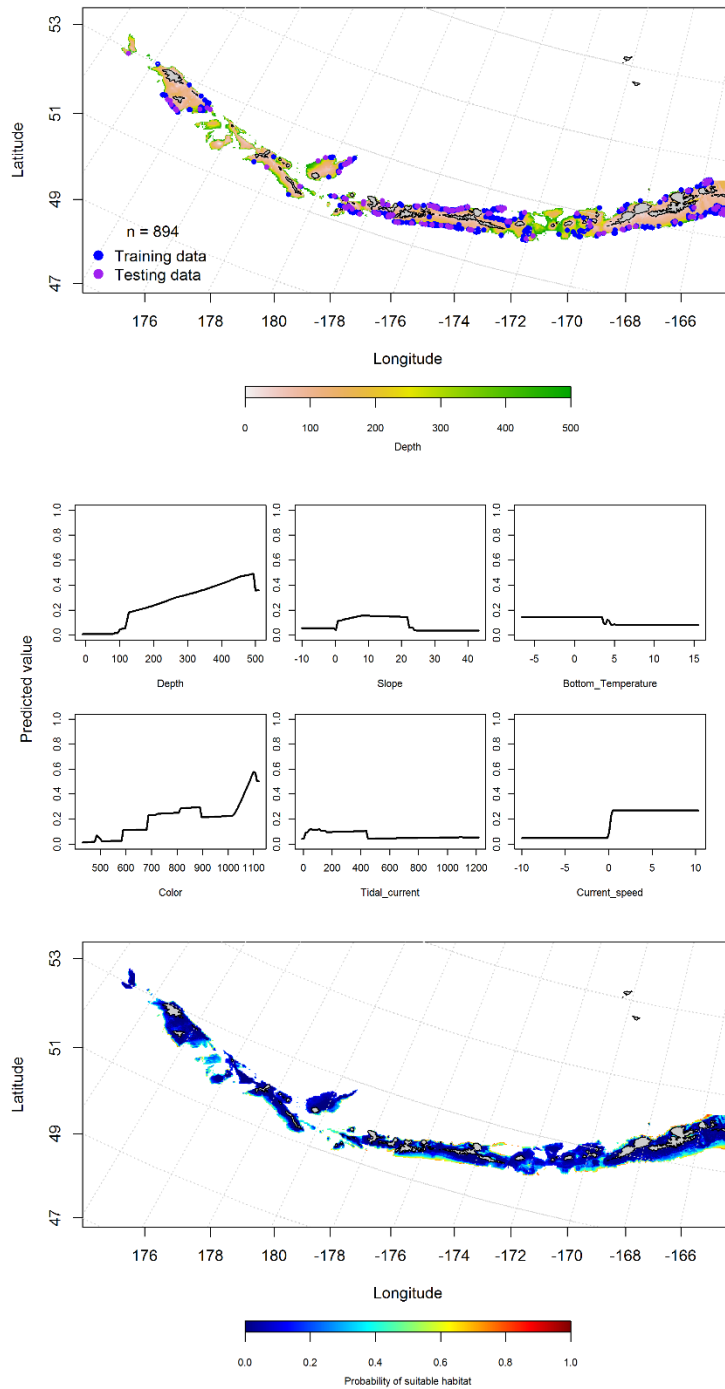


Figure 78. -- Locations of spring (March-May) commercial fisheries catches of adult sablefish (top panel), relationships between probability of presence and environmental variables for the maximum entropy model (middle panels), and predicted probability of suitable habitat for sablefish based on the model (bottom panel).

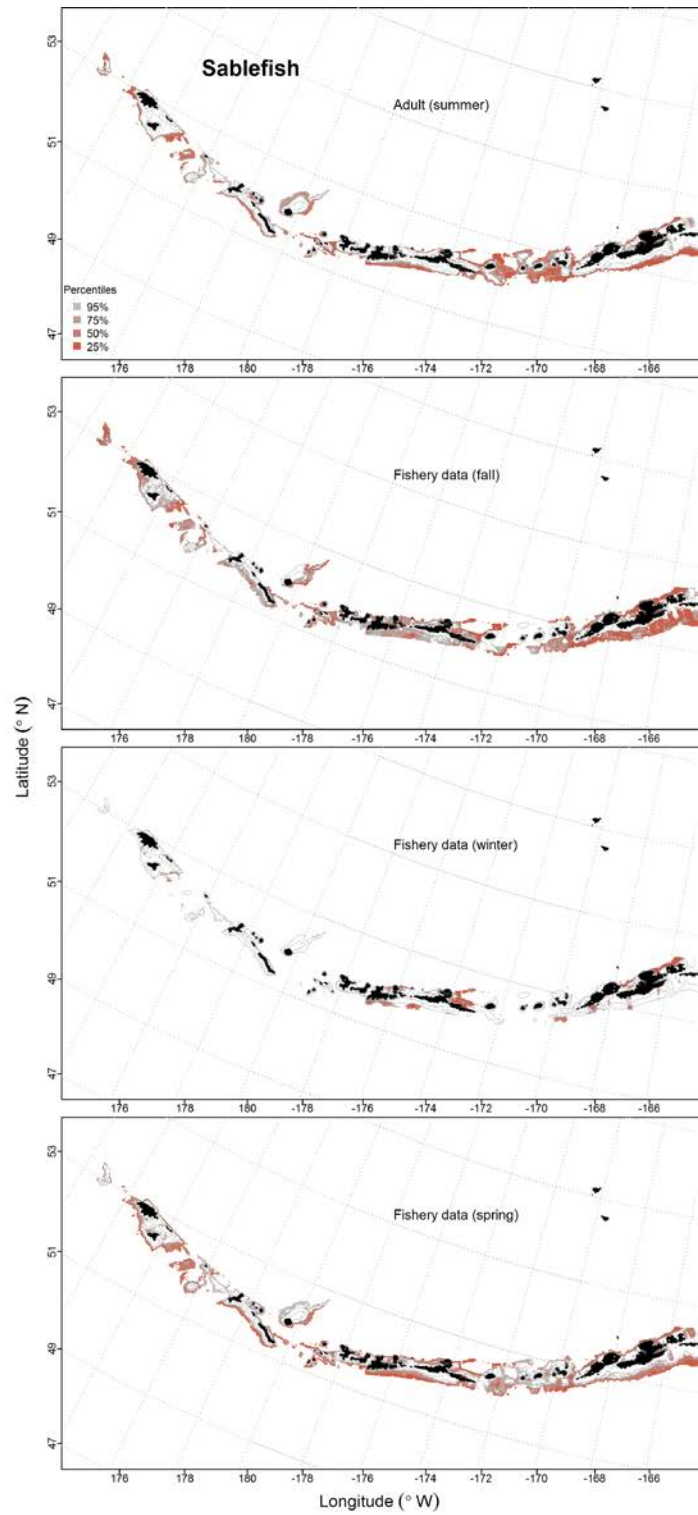


Figure 79. -- Predicted EFH quantiles for sablefish life history stages based on species distribution modeling. Adult stages are based on bottom trawl survey data, while seasonal stages (winter, spring, fall) are from commercial fishery data.

Great Sculpin (*Myoxocephalus polyacanthocephalus*)

Early life history stages of great sculpin --There were no identified records of great sculpin in the EcoFOCI database.

Juvenile and adult great sculpin distribution in the bottom trawl survey -- The catch of great sculpin in summer bottom trawl surveys of the Aleutian Islands indicates this species is broadly distributed. A MaxEnt model predicting suitable habitat of juvenile great sculpin had an AUC of 0.87 for the training data and 0.79 for the test data. Seventy-six percent of the training data and 79% of the test data were correctly classified. Bottom depth and tidal current were the most important variables explaining the distribution of juvenile great sculpin. The model predicted suitable habitat of juvenile great sculpin throughout the AI, though highest near Attu and Agattu islands in the west, and Unalaska Island in the east (Fig. 80).

A MaxEnt model predicting the suitable winter habitat of adult great sculpin had an AUC of 0.89 for the training data in the bottom trawl survey and 0.73 for the test data. Eighty-one percent of the training data and 73% of the test data were correctly classified. Depth, temperature and tidal current were the most important variables explaining suitable habitat of adult great sculpin. The predicted probability of suitable habitat was similar to juveniles (throughout the AI, though highest near Attu Agattu, and Unalaska islands) (Fig. 81).

Great sculpin distribution in commercial fisheries -- There were only 10 observations of great sculpin in the fall in the AI. In the winter, depth, ocean color, tidal current, and bottom temperature were the most important variables determining suitable habitat of great sculpin. The AUC of the winter MaxEnt model was 0.93 for the training data and 0.88 for the test data, and 88% of the cases in the training and test data set were predicted correctly. The model predicted

suitable habitat of great sculpin in the winter on the shallow shelf near Agattu Island in the west, and in shallow shelf waters near Atka and Unalaska islands in the east (Fig. 82).

In the spring, depth, ocean color, and tidal current were the most important variables determining suitable habitat of great sculpin. The AUC of the spring MaxEnt model was 0.95 for the training data and 0.77 for the test data, and the model correctly predicted 88% of the training data and 77% of the test data. As with the winter, the model predicted suitable habitat of great sculpin near Agattu Island in the west, and Atka Island in the east (Fig. 83).

Great sculpin essential fish habitat maps and conclusions -- Great sculpin EFH predicted by the modeling was similarly distributed across the Aleutian Islands for juvenile and adult life stages from summer bottom trawl surveys (Fig. 84). The winter and spring distribution of great sculpin EFH was generally the same in each season (Fig. 84), though more probable near Attu and Agattu islands in the winter.

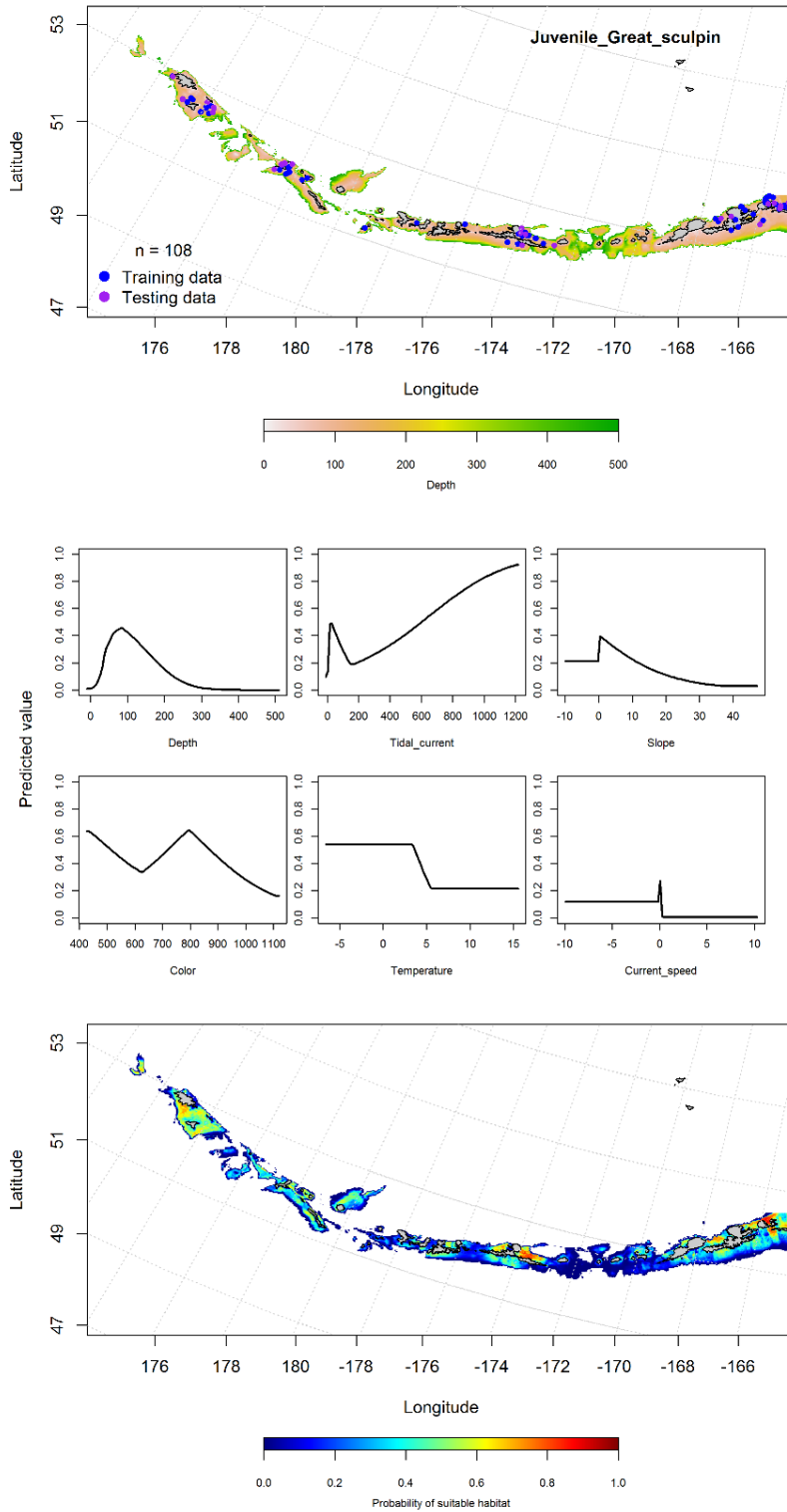


Figure 80. -- Distribution of catches of juvenile great sculpin in bottom trawl surveys (top panel), relationships between presence and environmental variables for the maximum entropy model of juvenile great sculpin (middle panels), and predicted probability of suitable habitat for juvenile great sculpin based on the model (bottom panel).

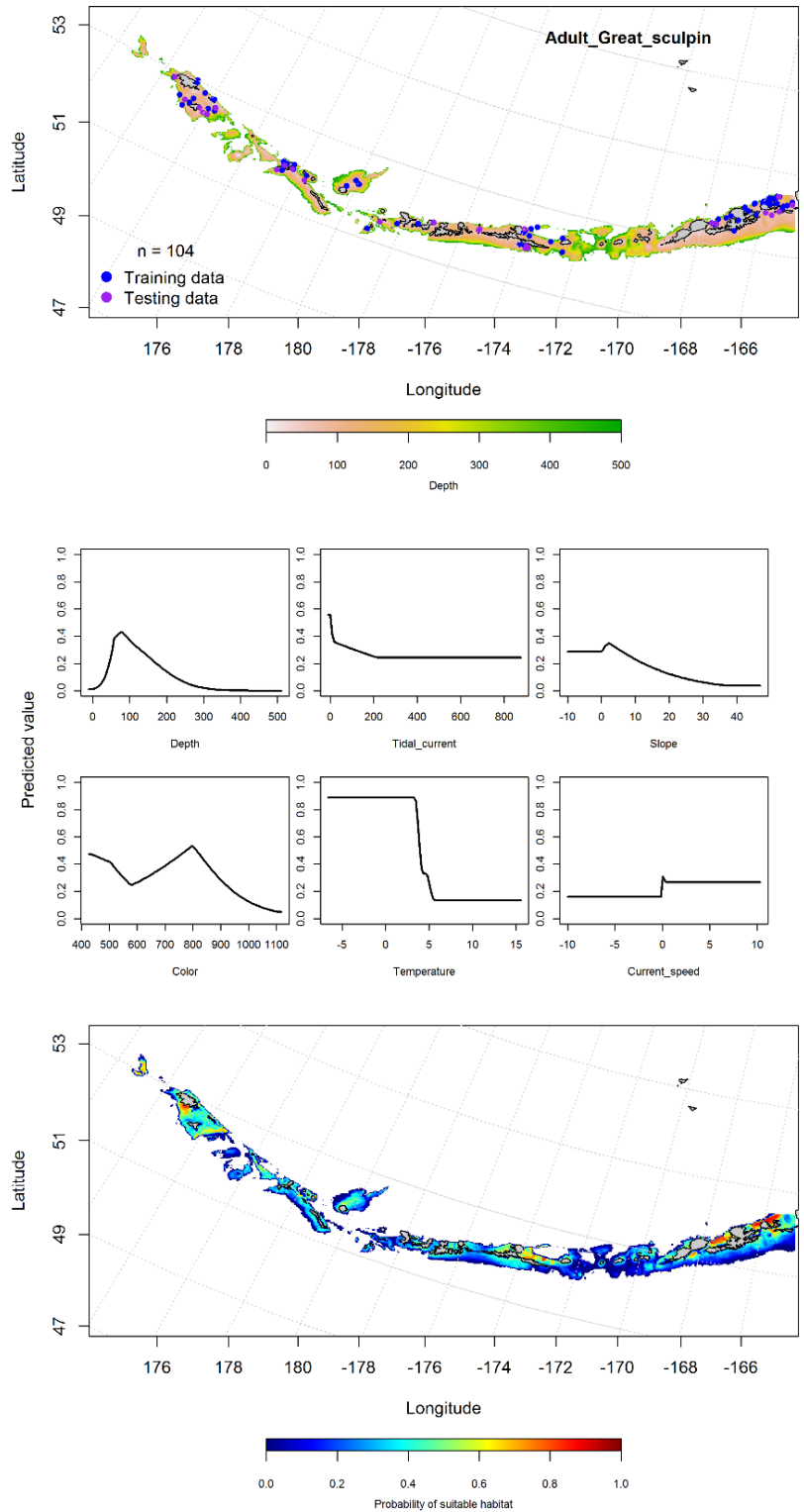


Figure 81. -- Distribution of catches of adult great sculpin in bottom trawl surveys (top panel), relationships between presence and environmental variables for the maximum entropy model of adult great sculpin (middle panels), and predicted probability of suitable habitat for adult great sculpin based on the model (bottom panel).

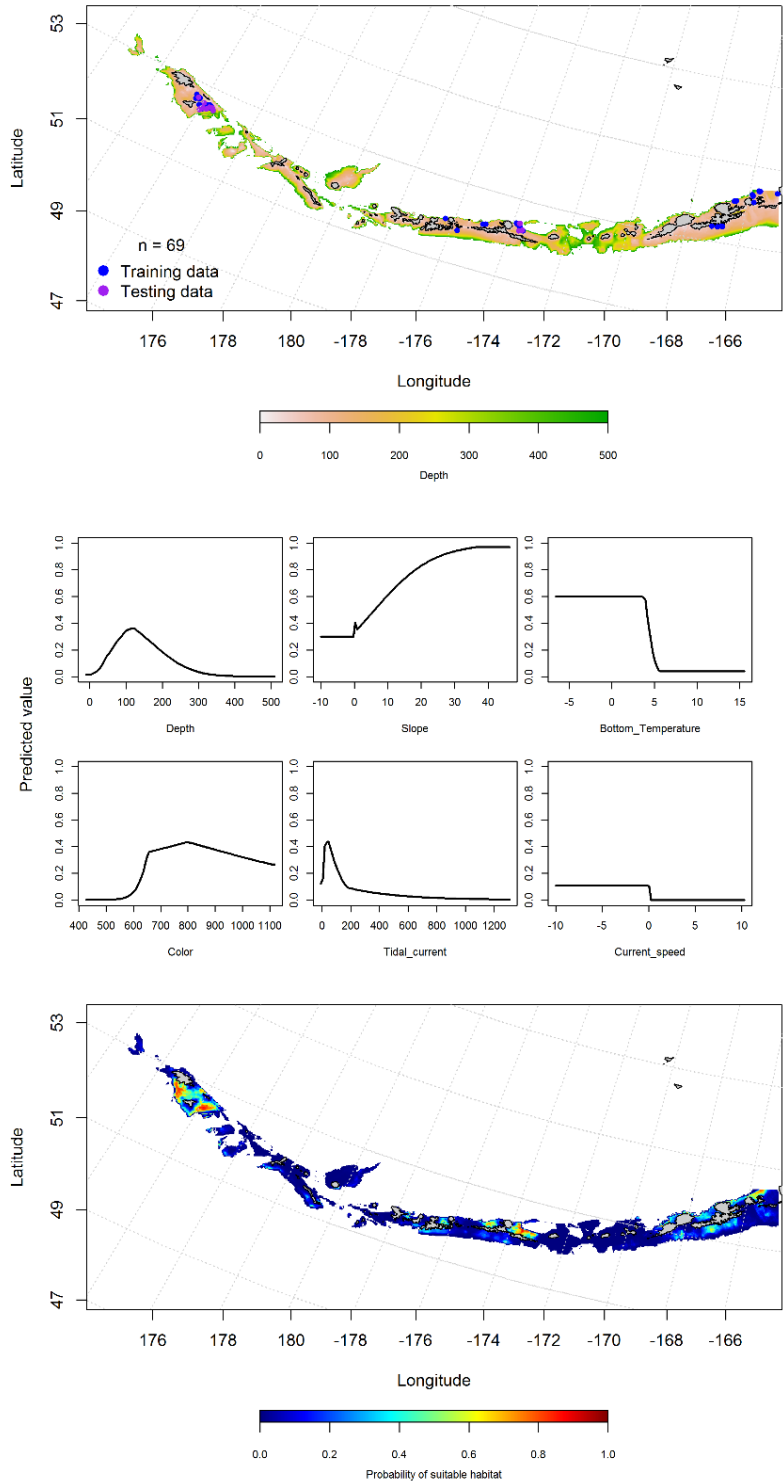


Figure 82. -- Locations of winter (December-February) commercial fisheries catches of great sculpin (top panel), relationships between probability of presence and environmental variables for the maximum entropy model (middle panels), and predicted probability of suitable habitat for sablefish based on the model (bottom panel).

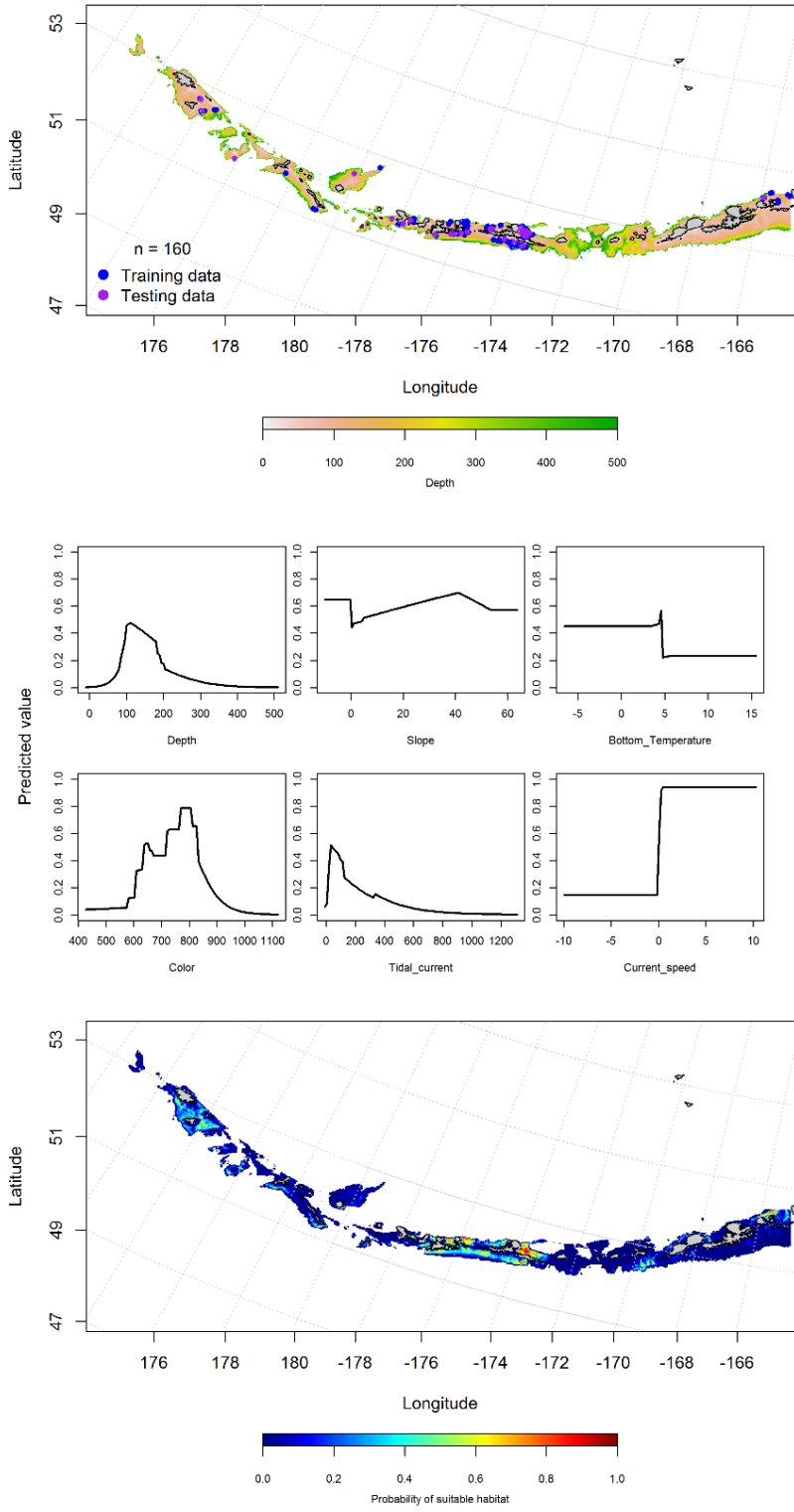


Figure 83. -- Locations of spring (March-May) commercial fisheries catches of great sculpin (top panel), relationships between probability of presence and environmental variables for the maximum entropy model (middle panels), and predicted probability of suitable habitat for sablefish based on the model (bottom panel).

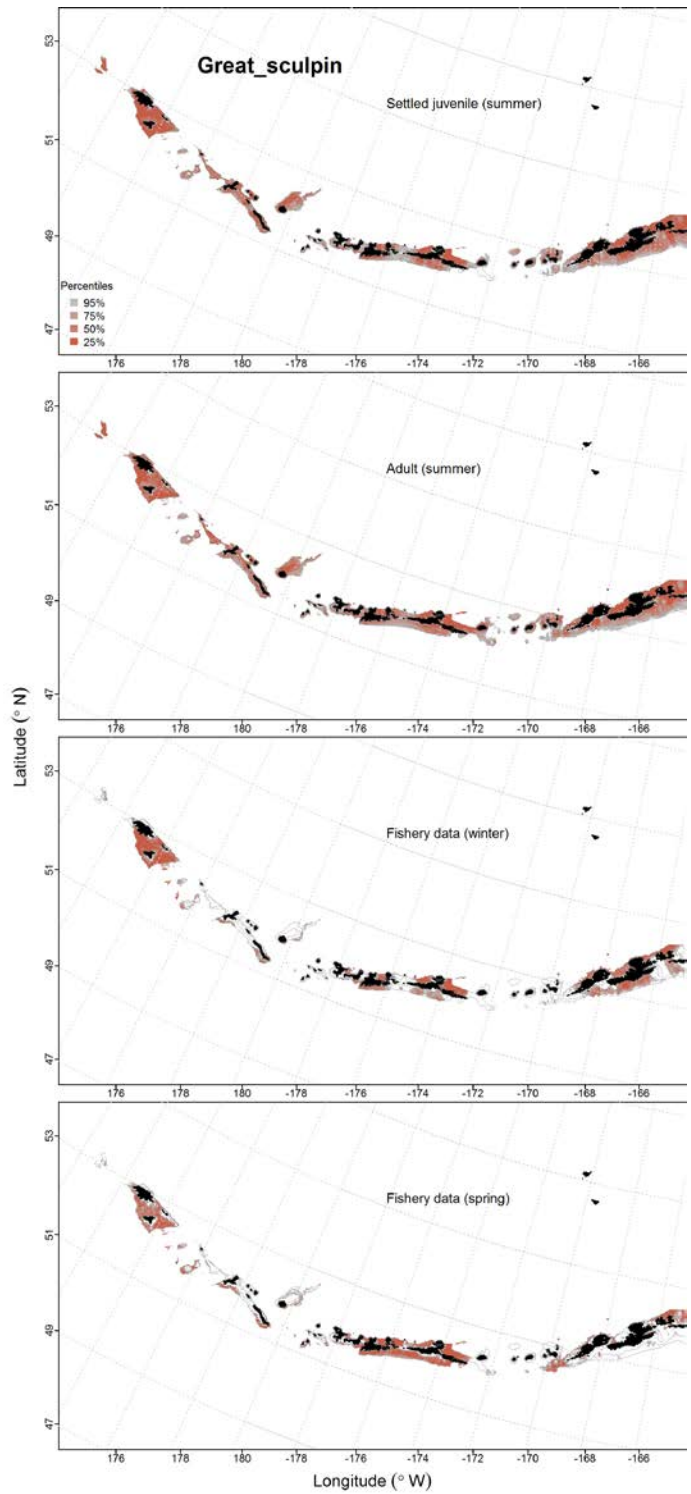


Figure 84. -- Predicted EFH quantiles for great sculpin life history stages based on species distribution modeling. Adult stages are based on bottom trawl survey data, while seasonal stages (winter, spring) are from commercial fishery data.

Yellow Irish Lord (*Hemilepidotus jordani*)

Early life history stages of great sculpin -- There were only 10 identified records (4 larvae and 6 pelagic juveniles) of yellow Irish lord in the EcoFOCI database.

Juvenile and adult great sculpin distribution in the bottom trawl survey -- The catch of yellow Irish lord in summer bottom trawl surveys of the Aleutian Islands indicates this species is broadly distributed. A MaxEnt model predicting the suitable habitat of juvenile yellow Irish lord resulted in AUC values of 0.91 for the training data and 0.73 for the test data set, and correctly classified 82% of the training data and 73% of the test data. Bottom depth and ocean color were the most important variables predicting the probability of suitable habitat of juvenile yellow Irish lord across the AI (Fig. 85).

A hurdle-GAM was used to predict the distribution of adult yellow Irish lord. The PA GAM resulted in an AUC of 0.80 for the training data where depth, location, and the presence of sponge were the most important variables in the model (Fig. 86). The AUC for predicting the test data was 0.78. Predicted suitable habitat was distributed throughout the AI, though highest probabilities were in the eastern AI (Fig. 86). The CPUE GAM explained 26% of the variability of the training data set and 26% of the test data set. Location, depth, and the presence of sponge were the most important variables explaining the CPUE of adult yellow Irish lord. The areas of highest abundance were in the central and eastern AI in shallow waters (Fig. 86).

Great sculpin distribution in commercial fisheries -- Distribution of adult yellow Irish lord in the Aleutian Islands in commercial fisheries catches was consistent throughout all seasons. In the fall, current speed, depth, and temperature were the most important variables determining suitable habitat of yellow Irish lord. The AUC of the fall MaxEnt model was 0.98 for the training

data and 0.91 for the test data with 92% of the cases in both the training data and 91% of the test data sets were predicted correctly. The model predicted suitable habitat of yellow Irish lord across the AI (Fig. 87).

In the winter, bottom depth and current speed were the most important variables determining suitable habitat of yellow Irish lord. The AUC of the winter MaxEnt model was 0.94 for the training data and 0.86 for the test data, with 85% of the cases in the training data and 86% of the test data were predicted correctly. As with the fall, the model predicted suitable habitat of yellow Irish lord across the AI (Fig. 88).

In the spring, bottom depth, ocean color and current speed were the most important variables determining suitable habitat of yellow Irish lord. The AUC of the spring MaxEnt model was 0.94 for the training data and 0.82 for the test data. The model correctly classified 87% of the training data and 82% of the test data. The model predicted suitable habitat of yellow Irish lord across the AI, though higher probability near Attu and Agattu islands, and in the central AI (Fig. 89).

Yellow Irish lord essential fish habitat maps and conclusions -- Summertime EFH of yellow Irish lord juveniles and adults varied in the western AI (Fig. 90). Juvenile EFH was more abundant in the central AI, while adult yellow Irish lord EFH was distributed across the AI and less abundant in the western AI. The fall, winter and spring distribution of yellow Irish lord was essentially the same throughout the seasons (Fig. 90).

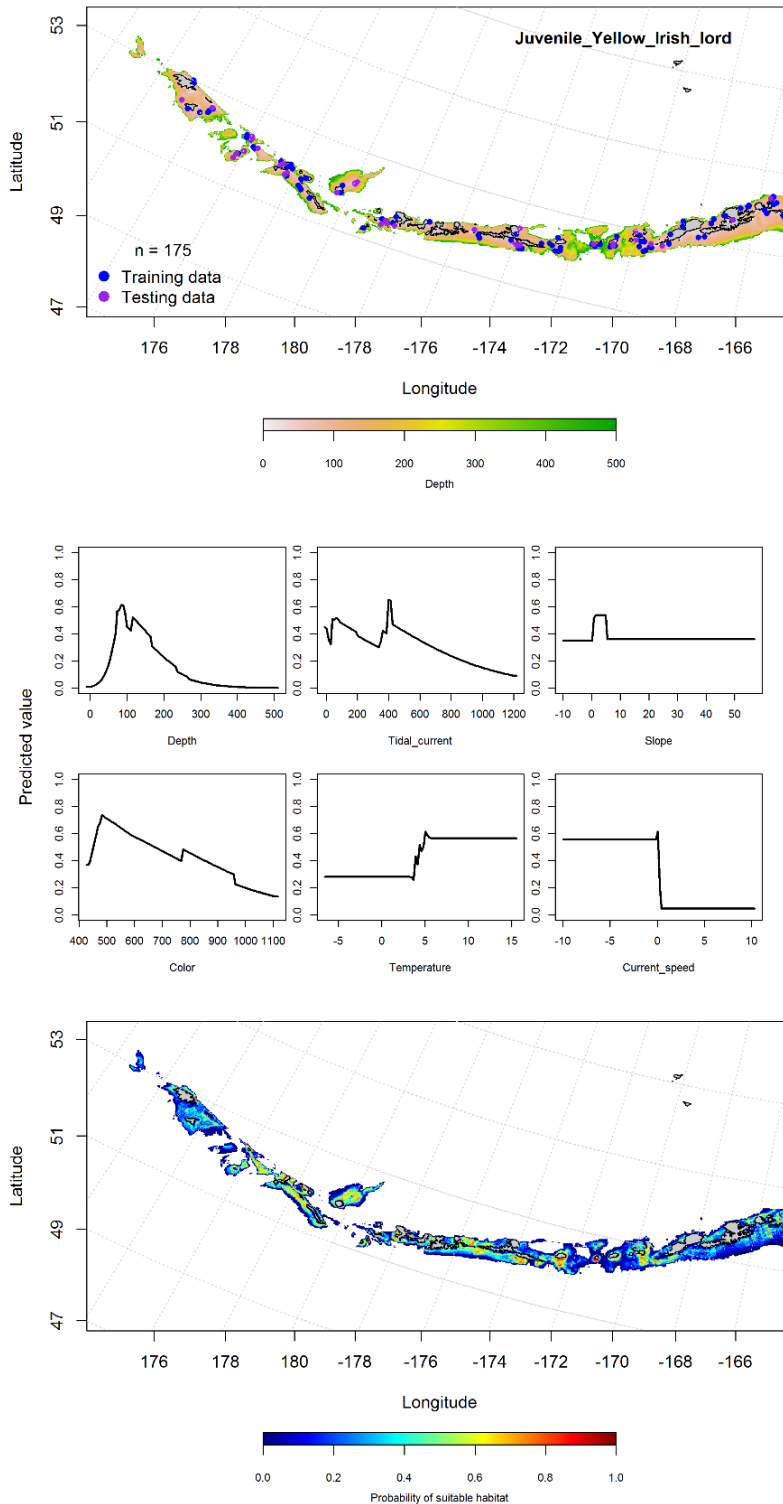


Figure 85. -- Distribution of catches of juvenile yellow Irish lord in bottom trawl surveys (top panel), relationships between presence and environmental variables for the maximum entropy model of juvenile yellow Irish lord (middle panels), and predicted probability of suitable habitat for juvenile yellow Irish lord based on the model (bottom panel).

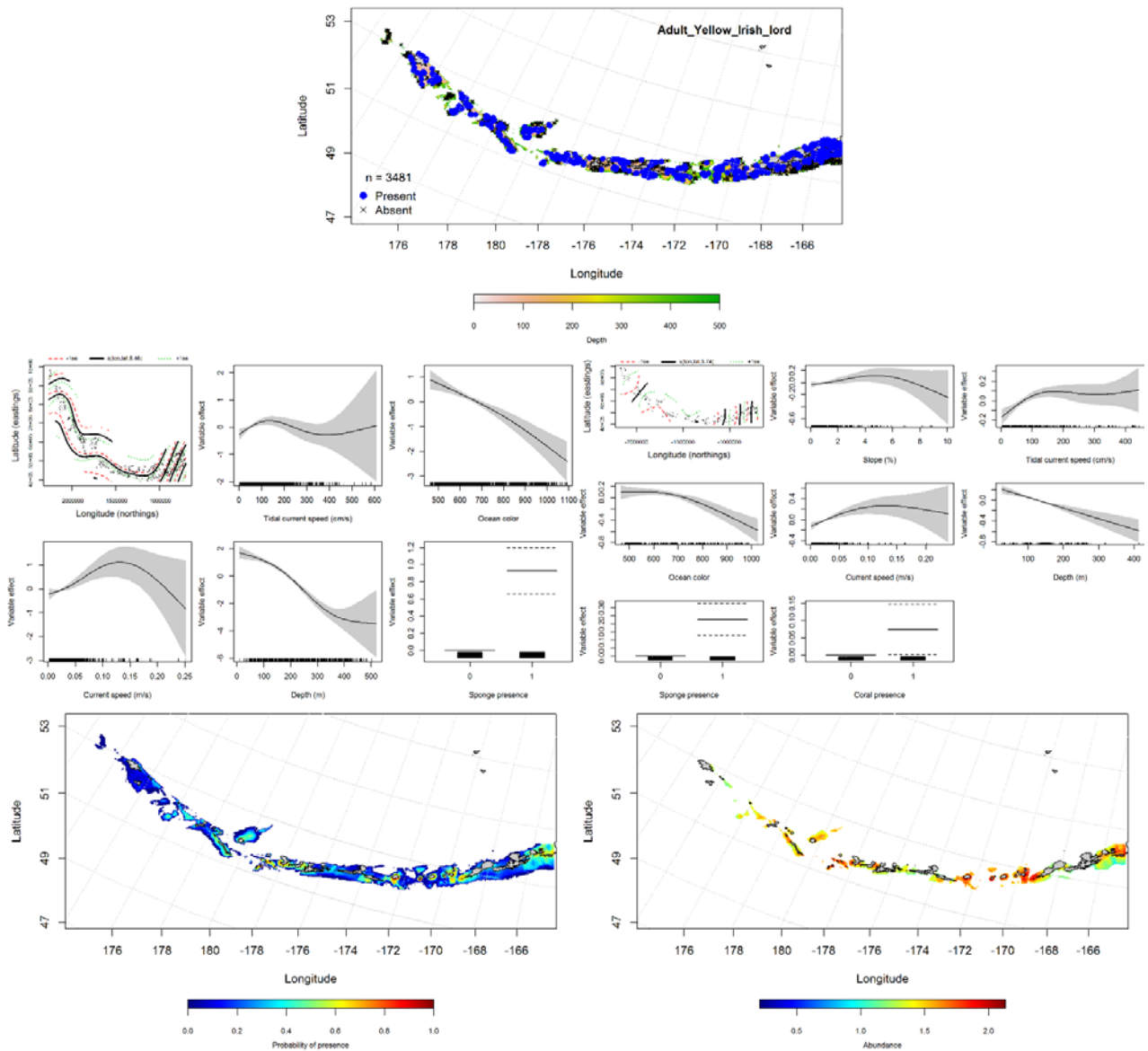


Figure 86. -- Distribution of catches of adult yellow Irish lord in bottom trawl surveys (top middle panel), significant relationships between CPUE and environmental variables for the best-fitting generalized additive model of adult yellow Irish lord (middle left and right panels), and predicted probability of presence and abundance of adult yellow Irish lord based on the models (bottom left and right panels).

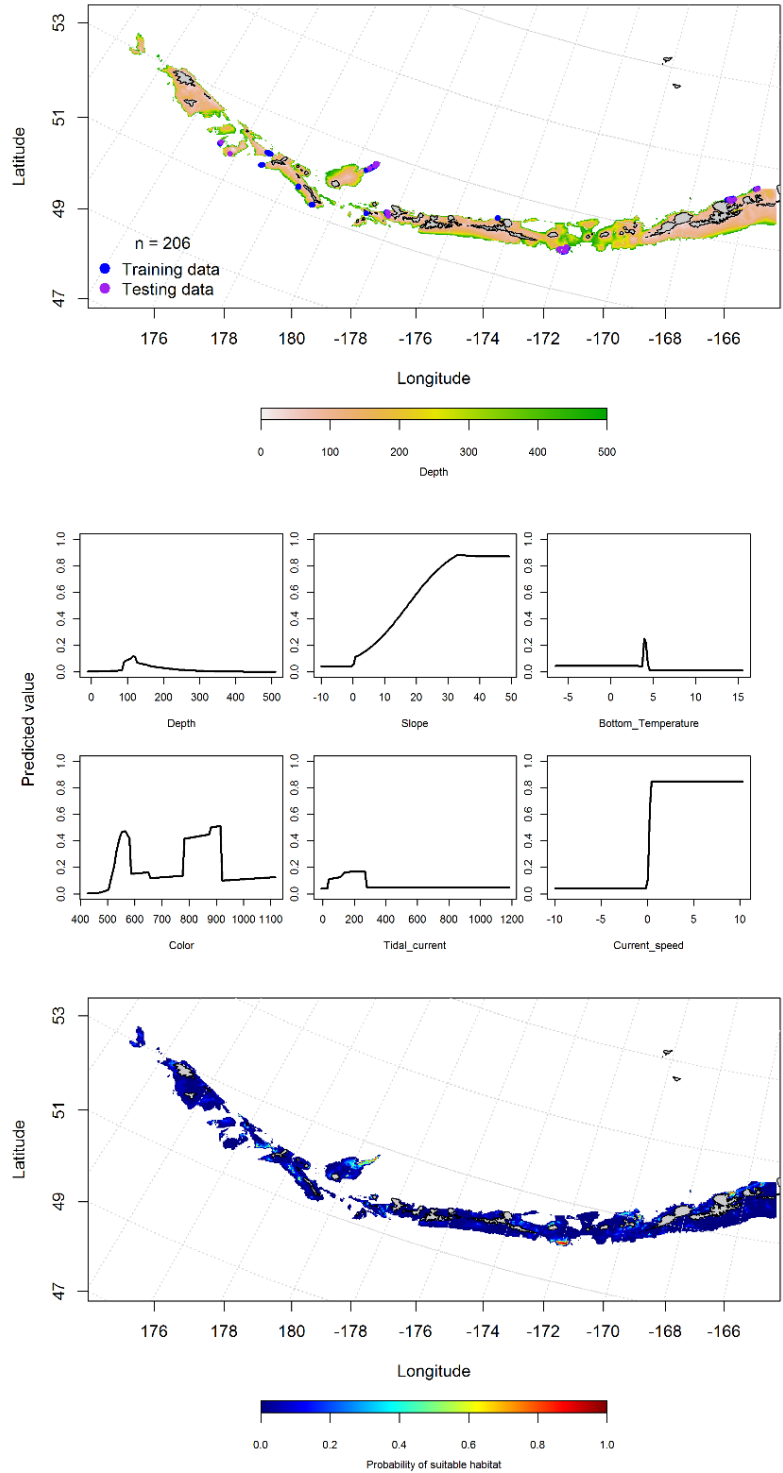


Figure 87. -- Locations of fall (September-November) commercial fisheries catches of yellow Irish lord (top panel), relationships between probability of presence and environmental variables for the maximum entropy model (middle panels), and predicted probability of suitable habitat for yellow Irish lord based on the model (bottom panel).

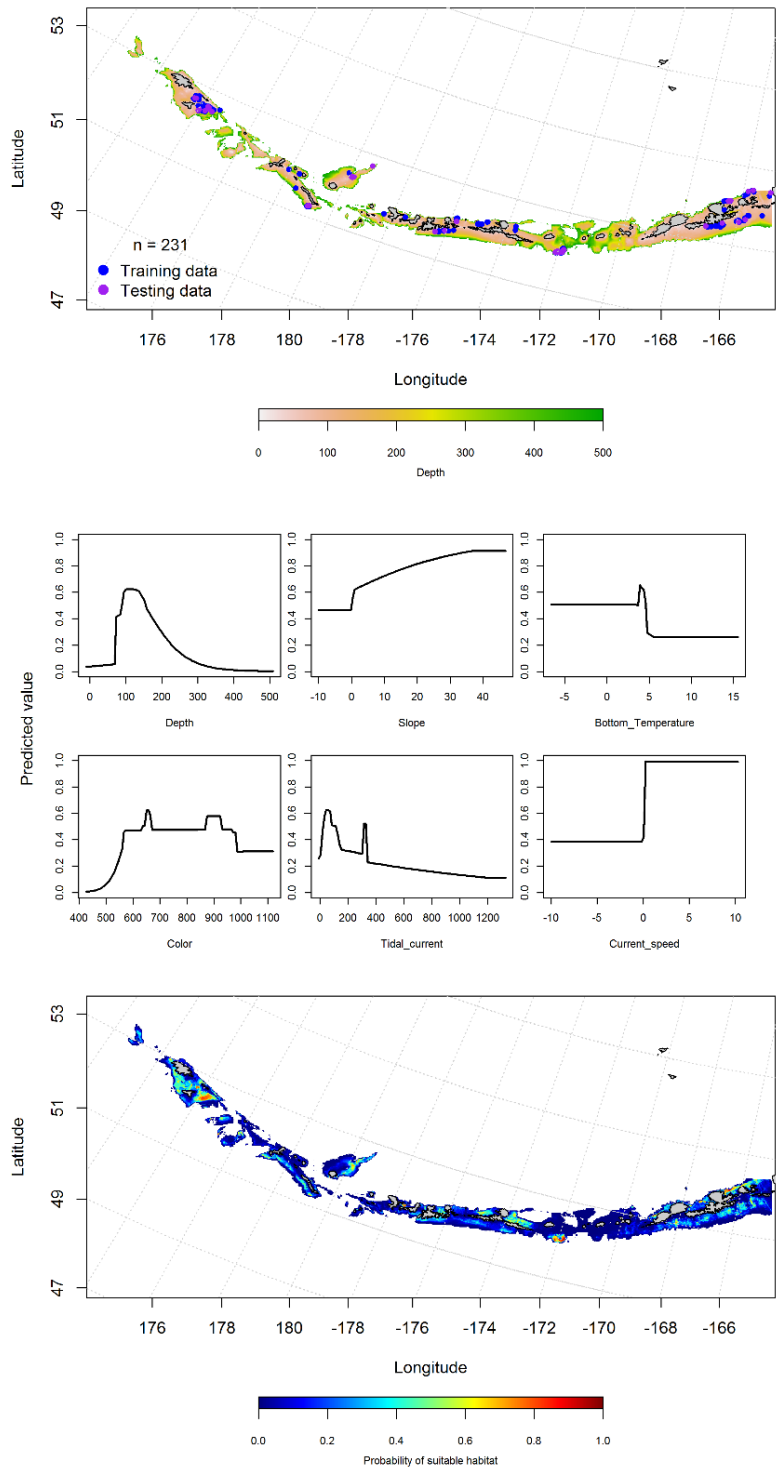


Figure 88. -- Locations of winter (December-February) commercial fisheries catches of yellow Irish lord (top panel), relationships between probability of presence and environmental variables for the maximum entropy model (middle panels), and predicted probability of suitable habitat for yellow Irish lord based on the model (bottom panel).

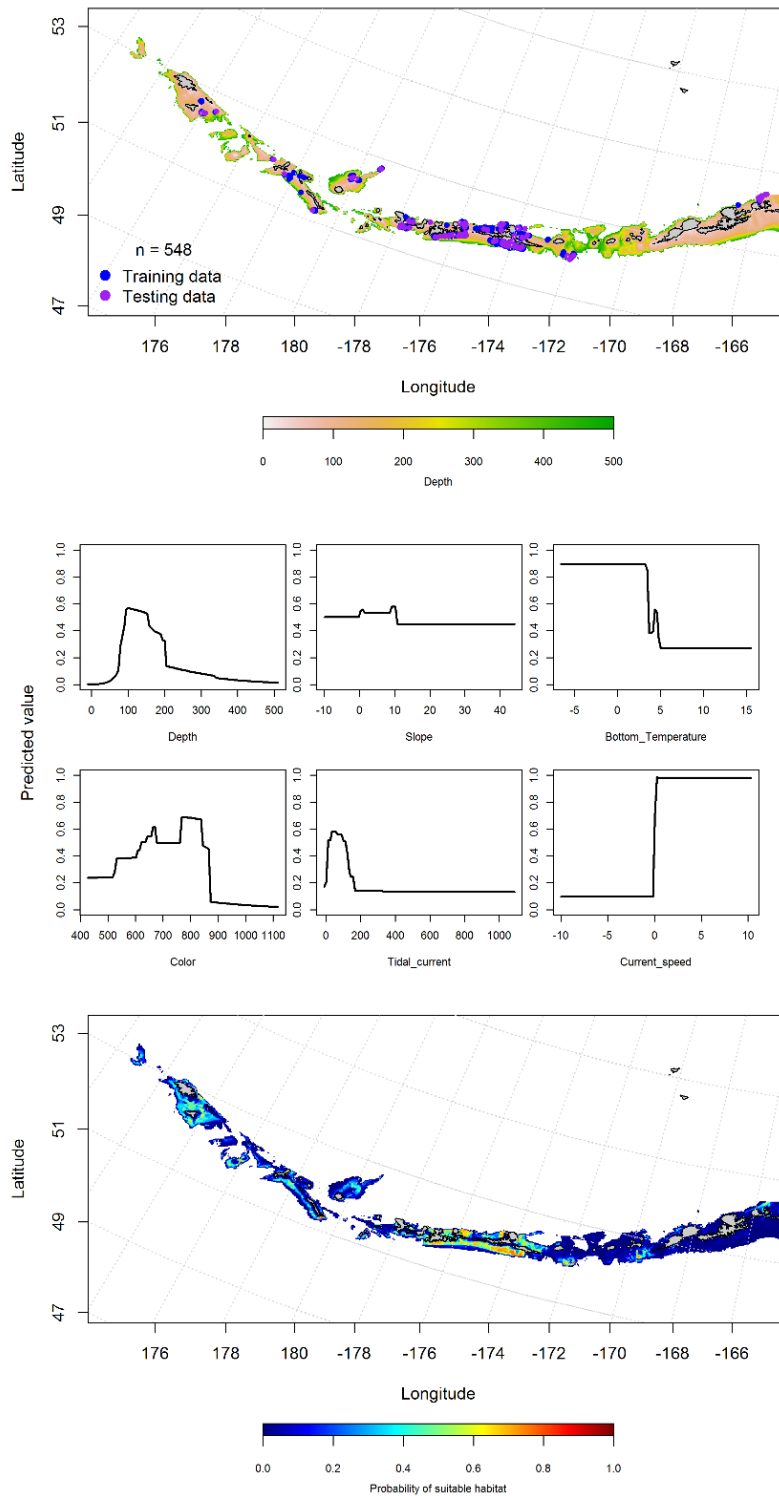


Figure 89. -- Locations of spring (March-May) commercial fisheries catches of yellow Irish lord (top panel), relationships between probability of presence and environmental variables for the maximum entropy model (middle panels), and predicted probability of suitable habitat for yellow Irish lord based on the model (bottom panel).

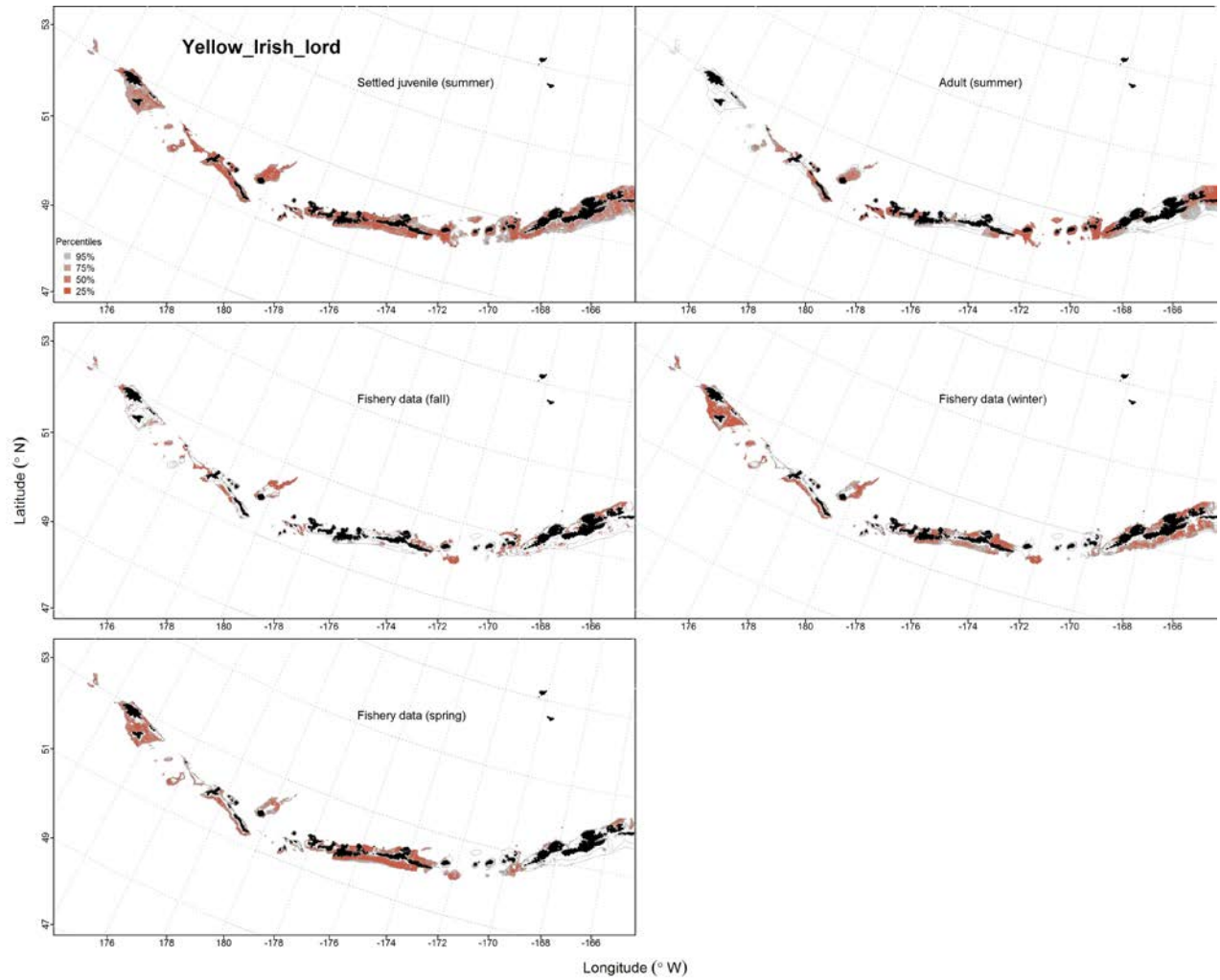


Figure 90. -- Predicted EFH quantiles for yellow Irish lord life history stages based on species distribution modeling. Settled juvenile and summer adult stages are based on bottom trawl survey data, while seasonal stages (winter, spring, fall) are from commercial fishery data.

Bigmouth Sculpin (*Hemitripterus bolini*)

Early life history stages of bigmouth sculpin --There were no instances of early life history stages of bigmouth sculpin in the EcoFOCI database.

Juvenile and adult bigmouth sculpin distribution in the bottom trawl survey -- The catch of bigmouth sculpin in summer bottom trawl surveys of the Aleutian Islands indicates this species is broadly distributed but relatively rare. There were not enough cases (n = 33) to model juvenile stages of bigmouth sculpin. A MaxEnt model predicting suitable habitat of adult bigmouth sculpin had an AUC of 0.85 for the training data and 0.75 for the test data. The model correctly classified 76% of the training data and 75% of the test data. Depth, temperature, and current speed were the most important variables explaining suitable habitat of adult bigmouth sculpin. The model predicted suitable habitat of adult bigmouth sculpin across the AI, though highest near Attu and Agattu islands in the west, Seguam Island in the central AI, and Akutan Island in the eastern AI (Fig. 91).

Bigmouth sculpin distribution in commercial fisheries -- Distribution of adult bigmouth sculpin in the Aleutian Islands in commercial fisheries catches was generally consistent throughout all seasons. In the fall, depth, temperature, and ocean color were the most important variables determining suitable habitat of bigmouth sculpin. The AUC of the fall MaxEnt model was 0.98 for the training data and 0.92 for the test data, with 94% of the training data and 92% of the test data correctly classified. The model predicted suitable habitat of adult bigmouth sculpin across the AI (Fig. 92).

In the winter, depth, tidal current and ocean color were the most important variables determining probable suitable habitat of bigmouth sculpin. The AUC of the winter MaxEnt

model was 0.96 for the training data and 0.85 for the test data, with 89% of the training data and 85% of the test data sets predicted correctly. The model predicted suitable winter habitat of bigmouth sculpin across the AI, though highest probabilities were in the western AI near Agattu and Attu islands, and in the central AI near Atka Island (Fig. 93).

In the spring, depth, ocean color and tidal current were the most important variables determining suitable habitat of bigmouth sculpin. The AUC of the spring MaxEnt model was 0.95 for the training data and 0.83 for the test data, and 87% of the training and 83% of the test data sets were correctly classified. The model predicted suitable habitat of bigmouth sculpin was distributed similar to the predictions in the winter (Fig. 94).

Bigmouth sculpin essential fish habitat maps and conclusions -- Bigmouth sculpin essential fish habitat predicted by the modeling is extensively distributed across the Aleutian Islands for adult life history stages although less abundant in some of the large passes in the west (Fig. 95). The fall, winter and spring distribution of bigmouth sculpin EFH was generally the same throughout the seasons in the Aleutian Islands (Fig. 95). Bigmouth sculpin were predicted to be more abundant in the western AI near Agattu and Attu islands in the winter, and in the central AI near Atka Island in the spring than in other seasons.

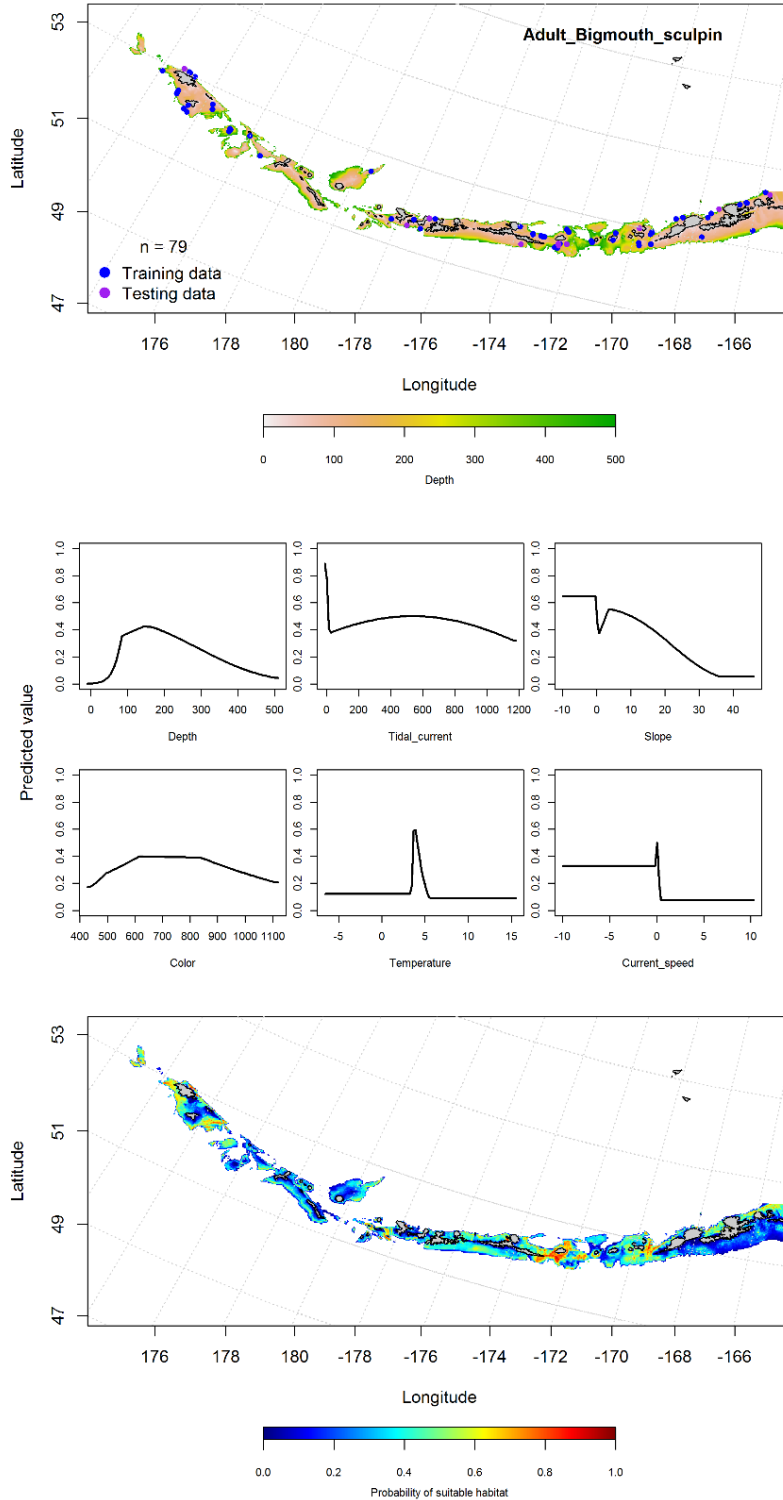


Figure 91. -- Distribution of catches of adult bigmouth sculpin in bottom trawl surveys (top panel), relationships between presence and environmental variables for the maximum entropy model of adult bigmouth sculpin (middle panels), and predicted probability of suitable habitat for adult bigmouth sculpin based on the model (bottom panel).

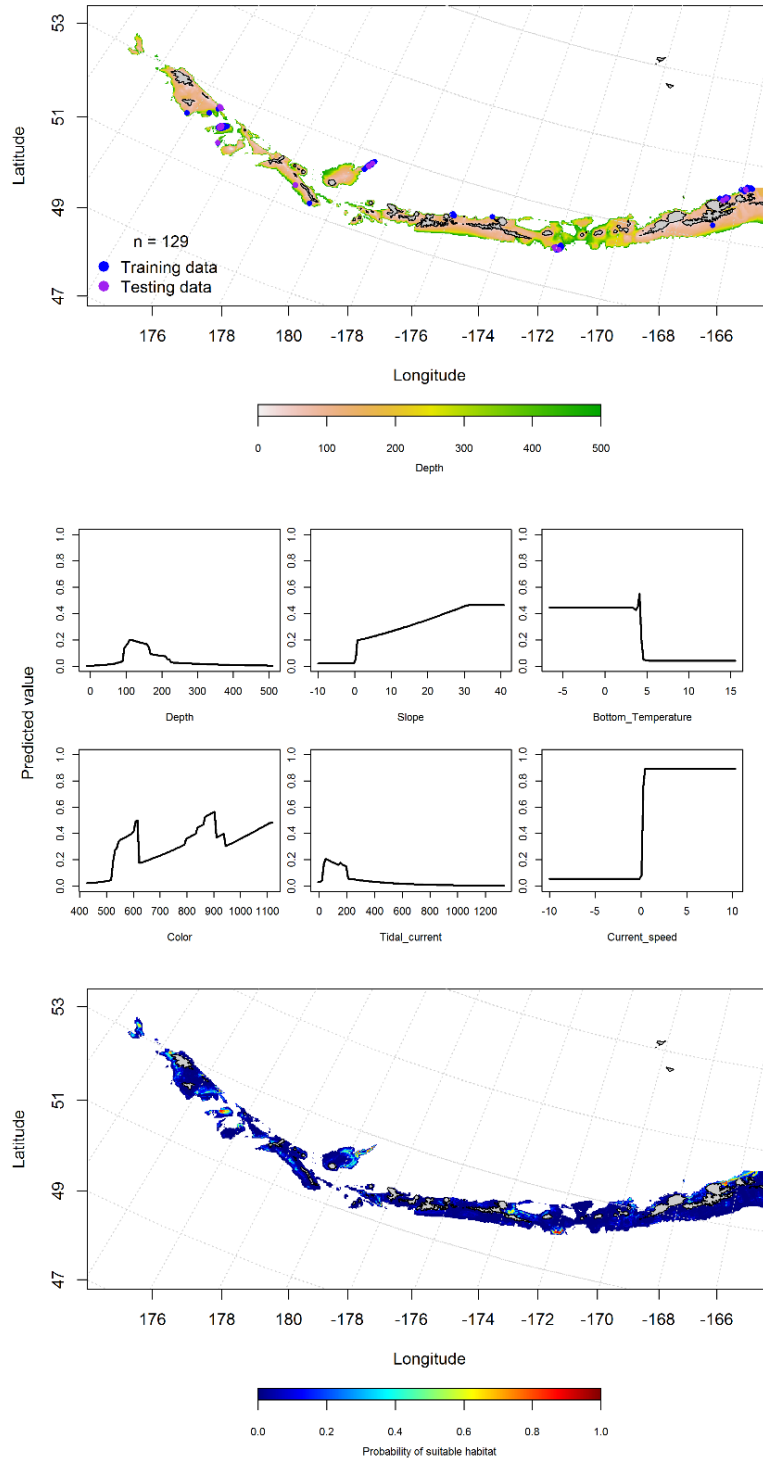


Figure 92. -- Locations of fall (September-November) commercial fisheries catches of adult bigmouth sculpin (top panel), relationships between probability of presence and environmental variables for the maximum entropy model (middle panels), and predicted probability of suitable habitat for bigmouth sculpin based on the model (bottom panel).

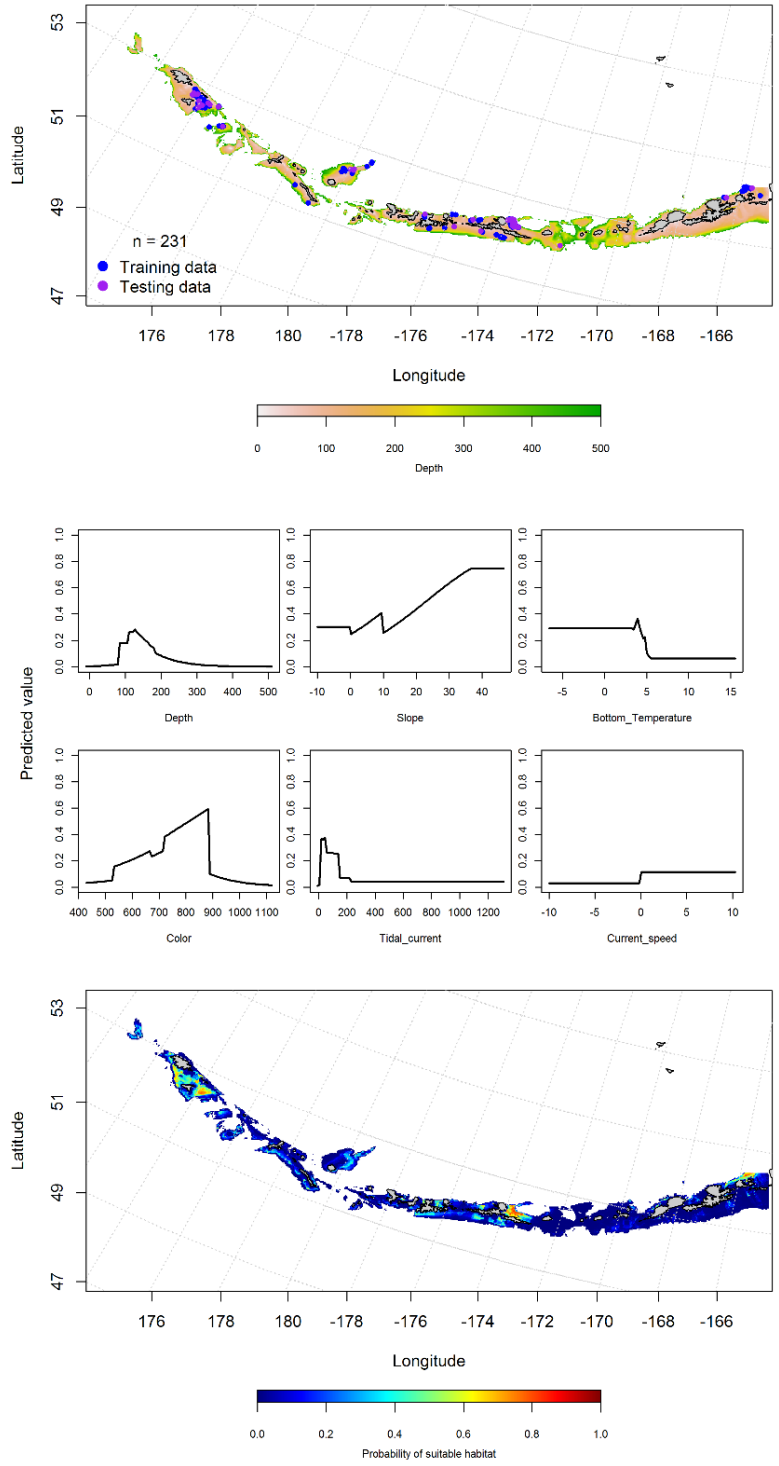


Figure 93. -- Locations of winter (December-February) commercial fisheries catches of adult bigmouth sculpin (top panel), relationships between probability of presence and environmental variables for the maximum entropy model (middle panels), and predicted probability of suitable habitat for bigmouth sculpin based on the model (bottom panel).

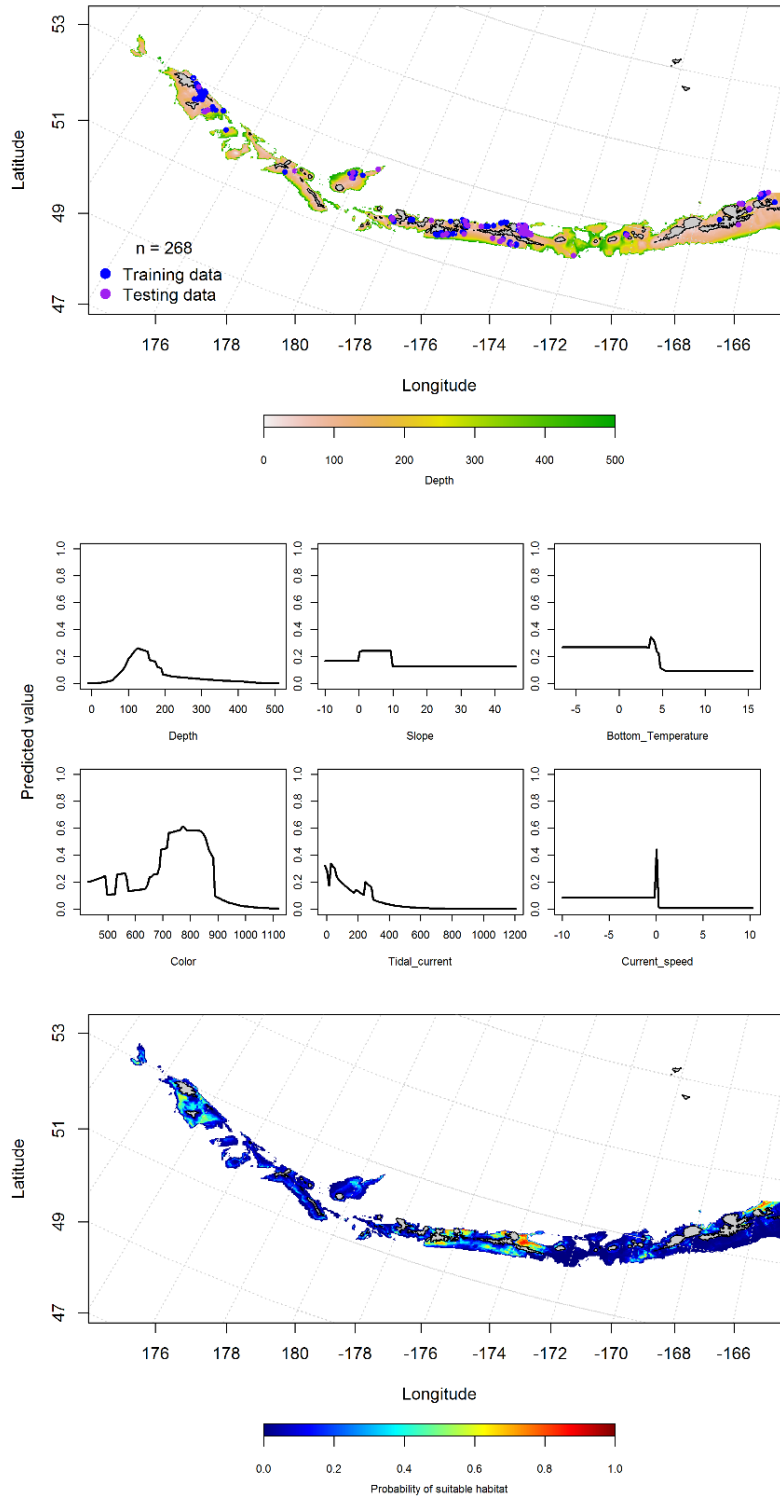


Figure 94. -- Locations of spring (March-May) commercial fisheries catches of adult bigmouth sculpin (top panel), relationships between probability of presence and environmental variables for the maximum entropy model (middle panels), and predicted probability of suitable habitat for bigmouth sculpin based on the model (bottom panel).

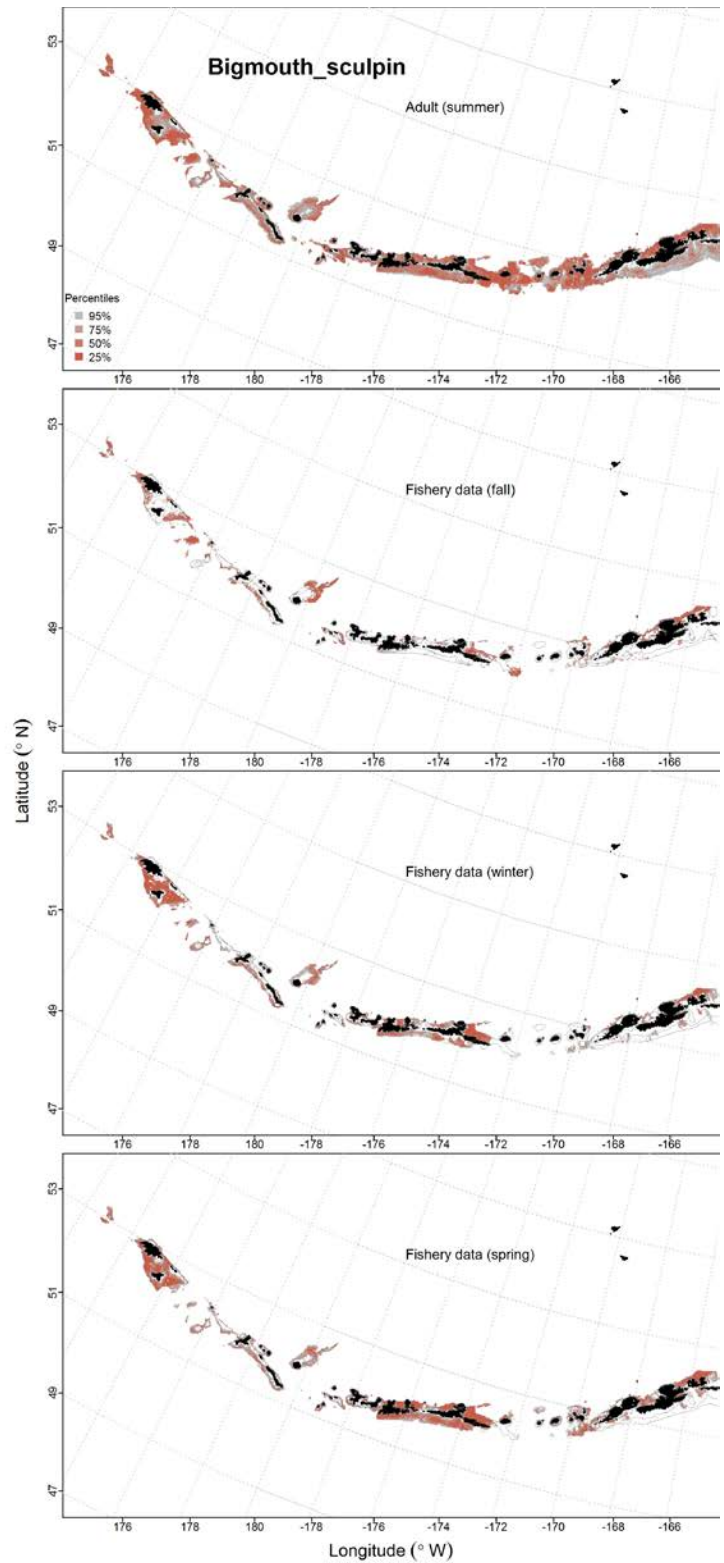


Figure 95. -- Predicted EFH quantiles for bigmouth sculpin life history stages based on species distribution modeling. Summer adult stages are based on bottom trawl survey data, while seasonal stages (winter, spring, fall) are from commercial fishery data.

Rockfishes

Pacific Ocean Perch (*Sebastes alutus*)

Early life history stages for *Sebastes* spp. weren't distinguished in the EcoFOCI database. Thus, EFH modeling for *Sebastes* larval stages were combined in the Pacific ocean perch (POP) section.

Early life history stages of *Sebastes* spp. -- There were 130 instances of larval *Sebastes* observed in the EcoFOCI database (Fig. 96), and all observations were found in the eastern AI. Surface temperature, ocean color, and current speed were the most significant variables in modeling probability of larval *Sebastes* spp. suitable habitat. The MaxEnt model AUC was 0.96 for the training and 0.94 for the test data, and correctly classified 91% of the training data and 94% of the test data set. The model predicted suitable habitat of spring *Sebastes* larvae in the eastern AI (Fig. 96).

Juvenile and adult Pacific ocean perch distribution in the bottom trawl survey -- A hurdle-GAM was used to predict the distribution of juvenile POP. The PA GAM indicated that depth, the presence of coral, location and the presence of sponge were the most important variables in the model. The AUC of the model was 0.77 for the training and test data. The model correctly classified 70% of the training data set and 71% of the test data set. The areas of predicted highest presence were concentrated from Atka Island to Samalga Pass and near Tahoma Reef in the western AI (Fig. 97). The CPUE GAM found location, depth, ocean color and the presence of coral were the most important determinants of CPUE. Overall, the hurdle model explained 16% of the variability in the training data and 11% in the test data. The model predicted the highest CPUE at Stalemate Bank and Tahoma Reef in the western AI (Fig. 97).

A GAM predicting the abundance of adult POP explained 43% of the variability in CPUE in the bottom trawl survey training data, and 46% of the variability in the test data. Depth, slope, geographic location, ocean color and the presence of coral were the most important variables explaining the catch of adult POP. Adult POP were distributed throughout the AI (Fig. 98).

Pacific ocean perch distribution in commercial fisheries -- Distribution of adult Pacific ocean perch in the Aleutian Islands in commercial fisheries catches was generally consistent in all seasons. In the fall, depth and temperature were the most important variables determining the distribution of POP. The AUC of the fall MaxEnt model was 0.94 for the training data and 0.88 for the test data. The model correctly predicted 87% of the training data set and 88% of the test data set. The model predicted probable suitable habitat of POP across the AI (Fig. 99).

In winter, depth, ocean color and temperature were the most important variables determining the distribution of POP. The AUC of the winter MaxEnt model was 0.96 for the training and 0.89 for the test data, and 90% of the catches in the training and 89% in the test data were predicted correctly. The model predicted suitable habitat of POP throughout the AI (Fig. 100).

In the spring, bottom depth and ocean color were the most important variables determining the distribution of adult POP. The AUC of the fall model was 0.91 for the training data and 0.86 for the test data. 83% of the training data and 86% of the test data sets were predicted correctly. As with fall and winter, the model predicted suitable habitat of POP throughout the AI (Fig. 100).

Pacific ocean perch essential fish habitat maps and conclusions -- Larval *Sebastes* spp. EFH was limited to the eastern AI (Fig. 102). Summertime EFH of juvenile POP was less broadly

distributed throughout the AI than the adult POP (Fig. 102). Similar to adult summertime bottom trawl survey data observations, the EFH predicted from commercial catches of POP in the fall, winter and spring was distributed throughout the Aleutian Islands chain (Fig. 102). There does not appear to be much seasonal variability to the EFH distribution and areas of high concentration are interspersed with areas of low concentration.

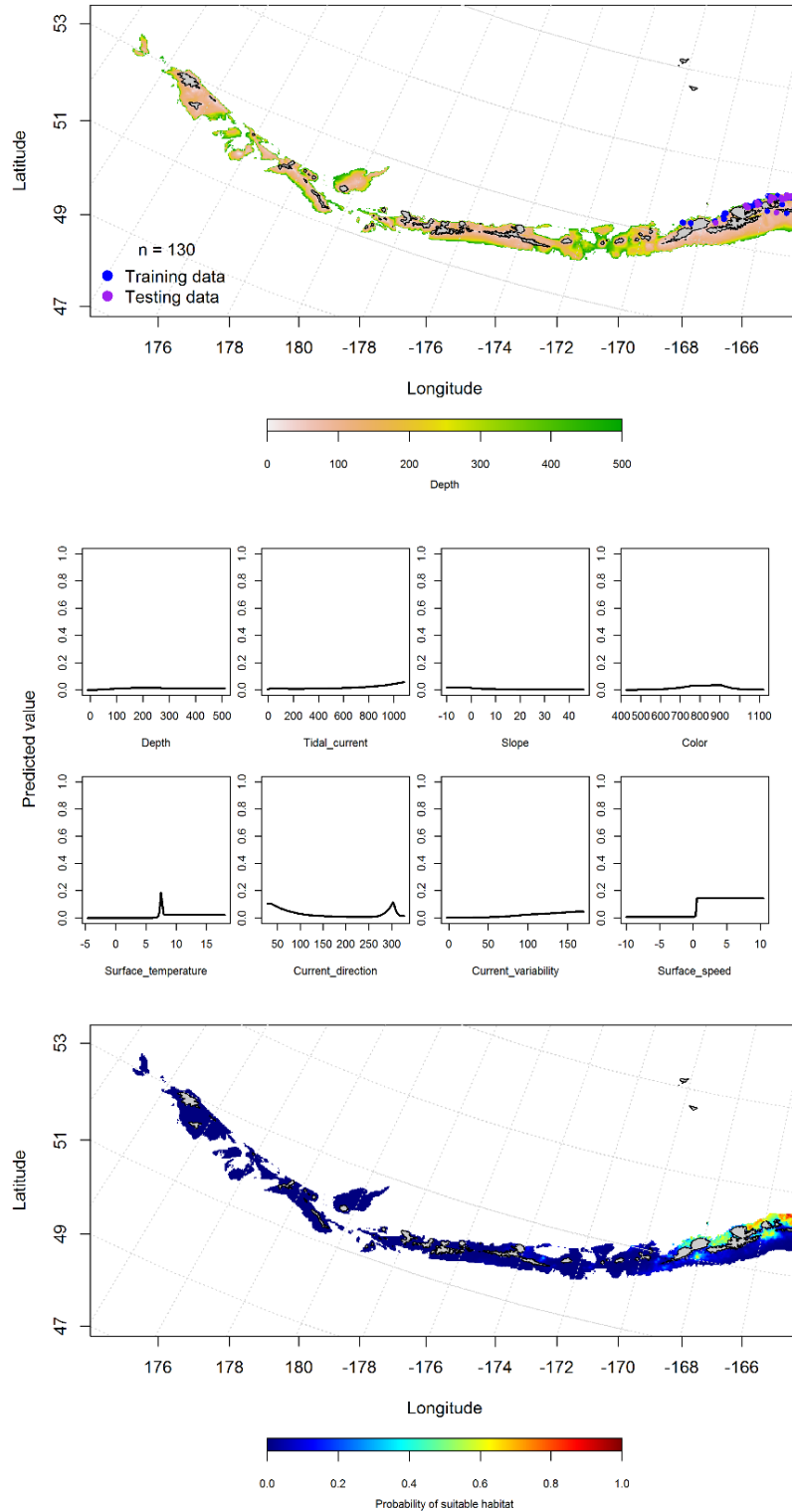


Figure 96. -- Observations of *Sebastes* spp. larvae from the Aleutian Islands the EcoFOCI data (top panel), relationships of suitable habitat and environmental variables (middle panels), and predicted probability of presence of suitable habitat for *Sebastes* spp. larvae from MaxEnt modeling of the Aleutian Islands (bottom panel).

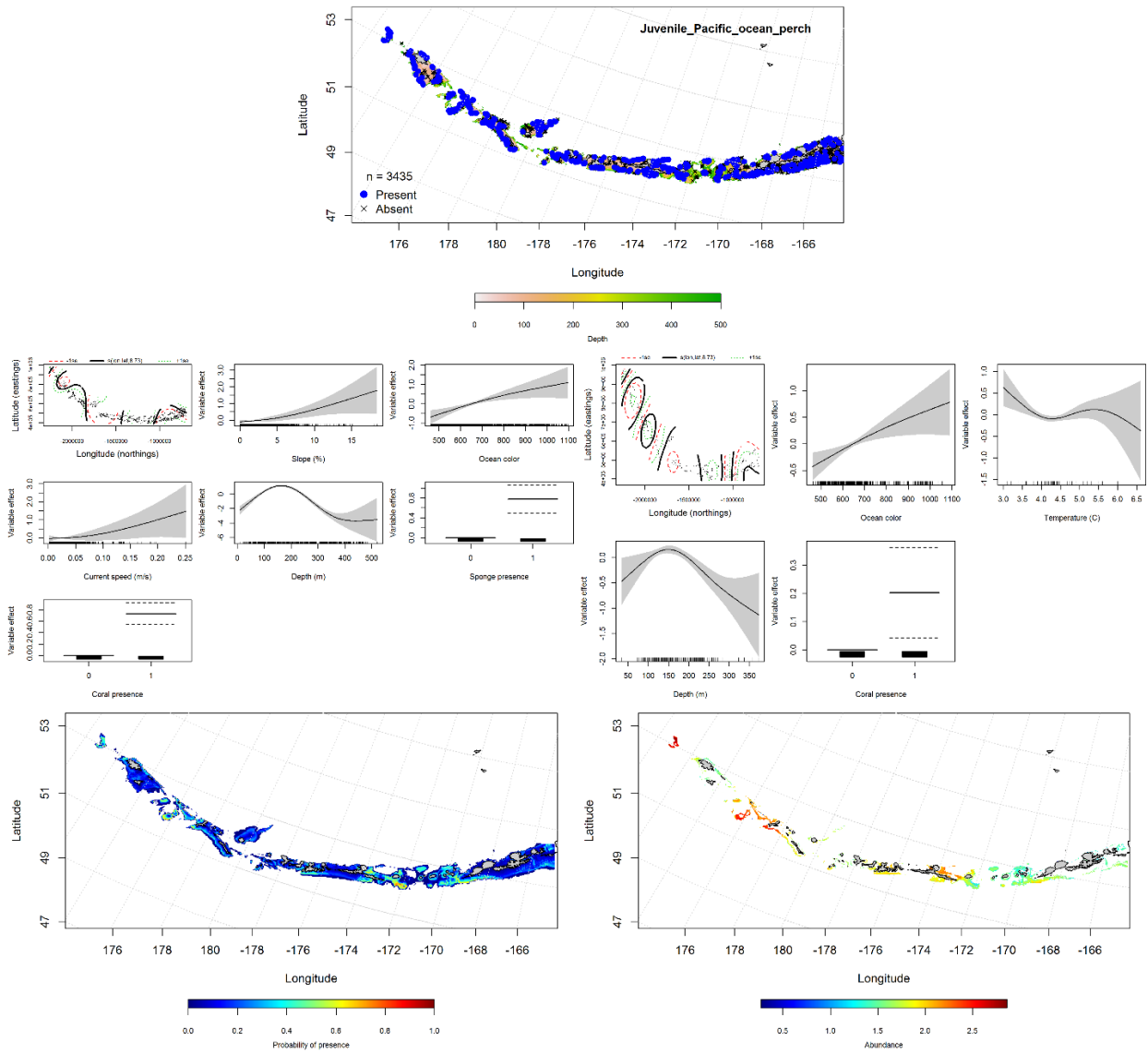


Figure 97. -- Distribution of catches of juvenile Pacific ocean perch in bottom trawl surveys (top middle panel), significant relationships between presence-absence and CPUE and environmental variables for the best-fitting generalized additive model of juvenile Pacific ocean perch (middle left and right panels), and predicted probability of presence and abundance of juvenile Pacific ocean perch based on the models (bottom left and right panels).

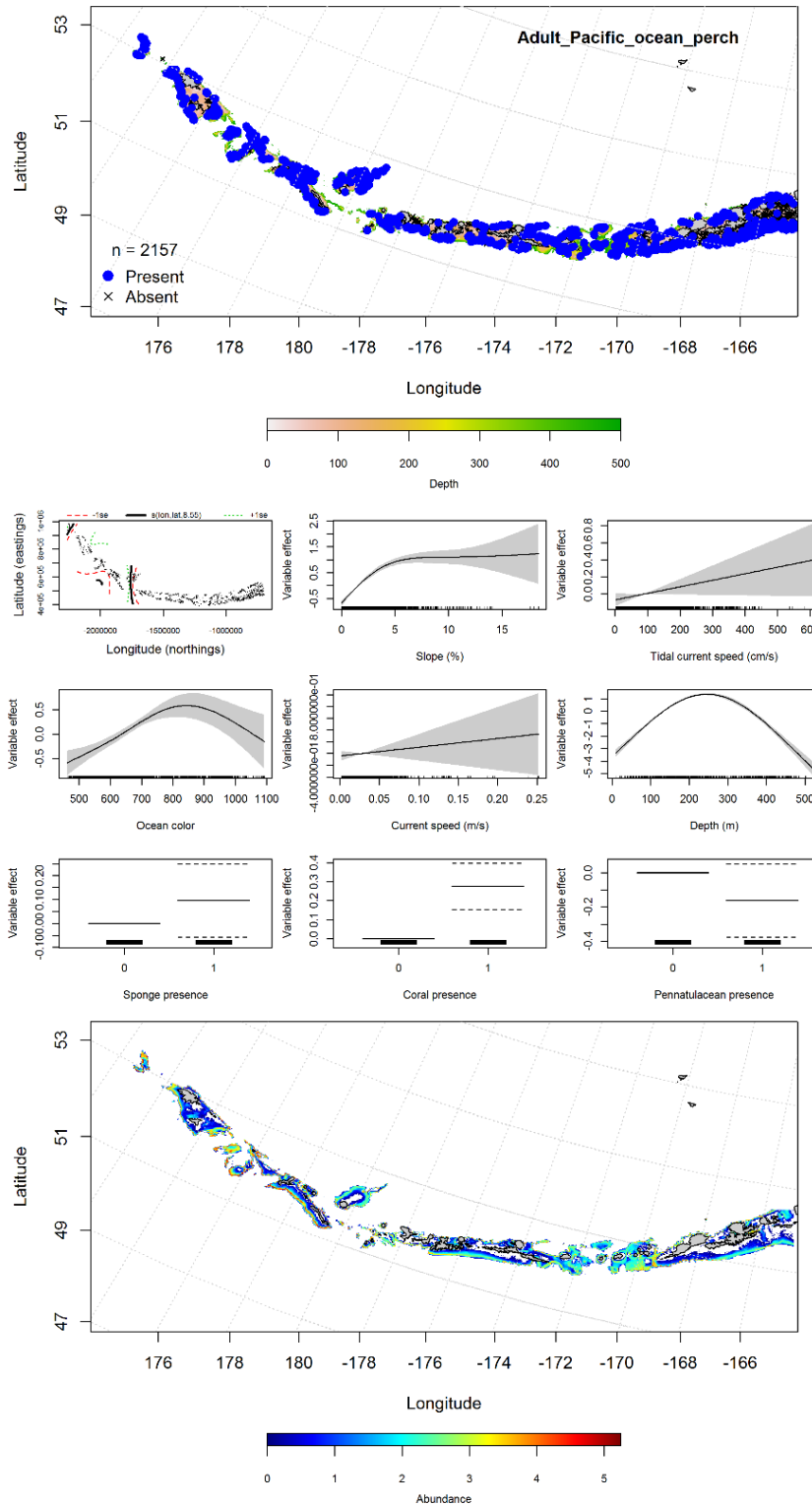


Figure 98. -- Distribution of catches of adult Pacific ocean perch in bottom trawl surveys (top panel), relationships between presence and environmental variables for the GAM model of adult Pacific ocean perch (middle panels), and predicted abundance of adult Pacific ocean perch based on the model (bottom panel).

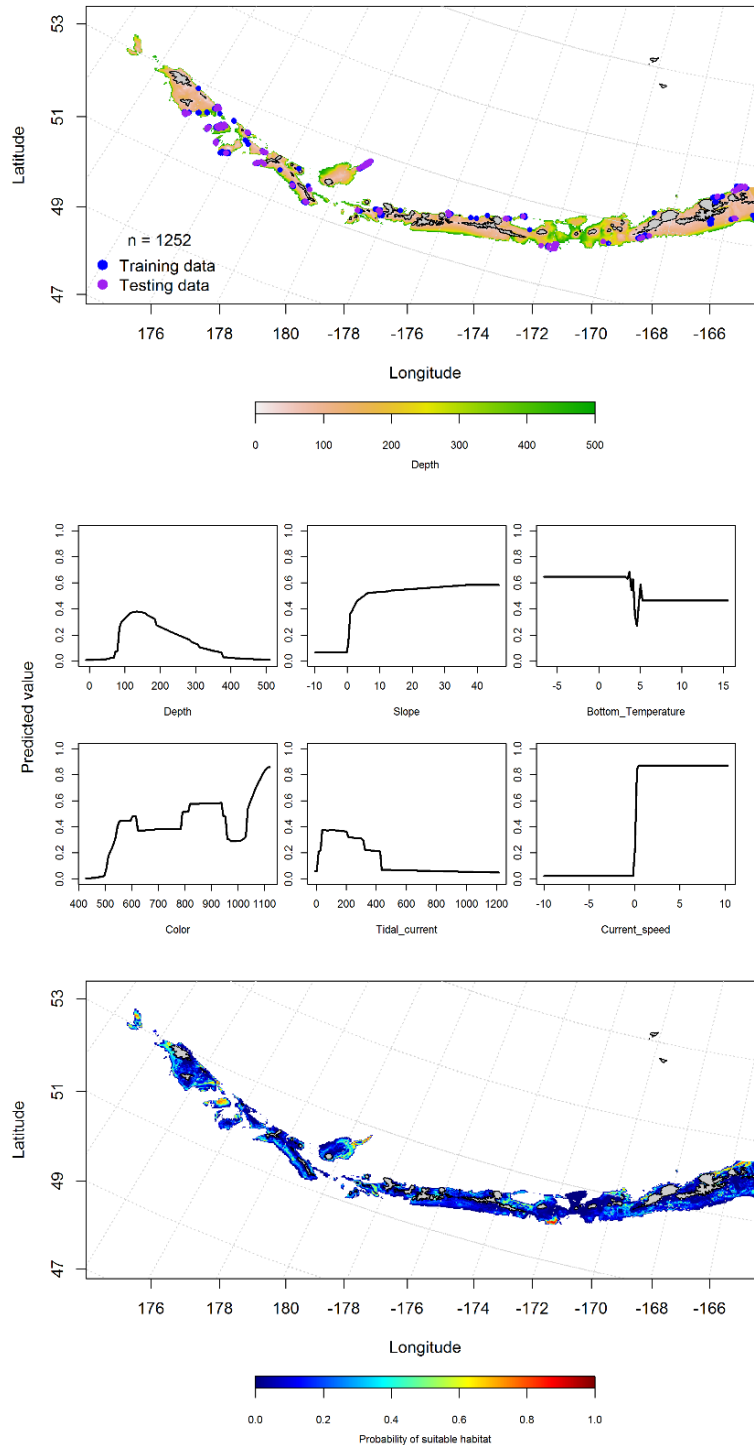


Figure 99. -- Locations of fall (September-November) commercial fisheries catches of Pacific ocean perch (top panel), relationships between probability of presence and environmental variables for the maximum entropy model (middle panels), and predicted probability of suitable habitat for Pacific ocean perch based on the model (bottom panel).

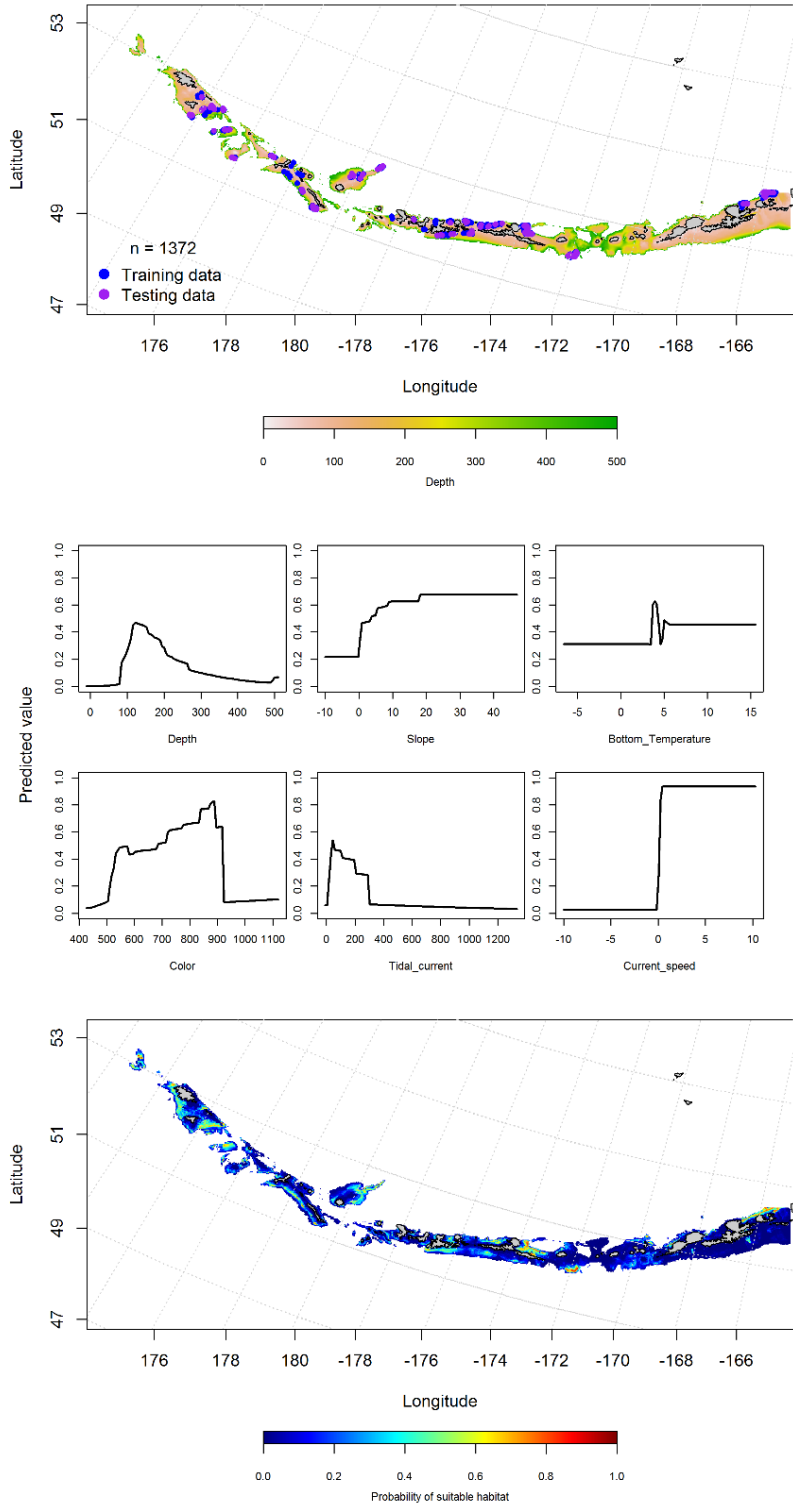


Figure 100. -- Locations of winter (December-February) commercial fisheries catches of Pacific ocean perch (top panel), relationships between probability of presence and environmental variables for the maximum entropy model (middle panels), and predicted probability of suitable habitat for Pacific ocean perch based on the model (bottom panel).

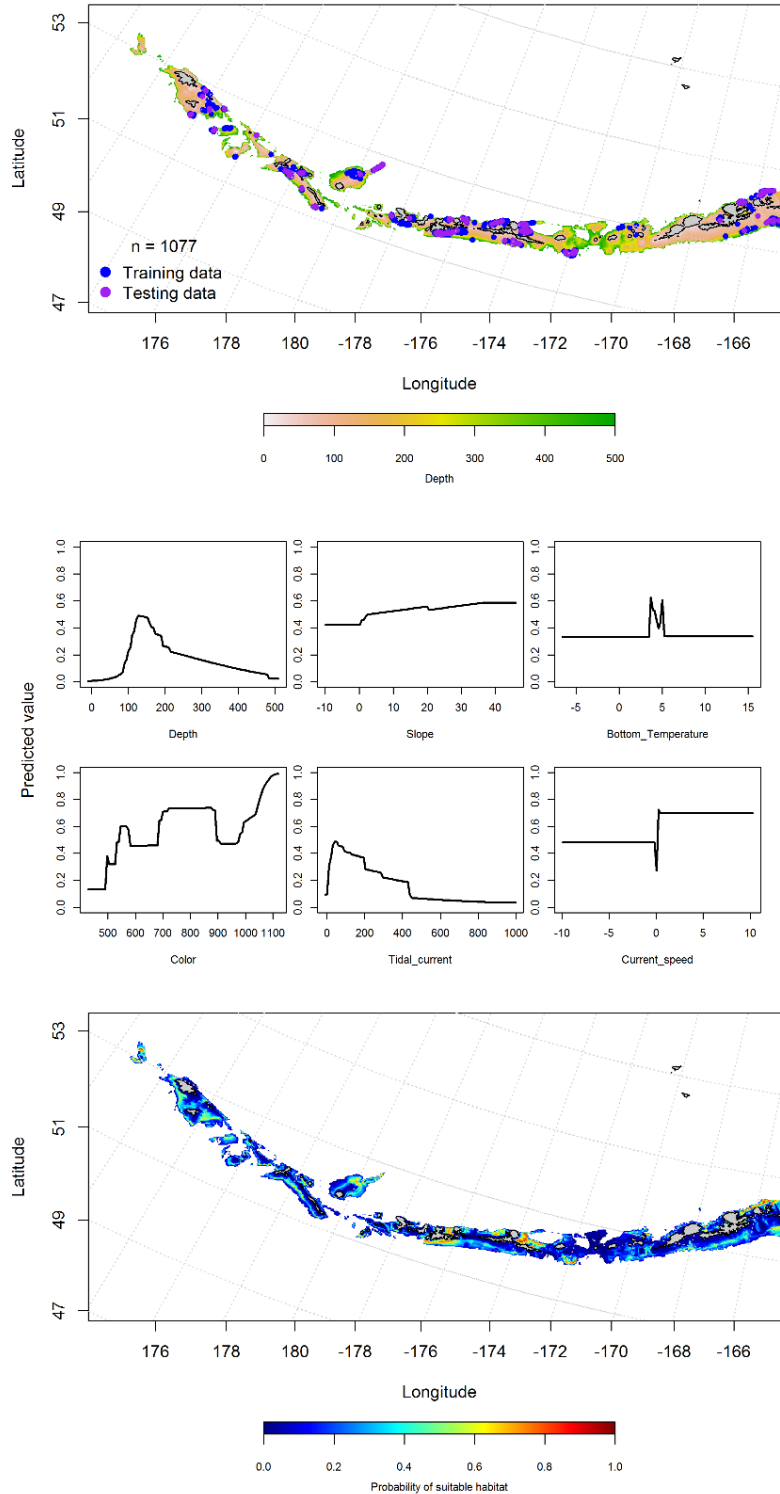


Figure 101. -- Locations of spring (March-May) commercial fisheries catches of Pacific ocean perch (top panel), relationships between probability of presence and environmental variables for the maximum entropy model (middle panels), and predicted probability of suitable habitat for Pacific ocean perch based on the model (bottom panel).

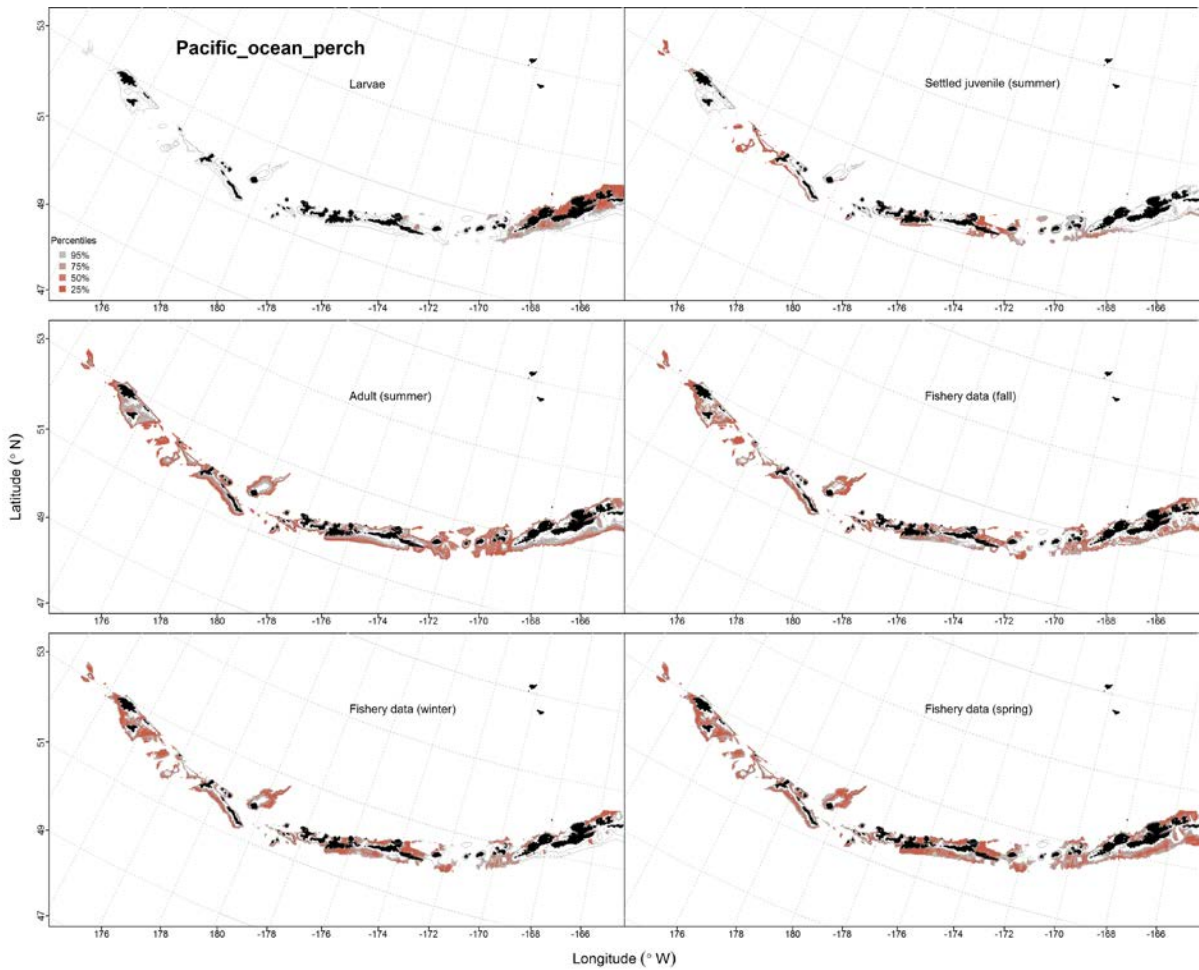


Figure 102. -- Predicted EFH quantiles for Pacific ocean perch life history stages based on species distribution modeling. Larval stage is based on EcoFOCI data and is for combined *Sebastes* spp. Settled juvenile and summer adult stages are based on bottom trawl survey data, while seasonal stages (winter, spring, fall) are from commercial fishery data.

Northern Rockfish (*Sebastes polyspinis*)

Early life history stages of *Sebastes* spp. -- Early life history stages of northern rockfish were not distinguishable from other *Sebastes* spp. Combined *Sebastes* spp. early life history stages are presented above with Pacific ocean perch.

Juvenile and adult northern rockfish distribution in the bottom trawl survey -- The catch of juvenile northern rockfish in summer bottom trawl surveys in the Aleutian Islands indicates this species presence varied across the Aleutian Islands survey area and was highest in the western Aleutian Islands (Fig. 103). A MaxEnt model was used to predict the suitable habitat of juvenile northern rockfish. The AUC of the model was 0.89 for the training data and 0.84 for the testing data. The most important variables in the model were depth and tidal current. The model predicted the highest probability of suitable habitat for juvenile northern rockfish at Stalemate Bank and north of Unalaska Island (Fig. 103).

The catch of adult northern rockfish in summer bottom trawl surveys of the Aleutian Islands was similar to juvenile catches (Fig. 104). A GAM predicting the abundance of adult northern rockfish explained 30% of the variability in the bottom trawl survey the training data and 29% of the test data. Location, depth, ocean color, and the presence of coral were the most important variables explaining the distribution of adult northern rockfish. The model predicted adult northern rockfish CPUE was highest west of Kiska Island to Stalemate Bank (Fig. 104).

Northern rockfish distribution in commercial fisheries -- In the fall, bottom depth and ocean color were the most important variables determining the distribution of northern rockfish. The AUC of the MaxEnt fall model was 0.93 for the training data and 0.85 for the test data, and 85% of the cases in the training data and test data set were predicted correctly. The model predicted

suitable habitat of northern rockfish throughout the Aleutian Islands with highest probabilities near Petrel Bank (Fig. 105).

In the winter, depth and ocean color were also the most important variables determining the distribution of northern rockfish. The AUC of the winter MaxEnt model was 0.94 for the training data and 0.85 for the test data and 87% of the training data and 85% of the test data were predicted correctly. As with the fall, the model predicted suitable habitat of northern rockfish throughout the Aleutian Islands, although less abundant in the east of Seguam Pass (Fig. 106).

Like the fall and winter, bottom depth and ocean color in the spring were the most important variables determining the distribution of northern rockfish. The AUC of the spring MaxEnt model was 0.90 for the training data and 0.84 for the test data. The model correctly classified 83% of the training data and 84% of the test data. The model predicted suitable habitat across the Aleutian Islands with highest probabilities from Seguam Pass to Adak Island (Fig. 107).

Northern rockfish essential fish habitat maps and conclusions -- In general, adult northern rockfish were widely distributed through the Aleutian Islands whereas the juveniles were more abundant in the central and western Aleutians (Fig. 108). EFH predicted from commercial catches of was widely distributed through the Aleutian Islands (Fig. 108). Seasonal similarities can be observed in areas of low abundance (e.g., large passes). There does not appear to be much seasonal variability to the EFH distribution from fall, winter and spring summertime commercial catches.

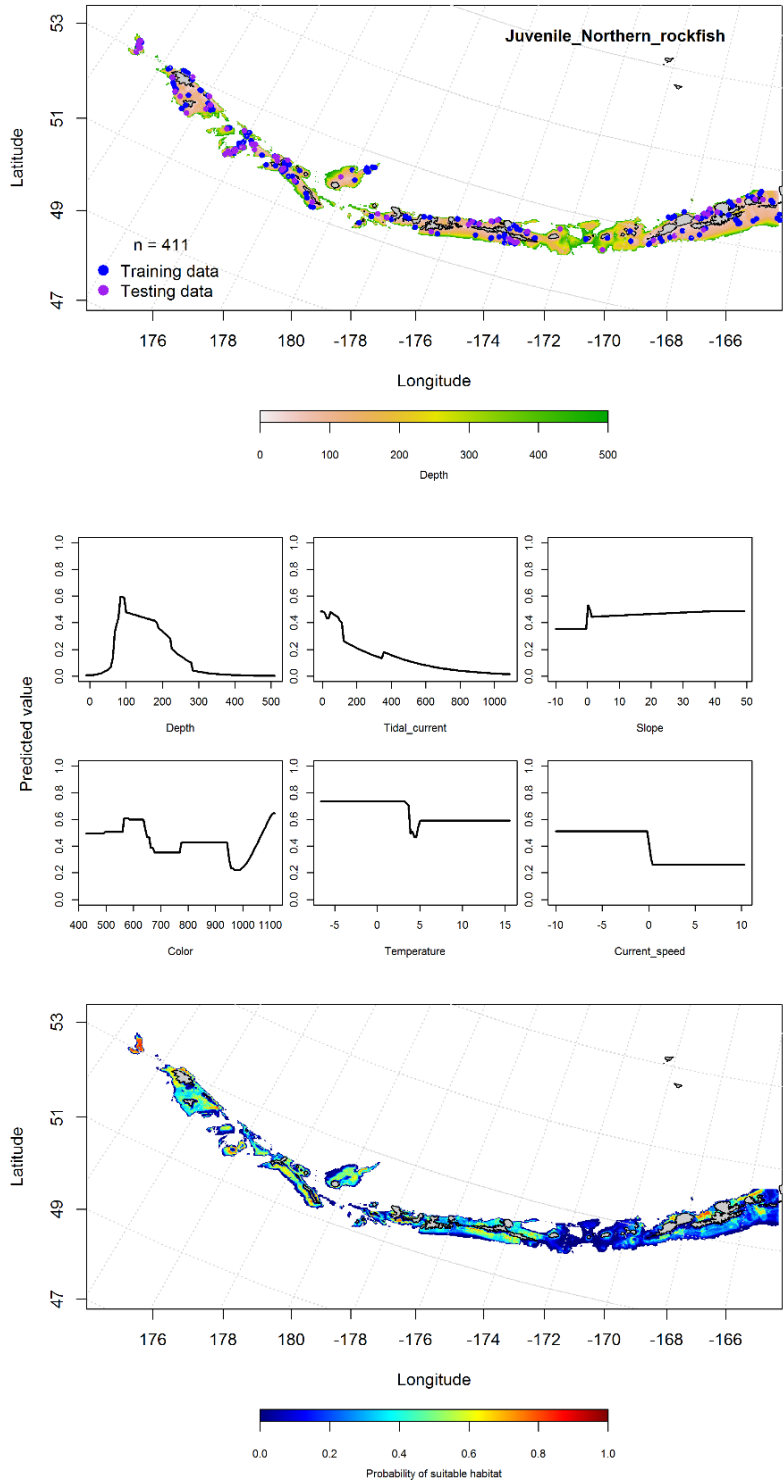


Figure 103. -- Distribution of catches of juvenile northern rockfish in bottom trawl surveys (top panel), relationships between presence and environmental variables for the maximum entropy model of juvenile northern rockfish (middle panels), and predicted probability of suitable habitat for juvenile northern rockfish based on the model (bottom panel).

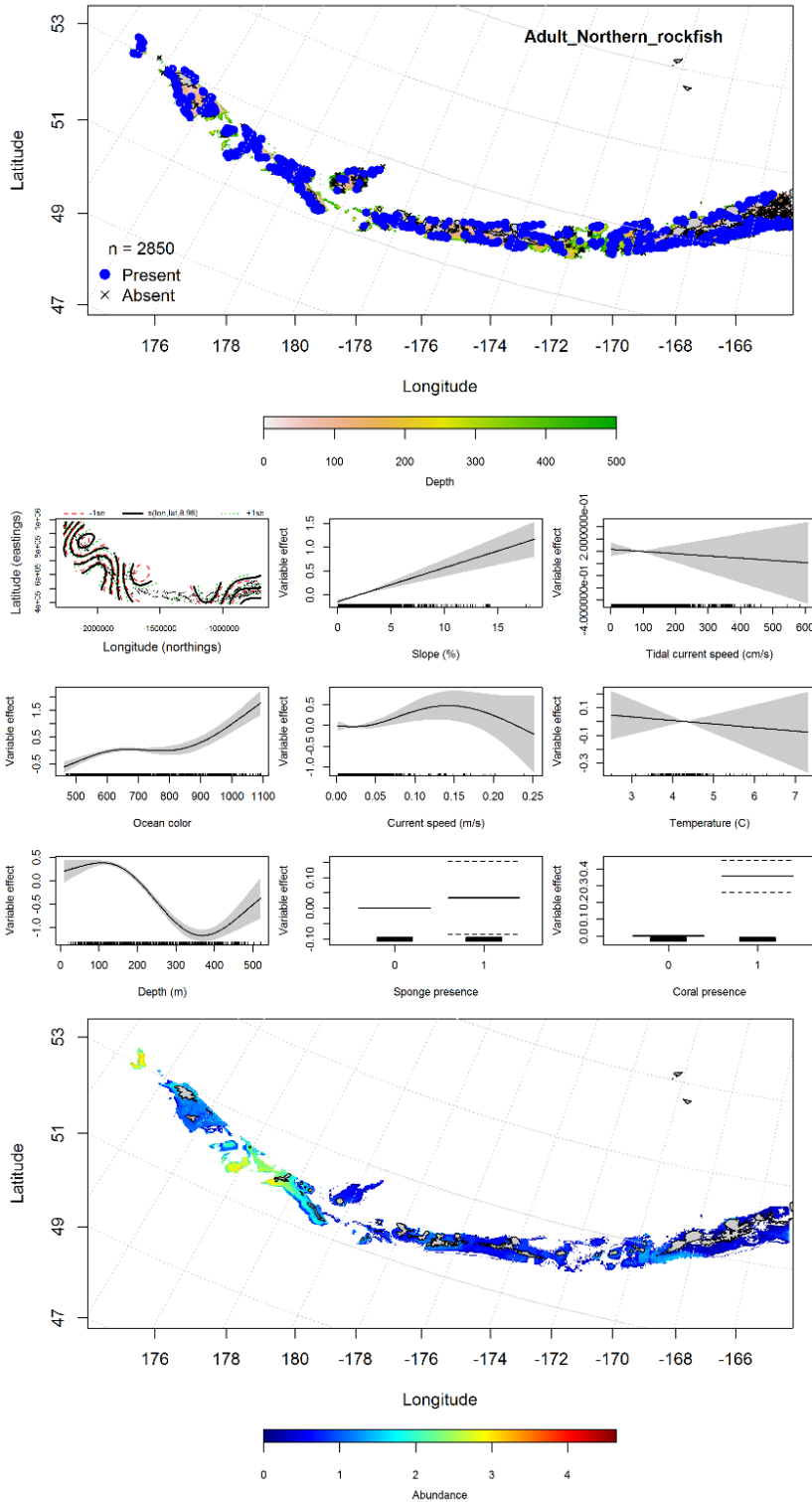


Figure 104. -- Distribution of catches of adult northern rockfish in bottom trawl surveys (top panel), relationships between presence and environmental variables for the GAM model of adult northern rockfish (middle panels), and predicted abundance of adult northern rockfish based on the model (bottom panel).

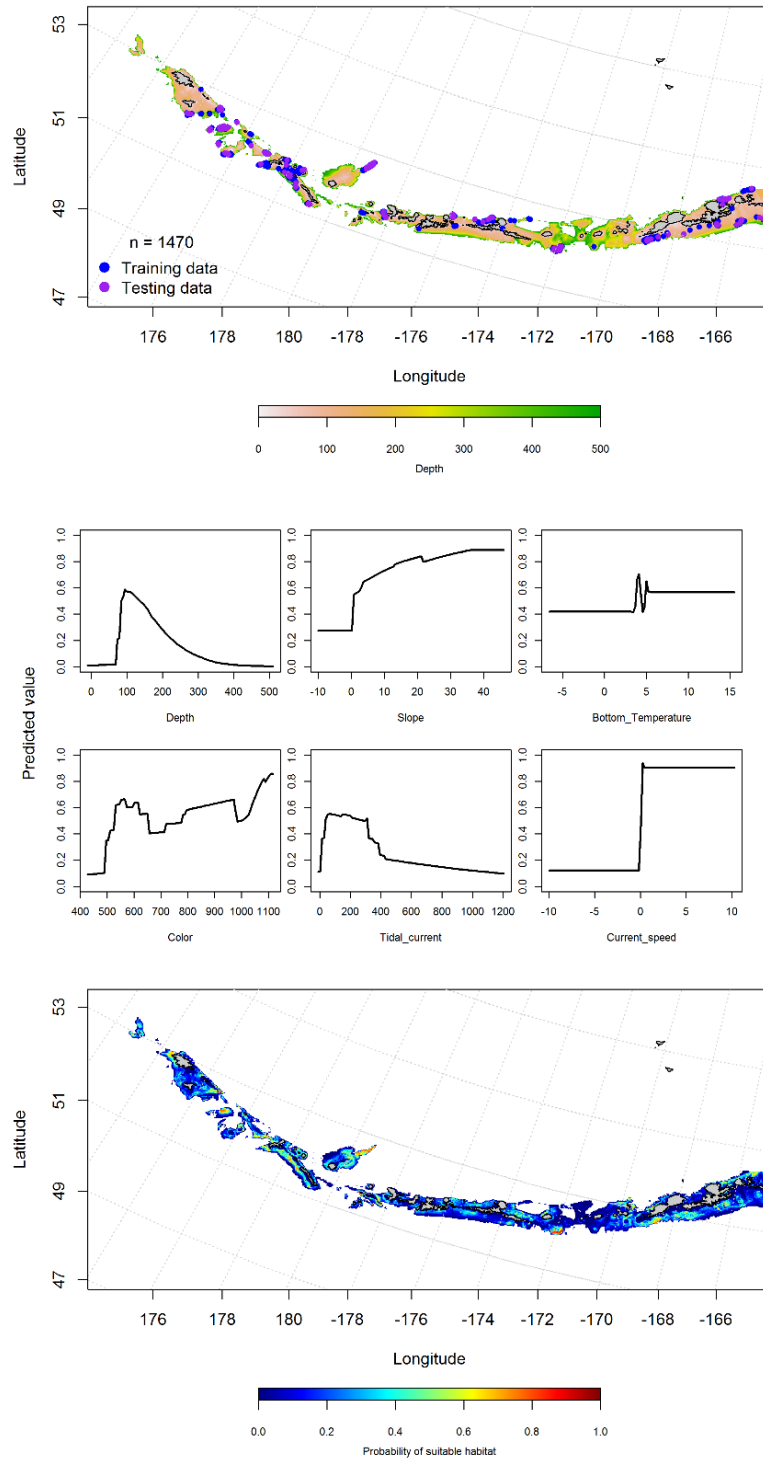


Figure 105. -- Locations of fall (September-November) commercial fisheries catches of northern rockfish (top panel), relationships between probability of presence and environmental variables for the maximum entropy model (middle panels), and predicted probability of suitable habitat for northern rockfish based on the model (bottom panel).

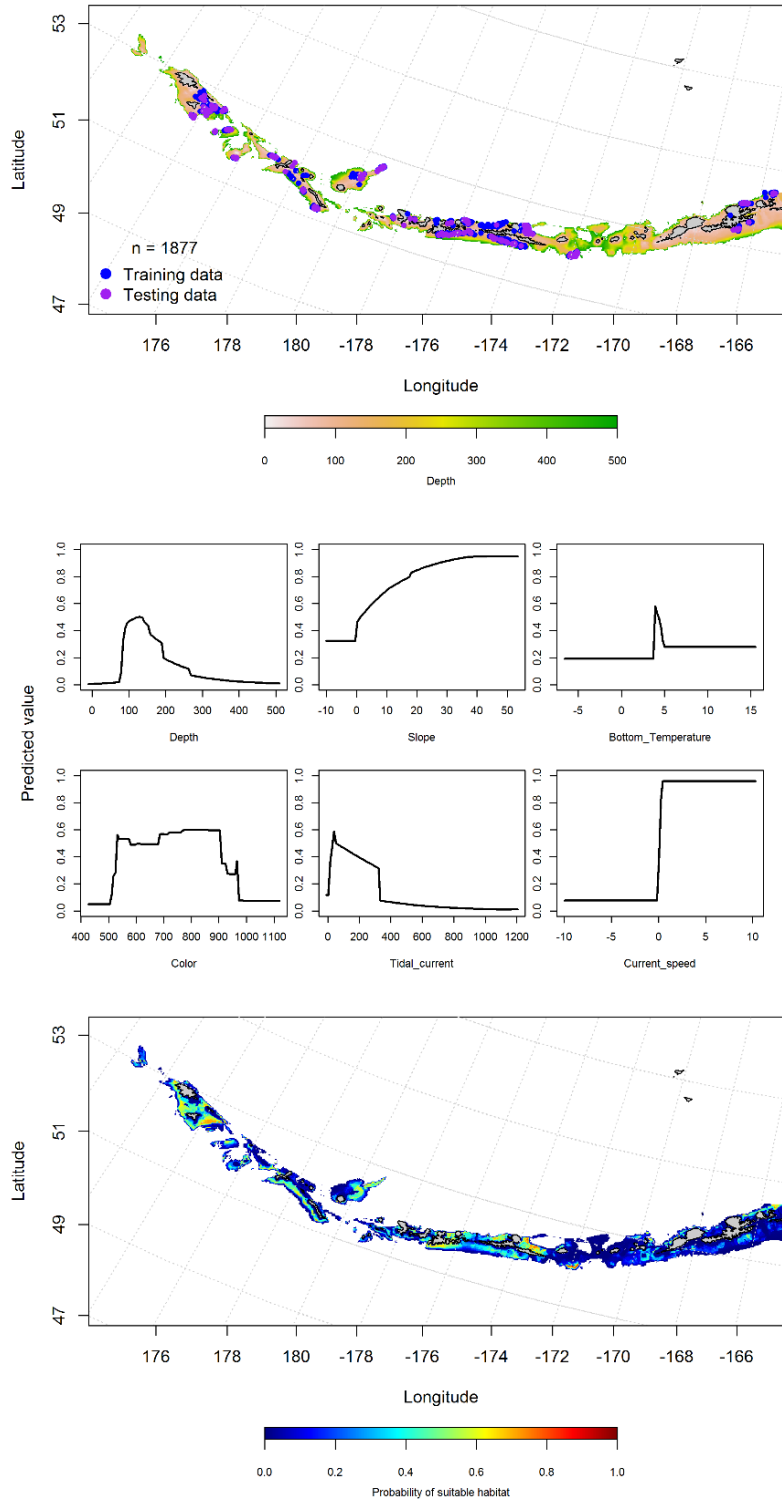


Figure 106. -- Locations of winter (December-February) commercial fisheries catches of northern rockfish (top panel), relationships between probability of presence and environmental variables for the maximum entropy model (middle panels), and predicted probability of suitable habitat for northern rockfish based on the model (bottom panel).

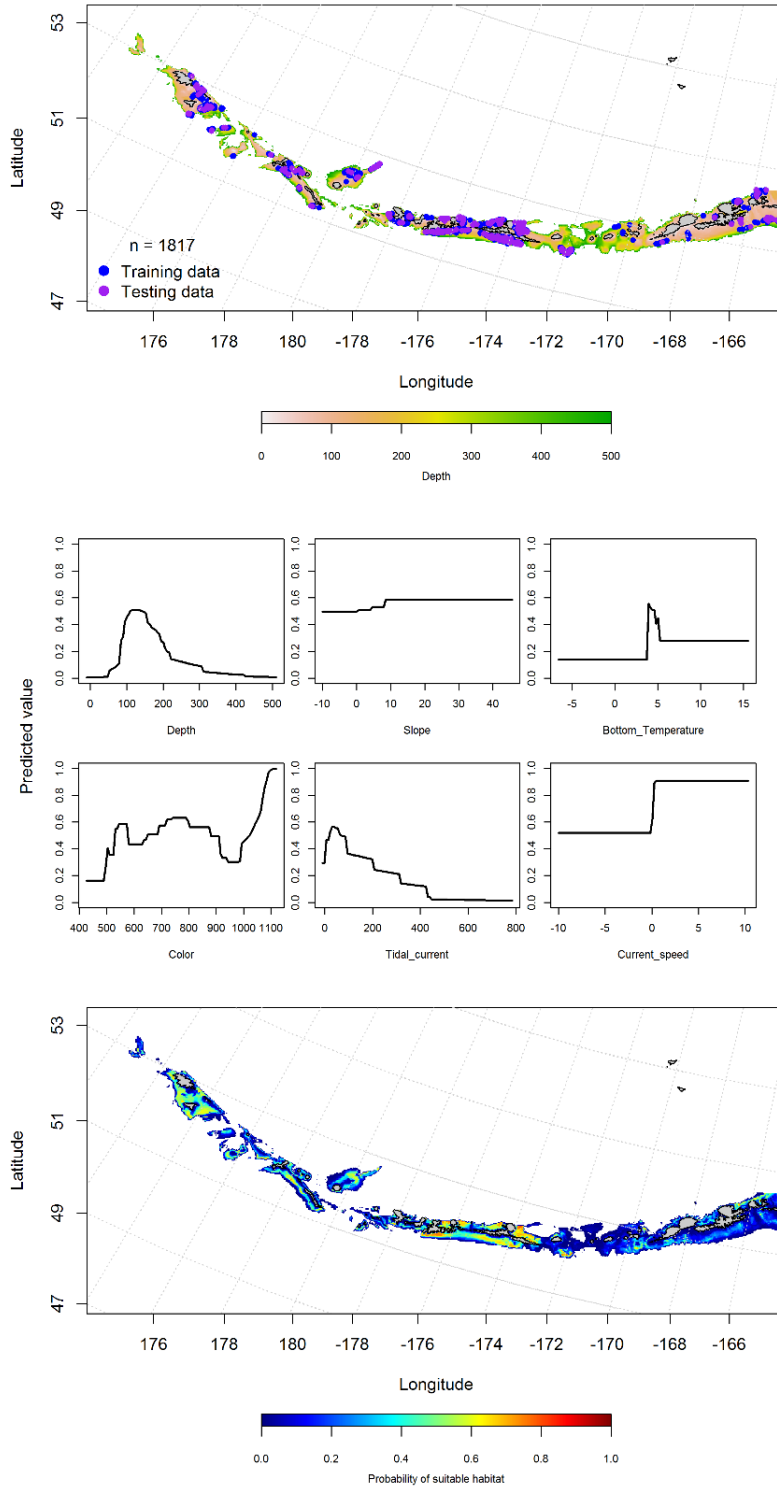


Figure 107. -- Locations of spring (March-May) commercial fisheries catches of northern rockfish (top panel), relationships between probability of presence and environmental variables for the maximum entropy model (middle panels), and predicted probability of suitable habitat for northern rockfish based on the model (bottom panel).

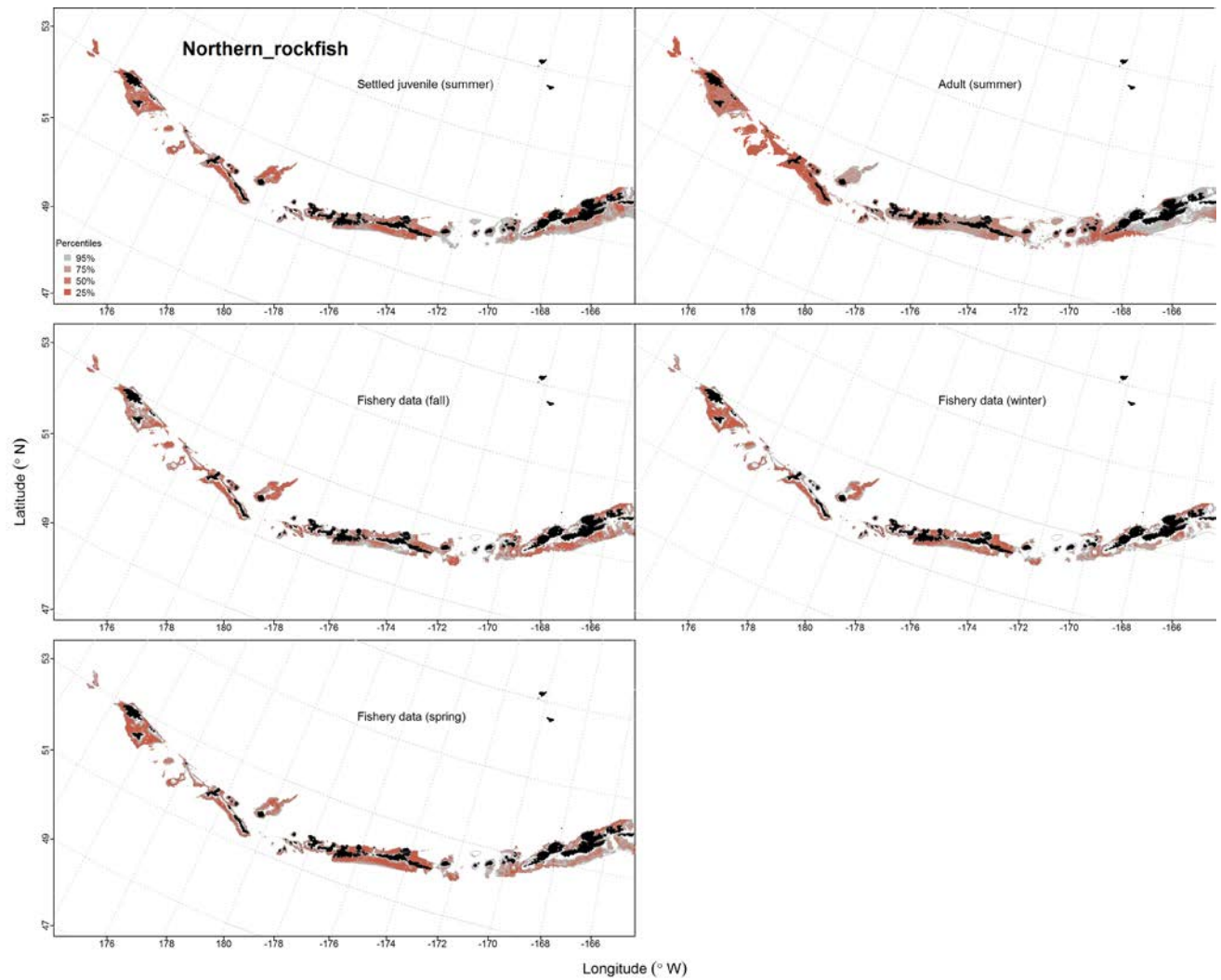


Figure 108. -- Predicted EFH quantiles for northern rockfish life history stages based on species distribution modeling. Larval stages are shown above in the Pacific ocean perch section (*Sebastes* spp.) Settled juvenile and summer adult stages are based on bottom trawl survey data, while seasonal stages (winter, spring, fall) are from commercial fishery data.

Shortraker Rockfish (*Sebastes borealis*)

Early life history stages of *Sebastes* spp. -- Early life history stages of shortraker rockfish were not distinguishable from other *Sebastes* spp. Combined *Sebastes* spp. early life history stages are presented above with Pacific ocean perch.

Juvenile and adult shortraker rockfish distribution in the bottom trawl survey -- A MaxEnt model was used to predict the distribution of juvenile shortraker rockfish. The model AUC was 0.96 for the training data and 0.86 for the test data. Depth and slope were the important variables to the model of juvenile shortraker rockfish. Juvenile shortraker rockfish were found at deeper depths along the continental shelf (Fig. 109).

A hurdle-GAM was used to predict the distribution of adult shortraker rockfish. The AUC for the PA GAM was 0.97 for the training data and 96% for the test data. Depth, location, and slope were the most important variables explaining the probability of presence of adult shortraker rockfish. The model correctly classified 92% of the training and 91% test data sets. Adult shortraker rockfish were predicted to occur at deeper depths across the Aleutians (Fig. 110).

The CPUE GAM found depth, geographic location and slope were the most influential variables on CPUE of adult shortraker rockfish. The model explained 37% of the variability in the training data and 20% of the test data. The model predicted abundance in a similar pattern as the PA GAM (throughout the Aleutians at deeper depths) (Fig. 110).

Shortraker rockfish distribution in commercial fisheries -- Distribution of adult shortraker rockfish in the Aleutian Islands in commercial fisheries catches was generally consistent throughout all seasons. In the fall, depth, ocean color, and tidal current were the most important

variables determining the distribution of shortraker rockfish. The AUC of the fall MaxEnt model was 0.89 for the training data and 0.63 for the test data. The model predicted suitable habitat of shortraker rockfish was high at deeper depths (Fig. 111).

In the winter, depth, tidal current and ocean color were the most important variables determining the distribution of shortraker rockfish. The AUC of the winter MaxEnt model was 0.86 for the training and 0.76 for the test data. As with the fall, the model predicted suitable habitat of shortraker rockfish throughout the Aleutians, although there was higher predicted probability in the east (Fig. 112).

In the spring, depth, ocean color and slope were the most important variables determining the distribution of shortraker rockfish. The AUC of the spring MaxEnt model was 0.92 for the training data and 0.81 for the test data. The model predicted suitable habitat of shortraker rockfish throughout the Aleutians, although with low probabilities (Fig. 113).

Shortraker rockfish essential fish habitat maps and conclusions -- In general, juvenile and adult shortraker rockfish were similarly distributed through the Aleutian Islands chain and co-occur in most places where they are found. Those collected in summertime bottom trawl surveys share similar predicted EFH distributions across the Aleutian Islands (Fig. 114). EFH for both juveniles and adults was predicted to occur at continental slope depths (> 200 m) throughout the AI. Similar to summertime bottom trawl survey data observations, the EFH predicted from commercial catches of shortraker rockfish is distributed throughout the Aleutian Islands chain (Fig. 114). There does not appear to be much seasonal variability to the EFH location throughout the AI. Large passes result in low values for EFH in all seasons.

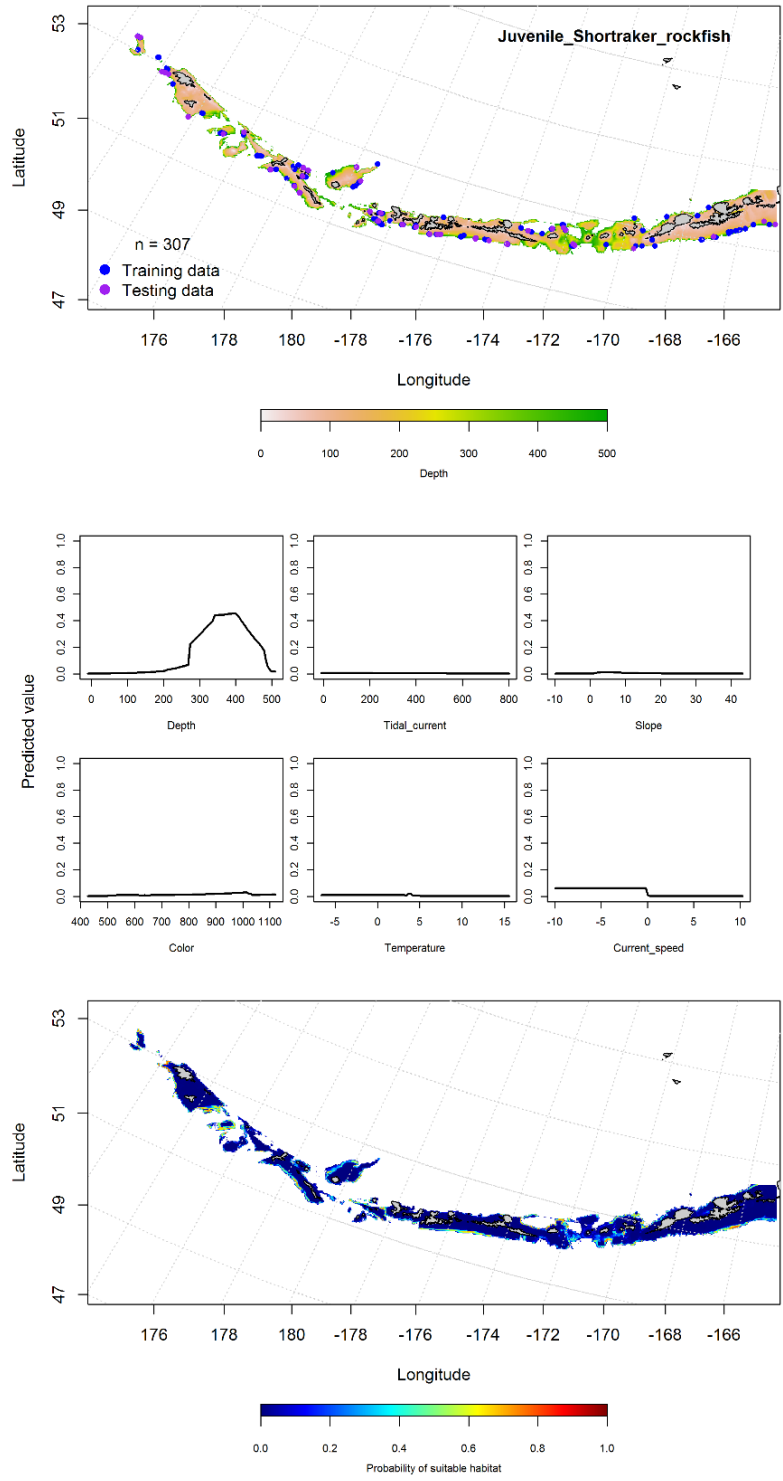


Figure 109. -- Distribution of catches of juvenile shorttraker rockfish in bottom trawl surveys (top panel), relationships between presence and environmental variables for the maximum entropy model of juvenile shorttraker rockfish (middle panels), and predicted probability of suitable habitat for juvenile shorttraker rockfish based on the model (bottom panel).

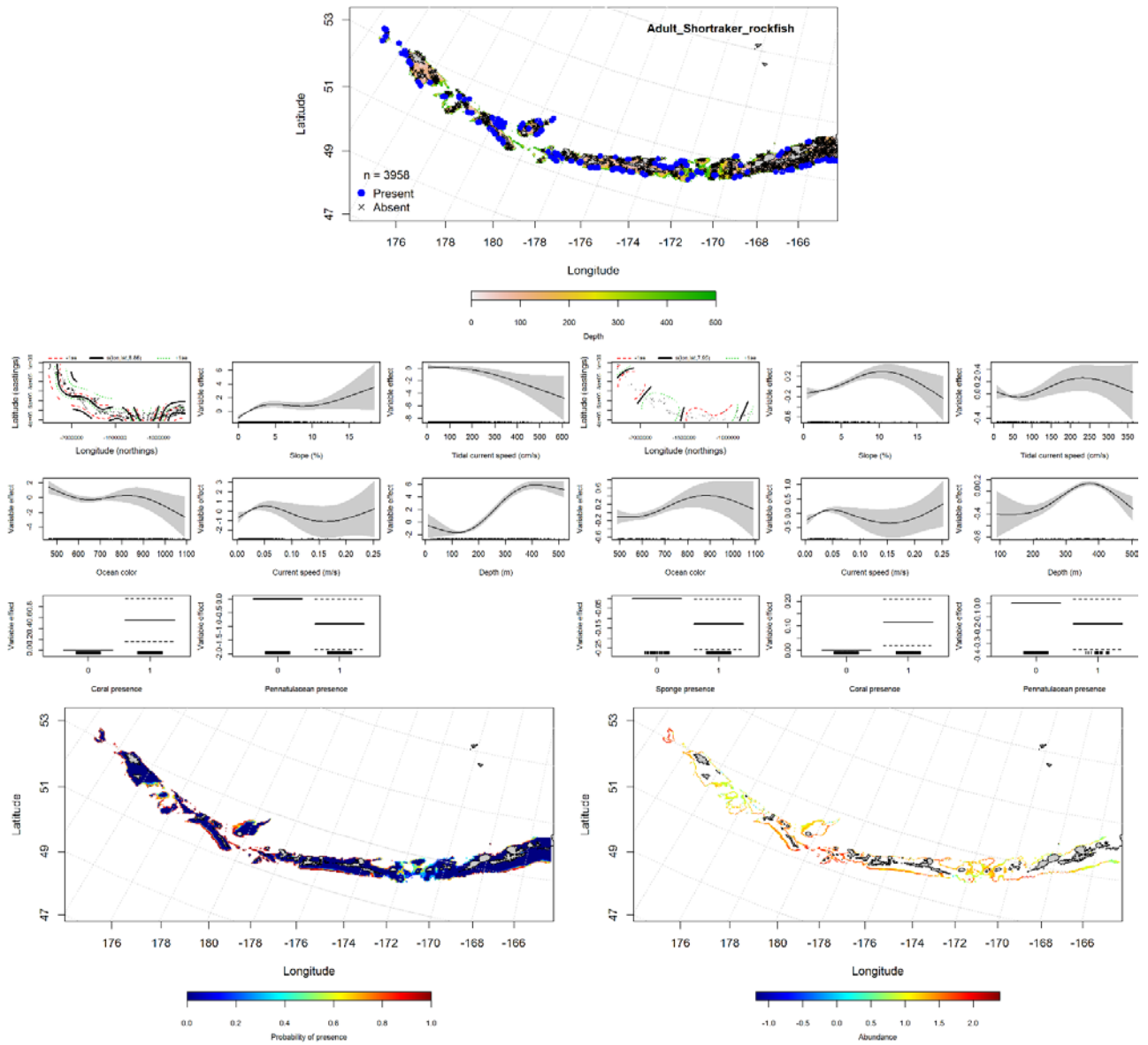


Figure 110. -- Distribution of catches of adult shorttraker rockfish in bottom trawl surveys (top middle panel), significant relationships between presence-absence and CPUE and environmental variables for the best-fitting generalized additive model adult shorttraker rockfish (middle left and right panels), and predicted probability of presence and abundance of adult shorttraker rockfish based on the models (bottom left and right panels).

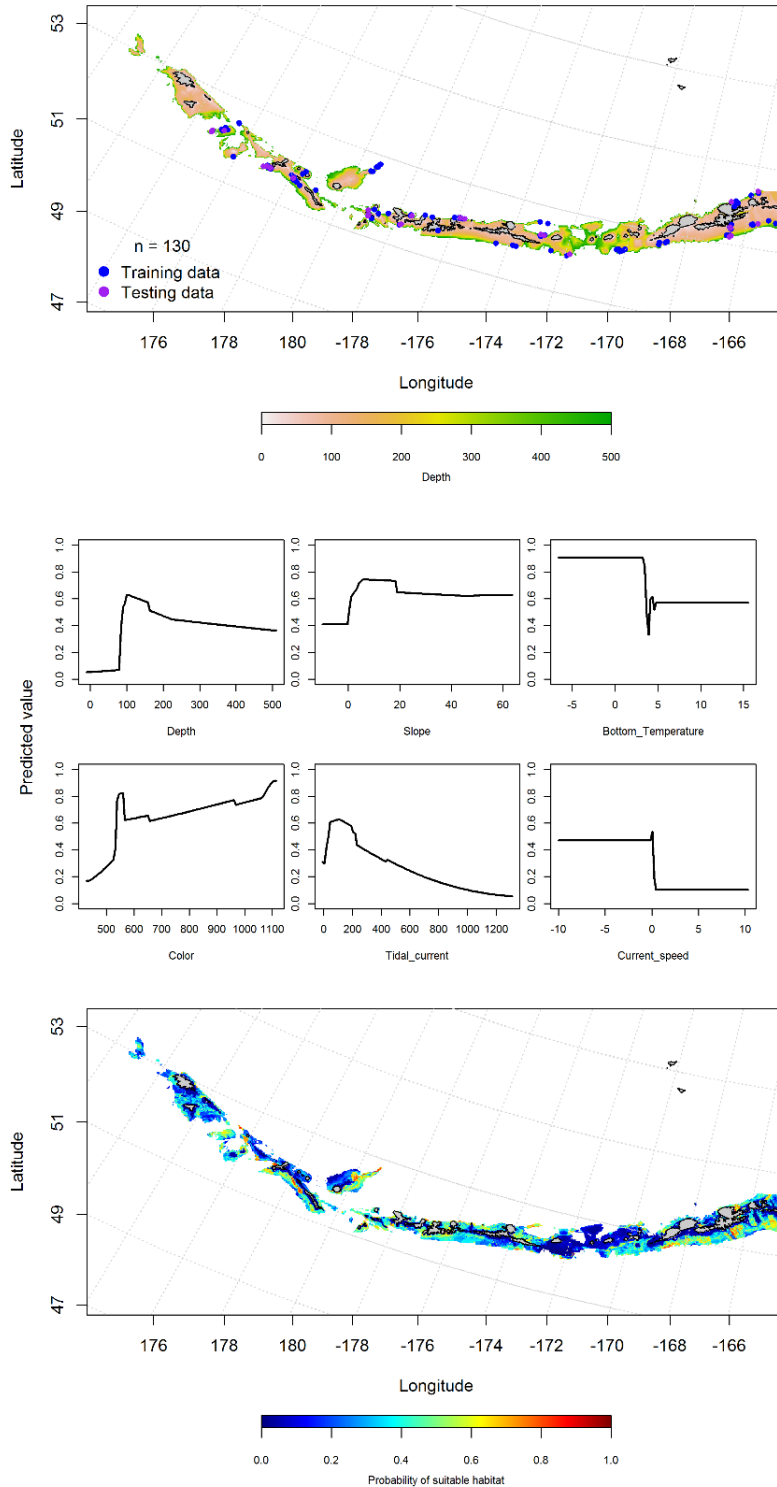


Figure 111. -- Locations of fall (September-November) commercial fisheries catches of shorttraker rockfish (top panel), relationships between probability of presence and environmental variables for the maximum entropy model (middle panels), and predicted probability of suitable habitat for shorttraker rockfish based on the model (bottom panel).

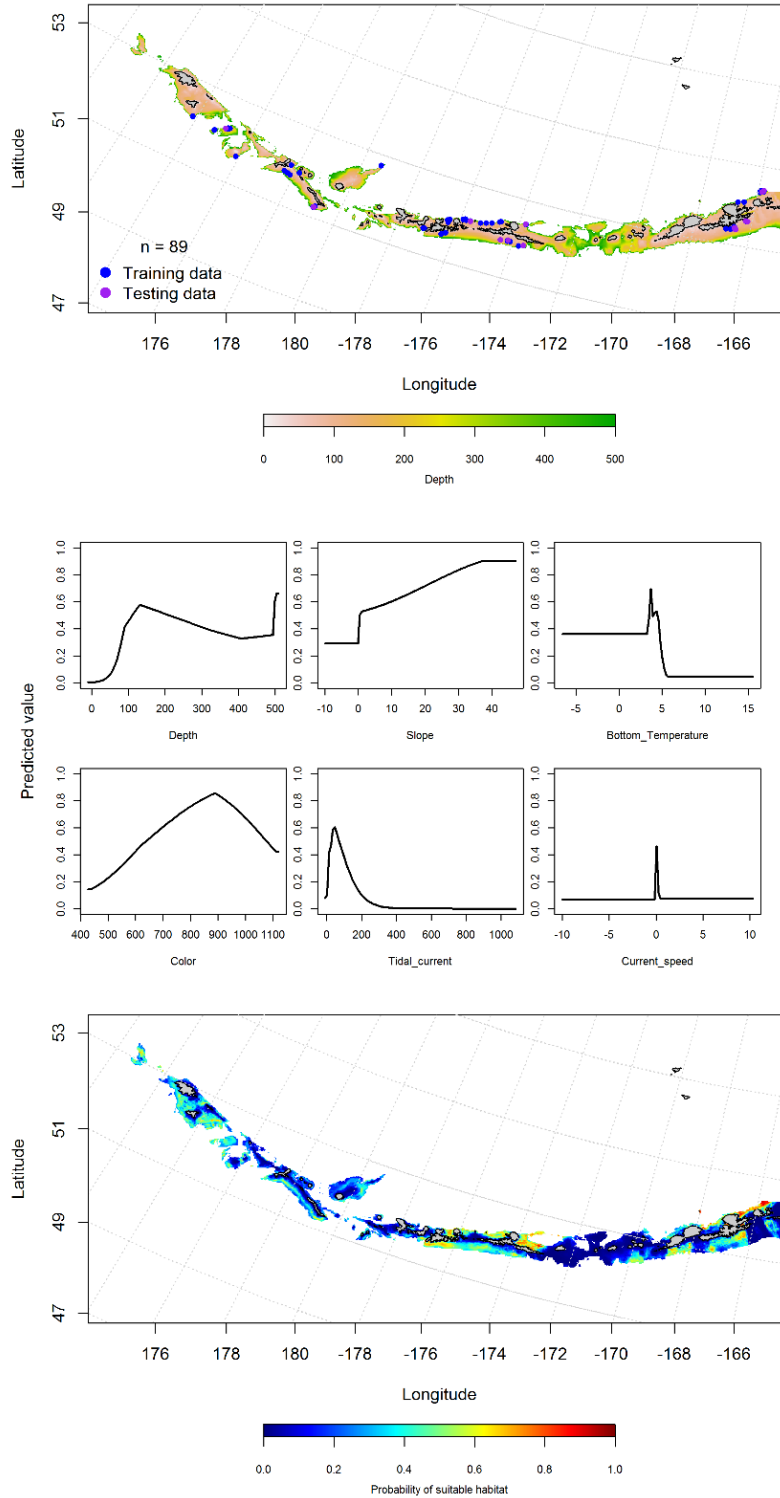


Figure 112. -- Locations of winter (December-February) commercial fisheries catches of shortraker rockfish (top panel), relationships between probability of presence and environmental variables for the maximum entropy model (middle panels), and predicted probability of suitable habitat for shortraker rockfish based on the model (bottom panel).

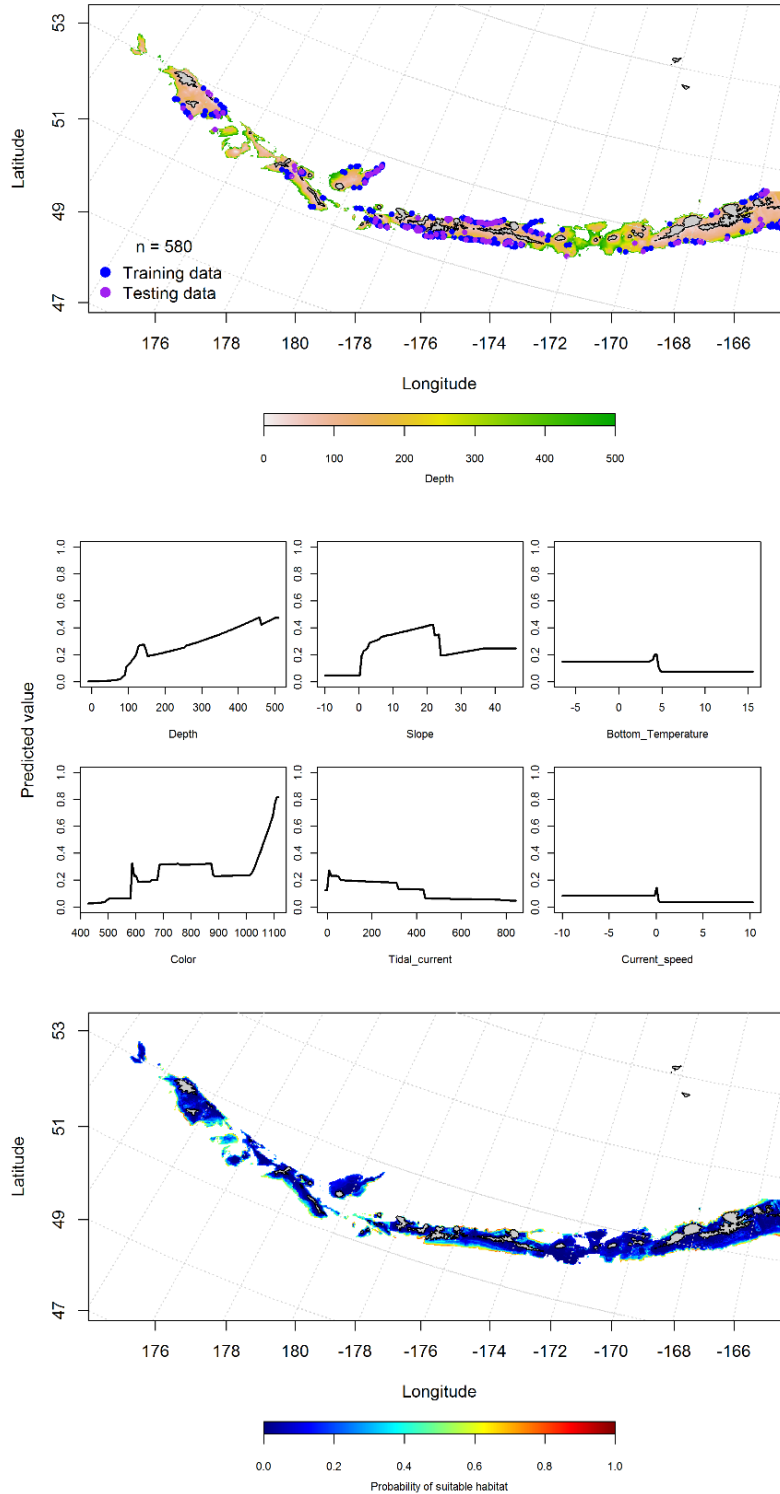


Figure 113. -- Locations of spring (March-May) commercial fisheries catches of shortraker rockfish (top panel), relationships between probability of presence and environmental variables for the maximum entropy model (middle panels), and predicted probability of suitable habitat for shortraker rockfish based on the model (bottom panel).

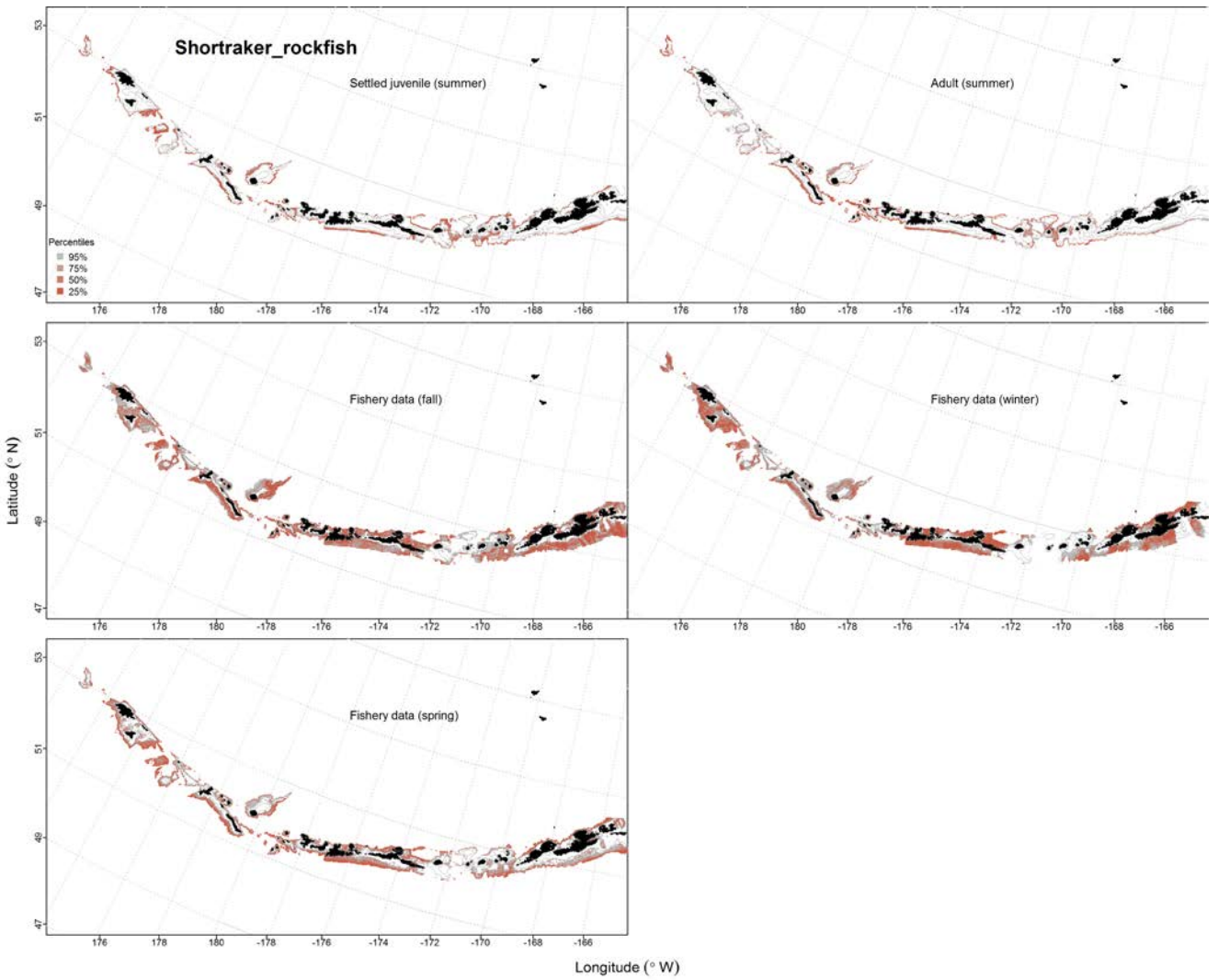


Figure 114. -- Predicted EFH quantiles for shorttraker rockfish life history stages based on species distribution modeling. Larval stages are shown above in the Pacific ocean perch section (*Sebastes* spp.) Settled juvenile and summer adult stages are based on bottom trawl survey data, while seasonal stages (winter, spring, fall) are from commercial fishery data.

Rougheye Rockfish (*Sebastes aleutianus*)

Rougheye and blackspotted rockfish were considered a single species until recently when blackspotted rockfish were rediscovered as a distinct species (Orr and Hawkins 2008). In the bottom trawl survey operations the species have been separated since 2006.

Early life history stages of *Sebastes* spp. -- Early life history stages of rougheye rockfish were not distinguishable from other *Sebastes* spp. Combined *Sebastes* spp. early life history stages are presented above with Pacific ocean perch.

Adult rougheye rockfish distribution in the bottom trawl survey -- There were only 36 catches of juvenile rougheye rockfish in the bottom trawl survey, so modeling was not conducted.

Depth and slope were the most important variables explaining the distribution of adult rougheye rockfish. The MaxEnt model predicting probability of suitable habitat of adult rougheye rockfish had an AUC of 0.89 for the training and 0.75 for the test data. Suitable habitat of adult rougheye rockfish was highest south of Unalaska Island and near Seguam Pass (Fig. 115).

Rougheye rockfish distribution in commercial fisheries -- Rougheye rockfish are not distinguished from blackspotted rockfish in commercial fisheries data. Therefore, no modeling of commercial catches was conducted for these species.

Rougheye rockfish essential fish habitat maps and conclusions -- Rougheye rockfish EFH was predicted to occur predominantly in the eastern Aleutian Islands at deeper depths (Fig. 116).

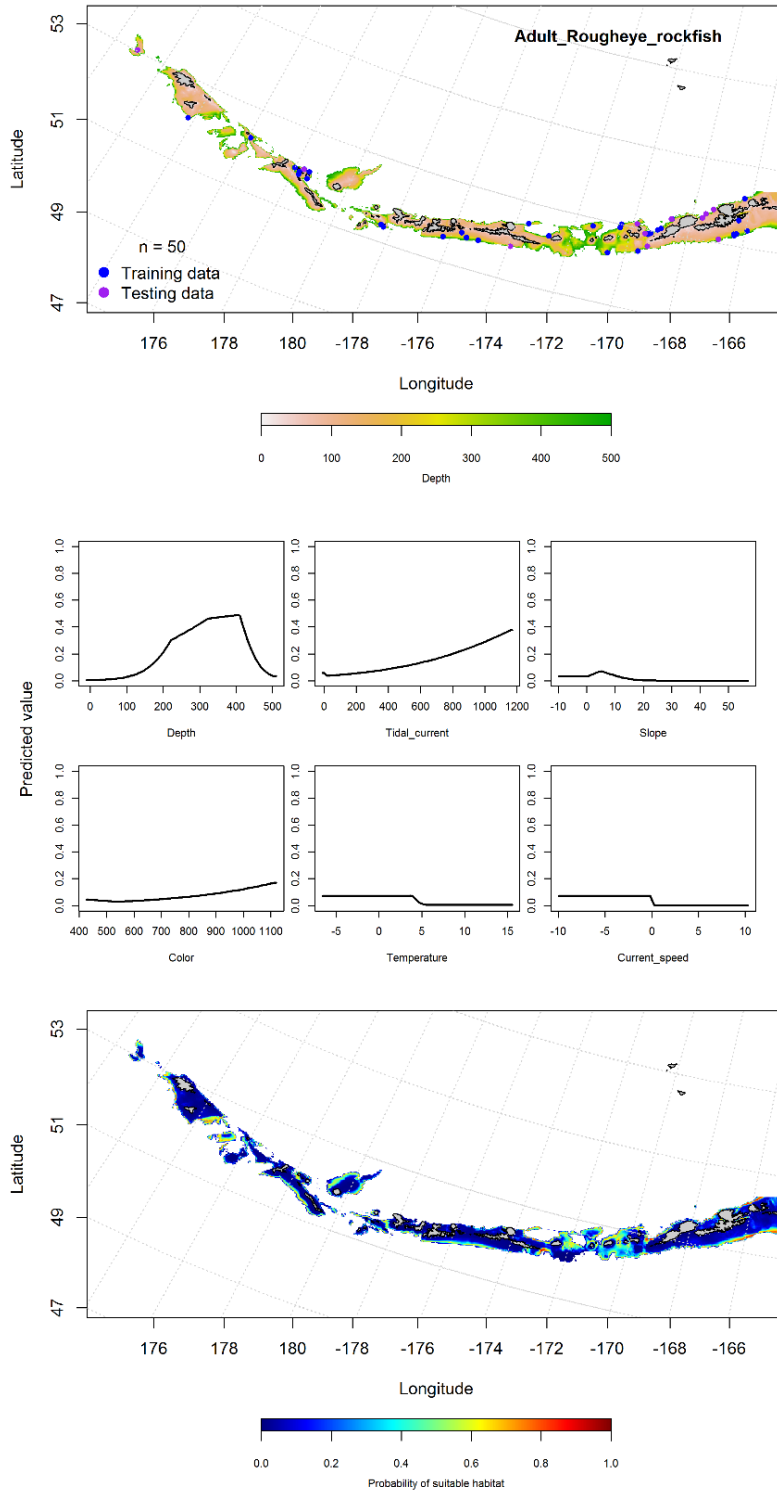


Figure 115. -- Distribution of catches of adult rougheye rockfish in bottom trawl surveys (top panel), relationships between presence and environmental variables for the maximum entropy model of adult rougheye rockfish (middle panels), and predicted probability of suitable habitat for adult rougheye rockfish based on the model (bottom panel).

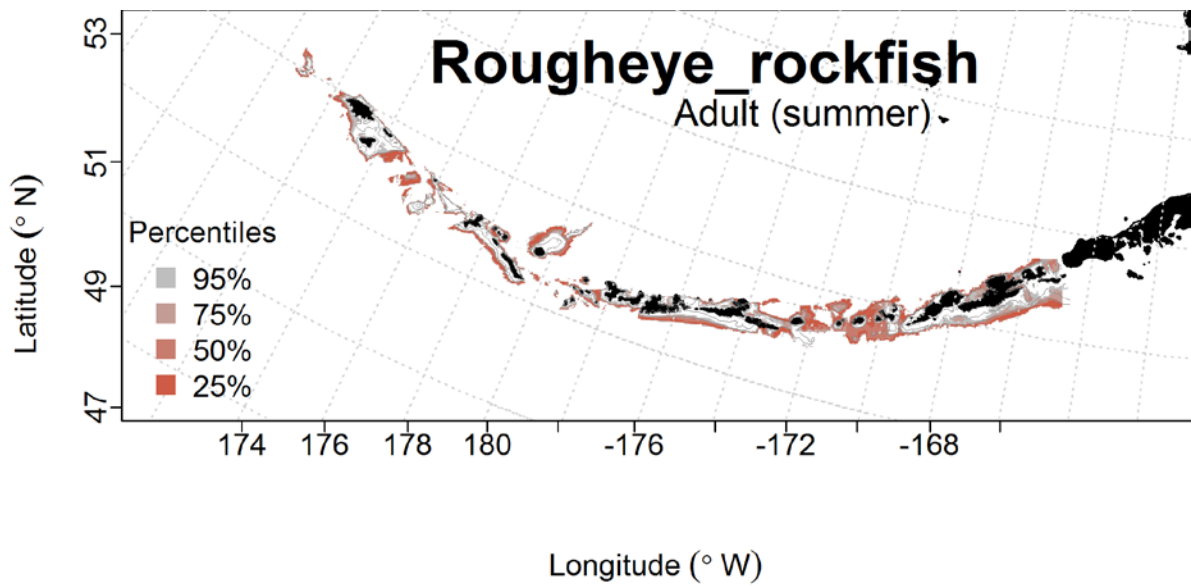


Figure 116. -- Predicted EFH quantiles for adult rougheye rockfish based on species distribution modeling. Larval stages are shown above in the Pacific ocean perch section (*Sebastes* spp.) Settled summer adult stage is based on bottom trawl survey data.

Blackspotted Rockfish (*Sebastes melanostictus*)

Rougheye and blackspotted rockfish were considered a single species until recently (Orr and Hawkins 2008). In the bottom trawl survey data the species have been separated since 2006.

Early life history stages of *Sebastes* spp. -- Early life history stages of blackspotted rockfish were not distinguishable from other *Sebastes* spp. Combined *Sebastes* spp. early life history stages are presented with Pacific Ocean perch.

Juvenile and adult blackspotted rockfish distribution in the bottom trawl survey -- A MaxEnt model was used to predict the distribution of suitable habitat for juvenile blackspotted rockfish. Bottom depth and slope were most important variables in the model, and the AUC was 0.89 for the training data and 0.74 for the test data. Juvenile blackspotted rockfish suitable habitat was predicted across the AI though higher near Kiska and Adak islands, Tahoma Bank and Walls Plateau (Fig. 117).

A MaxEnt model was used to predict the distribution of suitable habitat for adult blackspotted rockfish. Bottom depth and slope were again most important variables in the model, and the AUC was 0.92 for the training data and 0.83 for the test data. Adult blackspotted rockfish suitable habitat was predicted across the AI, though higher near passes (Fig. 118).

Blackspotted rockfish distribution in commercial fisheries -- Blackspotted rockfish are not distinguished from rougheye rockfish in commercial fisheries data. Therefore, no modeling of commercial catches was conducted for these species.

Blackspotted rockfish essential fish habitat maps and conclusions -- Blackspotted rockfish summertime EFH of juveniles and adults were similarly distributed across the AI with highest

probabilities around Seguam Pass to the Islands of Four Mountains and in deeper areas near the shelf break throughout the Aleutians (Fig. 119).

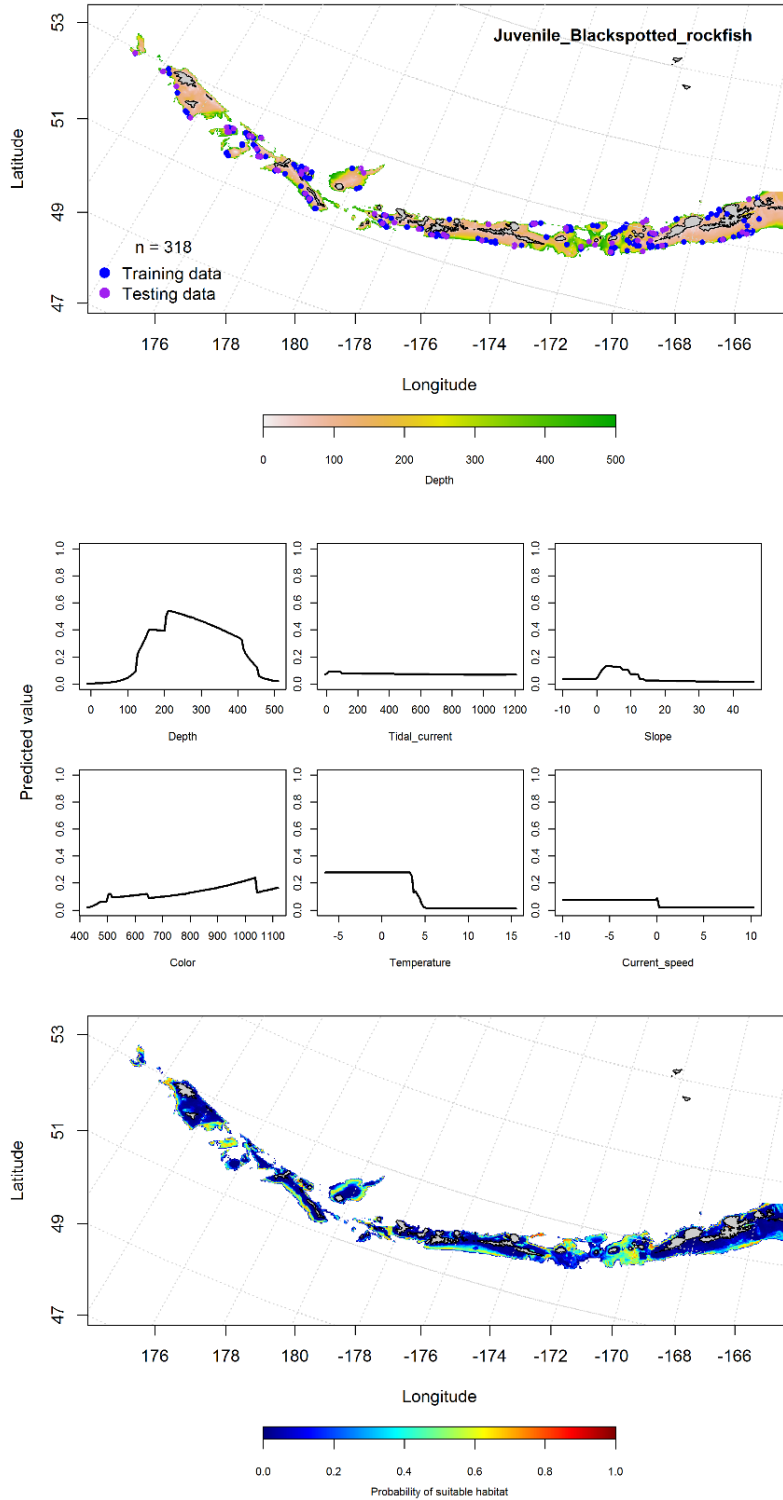


Figure 117. -- Distribution of catches of juvenile blackspotted rockfish in bottom trawl surveys (top panel), relationships between presence and environmental variables for the maximum entropy model of juvenile blackspotted rockfish (middle panels), and predicted probability of suitable habitat for juvenile blackspotted rockfish based on the model (bottom panel).

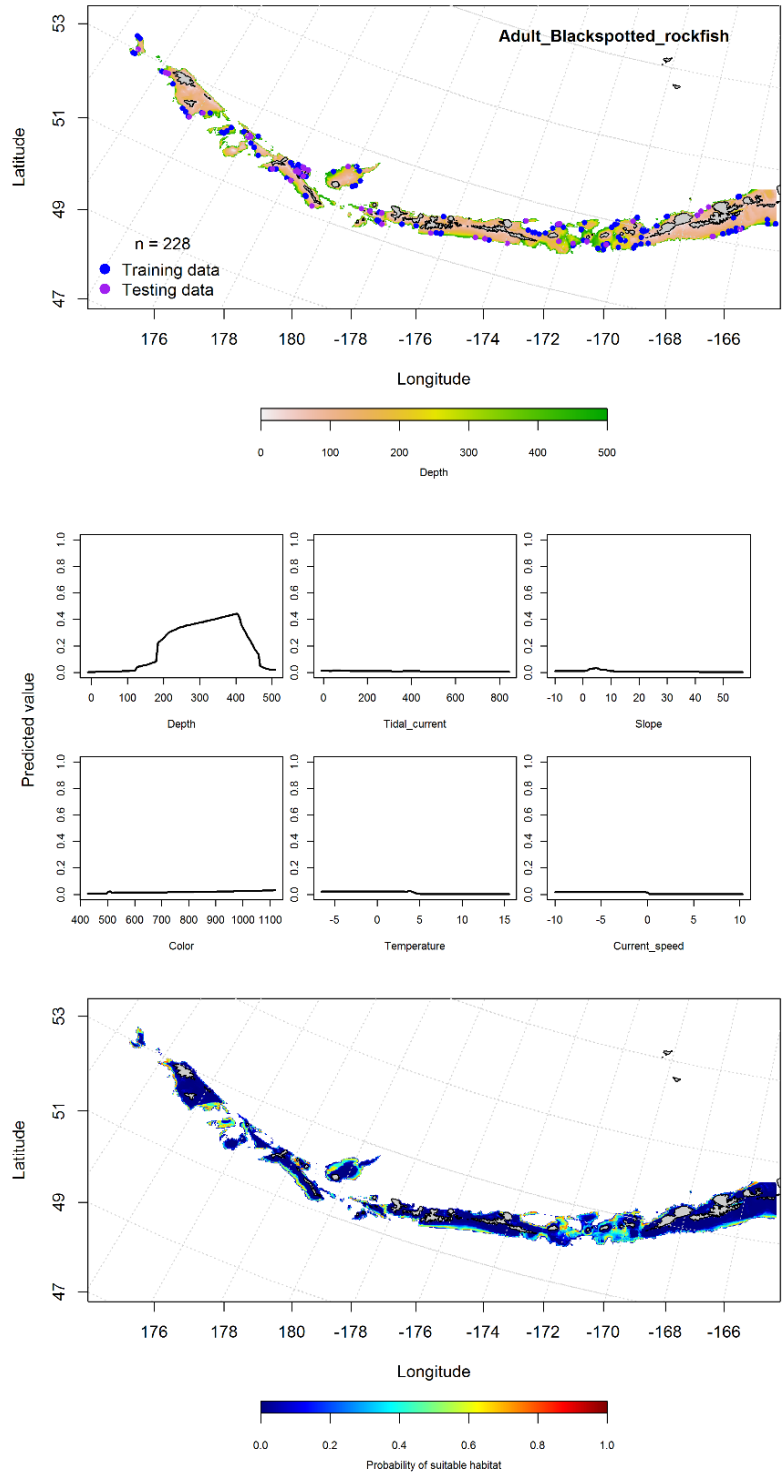


Figure 118. -- Distribution of catches of adult blackspotted rockfish in bottom trawl surveys (top panel), relationships between presence and environmental variables for the maximum entropy model of adult blackspotted rockfish (middle panels), and predicted probability of suitable habitat for adult blackspotted rockfish based on the model (bottom panel).

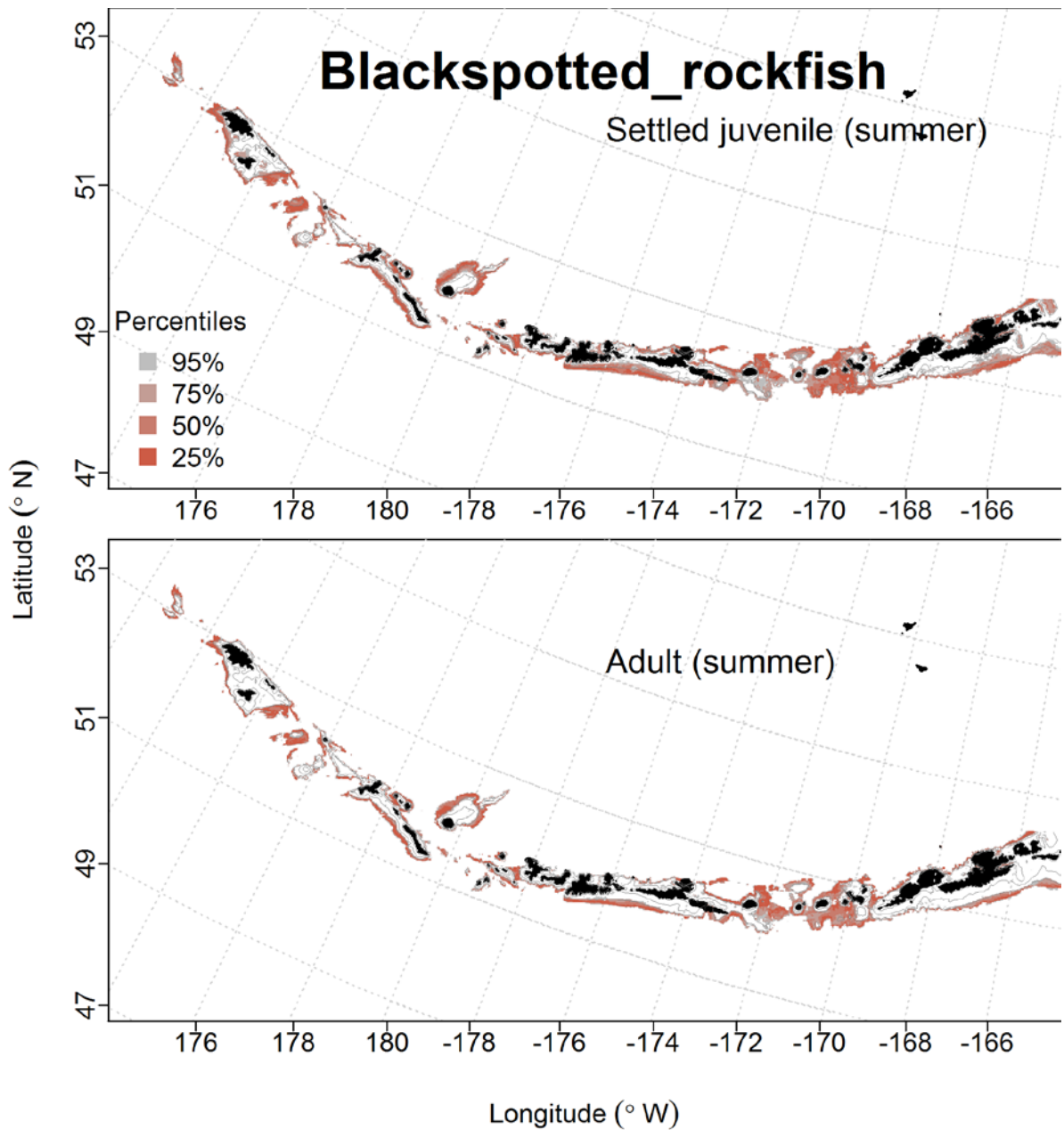


Figure 119. -- Predicted EFH quantiles for juvenile and adult blackspotted rockfish based on species distribution modeling. Larval stages are shown above in the Pacific ocean perch section (*Sebastes* spp.) Settled summer juvenile and adult stages are based on bottom trawl survey data.

Dusky Rockfish (*Sebastes variabilis*)

Early life history stages of *Sebastes* spp. -- Early life history stages of dusky rockfish were not distinguishable from other *Sebastes* spp. Combined *Sebastes* spp. early life history stages are presented with Pacific ocean perch.

Juvenile and adult dusky rockfish distribution in the bottom trawl survey -- There were only 22 instances of juvenile Dusky rockfish from summertime bottom trawl survey catches not enough to model.

A MaxEnt model was used to predict the distribution of suitable habitat for adult dusky rockfish. The AUC was 0.82 for the training data and 0.68 for the test data. The most important variables predicting the probability of suitable habitat were depth and ocean color. The areas of suitable habitat were mostly in the eastern Aleutians from Adak Island to Unimak Pass (Fig. 120).

Dusky rockfish distribution in commercial fisheries -- In the fall, depth, mean current speed and tidal current were the most important variables determining the distribution of dusky rockfish. The AUC of the fall MaxEnt model was 0.94 for the training data and 0.81 for the test data. The model predicted suitable habitat of dusky rockfish was highest south of Seguam Pass and Umnak Island (Fig. 121).

In the winter, depth, ocean color and temperature were the most important variables determining the distribution of dusky rockfish. The AUC of the winter MaxEnt model was 0.95 for the training and 0.84 for the test data. The model predicted suitable habitat of dusky rockfish throughout the Aleutians on the continental shelf (Fig. 122).

In the spring, depth and ocean color were the most important variables determining the distribution of dusky rockfish. The AUC of the spring MaxEnt model was 0.92 for the training data and 0.80 for the test data. The model predicted suitable habitat of dusky rockfish throughout the Aleutians, similar to the winter distribution (Fig. 123).

Dusky rockfish essential fish habitat maps and conclusions -- Summertime EFH of adult dusky rockfish adults was distributed across AI, with a general decrease from east to west (Fig. 124). The fall, winter and spring distribution of dusky rockfish predicted EFH changed from fall to winter and spring (which were similar). EFH was concentrated in the central and far western Aleutian Islands in the latter two seasons, while less concentrated during the fall (Fig. 124).

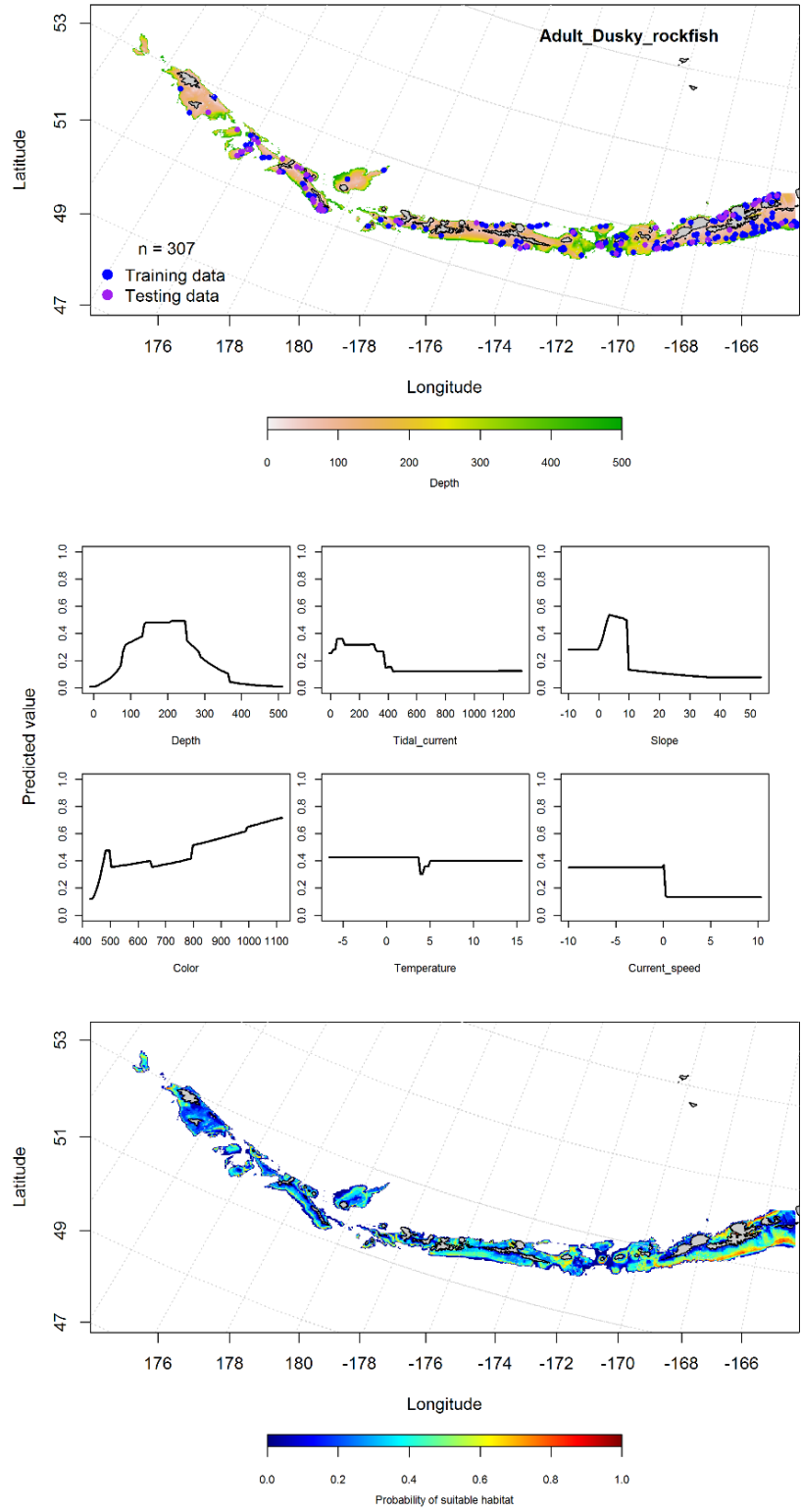


Figure 120. -- Distribution of catches of adult dusky rockfish in bottom trawl surveys (top panel), relationships between presence and environmental variables for the maximum entropy model of adult dusky rockfish (middle panels), and predicted probability of suitable habitat for adult dusky rockfish based on the model (bottom panel).

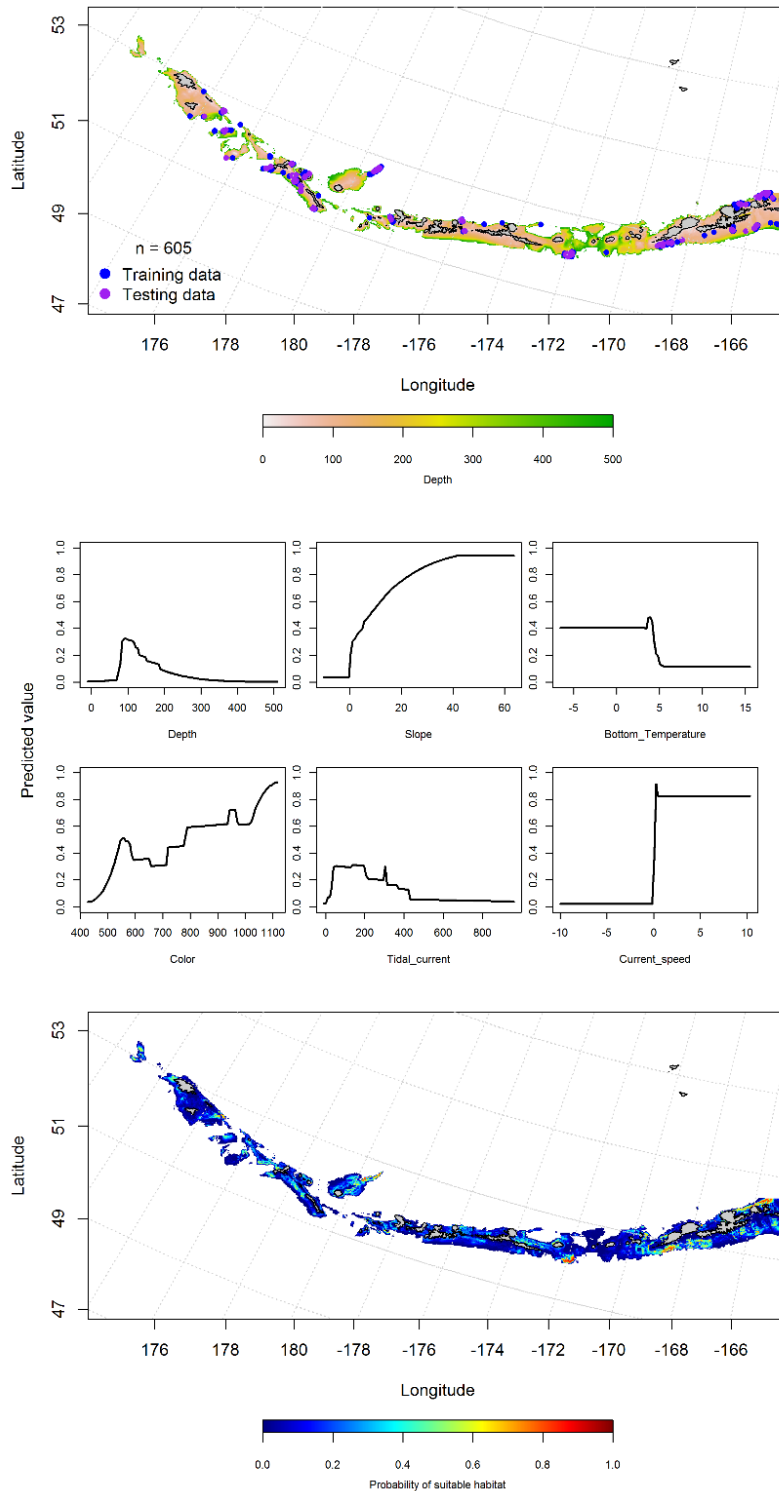


Figure 121. -- Locations of fall (September-November) commercial fisheries catches of dusky rockfish (top panel), relationships between probability of presence and environmental variables for the maximum entropy model (middle panels), and predicted probability of suitable habitat for dusky rockfish based on the model (bottom panel).

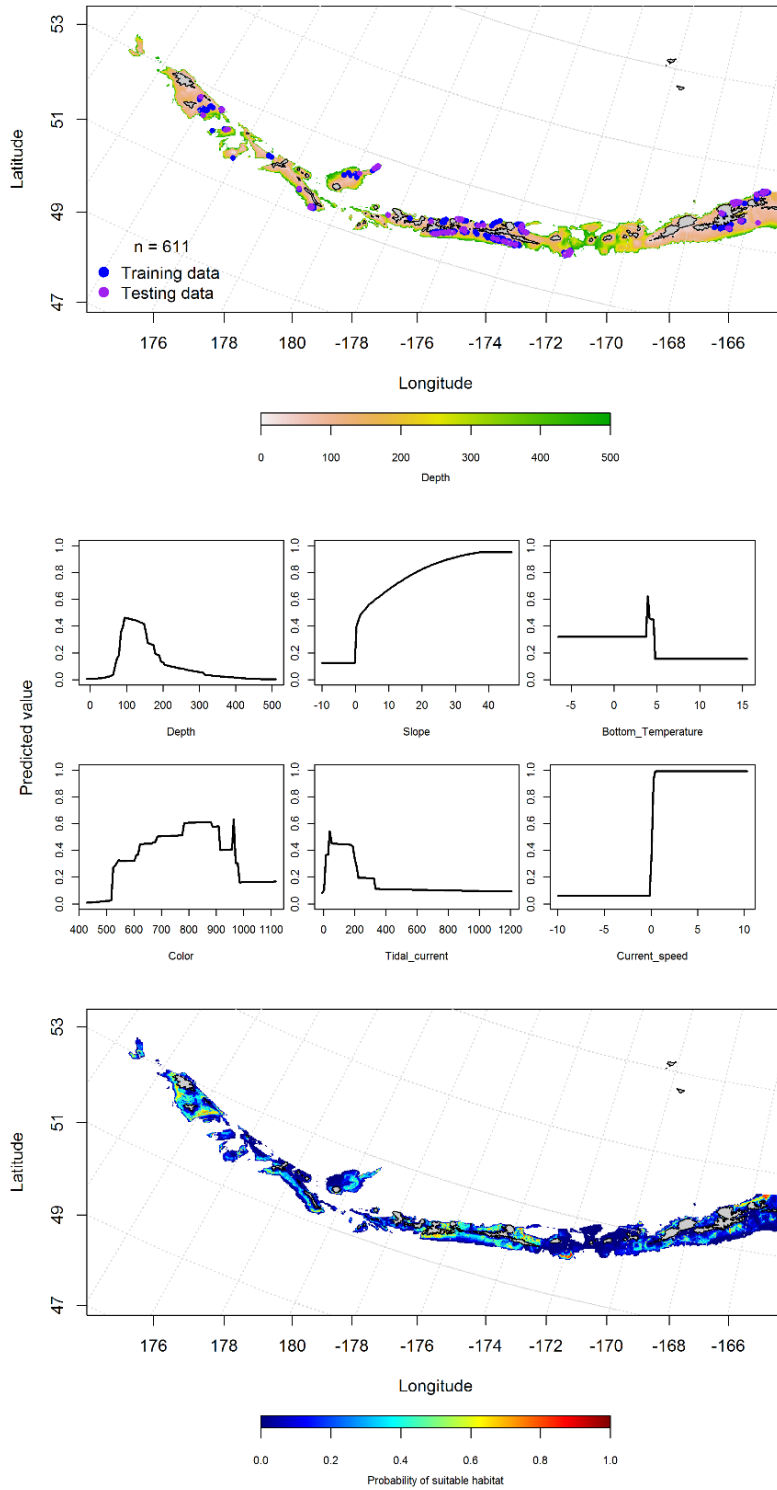


Figure 122. -- Locations of winter (December-February) commercial fisheries catches of dusky rockfish (top panel), relationships between probability of presence and environmental variables for the maximum entropy model (middle panels), and predicted probability of suitable habitat for dusky rockfish based on the model (bottom panel).

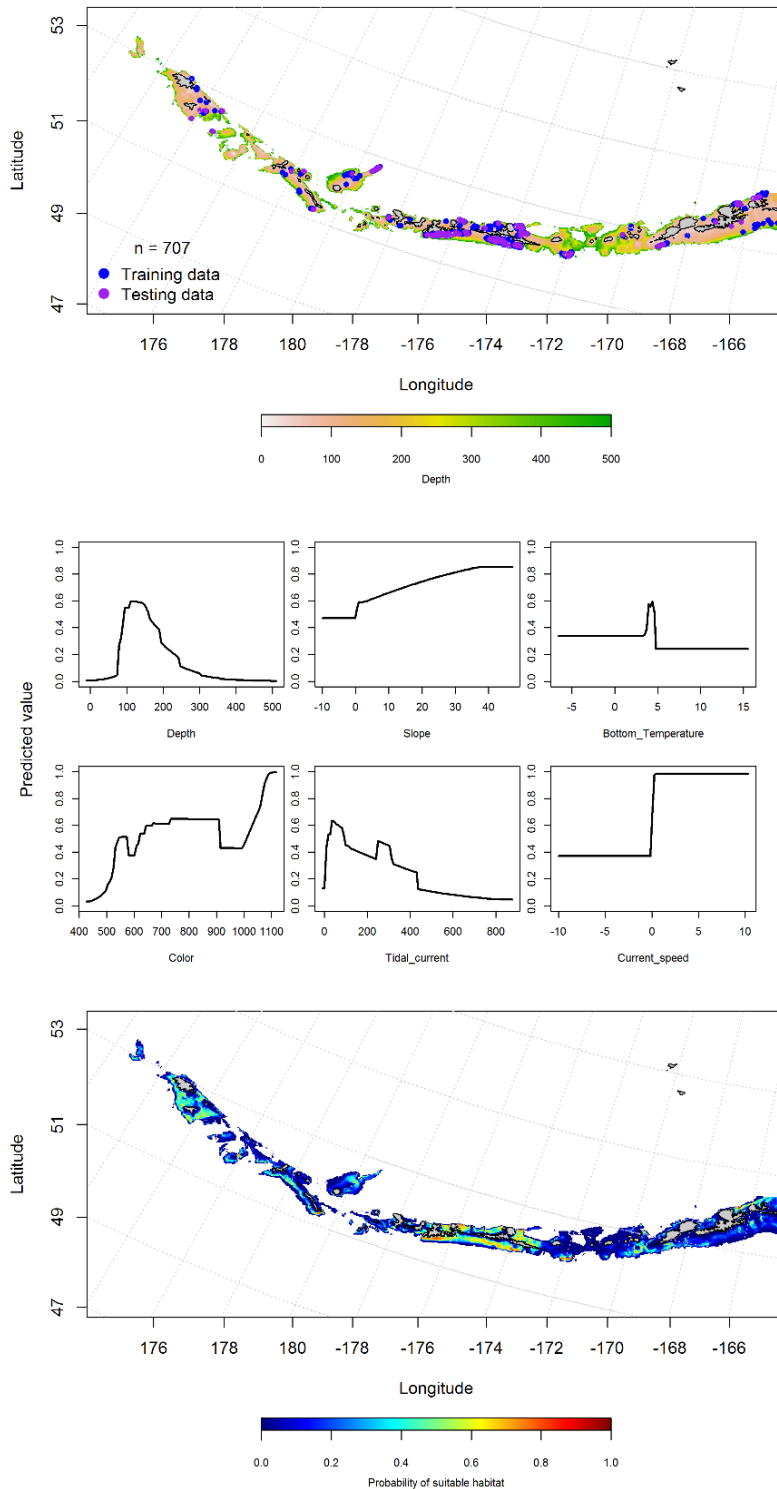


Figure 123. -- Locations of spring (March-May) commercial fisheries catches of dusky rockfish (top panel), relationships between probability of presence and environmental variables for the maximum entropy model (middle panels), and predicted probability of suitable habitat for dusky rockfish based on the model (bottom panel).

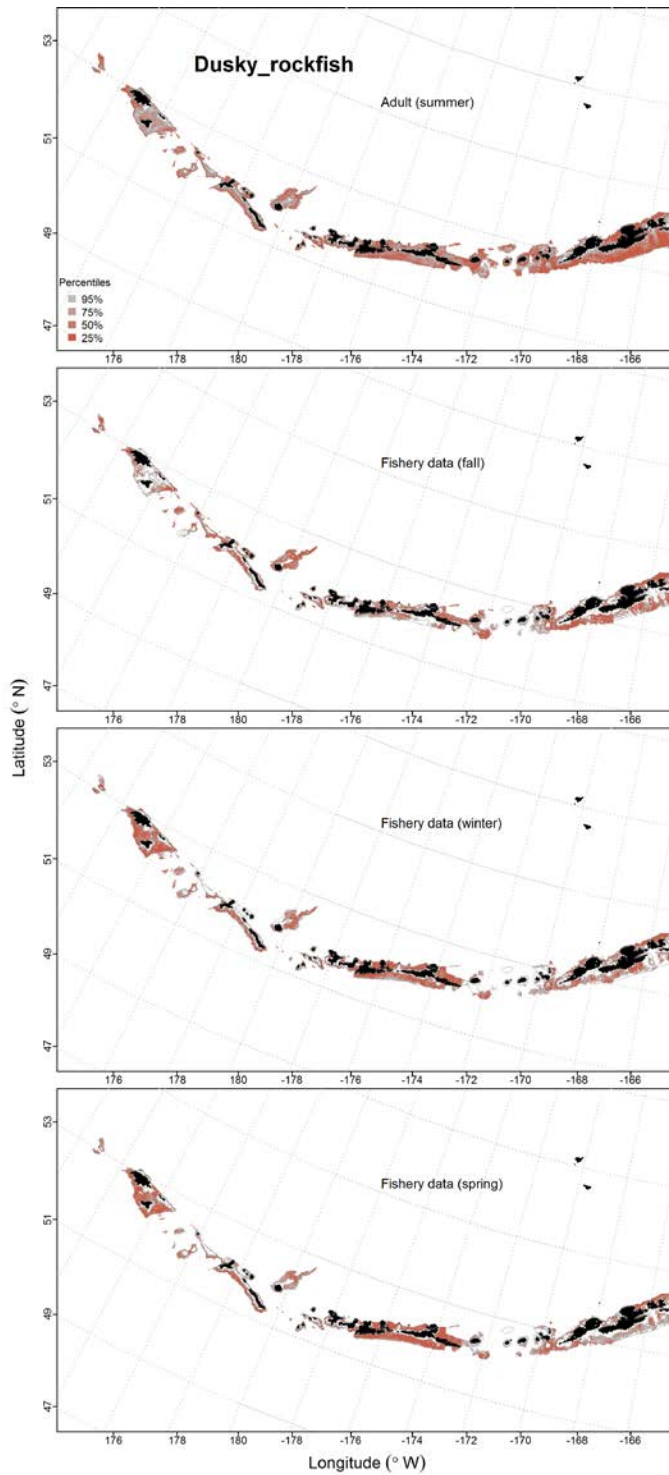


Figure 124. -- Predicted EFH quantiles for dusky rockfish life history stages based on species distribution modeling. Larval stages are shown above in the Pacific ocean perch section (*Sebastes* spp.) Summer adult stages are based on bottom trawl survey data, while seasonal stages (winter, spring, fall) are from commercial fishery data.

Harlequin Rockfish (*Sebastes variegatus*)

Early life history stages of *Sebastes* spp. -- Early life history stages of harlequin rockfish were not distinguishable from other *Sebastes* spp. Combined *Sebastes* spp. early life history stages are presented above with Pacific ocean perch.

Adult harlequin rockfish distribution in the bottom trawl survey -- There were only five instances of juvenile harlequin rockfish in the bottom trawl survey data, not enough data to run a model.

A MaxEnt model predicting the probability of suitable habitat of adult harlequin rockfish resulted in AUC's of 0.90 in the training data and 0.85 in the test data. Depth, ocean color and slope were the most important variables explaining suitable habitat of adult harlequin rockfish. The model predicted suitable habitat of adult harlequin rockfish in shallow mid-shelf areas throughout the Aleutian Islands at relatively low probabilities (Fig. 125).

Harlequin rockfish distribution in commercial fisheries -- In the fall, bottom depth, current speed, ocean color and bottom temperature were the most important variables determining probability of suitable habitat of harlequin rockfish for commercial fishery data. The AUC of the fall MaxEnt model was 0.98 for the training data and 0.92 for the test data. The model predicted suitable habitat of adult harlequin rockfish in relatively small areas such as the patch south of Seguam Pass (Fig. 126).

In the winter, depth, current speed, bottom temperature and ocean color were the most important variables determining probability of suitable habitat of harlequin rockfish. The AUC of the winter MaxEnt model was 0.98 for the training data and 0.92 for the test data. As with the fall, the model predicted suitable habitat of harlequin rockfish was patchy (Fig. 127).

In the spring, bottom depth, current speed, and ocean color were also the most important variables determining the probability of suitable habitat of harlequin rockfish. The AUC of the spring MaxEnt model was 0.95 for the training data and 0.89 for the test data. The model predicted patchy suitable habitat of harlequin rockfish in the spring across the Aleutian Islands (Fig. 128). As with the other seasons, there was a hotspot of suitable habitat south of Seguam Island.

Harlequin rockfish essential fish habitat maps and conclusions -- Summertime EFH of adult harlequin rockfish was predicted across the Aleutian Islands in shallow zones on the continental shelf based on bottom trawl survey data (Fig. 129). The fall, winter and spring predicted EFH of harlequin rockfish was very concentrated in a few locations such as south of Seguam Island and on Petrel Bank (Fig. 129). These areas of concentration were consistent across seasons.

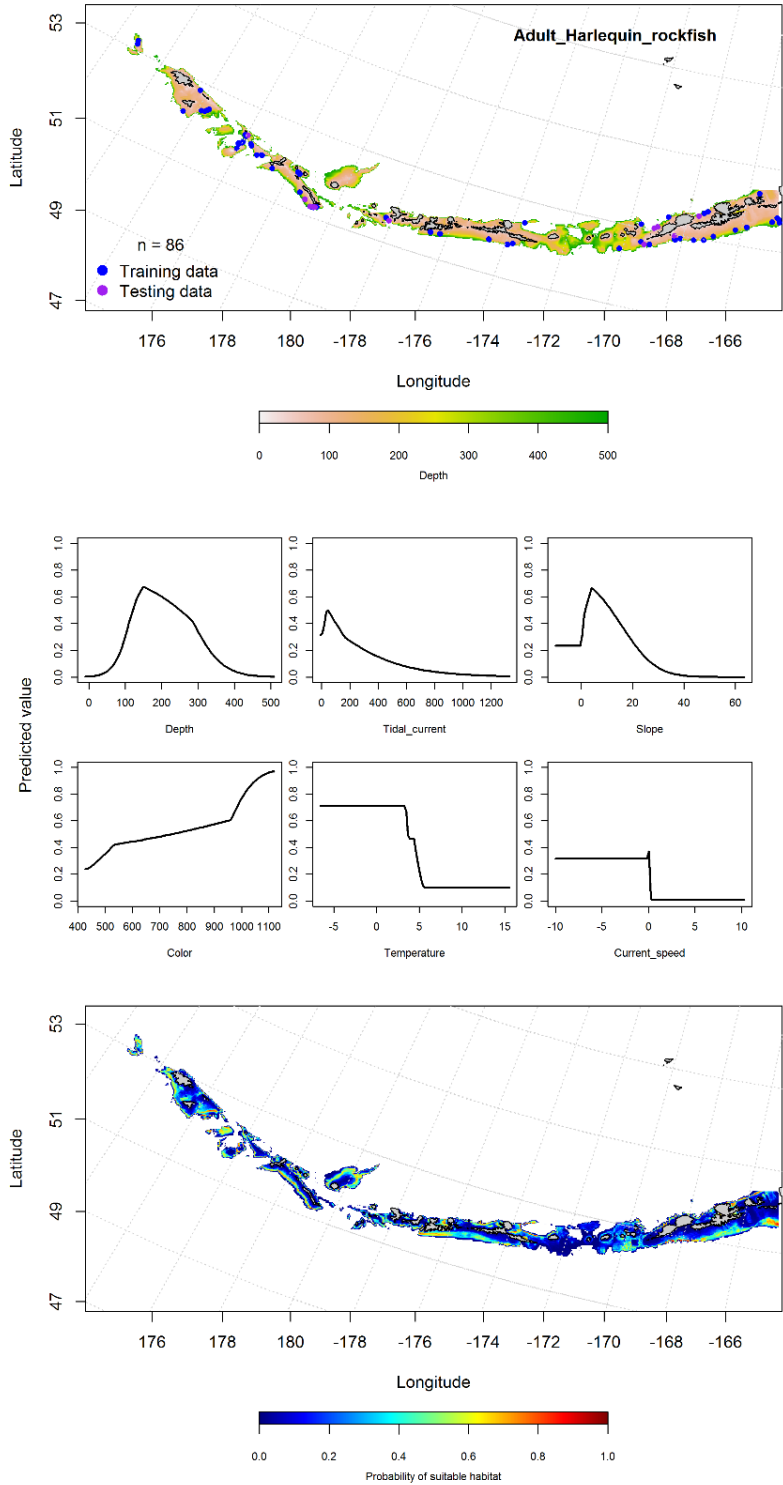


Figure 125. -- Distribution of catches of adult harlequin rockfish in bottom trawl surveys (top panel), relationships between presence and environmental variables for the maximum entropy model of adult harlequin rockfish (middle panels), and predicted probability of suitable habitat for adult harlequin rockfish based on the model (bottom panel).

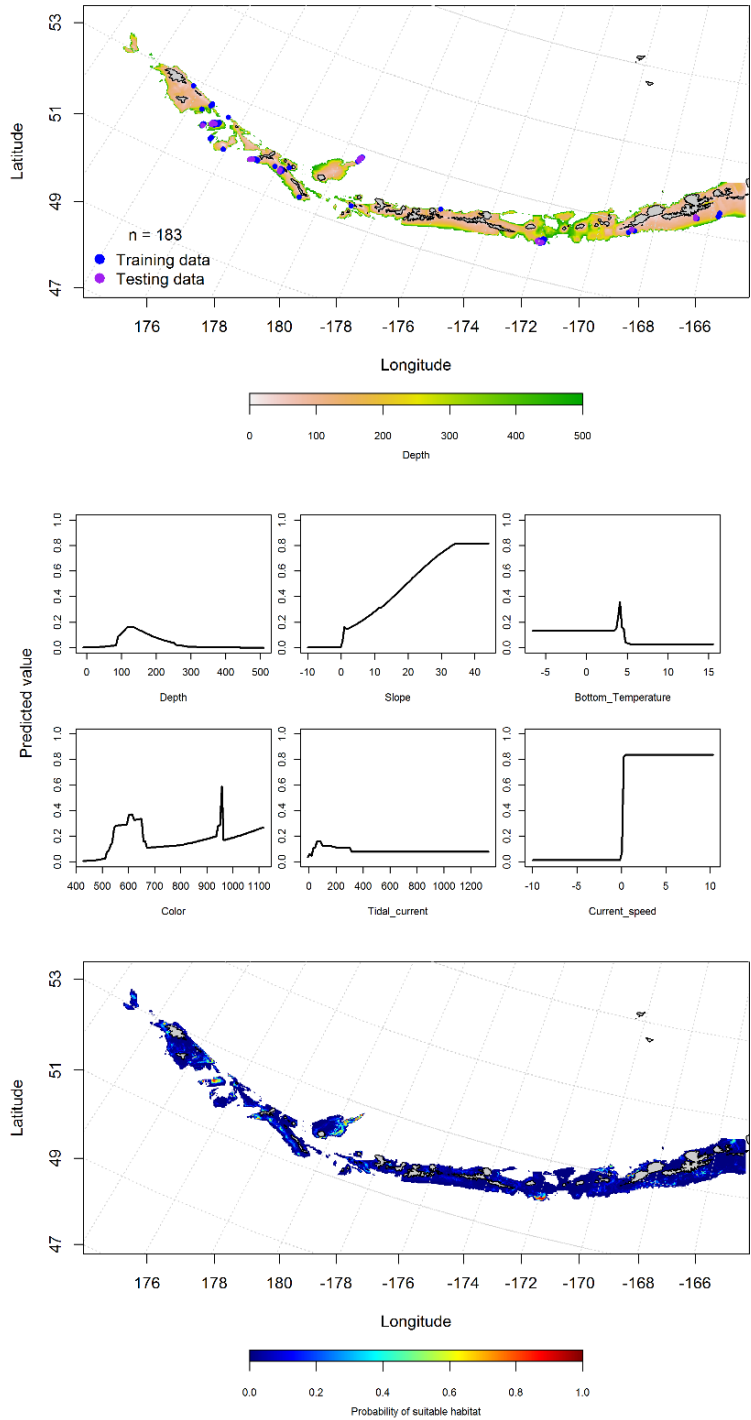


Figure 126. -- Locations of fall (September-November) commercial fisheries catches of harlequin rockfish (top panel), relationships between probability of presence and environmental variables for the maximum entropy model (middle panels), and predicted probability of suitable habitat for harlequin rockfish based on the model (bottom panel).

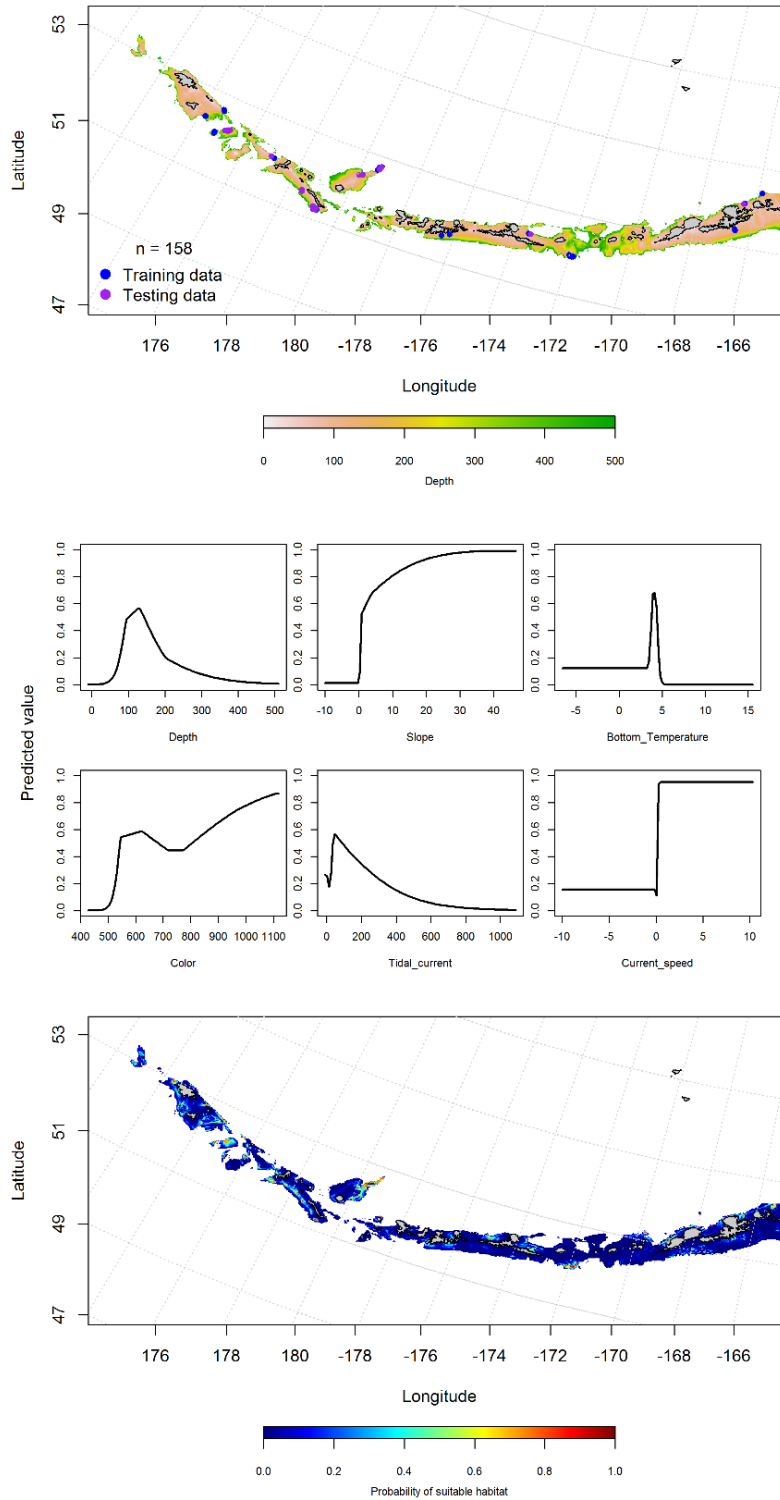


Figure 127. -- Locations of winter (December-February) commercial fisheries catches of harlequin rockfish (top panel), relationships between probability of presence and environmental variables for the maximum entropy model (middle panels), and predicted probability of suitable habitat for harlequin rockfish based on the model (bottom panel).

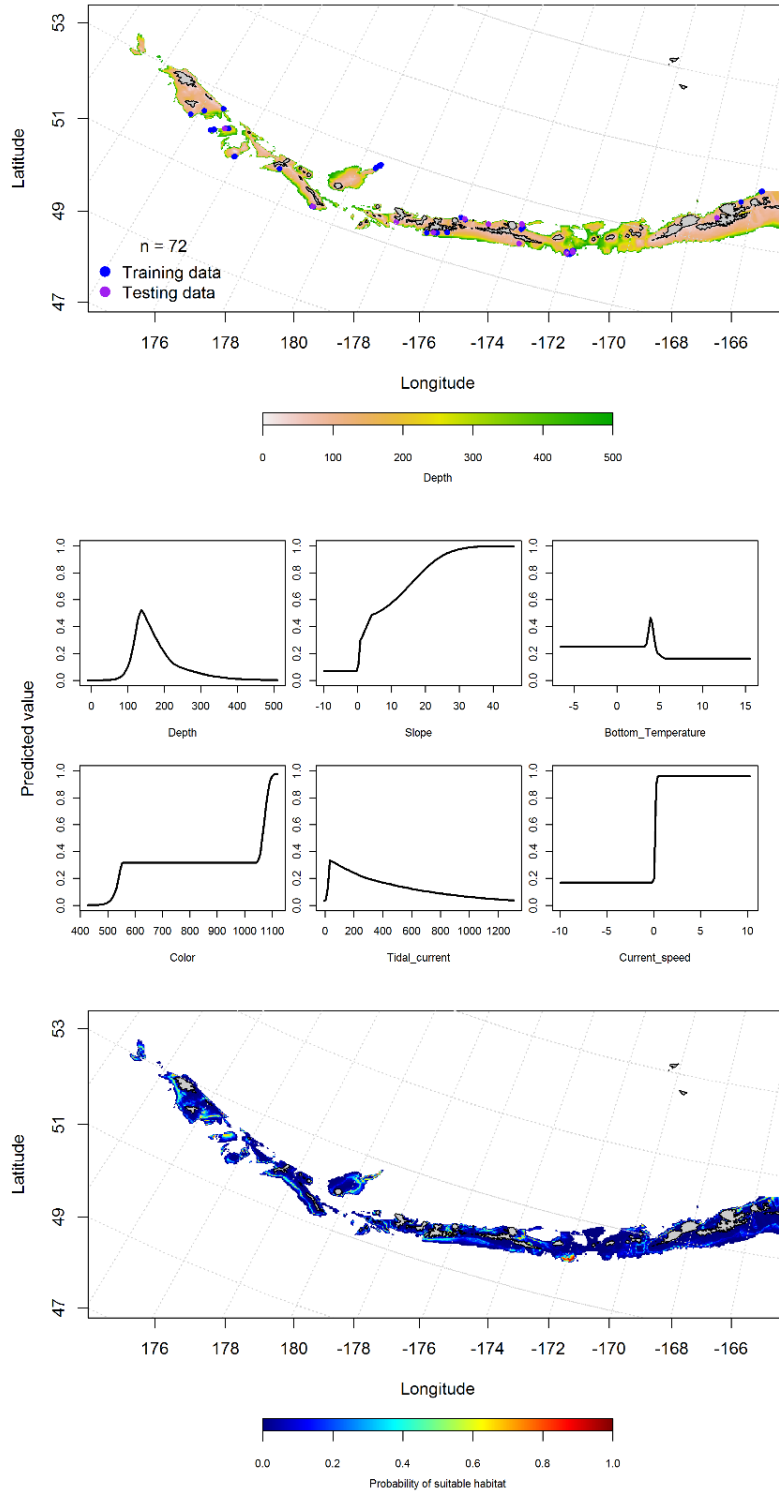


Figure 128. -- Locations of spring (March-May) commercial fisheries catches of harlequin rockfish (top panel), relationships between probability of presence and environmental variables for the maximum entropy model (middle panels), and predicted probability of suitable habitat for harlequin rockfish based on the model (bottom panel).

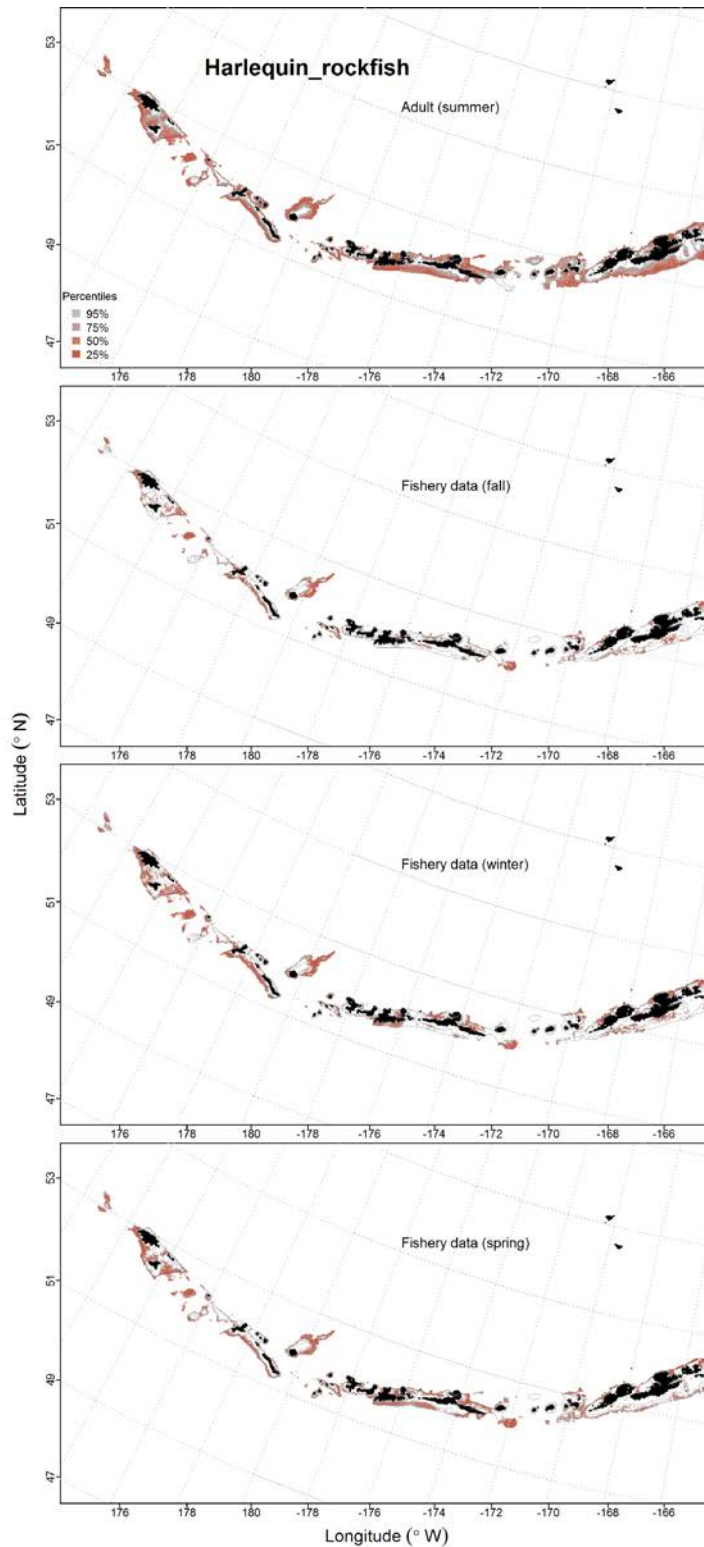


Figure 129. -- Predicted EFH quantiles for harlequin rockfish life history stages based on species distribution modeling. Larval stages are shown above in the Pacific ocean perch section (*Sebastes* spp.) Summer adult stages are based on bottom trawl survey data, while seasonal stages (winter, spring, fall) are from commercial fishery data.

Shortspine Thornyhead (*Sebastolobus alascanus*)

Early life history stages of shortspine thornyhead -- There was no data for early life history stages of shortspine thornyhead.

Juvenile and adult shortspine thornyhead distribution in the bottom trawl survey -- A MaxEnt model was used to predict the probability of suitable habitat for juvenile shortspine thornyhead. Depth and ocean color were the most important variables explaining the probability of suitable habitat for juvenile shortspine thornyhead. The model AUC was 0.96 for the training data and 0.87 for the test data. The areas of probable suitable habitat were found in deeper water south of Unalaska Island and in areas to the west of Petrel Bank (Fig. 130).

A hurdle-GAM was used to predict the distribution of adult shortspine thornyhead. The AUC of the PA GAM was 0.95 for the training data and 0.96 for the test data. Depth, geographic location, and ocean color were the most important variables. The model correctly classified 88% of the training data and 89% of the test data. The model predicted the highest probability of presence in deeper water all across the Aleutians, except from Samalga Pass to Adak Island (Fig. 131). Geographic location, depth and slope were the most important variables in the CPUE GAM. The model explained 50% of the variance in the training data and 42% in the test data. The model predicted high CPUE in deeper waters throughout the Aleutians (Fig. 131).

Shortspine thornyhead distribution in commercial fisheries -- In the fall, depth, ocean color, and current speed were the most important variables determining suitable habitat of shortspine thornyhead. The AUC of the fall MaxEnt model was 0.92 for the training data and 0.73 for the test data. The model predicted suitable habitat of shortspine thornyhead in the fall was highest near Unalaska Island (Fig. 132).

In the spring, depth, ocean color, current speed and bottom temperature were the most important variables determining suitable habitat of shortspine thornyhead. The AUC of the fall MaxEnt model was 0.99 for the training data and 0.86 for the test data. The model predicted suitable habitat of shortspine thornyhead in the winter was uniformly low except near Unalaska Island (Fig. 133).

In the spring, depth and ocean color were the most important variables determining suitable habitat of shortspine thornyhead. The AUC of the spring MaxEnt model was 0.94 for the training data and 0.81 for the test data. The model predicted suitable habitat of shortspine thornyhead in the spring was highest in the eastern Aleutians south of Unalaska Island (Fig. 134).

Shortspine thornyhead essential fish habitat maps and conclusions -- Predicted summertime EFH of shortspine thornyhead juveniles and adults was similar across the AI (Fig. 135). It included areas of the continental slope deeper than about 200 m, throughout the region. The fall and winter distribution of shortspine thornyhead EFH in the commercial fishery was more broadly distributed than the other seasons, but again shortspine thornyhead EFH was found mostly in the deeper waters with slightly higher concentration in the eastern Aleutian Islands (Fig. 135).

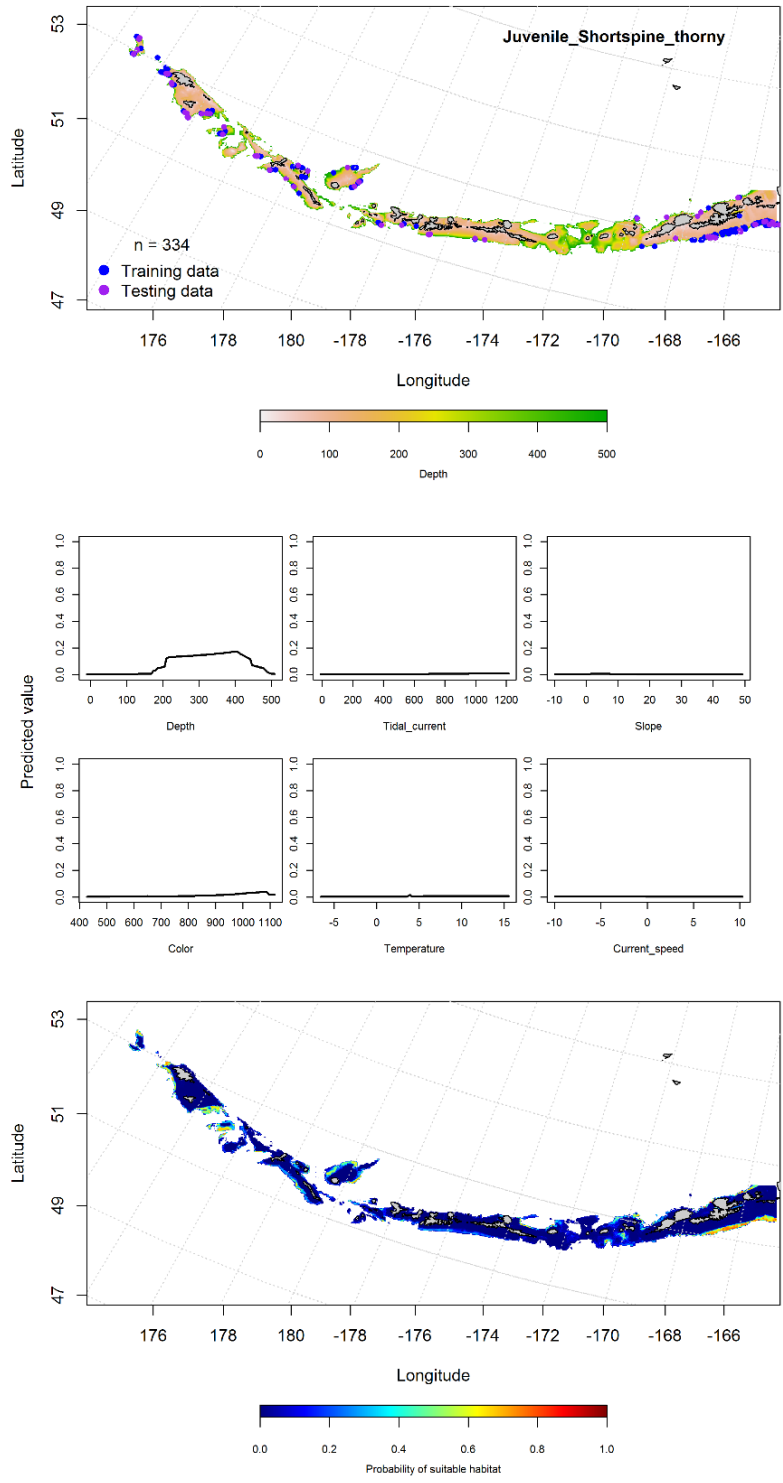


Figure 130. -- Distribution of catches of juvenile shortspine thornyhead in bottom trawl surveys (top panel), relationships between presence and environmental variables for the maximum entropy model of juvenile shortspine thornyhead (middle panels), and predicted probability of suitable habitat for juvenile shortspine thornyhead based on the model (bottom panel).

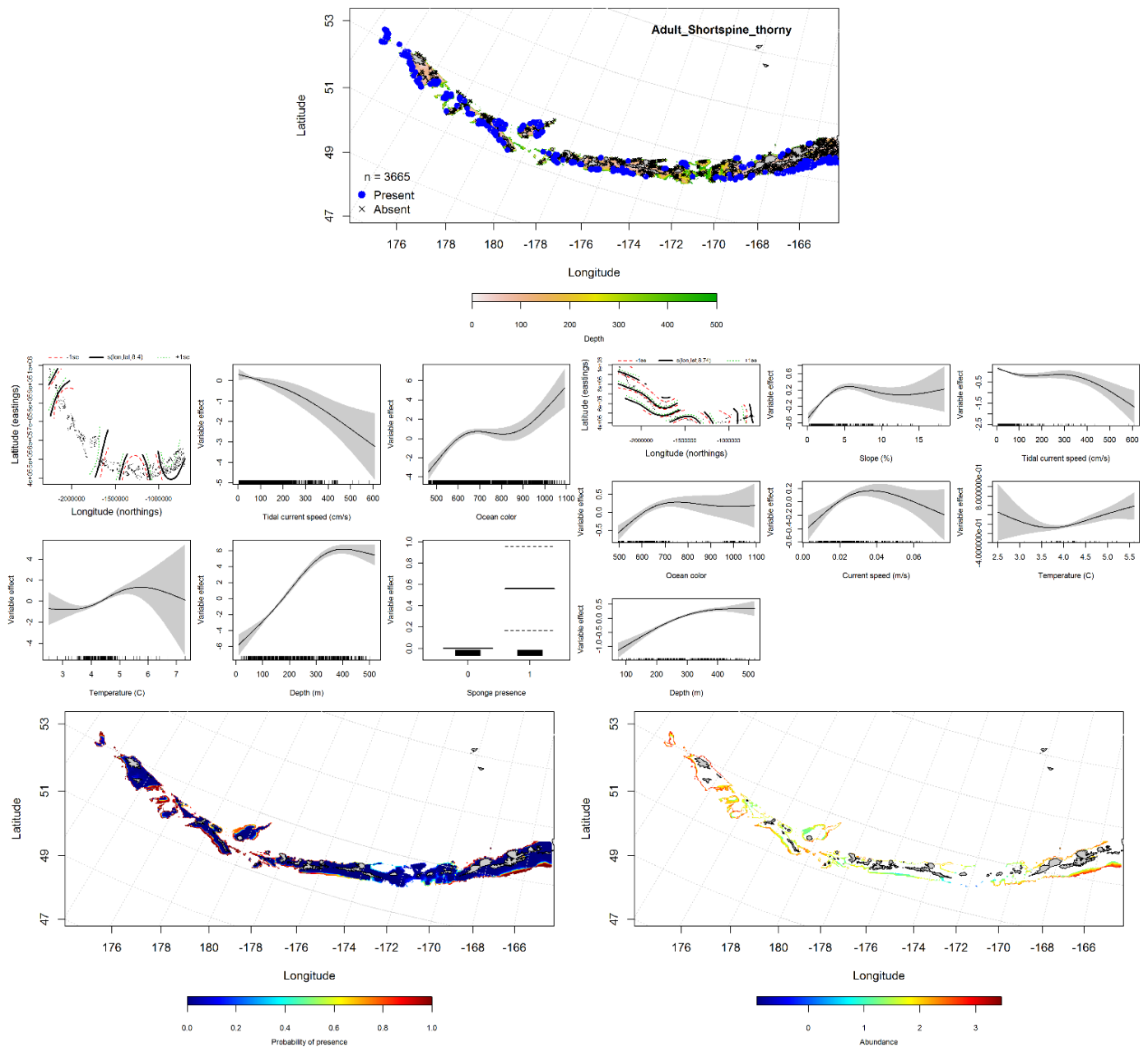


Figure 131. -- Distribution of catches of adult shortspine thornyhead in bottom trawl surveys (top middle panel), significant relationships between presence-absence and CPUE and environmental variables for the best-fitting generalized additive model adult shortspine thornyhead (middle left and right panels), and predicted probability of presence and abundance of adult shortspine thornyhead based on the models (bottom left and right panels).

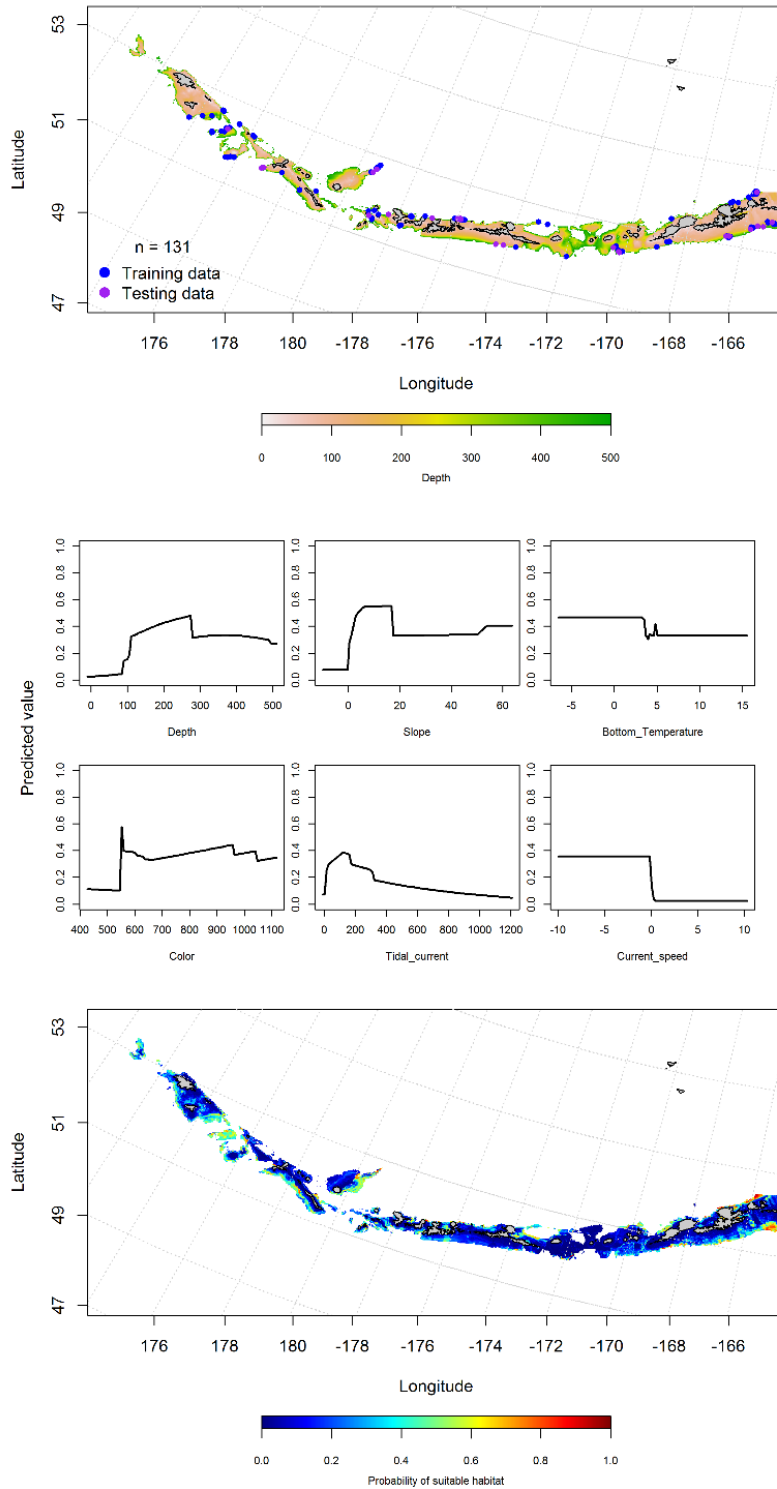


Figure 132. -- Locations of fall (September-November) commercial fisheries catches of shortspine thornyhead (top panel), relationships between probability of presence and environmental variables for the maximum entropy model (middle panels), and predicted probability of suitable habitat for shortspine thornyhead based on the model (bottom panel).

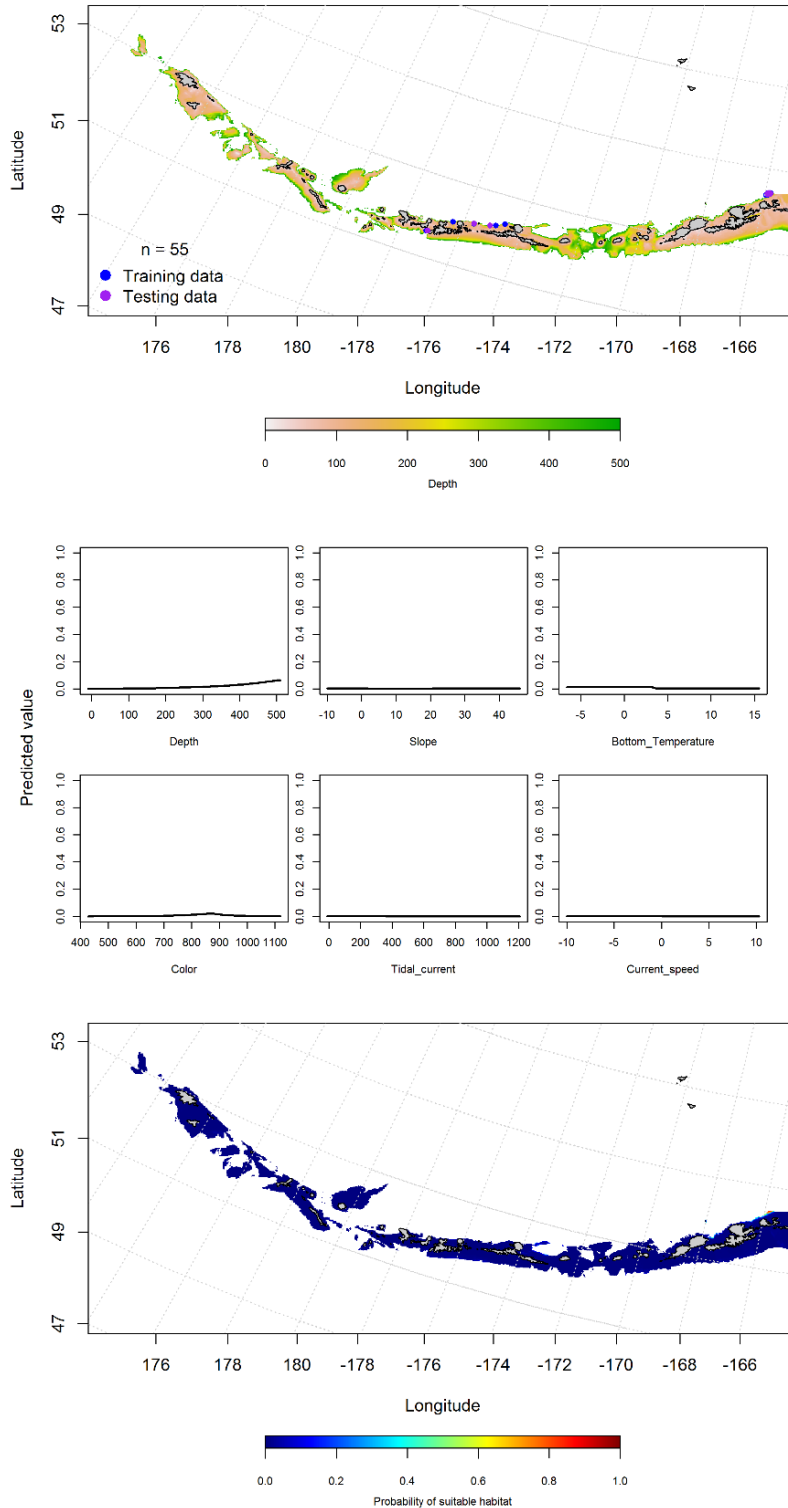


Figure 133. -- Locations of fall (December-February) commercial fisheries catches of shortspine thornyhead (top panel), relationships between probability of presence and environmental variables for the maximum entropy model (middle panels), and predicted probability of suitable habitat for shortspine thornyhead based on the model (bottom panel).

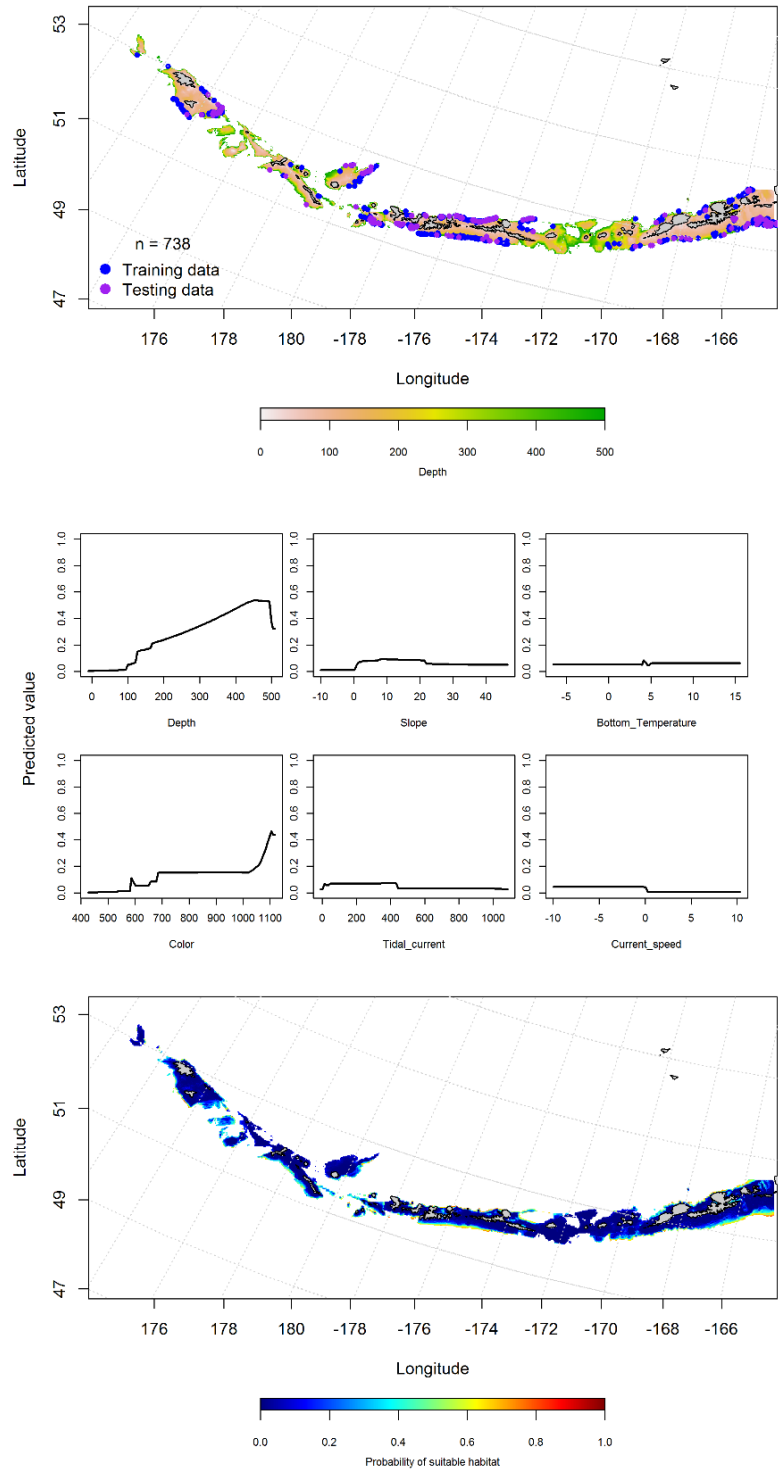


Figure 134. -- Locations of spring (March-May) commercial fisheries catches of shortspine thornyhead (top panel), relationships between probability of presence and environmental variables for the maximum entropy model (middle panels), and predicted probability of suitable habitat for shortspine thornyhead based on the model (bottom panel).

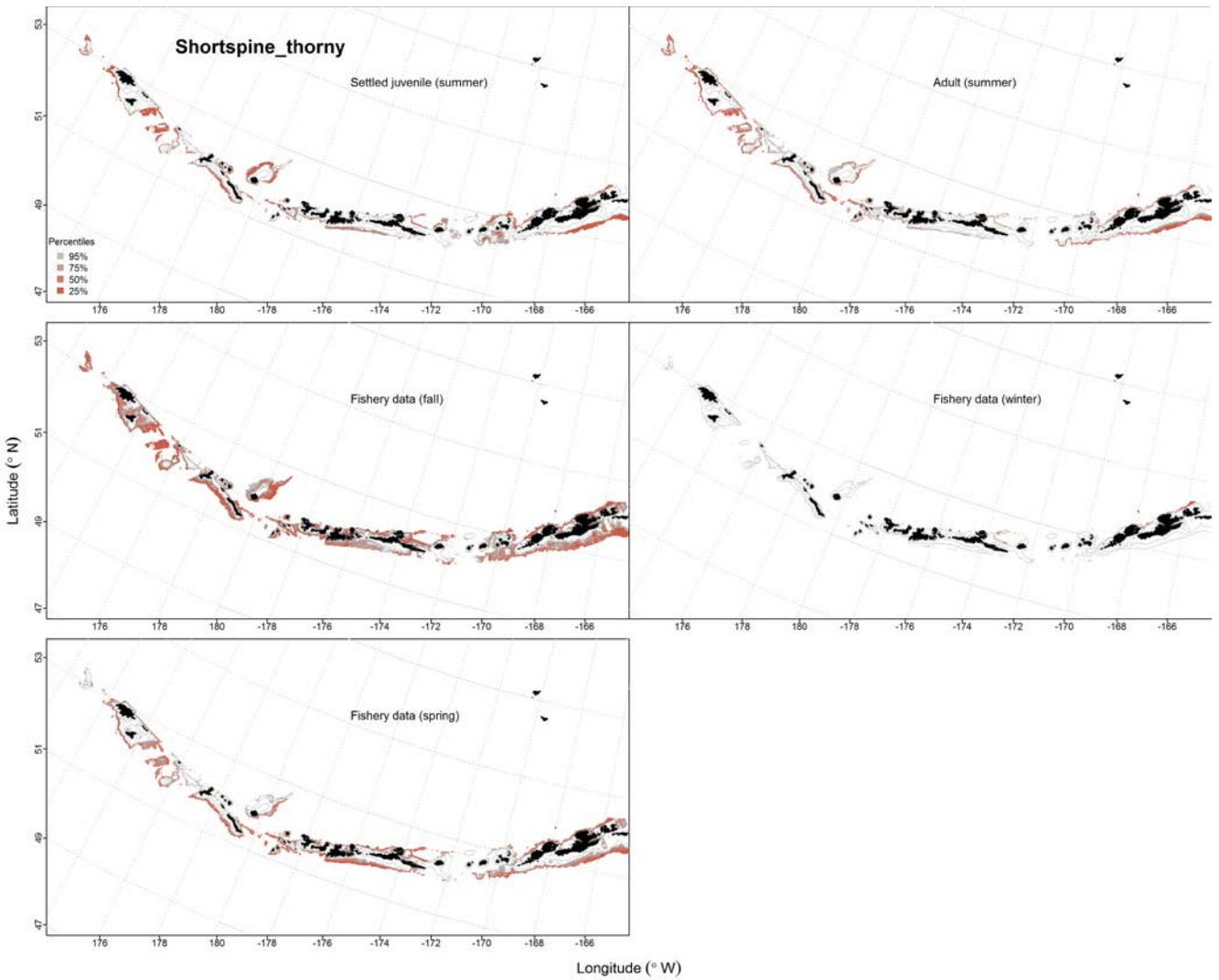


Figure 135. -- Predicted EFH quantiles for shortspine thornyhead life history stages based on species distribution modeling. Settled juvenile and summer adult stages are based on bottom trawl survey data, while seasonal stages (winter, spring, fall) are from commercial fishery data.

Skates

Early life history information for skates is limited. Skates are known to lay eggs in nursery areas in Alaska (Hoff 2010). These are typically small areas of high concentrations of eggs on the upper continental slope of the Bering Sea. Nursery areas have been identified in the eastern Bering Sea, but none have been identified within the Aleutian Islands so we do not consider EFH for early life history stages for skates in this report.

Alaska Skate (*Bathyraja parmifera*) and Leopard Skate (*Bathyraja panthera*)

The Alaska skate and leopard skate were until very recently (~2015) considered as a single species in the bottom trawl surveys and the commercial fisheries data from the Aleutian Islands. For this report we grouped the two species together (hereafter referred to as Alaska skate).

Juvenile and adult Alaska skate distribution in the bottom trawl survey -- A MaxEnt model predicting suitable habitat of juvenile Alaska skate had AUC's of 0.80 for the training and 0.62 for the test data. Depth and current speed were the most important variables explaining the distribution of juvenile Alaska skate. The juvenile Alaska skate model predicted highest probability of suitable habitat in the central and western Aleutians (Fig. 136).

A MaxEnt model predicting suitable habitat of adult Alaska skate had AUC's of 0.88 for the training and 0.77 for the test data. Depth and ocean color were the most important variables explaining the distribution of adult Alaska skate suitable habitat. The model predicted high habitat suitability in the central and western Aleutians (at Stalemate Bank, Fig. 137).

Alaska skate distribution in commercial fisheries -- In the fall, depth and tidal current were the most important variables determining the distribution of Alaska skate. The AUC of the fall MaxEnt model was 0.90 for the training data and 0.82 for the test data. Areas of high predicted suitable habitat of Alaska skate in the fall were distributed throughout the Aleutians, except in large passes (Fig. 138).

In the winter, depth, ocean color and tidal current were the most important variables determining the distribution of Alaska skate habitat. The AUC of the winter MaxEnt model was 0.92 for the training data, 0.89 for the test data. The model predicted suitable habitat of Alaska skate near Agattu and Attu islands in the western and Atka Island in the central Aleutians (Fig. 139).

In the spring, depth, ocean color and tidal current were also the most important variables determining the distribution of Alaska skate habitat. The AUC of the spring MaxEnt model was 0.92 for the training data and 0.81 for the test data. The model predicted suitable habitat of Alaska skate throughout the Aleutians, although highest in the central Aleutians (Fig. 140).

Alaska skate essential fish habitat maps and conclusions -- Alaska skate were distributed across AI, and less abundant in the passes. Predicted summertime EFH of Alaska skate juveniles was similar to the adults (Fig. 141). The fall, winter and spring distribution of Alaska skate EFH was essentially the same (Fig. 141). Areas of higher predicted EFH was in the western AI near Agattu and Attu islands, and in the central AI near Adak and Atka islands.

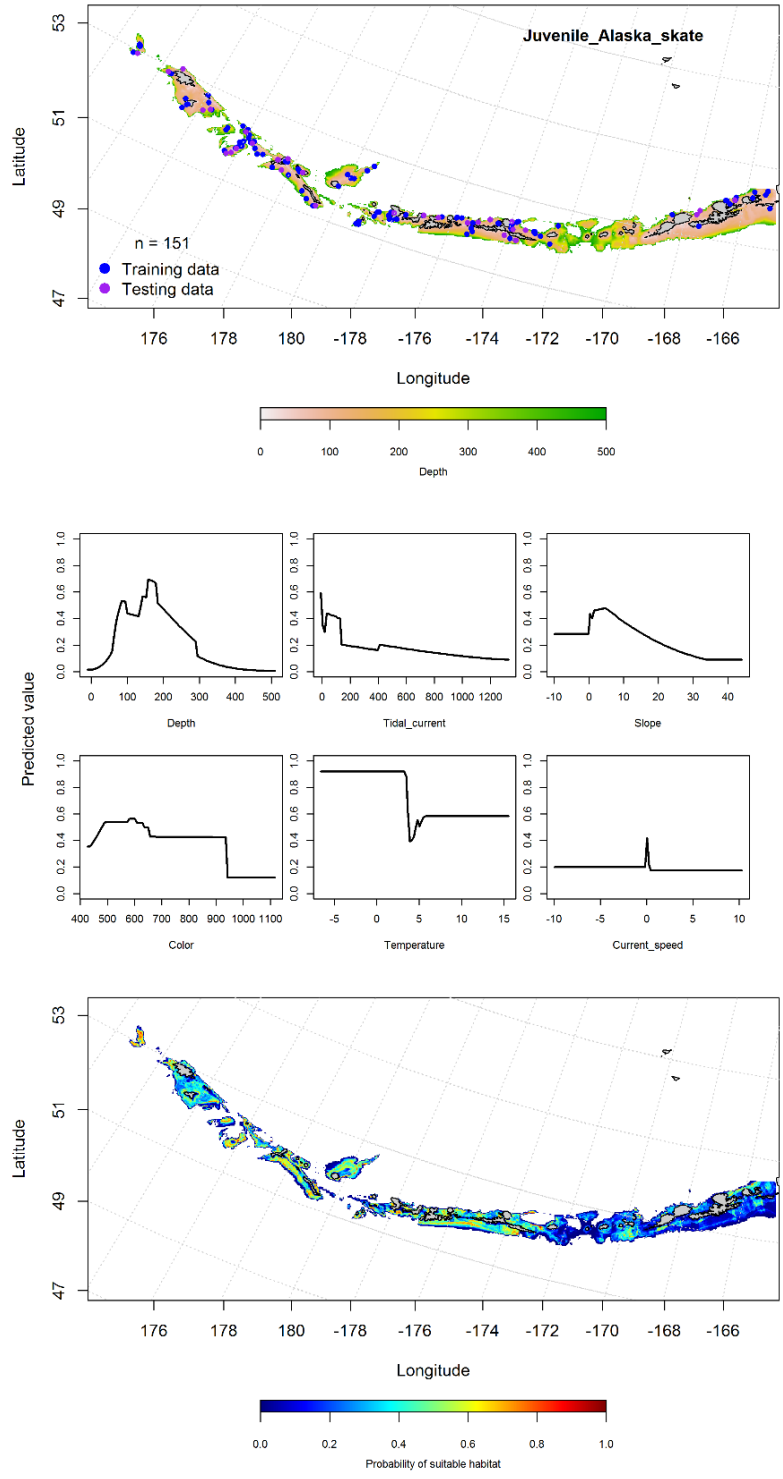


Figure 136. -- Distribution of catches of juvenile Alaska skate in bottom trawl surveys (top panel), relationships between presence and environmental variables for the maximum entropy model of juvenile Alaska skate (middle panels), and predicted probability of suitable habitat for juvenile Alaska skate based on the model (bottom panel).

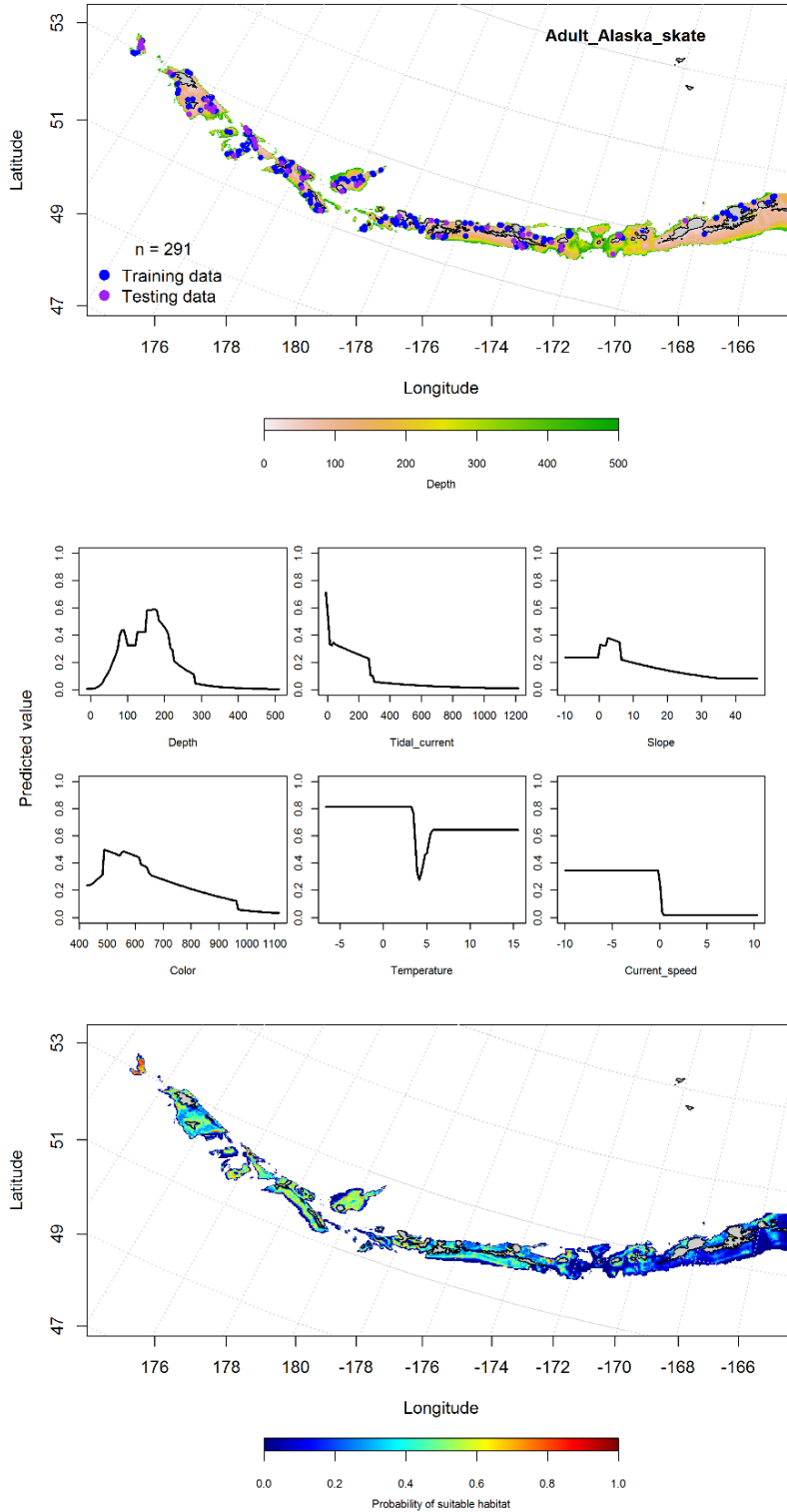


Figure 137. -- Distribution of catches of adult Alaska skate in bottom trawl surveys (top panel), relationships between presence and environmental variables for the maximum entropy model of adult Alaska skate (middle panels), and predicted probability of suitable habitat for adult Alaska skate based on the model (bottom panel).

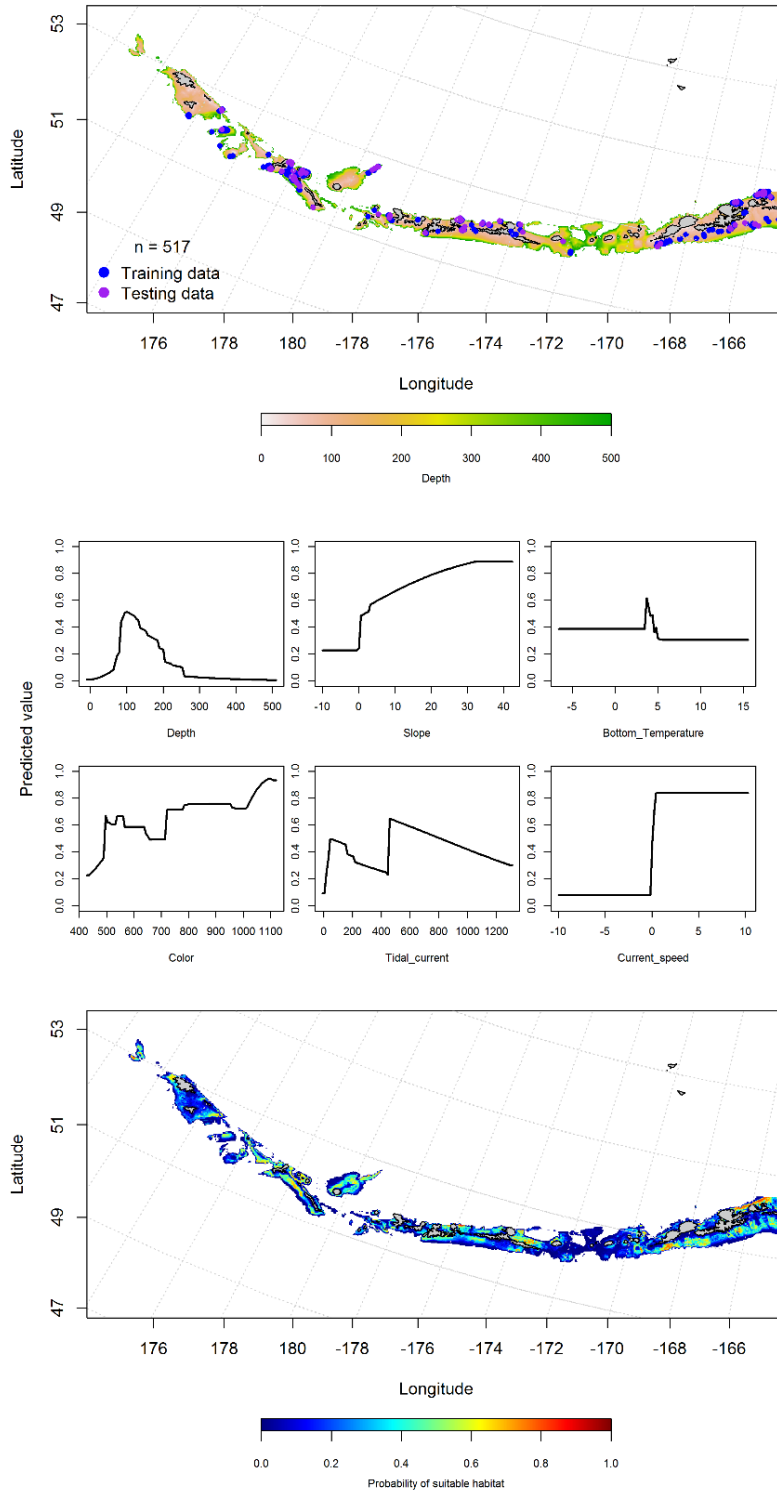


Figure 138. -- Locations of fall (September-November) commercial fisheries catches of Alaska skate (top panel), relationships between probability of presence and environmental variables for the maximum entropy model (middle panels), and predicted probability of suitable habitat for Alaska skate based on the model (bottom panel).

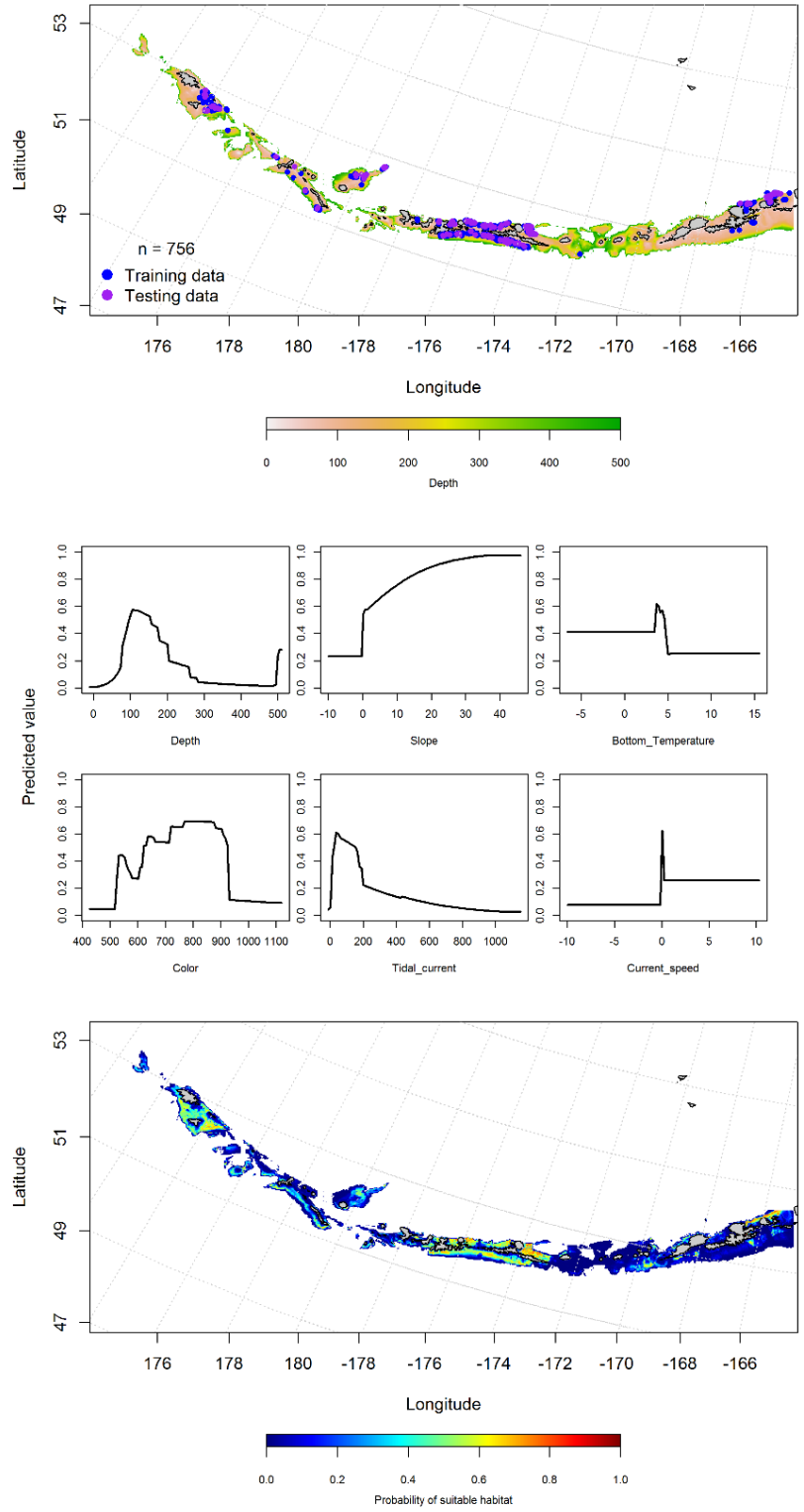


Figure 139. -- Locations of winter (December-February) commercial fisheries catches of Alaska skate (top panel), relationships between probability of presence and environmental variables for the maximum entropy model (middle panels), and predicted probability of suitable habitat for Alaska skate based on the model (bottom panel).

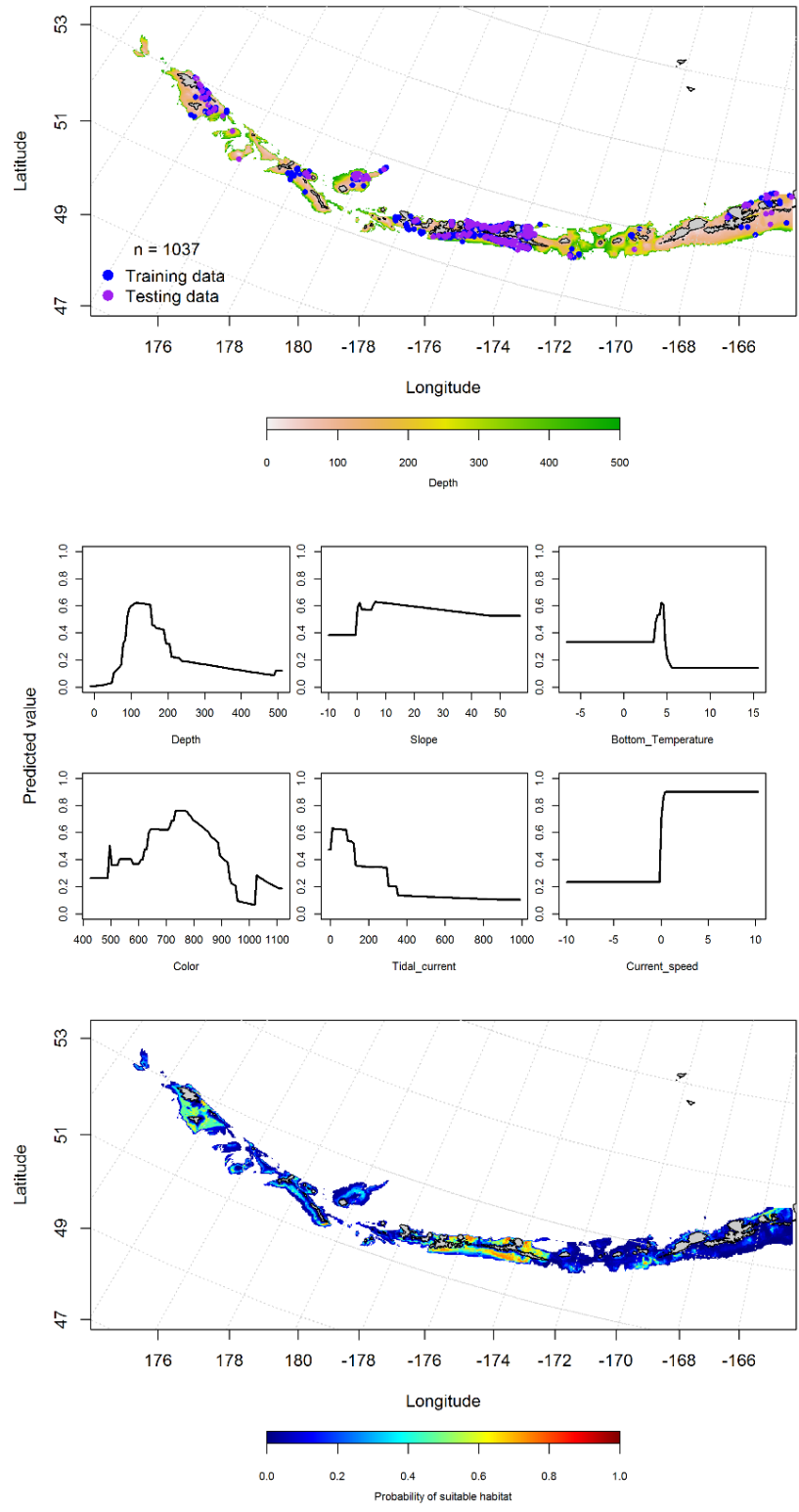


Figure 140. -- Locations of spring (March-May) commercial fisheries catches of Alaska skate (top panel), relationships between probability of presence and environmental variables for the maximum entropy model (middle panels), and predicted probability of suitable habitat for Alaska skate based on the model (bottom panel).

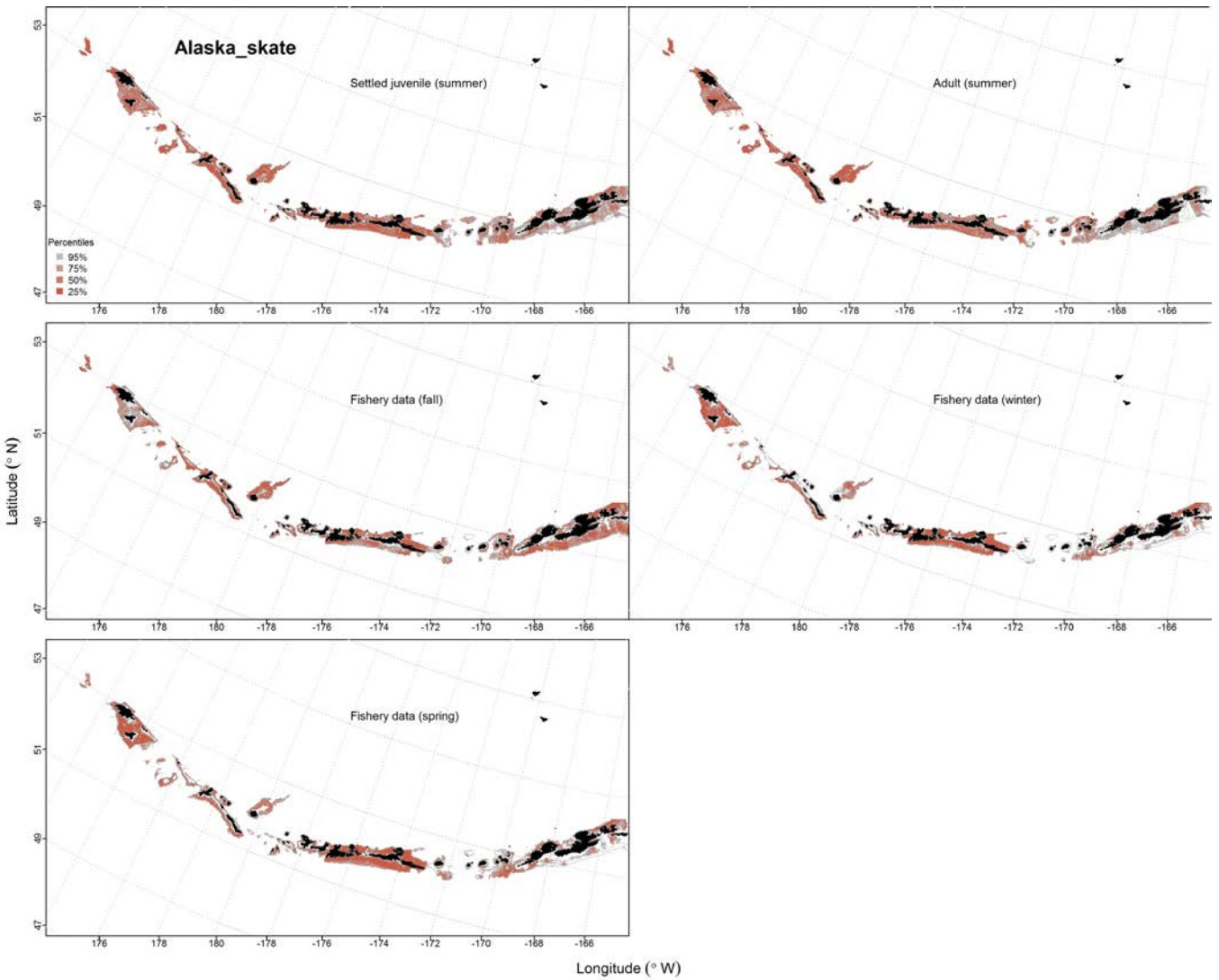


Figure 141. -- Predicted EFH quantiles for Alaska skate life history stages based on species distribution modeling. Summer juvenile and adult stages are based on bottom trawl survey data, while seasonal stages (winter, spring, fall) are from commercial fishery data.

Aleutian Skate (*Bathyraja aleutica*)

Juvenile and adult Aleutian skate distribution in the bottom trawl survey -- Although there were enough data points to use hurdle-GAM model to predict the distribution of juvenile Aleutian skate, the resulting models were very poor fits to the data, so a MaxEnt approach was used instead. The MaxEnt model predicting the probability of suitable habitat for juvenile Aleutian skate resulted in AUC's of 0.80 for the training data and 0.62 for the test data. Depth and current speed were the most important variables determining the distribution of juvenile Aleutian skate. Predicted suitable habitat of juvenile Aleutian skate was distributed throughout the Aleutians with higher probabilities west of Samalga Pass (Fig. 142).

A MaxEnt model predicting the probability of suitable habitat of adult Aleutian skate resulted in an AUC of 0.88 for the training data and 0.79 for the test data. Depth, temperature, and ocean color were the most important variables explaining the probability of suitable habitat of adult Aleutian skate. Predicted suitable habitat was found throughout the Aleutians but was highest around Seguam Island and Stalemate Bank (Fig. 143).

Aleutian skate distribution in commercial fisheries -- In the fall, ocean color and depth were the most important variables determining the distribution of Aleutian skate. The AUC of the fall MaxEnt model was 0.90 for the training data and 0.78 for the test data. The model predicted suitable habitat of Aleutian skate was highest in the eastern Aleutians south of Umnak and Unalaska islands (Fig. 144).

In the winter, depth, ocean color and bottom temperature were the most important variables determining the distribution of Aleutian skate habitat. The AUC of the winter MaxEnt model was 0.94 for the training data and 0.80 for the test data. The model predicted the

probability of suitable habitat Aleutian skate was of higher near Atka and Unalaska islands (Fig. 145).

In the spring, depth and ocean color were the most important variables determining the distribution of Aleutian skate habitat. The AUC of the MaxEnt spring model was 0.89 for the training data and 0.74 for the test data. The predicted the probability of suitable habitat of Aleutian skate in the spring was highest in the central Aleutians (Fig. 146).

Aleutian skate essential fish habitat maps and conclusions -- Summertime EFH of Aleutian skate juveniles and adults were similarly distributed throughout the Aleutian Islands (Fig. 147). Predictions of juvenile and adult Aleutian skate EFH were highest in the central and western Aleutians. The fall, winter and spring distribution of Aleutian skate EFH were similarly distributed (Fig. 147). The central Aleutians near Atka and Amlia islands was the most essential habitat in all seasons, followed by the eastern Aleutians.

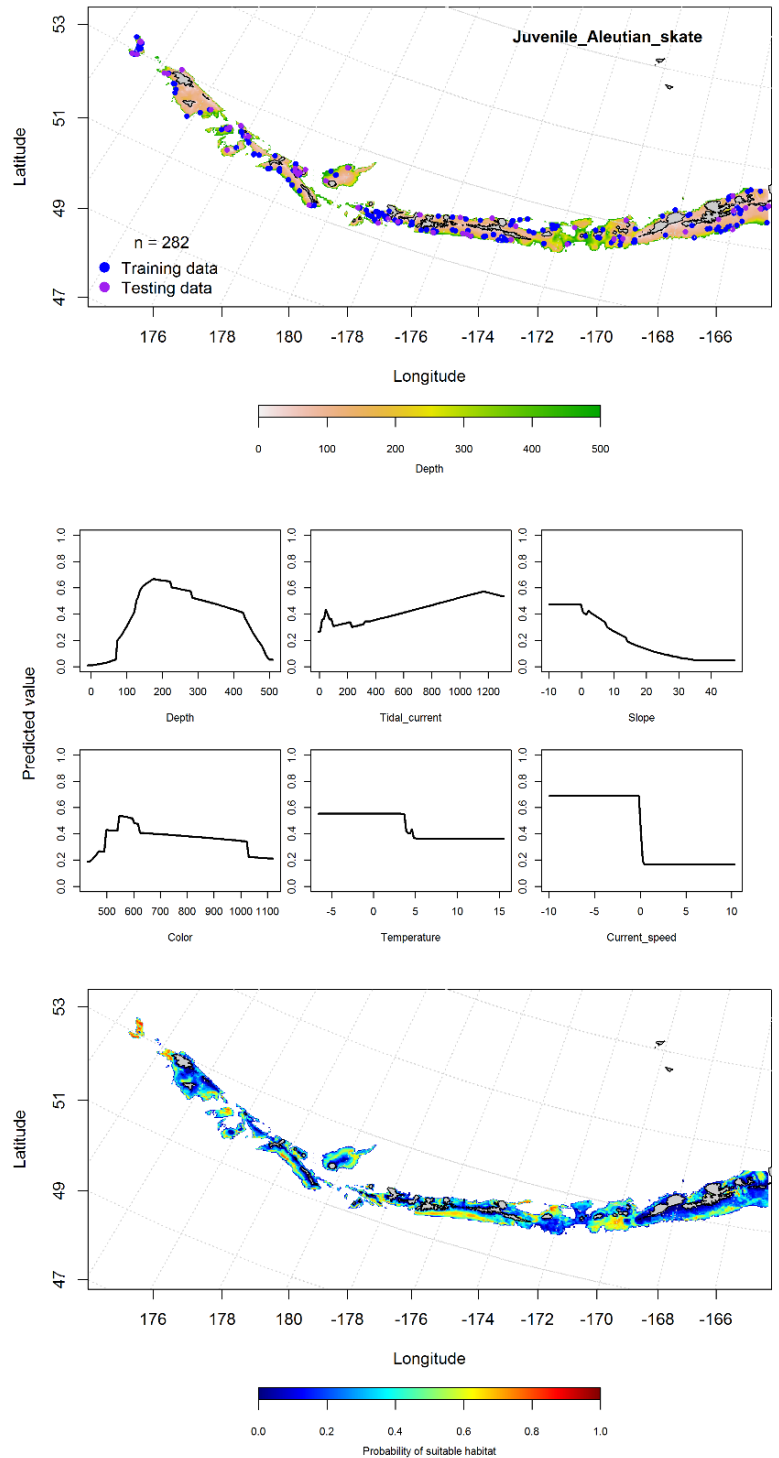


Figure 142. -- Distribution of catches of juvenile Aleutian skate in bottom trawl surveys (top panel), relationships between presence and environmental variables for the maximum entropy model of juvenile Aleutian skate (middle panels), and predicted probability of suitable habitat for juvenile Aleutian skate based on the model (bottom panel).

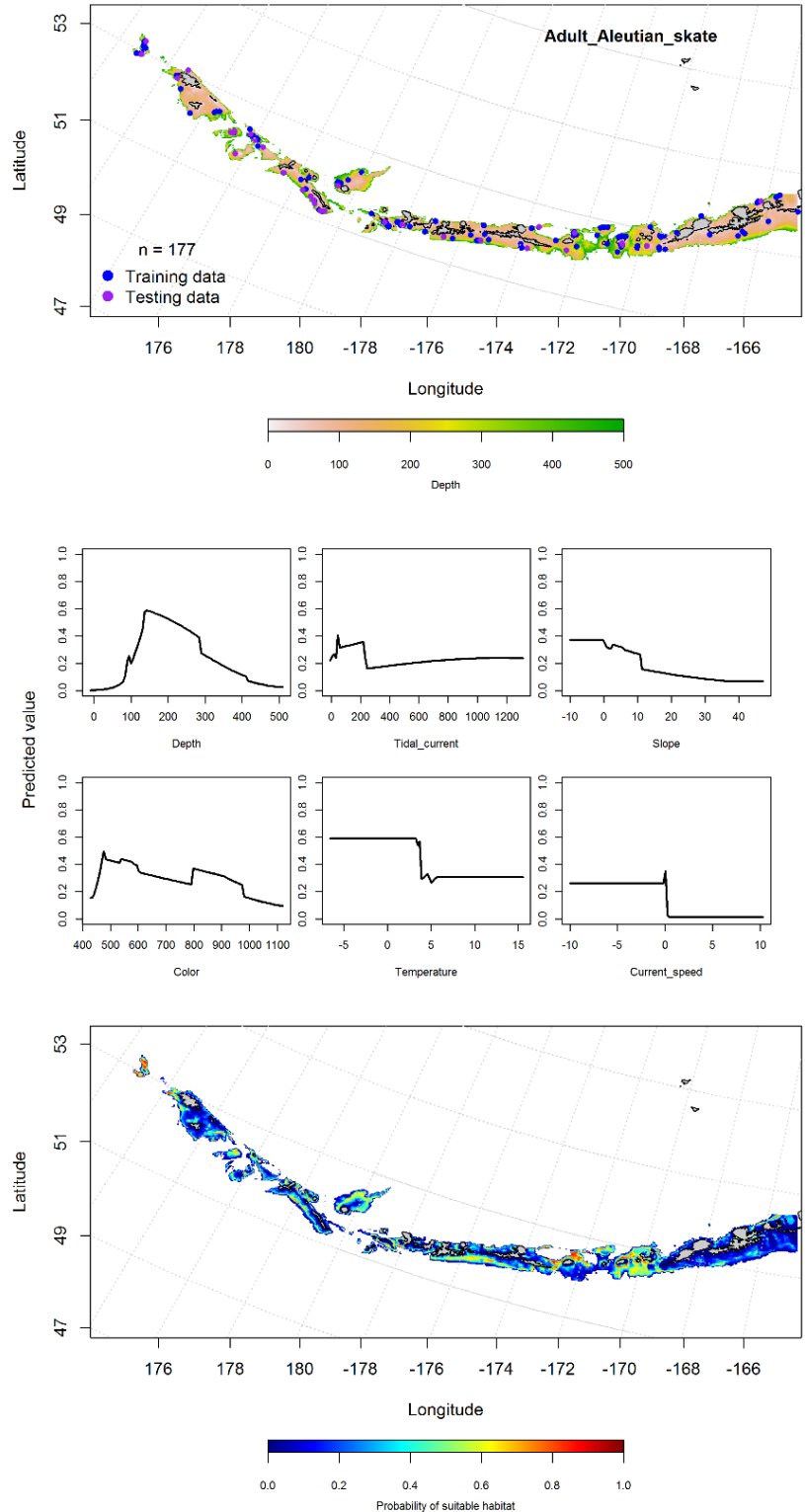


Figure 143. -- Distribution of catches of adult Aleutian skate in bottom trawl surveys (top panel), relationships between presence and environmental variables for the maximum entropy model of adult Aleutian skate (middle panels), and predicted probability of suitable habitat for adult Aleutian skate based on the model (bottom panel).

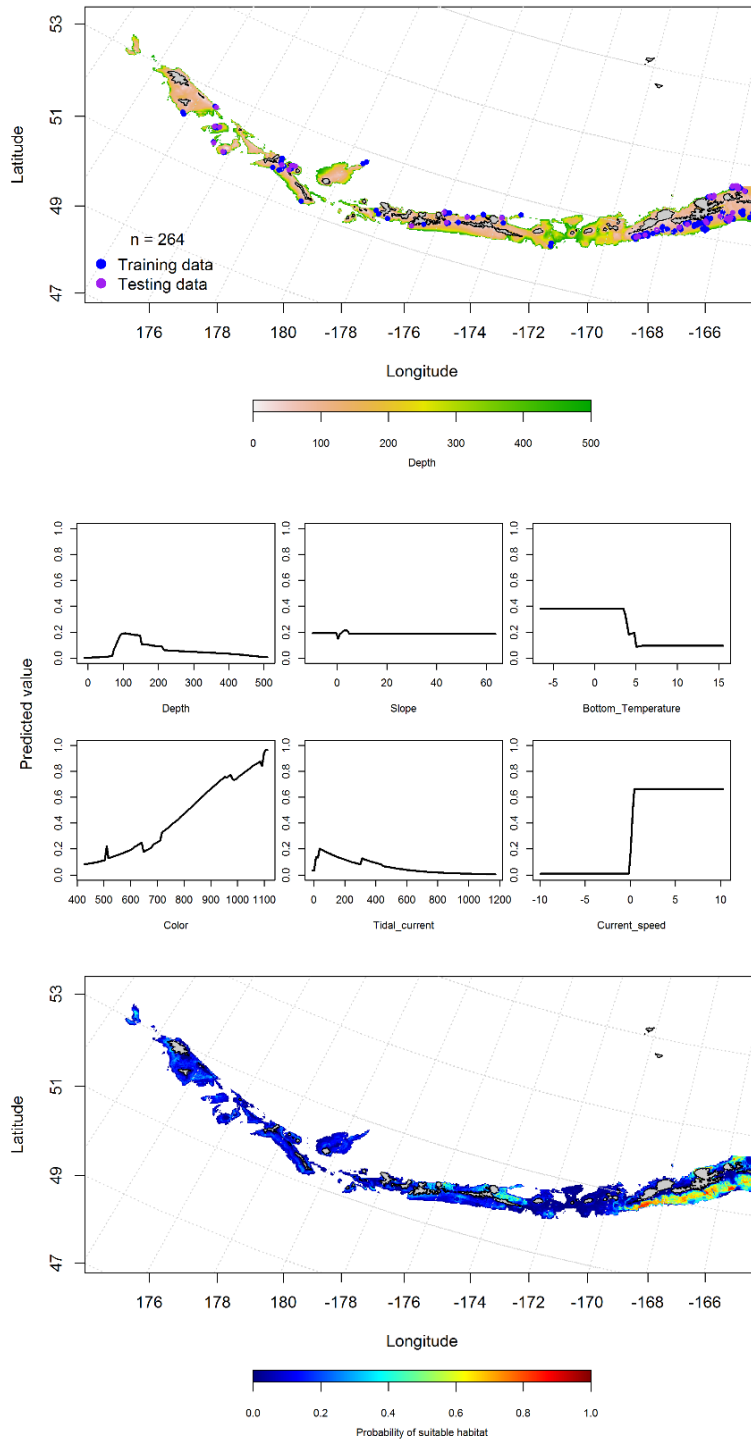


Figure 144. -- Locations of fall (September-November) commercial fisheries catches of Aleutian skate (top panel), relationships between probability of presence and environmental variables for the maximum entropy model (middle panels), and predicted probability of suitable habitat for Aleutian skate based on the model (bottom panel).

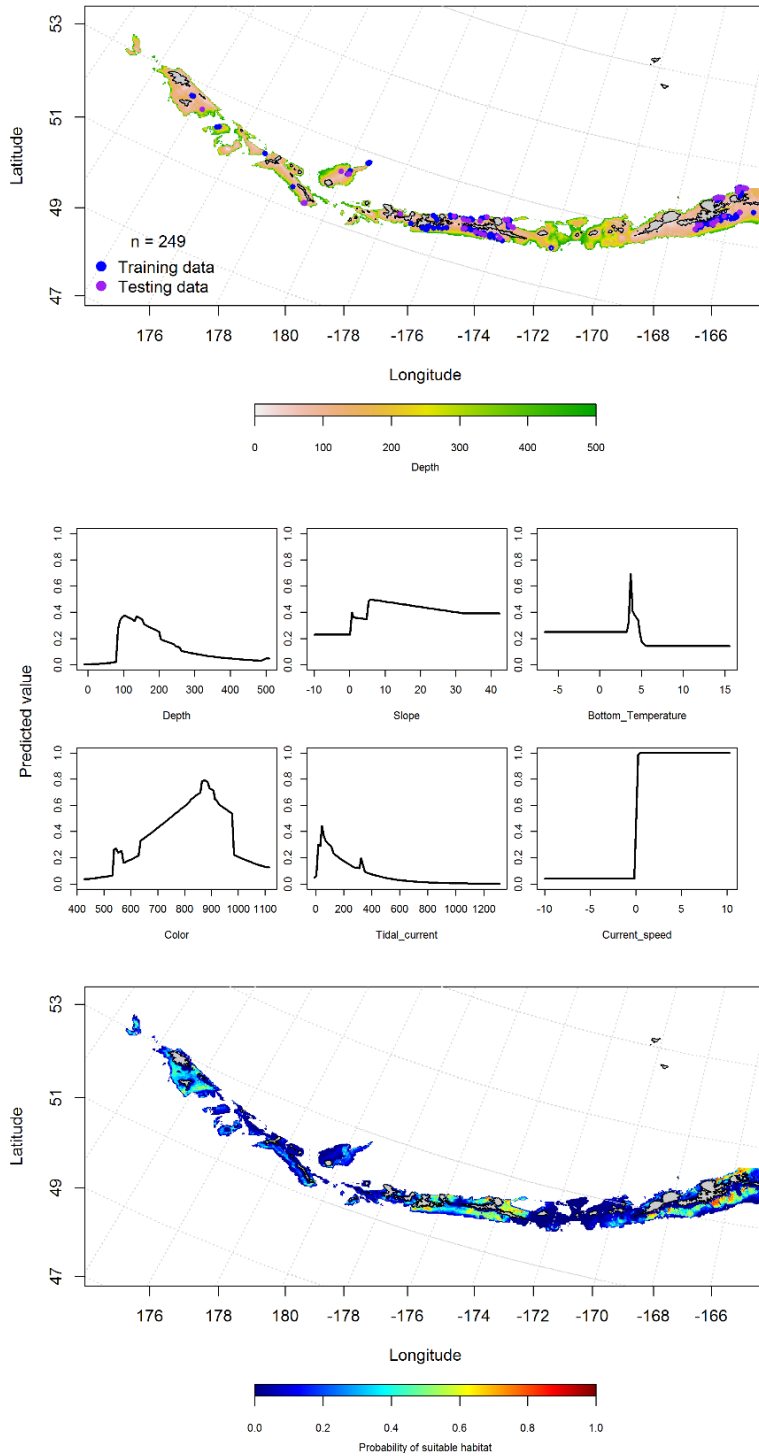


Figure 145. -- Locations of winter (December-February) commercial fisheries catches of adult Aleutian skate (top panel), relationships between probability of presence and environmental variables for the maximum entropy model (middle panels), and predicted probability of suitable habitat for Aleutian skate based on the model (bottom panel).

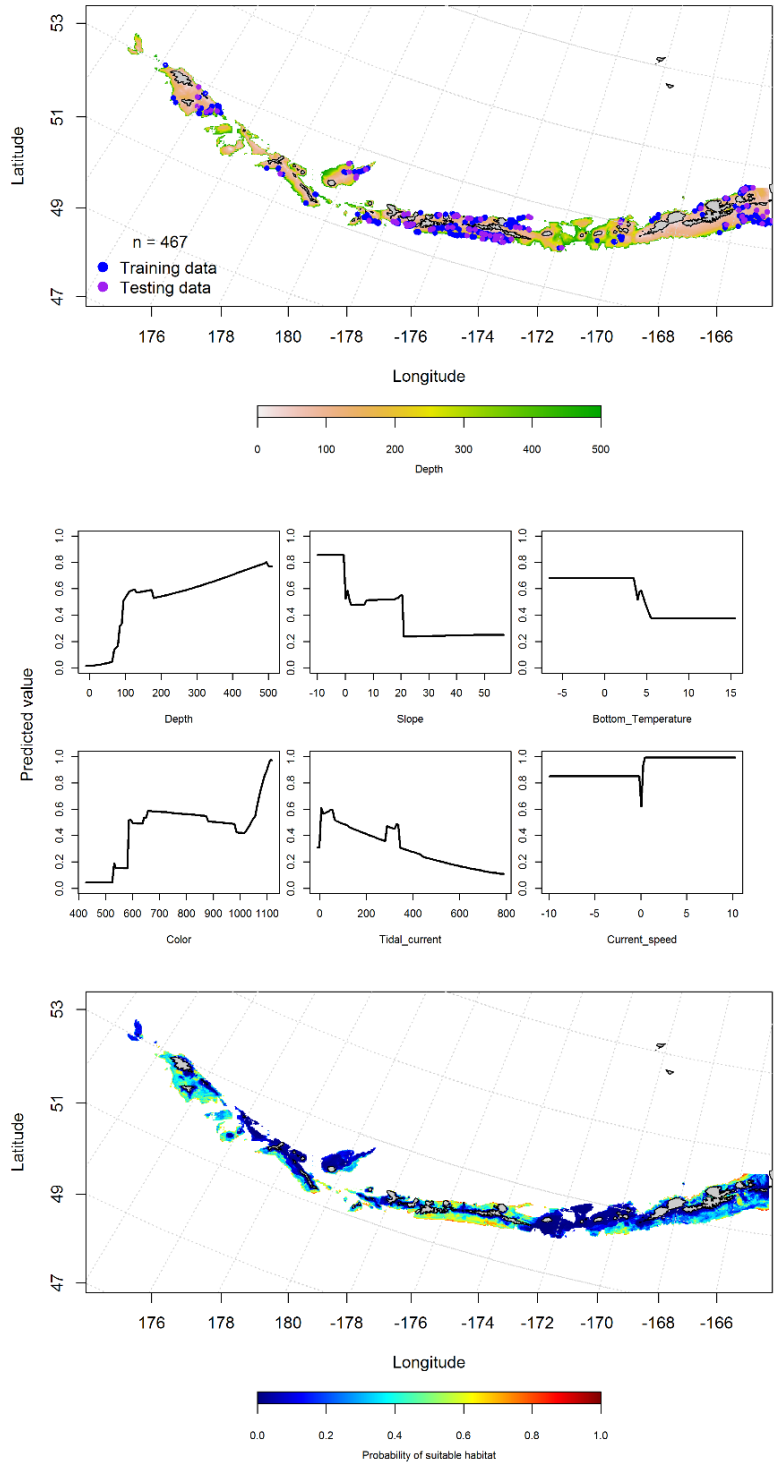


Figure 146. -- Locations of spring (March-May) commercial fisheries catches of adult Aleutian skate (top panel), relationships between probability of presence and environmental variables for the maximum entropy model (middle panels), and predicted probability of suitable habitat for Aleutian skate based on the model (bottom panel).

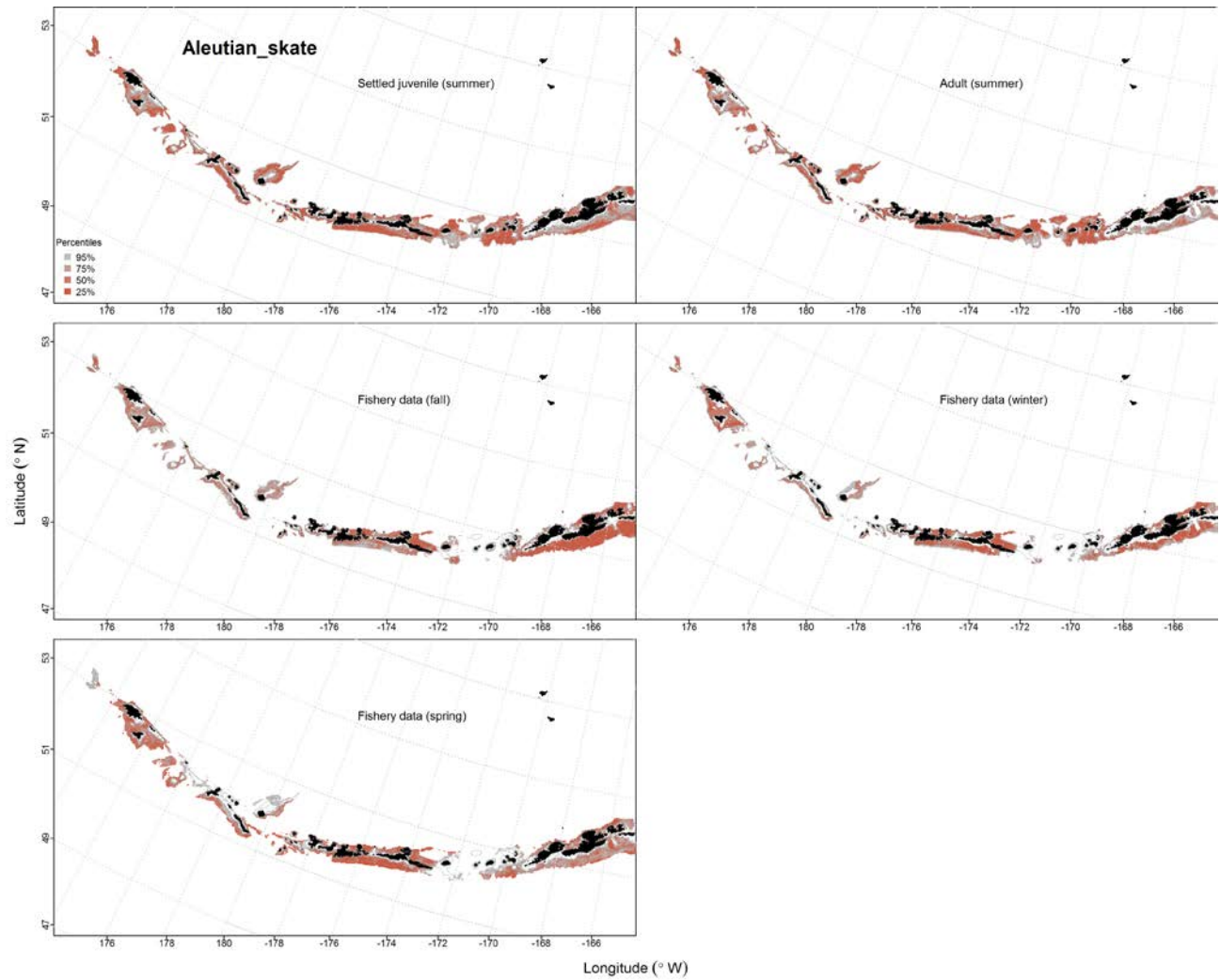


Figure 147. -- Predicted EFH quantiles for Aleutian skate life history stages based on species distribution modeling. Summer juvenile and adult stages are based on bottom trawl survey data, while seasonal stages (winter, spring, fall) are from commercial fishery data.

Invertebrates

Golden King Crab (*Lithodes aequispinus*)

Golden king crab distribution in the bottom trawl survey -- A hurdle-GAM model was used to predict the distribution of golden king crab. The AUC of the PA GAM was 0.90 for the training and test data. Depth, geographic location, tidal current and coral presence were the most important variables explaining the presence or absence of golden king crab. The model correctly classified 83% of the training and test data. The model predicted suitable habitat was highest in Seguam pass and Near pass (Fig. 148).

The CPUE GAM found current speed influenced the CPUE of golden king crab the most and the model explained 10% of the variance in the training data, and only 2% of the variance in the test data. The model predicted highest abundance in a similar pattern as the PA GAM (in Seguam and Near passes), but also on Petrel Bank (Fig. 148).

Golden king crab distribution in commercial fisheries -- Distribution of golden king crab in the Aleutian Islands in commercial fisheries catches was generally consistent with the bottom trawl survey. Bottom temperature, ocean color and tidal current were the most important variables determining the distribution of golden king crab habitat in the fall. The AUC of the fall MaxEnt model was 0.91 for the training data and 0.73 for the test data. The model predicted suitable habitat of golden king crab was highest in large passes (Fig. 149).

There were only six instances of golden king crab catch in the commercial fishery during winter months (a model was not run).

In the spring, depth and bottom temperature were the most important variables determining the distribution of golden king crab. The AUC of the spring MaxEnt model was 0.91 for the training data and 0.76 for the test data. The model predicted the probability of suitable habitat of golden king crab was highest in Near Pass (Fig. 150).

Golden king crab essential fish habitat maps and conclusions -- Golden king crab EFH predicted by the model using summertime bottom trawls is distributed across the Aleutian Islands, though highest in areas with large passes (Fig. 151). The fall and spring distribution of golden king crab EFH was essentially the same as the summer, with EFH distributed across the AI and highest in areas with large passes (Fig. 151).

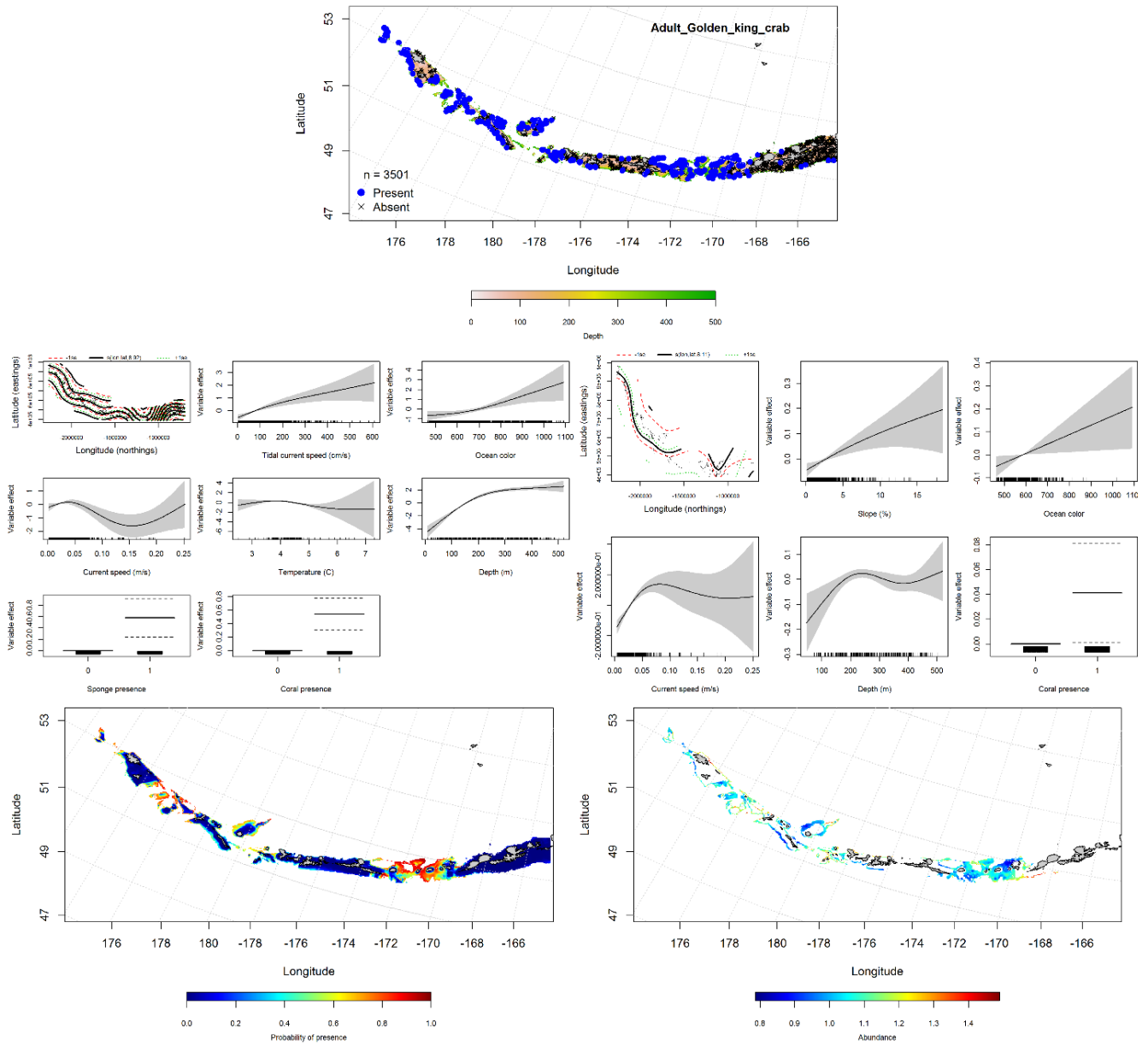


Figure 148. -- Distribution of catches of golden king crab in bottom trawl surveys (top middle panel), significant relationships between presence-absence and CPUE and environmental variables for the best-fitting generalized additive model golden king crab (middle left and right panels), and predicted probability of presence and abundance of golden king crab based on the models (bottom left and right panels).

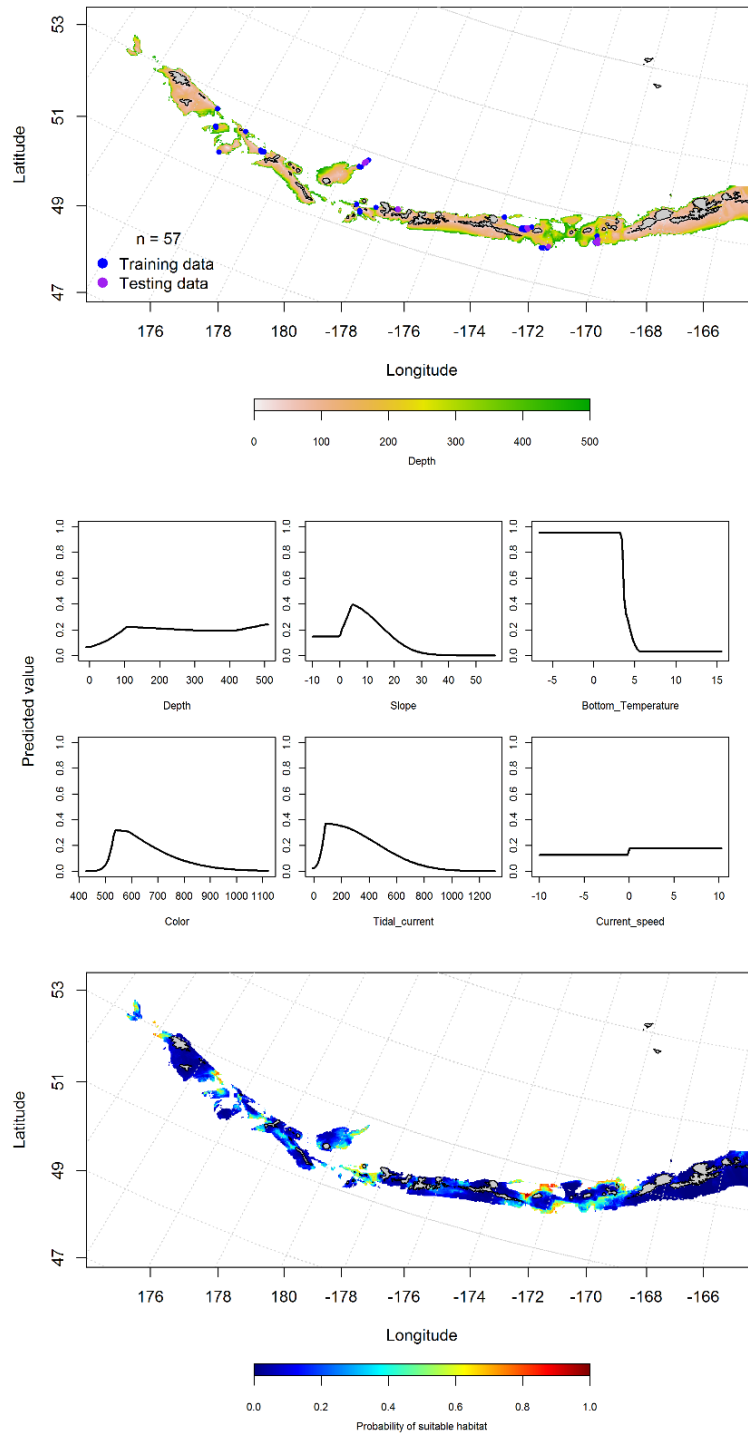


Figure 149. -- Locations of fall (September-November) commercial fisheries catches of golden king crab (top panel), relationships between probability of presence and environmental variables for the maximum entropy model (middle panels), and predicted probability of suitable habitat for golden king crab based on the model (bottom panel).

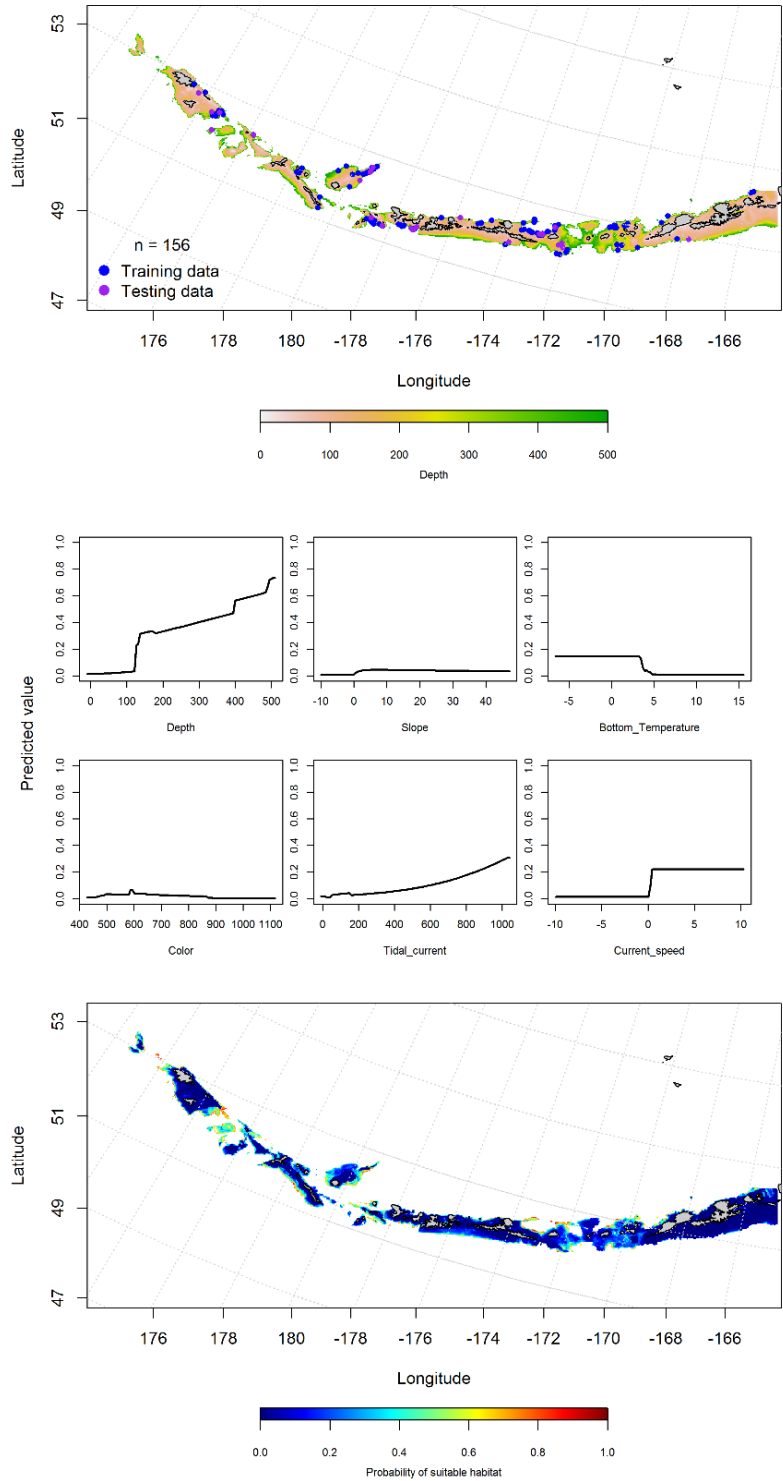


Figure 150. -- Locations of spring (March-May) commercial fisheries catches of golden king crab (top panel), relationships between probability of presence and environmental variables for the maximum entropy model (middle panels), and predicted probability of suitable habitat for golden king crab based on the model (bottom panel).

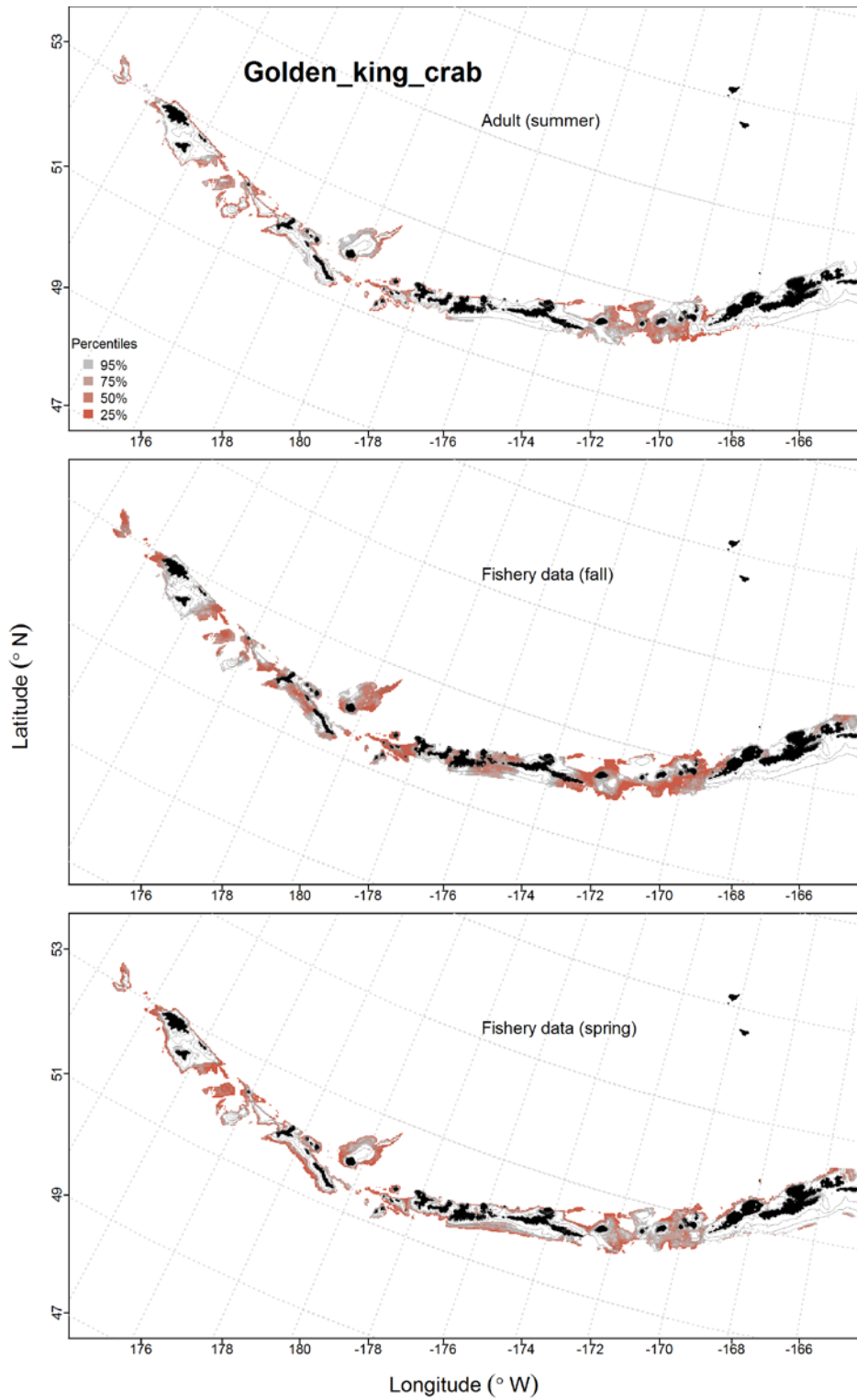


Figure 151. -- Predicted EFH quantiles for golden king crab based on species distribution modeling. Summer EFH is based on bottom trawl survey data, while seasonal stages (winter, spring, fall) are from commercial fishery data.

Pacific Giant Octopus (*Enteroctopus dofleini*)

Pacific giant octopus distribution in the bottom trawl survey -- A hurdle-GAM model was used to predict the distribution of Pacific giant octopus. The AUC of the PA GAM was 0.71 for the training data and 0.66 for the test data. Sponge presence and location were the most important variables explaining the probability of presence of Pacific giant octopus. The model correctly classified 63% of the training data set and 59% of the test data. The model predicted higher probability of presence for octopus near Amlia Island and south of Umnak Island (Fig. 152). The CPUE GAM found slope and depth influence the CPUE of Pacific giant octopus the most, but the model explained 6% of the variability in the training and 8% of the variability in the test data sets. The model predicted suitable habitat across the Aleutians in roughly similar levels, but the model fits were not great for CPUE (Fig. 152). Pacific giant octopus are not identified to species in the commercial fishery database.

Pacific giant octopus essential fish habitat maps and conclusions -- Pacific giant octopus essential fish habitat predicted from summer bottom trawl surveys modeling is distributed across the central and western Aleutian Islands near Kiska Island and the Tahoma Bank and Walls Plateau, with some EFH south of Umnak Island (Fig. 153).

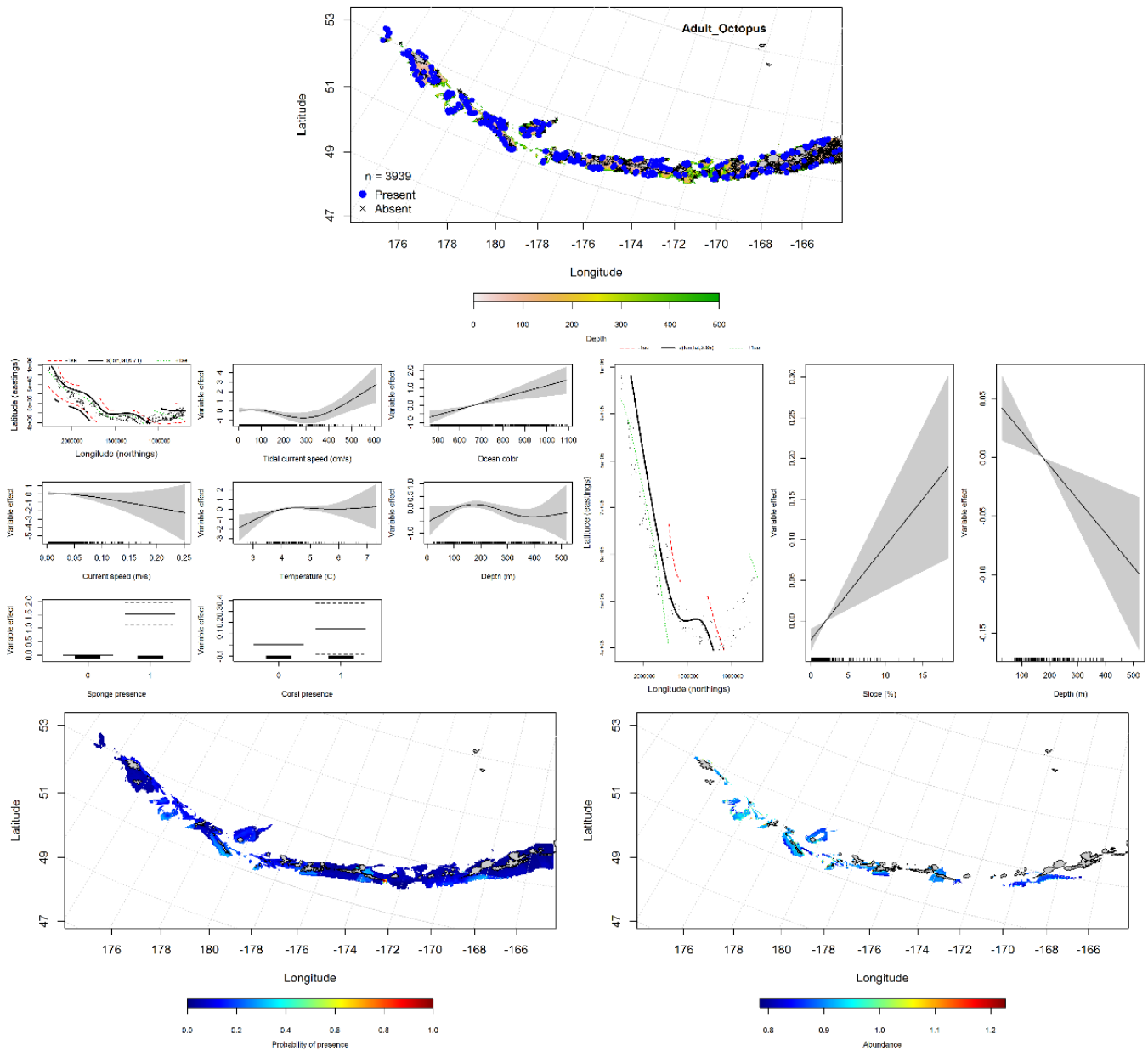


Figure 152. -- Distribution of catches of Pacific giant octopus in bottom trawl surveys (top middle panel), significant relationships between presence-absence and CPUE and environmental variables for the best-fitting generalized additive model Pacific giant octopus (middle left and right panels), and predicted probability of presence and abundance of Pacific giant octopus based on the models (bottom left and right panels).

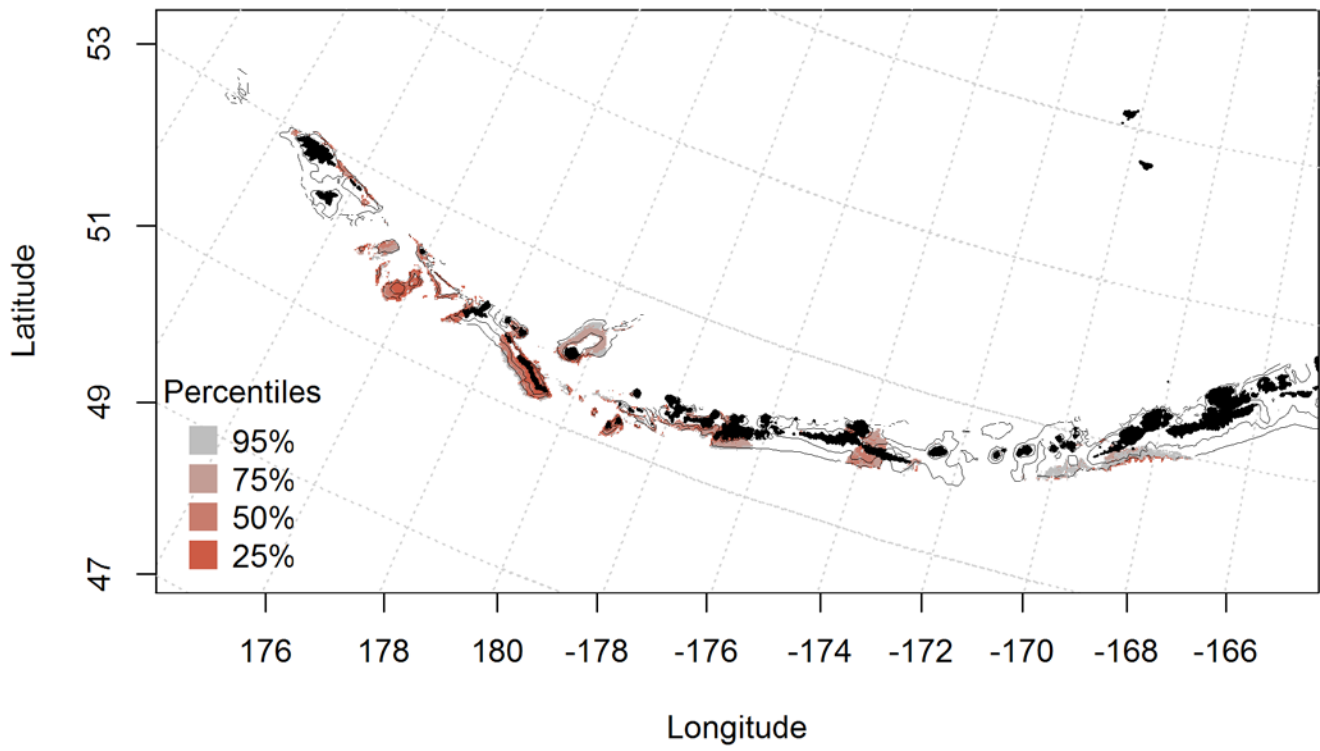


Figure 153. -- Predicted EFH quantiles for Pacific giant octopus based on species distribution modeling of bottom trawl survey catches.

ACKNOWLEDGMENTS

We wish to thank Kim Rand, John Olson and Wayne Palsson for their reviews of this report. We would also like to thank the numerous stock assessment scientists from the AFSC and Steve MacLean from the NPFMC for their helpful reviews and criticisms. This project was funded by the AKRO/AFSC Essential Fish Habitat Research Funds.

CITATIONS

- Behrenfeld, M. J., and P. G. Falkowski. 1997. Photosynthetic rates derived from satellite-based chlorophyll concentration. *Limnol. Oceanogr.* 42(1):1-20.
- Cochran, W.G. 1977. *Sampling Techniques*. 3rd ed. Wiley Series in Probability and Mathematical Statistics - Applied. John Wiley & Sons. N.Y., NY 428 p.
- Cragg, J.G. 1971. Some statistical models for limited dependent variables with application to the demand for durable goods. *Econometrica* 39:829-844.
- Danielson, S., E. Curchitser, K. Hedstrom, T. Weingartner, and P. Stabeno. 2011. On ocean and sea ice modes of variability in the Bering Sea. *J. Geophys. Res.* 116:C12034.
- DeLong, E. R., D. M. DeLong, and D. L. Clarke-Pearson. 1988. Comparing the area under two or more correlated receiver operating characteristic curves: a nonparametric approach. *Biometrics* 44(3):837-845.
- DeLong, A.K., and J.S. Collie. 2004. *Defining Essential Fish Habitat: A Model- Based Approach*. Rhode Island Sea Grant, Narragansett, R.I. 4pp. Rhode Island Sea Grant Communications Office, University of Rhode Island Bay Campus, Narragansett, RI 02882-1197.
- Egbert, G. D., and S. Y. Erofeeva. 2002. Efficient inverse modeling of barotropic ocean tides. *J. Atmos. Ocean. Tech.* 19(2):183-204.
- Elith, J., S. J. Phillips, T. Hastie, M. Dudik, Y. E. Chee, and C. J. Yates. 2011. A statistical explanation of MaxEnt for ecologists. *Diversity Distrib.* 17:43-57.
- Hastie, T. J., and R. J. Tibshirani. 1990. *Generalized Additive Models*. Monographs on Statistics and Applied Probability (43). 338 p.
- Hoff, G. R. 2010. Identification of skate nursery habitat in the eastern Bering Sea. *Mar. Ecol- Prog. Ser.* 403:243-254.
- Hosmer, D. W., and S. Lemeshow. 2005. *Applied Logistic Regression*. John Wiley and Sons, Inc.
- Ladd, C., G. L. Hunt Jr, C. W. Mordy, S. A. Salo, and P. J. Stabeno. 2005. Marine environment of the eastern and central Aleutian Islands. *Fish. Oceanogr.* 14:22-38.
- Laman, E. A., C. N. Rooper, S. C. Rooney, K. A. Turner, D. W. Cooper, and M. Zimmermann. 2017. Model-based essential fish habitat definitions for Bering Sea groundfish species. U.S. Dep. Commer., NOAA Tech. Memo. NMFS-AFSC-357, 265 p.
- Lauth, R. R., S. W. McEntire, and H. H. Zenger Jr. 2007. Geographic distribution, depth range, and description of Atka mackerel *Pleurogrammus monopterygius* nesting habitat in Alaska. *Alaska Fish. Res. Bull.* 12:165-186.

- Lozier, J. D., P. Aniello, and M. J. Hickerson. 2009. Predicting the distribution of Sasquatch in western North America: Anything goes with ecological niche modelling. *J. Biogeog.* 36(9):1623-1627.
- Orr, J. W., and S. Hawkins. 2008. Species of the rougheye rockfish complex: resurrection of *Sebastes melanostictus* (Matsubara, 1934) and a redescription of *Sebastes aleutianus* (Jordan and Evermann, 1898) (Teleostei: Scorpaeniformes). *Fish. Bull., U. S.* 106(2):111-134.
- Phillips, S. J., R. P. Anderson, and R. E. Schapire. 2006. Maximum entropy modeling of species geographic distributions. *Ecol. Model.* 190(3-4):231-59.
- Potts, J., and J. Elith. 2006. Comparing species abundance models. *Ecol. Model.* 199:153-163.
- R Core Development Team. 2013. R: A language and environment for statistical computing. R Foundation for Statistical Computing, Vienna, Austria. URL: <http://www.R-project.org/>.
- Rooney, S., E. A. Laman, C. N. Rooper, K. Turner, D. Cooper, M. Zimmermann. In prep. Model-based essential fish habitat definitions for Gulf of Alaska groundfish species. U.S. Dep. Commer., NOAA Tech. Memo. NMFS-AFSC-XXX, xxx p.
- Rooper, C. N., M. F. Sigler, P. Goddard, P. Malecha, R. Towler, K. Williams, R. Wilborn, and M. Zimmermann. 2016. Validation and improvement of species distribution models for structure forming invertebrates in the eastern Bering Sea with an independent survey. *Mar. Ecol. Prog. Ser.* 551:117-130.
- Rooper, C. N., M. Zimmermann, M. M. Prescott, and A. J. Hermann. 2014. Predictive models of coral and sponge distribution, abundance, and diversity in bottom trawl surveys of the Aleutian Islands, Alaska. *Mar. Ecol. Prog. Ser.* 503:157-176.
- Sagarese, S. R., M. G. Frisk, R. M. Cerrato, K. A. Sosebee, J. A. Musick, and P. J. Rago. 2014. Application of generalized additive models to examine ontogenetic and seasonal distributions of spiny dogfish (*Squalus acanthias*) in the Northeast (US) shelf large marine ecosystem. *Can. J. Fish. Aquat. Sci.* 71(6): 847-877.
- Sigler, M. F., C. N. Rooper, G. R. Hoff, R. P. Stone, R. A. McConnaughey, and T. K. Wilderbuer. 2015. Faunal features of submarine canyons on the eastern Bering Sea slope. *Mar. Ecol. Prog. Ser.* 526:21-40.
- Stabeno, P. J., J. D. Schumacher, and K. Ohtani. 1999. The physical oceanography of the Bering Sea. In: Loughlin T. R., and K. Ohtani (eds) *Dynamics of the Bering Sea: A Summary of Physical, Chemical, and Biological Characteristics, and a Synopsis of Research on the Bering Sea*, North Pacific Marine Science Organization (PICES), University of Alaska Sea Grant, AK-SG-99-03. Fairbanks, Alaska, p. 1-59.
- Stabeno, P. J., R. K. Reed, and J. M. Napp. 2002. Transport through Unimak Pass, Alaska. *Deep-Sea Res. II* 49:5919-5930.
- Stauffer, G. 2004. NOAA protocols for groundfish bottom trawl surveys of the Nation's fishery resources. U. S. Dep. Commer., NOAA Tech. Memo. NMFS-F/SPO-65, 205 p.

- Venables W. N., and B. D. Ripley. 2002. *Modern Applied Statistics with S*. Fourth Edition. Springer Science+Business Media, New York, N.Y.
- Wood, S. N. 2006. *Generalized Additive Models: An Introduction with R*. Chapman and Hall/CRC, Boca Raton, FL. 392 p.
- Zimmermann M., M. M. Prescott, and C. N. Rooper. 2013. Smooth sheet bathymetry of the Aleutian Islands. U. S. Dep. Commer. NOAA Tech. Memo. NMFS-AFSC-250, 43 p.
- Zimmermann, M., and J. L. Benson. 2013. Smooth sheets: How to work with them in a GIS to derive bathymetry, features, and substrates. U. S. Dep. Commer. NOAA Tech. Memo. NMFS-AFSC-249, 52 p.
- Zuur, A. F., E. N. Ieno, N. J. Walker, A. A. Saveliev, and G. M. Smith. 2009. *Mixed Effects Models and Extensions in Ecology with R*, 596 p.

RECENT TECHNICAL MEMORANDUMS

Copies of this and other NOAA Technical Memorandums are available from the National Technical Information Service, 5285 Port Royal Road, Springfield, VA 22167 (web site: www.ntis.gov). Paper and electronic (.pdf) copies vary in price.

AFSC-

- 359 RODGVELLER, C. J., P. W. MALECHA, and C. R. LUNSFORD. 2017. Long-term survival and observable healing of two deepwater rockfishes, *Sebastes*, after barotrauma and subsequent recompression in pressure tanks, 37 p. NTIS number pending.
- 358 FAUNCE, C., J. SULLIVAN, S. BARBEAUX, J. CAHALAN, J. GASPER, S. LOWE, and R. WEBSTER. 2017. Deployment performance review of the 2016 North Pacific Groundfish and Halibut Observer Program. U.S. Dep. Commer., NOAA Tech. Memo. NMFS-AFSC-358, 75 p. NTIS number pending.
- 357 LAMAN, E. A., C. N. ROOPER, S. C. ROONEY, K. A. TURNER, D. W. COOPER, and M. ZIMMERMANN. 2017. Model-based essential fish habitat definitions for Bering Sea groundfish species, 75 p. NTIS number pending.
- 356 CSEPP, D. J., D. C. HONEYFIELD, J. J. VOLLENWEIDER, and J. WOMBLE. 2017. Estuarine distribution, nutritional and thiaminase content of eulachon (*Thaleichthys pacificus*) in Southeast Alaska, with implications for Steller sea lions, 56 p. NTIS number pending.
- 355 M. M. MUTO, V. T. HELKER, R. P. ANGLISS, B. A. ALLEN, P. L. BOVENG, J. M. BREIWICK, M. F. CAMERON, P. J. CLAPHAM, S. P. DAHLE, M. E. DAHLHEIM, B. S. FADELY, M. C. FERGISON, L. W. FRITZ, R. C. HOBBS, Y. V. IVASHCHENKO, A. S. KENNEDY, J. M. LONDON, S. A. MIZROCH, R. R. REAM, E. L. RICHMOND, K. E. W. SHELDEN, R. G. TOWELL, P. R. WADE, J. M. WAITE, and A. N. ZERBINI. 2017. Alaska marine mammal stock assessments, 2016, 366 p. NTIS No. PB2017-102381
- 354 HELKER, V. T., M. M. MUTO, K. SAVAGE, S. TEERLINK, L. A. JEMISON, K. WILKINSON, and J. JANNOTT. 2017. Human-caused mortality and injury of NMFS-managed Alaska marine mammal stocks, 2011-2015. U.S. Dep. Commer., NOAA Tech. Memo. NMFS-AFSC-354, 112 p. NTIS No. PB2016102765.
- 353 CONNER, J., D. G. NICHOL, and R. R. LAUTH. 2017. Results of the 2015 eastern Bering Sea continental shelf bottom trawl survey of groundfish and invertebrate resources, 154 p. NTIS No. PB2017-102385.
- 352 CONNER, J., and R. R. LAUTH. 2017. Results of the 2016 eastern Bering Sea continental shelf bottom trawl survey of groundfish and invertebrate resources, 159 p. NTIS No. PB2017-102386.
- 351 GODDARD, P., R. E. WILBORN, C. N. ROOPER, K. WILLIAMS, and R. TOWLER. 2017. Results of the 2012 and 2014 underwater camera surveys of the Aleutian Islands, 505 p. NTIS No. PB2017-102387.
- 350 CONNER, J., D. E. STEVENSON, and R. R. LAUTH. 2017. Results of the 2014 eastern Bering Sea continental shelf bottom trawl survey of groundfish and invertebrate resources, 154 p. NTIS No. PB2017-102195.
- 349 von SZALAY, P. G., N. W. RARING, C. N. ROOPER, and E. A. LAMAN. 2017. Data Report: 2016 Aleutian Islands bottom trawl survey. U.S. Dep. Commer., NOAA Tech. Memo. NMFS-AFSC-349, 161 p. NTIS No. PB2017-102170.